GEODYNAMIC SETTING AND MINERALIZATION IN THE WESTERN NEO-TETHYS

A Thesis Submitted to the
College of Graduate and Postdoctoral Studies
In Partial Fulfillment of the Requirements
For the Degree of Master of Science
In the Department of Geological Sciences
University of Saskatchewan
Saskatoon

By

KHALIL ALLAHYARI

PERMISSION TO USE

In presenting this thesis/dissertation in partial fulfillment of the requirements for a Postgraduate degree from the University of Saskatchewan, I agree that the Libraries of this University may make it freely available for inspection. I further agree that permission for copying of this thesis/dissertation in any manner, in whole or in part, for scholarly purposes may be granted by the professor or professors who supervised my thesis/dissertation work or, in their absence, by the Head of the Department or the Dean of the College in which my thesis work was conducted. It is understood that any copying or publication or use of this thesis/dissertation or parts thereof for financial gain shall not be allowed without my written permission. It is also understood that due recognition shall be given to me and to the University of Saskatchewan in any scholarly use which may be made of any material in my thesis/dissertation.

DISCLAIMER

This thesis was exclusively created to meet the thesis and/or exhibition requirements for the degree of Master of Science at the University of Saskatchewan. References in this thesis to any specific commercial products, process, or service by trade name, trademark, manufacturer, or otherwise do not constitute or imply its endorsement, recommendation, or favouring by the University of Saskatchewan. The views and opinions of the author expressed herein do not state or reflect those of the University of Saskatchewan and shall not be used for advertising or product endorsement purposes.

Requests for permission to copy or to make other uses of materials in this thesis/dissertation in whole or part should be addressed to:

Head of Geological Sciences

University of Saskatchewan

Saskatoon, Saskatchewan S7N 5E2 Canada

OR

Dean

College of Graduate and Postdoctoral Studies

University of Saskatchewan

116 Thorvaldson Building, 110 Science Place

Saskatoon, Saskatchewan S7N 5C9 Canada

ABSTRACT

The southern section of the Neo-Tethys Ocean was located between the Arabian shield and the Sanandaj-Sirjan Zone. To understand the mineral exploration potential in this area, a new database including 420 U-Pb and 1147 lithogeochemical samples, 1552 Lu-Hf, and 353 Sm-Nd isotopic composition results were constructed from published articles. This research is the first attempt to provide quantitative constraints on the development of the Western Neo-Tethys by utilizing the available published geochronological and geochemical data on the Mesozoic evolution of the Neo-Tethys. The collected dataset potentially provides insights into the relationship between tectono-magmatic environments and geochemical signatures in the overall study area.

The geodynamic evolution of the Neo-Tethys in Iran started potentially as a rift by the Late Permian. Thus, igneous and metamorphic rocks older than Permian has been considered as basement and crustal blocks. The calculated ε_{Hf} and ε_{Nd} values distinguish five large crustal blocks in the western Neo-Tethys. However, the isotopic composition in the central and northwest of the Urumieh-Dokhtar Magmatic Arc confirms the rifting and seafloor spreading of Neo-Tethys during the Permian–Triassic times.

Contrary to previous studies, the GPlates-based reconstructions showed that the closure of Paleo-Tethys occurred in the Late Jurassic, not in the Permian–Triassic period. Moreover, based on this paleo-plate reconstruction, the opening of the Neo-Tethys was formed in the Late Triassic - Early Jurassic period and the initiation of subduction has occurred during the Middle Jurassic - Late Jurassic. Furthermore, the GPlates reconstructions, indicate that the initiation of collision between Arabia and Eurasia occurred between the upper Miocene to Pliocene (10-5 Ma).

The geodynamic evolution of the southern Neo-Tethys Ocean involved a significant flare-up of arc magmatism affecting a large part of Iran and western Neo-Tethys from Cretaceous until the mid-Tertiary. The peak of magmatism occurred between 55 and 35Ma. This flare-up has formed two parallel arc regions, the Sanandaj-Sirjan Zone in the fore-arc and Urumieh-Dokhtar Magmatic Arc in the back-arc. These two parallel domains are believed to be the result of the NE-dipping subduction of the Neo-Tethys in the Western Neo-Tethys. The geochemical features and adakitic signatures in these areas are interpreted similarly to the Andean-type magmatism. The mineralization in this realm is linked to the intrusion-related porphyry copper system of the

Urumieh-Dokhtar Magmatic Arc. This area is significantly dominated by substantial volcanic activity. Alternatively, volcanic massive sulfide deposit formation is related to the evolution of an extensional continental margin in a back-arc environment that affected the Central Iranian Microcontinent.

This study has shown that no adakitic signatures are observed in Western Neo-Tethys rocks until the Early Jurassic. The first signs of adakitic magmatism appeared during the Middle to Late Jurassic period for the Ghorveh area in the northwest of Sanandaj-Sirjan Zone. However, the subduction of the Neo-Tethys oceanic crust under the Central Iranian Microcontinent has continued from Jurassic to Paleogene time, and adakitic magmatism has occurred in some segments along Western Neo-Tethys.

ACKNOWLEDGMENTS

I would first like to acknowledge the support and valuable guidance provided by my supervisors **Dr. Kevin Ansdell** and **Dr. Bruce Eglington**, throughout the completion of this thesis. Many thanks for your patience through the extended timeline of this project and guidance in data interpretation, conference preparation, and writing.

Thank you to my committee members, **Dr. Camille Partin, Dave Thomas,** and **Dr. Luis Buatois**, for taking the time to review my thesis and provide valuable comments.

My eternal gratitude to Dean Meek for providing suggestions and sharing valuable GIS and GPlates related insights. To Lavie Nyguen, Isabelle Baconnais, and Mojtaba Abdolahnezhad thank you for being continuously optimistic and providing endless moral support.

I am also grateful for the technical support I received from Jim Rosen and Tim Prokopiuk at the Department of Geological Sciences.

The completion of this thesis would not have been possible without the help and support I've received from my colleagues, family, and friends. Finally, a special thanks to my wife, **Hamraz**, for her love and valued supports throughout the writing of this thesis.

This research was supported by funding provided by a Dean's Scholarship from the University of Saskatchewan and the Department of Geological Sciences, NSERC Discovery grant to Kevin Ansdell, and the Pyke Chair research fund to Bruce Eglington.

DEDICATION

To my loves: **Hamraz**, **Evian**, and **Ryan**,

without your support, this would not have been possible.

and

To the memory of my parents

that you have always been here with me

and you will be in my heart forever.

TABLE OF CONTENTS

LIST OF TABLES

LIST OF FIGURES

ACRONYMS AND ABBREVIATIONS USED

AP – Accretionary Prism
Cpy – Chalcopyrite
CHUR– Chondritic Uniform Reservoir
CIM – Central Iranian Microcontinent
GIS – Geographic Information Systems
HMREE – Heavy Rare Earth Element
Hem – Hematite
IB – inner belt
KCMA - Kerman Cenozoic magmatic assemblage
LREE – Light Rare Earth Element
MREE – Medium Rare Earth Element
MC-ICP-MS - Multi- collector inductively coupled mass spectrometry
MZTZ – Main Zagros Thrust Zone
OIB – Oceanic Island Basalts
OB – outer belt
OPB – Oceanic Plateau Basalts
ORG – Oceanic Ridge Granites
PIC – Proven Igneous Complex
Po – Pyrrhotite
Py – Pyrite
Qtz – Quartz
REE – Rare Earth Element
SEDEX – Sedimentary-exhalative deposits
SQL – Structured Query Language
SSZ – Sanandaj-Sirjan Zone
SiSZ – Sistan Suture Zone
syn-COLG – syn-Collisional Granites
T_{DM} – Depleted mantle model age
T_{2DM} – two-stage depleted mantle model
UDMA – Urumieh-Dokhtar Magmatic Arc
VMS – Volcanic Massive Sulfide
VAB – Volcanic Arc Basalt
VAG – Volcanic Arc Granites
WPG – Within Plate Granites
WNT– Western Neo-Tethys
Fig – Figure

CHAPTER 1: INTRODUCTION

1.1 Introduction

The western part of the Tethys Ocean was the realm of major plate tectonic reconfiguration during the Late Paleozoic – Early Mesozoic time. The opening of the Neo-Tethys Ocean along the eastern margin of Gondwana occurred accompanying the closing of the Paleo-Tethys Ocean along the southern margin of Eurasia (Muttoni et al., 2009). This is important in the tectonic development of southwestern Asia because the Cimmerian terranes, including Iran, Afghanistan, Karakoram, and Qiangtang, broke off from the eastern edge of Gondwanan. They drifted northward across the Paleo-Tethys and ultimately collided with the Eurasian margin. (e.g., Şengör, 1979; Muttoni et al., 2009). Most of the mineralization in the Western Neo-Tethys (WNT) is related to the Neo-Tethys and related back-arc basins on the south side of Eurasia, including volcanogenic massive sulfide (VMS) (Badrzadeh et al., 2011; Mousivand et al., 2007; Mousivand et al., 2011), porphyry deposits (Arjmandzadeh et al., 2011b; Jamali & Mehrabi, 2015; Richards, 2015; Richards, 2014; Zürcher et al., 2015; Nabatian, Wan, & Honarmand, 2017; Zarasvandi et al., 2015; Hosseini et al., 2017a; Shahsavari Alavijeh et al., 2017; Alaminia et al., 2017; Heidari et al., 2015), and Mesozoic ophiolites (Saccani et al., 2013; Allahyari et al., 2010).

However, in order to fully understand the mineral exploration potential in this area, it is essential to understand the geodynamics and different tectonic associations in the mineralized belts. This research is the first attempt to provide quantitative constraints on the development of the WNT by utilizing the available published geochronological and geochemical data on the Mesozoic evolution of the Neo-Tethys. The timing and geochemical signatures related to mineralization in ophiolites, VMS, and porphyry deposits are fundamental to predicting the likelihood of mineralization in the geological entities of the western Neo-Tethys.

In this regard, it was necessary to collect the available data in a new data set. Certain aspects for which data were compiled for this study were: geochronology, geochemistry, isotope geochemistry, and bringing these data together to infer the most likely scenario for the development history of the western Neo-Tethys.

The main evolution of the Neo-Tethys lithosphere occurred during the Mesozoic; the region is also well known for its Cu and Cu-Au porphyry mineralization. Therefore, integrating,

geochronological, geochemical, and isotopic data from the Neo-Tethys region might provide further insights into the spatial and temporal relationships between crustal geochemical signatures and Cu and Cu-Au porphyry formation. In addition, this dataset provides an improved understanding of tectono-magmatic events in the study areas. Meanwhile, the correlation between the geochemistry and the geochronological data leads to a better understanding of the location of mineral deposits in the western Neo-Tethys.

1.2 Project Scope

This Master of Science thesis project is focused on the geodynamic evolution of the WNT and understanding the geochronological and geochemical signatures leading to potential mineralization in this area at a particular time. This thesis focuses on a better understanding of the geochemical signatures leading to potential mineralization in VMS and porphyry deposits during the development of the Neo-Tethys in southwest Asia. In this study, geochronology, geochemistry, and isotope geochemistry data have been compiled from the published literature.

In addition, the important focus of this thesis is on why there is no mineralization in some WNT areas at specific times. This work aims to provide better exploration parameters for future Cu-Au-Mo porphyry and VMS mineralization exploration in this area.

1.3 Research Question and Hypotheses

In this study, our aim is to clarify the various assumptions about potential mineralization in the western Neo-Tethys. In this regard, the following research question:

Question: Why do some arc segments in the Urumieh-Dokhtar Magmatic Arc (UDMA) in WNT orogenic systems show significant copper ore deposits while in others they are absent?

Hypothesis:

Magmatic activity and Cu mineralization along the main UDMA are attributed to three main episodes: (1) Eocene–Oligocene (Ahmadian et al., 2009); (2) Mid-Late Oligocene and (3) Mid-Late Miocene (Shahabpour & Kramers, 1987; Shafiei et al., 2009). Because of the long-recognized analogy between the cordilleran-type UDMA and Andean arcs (Dewey et al., 1979), porphyry copper deposits form in mature arc settings with the enriched and thickened lithosphere during the evolution of the UDMA.

1.4 Thesis Layout

The thesis has been written in seven chapters and organized in the thesis-based style. Each chapter has a specific focus and objective. The titles of the chapters are (1) Introduction, (2) Regional geological setting, (3) Methodology, (4) Results, (5) Discussion Part 1, (6) Discussion Part 2, and (7) Conclusion.

CHAPTER 2: REGIONAL GEOLOGICAL SETTING

2.1 Literature review and Previous work

This section consists of the compilation of geological, geochemical, and geochronological data of the study areas, existing in published scientific articles, available databases, books, thesis, geological maps, and other sources, allowing the author to gain the main geological background of the Neo-Tethys. This forms the relevant framework for constructing an extensive geochronological and geochemical database (see chapter 4), which is utilized in this thesis.

2.2. The Neo-Tethys realm in Iran

In southwest Asia, the Mesozoic southern branch of the Neo-Tethys Ocean (**Fig. 2.1, 2.2**) was situated between the Arabian shield and the Sanandaj Sirjan Zone (SSZ) of Iran (e.g., Berberian & King, 1981; Şengör et al., 1988; Robertson, 2007; Allahyari et al., 2010). Ophiolites segments cropping out along the Main Zagros Thrust Zone (MZTZ, **Fig 2.2**) indicate the suture zone between the Arabian (Zagros domain) and Sanandaj Sirjan Zone. They represent portions of the southern Neo-Tethyan oceanic lithosphere, which initially existed between the Arabian plate and Eurasian continental margins (**Fig.2.1, 2.2**). Geology, geodynamics, stratigraphy, tectonics, and petroleum resources of the Zagros domain have been comprehensively studied in recent years (Berberian & King, 1981; Dercourt et al., 1986; Ricou, Braud, & Brunn, 1977; Ricou, 1976; Şengör et al., 1988; Stampfli & Borel, 2002), as well as in the latest literature (e.g., Agard et al., 2005; Allahyari et al., 2014; Leturmy & Robin, 2010; Saccani et al., 2014). Several authors suggested an intra-oceanic supra-subduction zone setting developed in this ocean during the Late Cretaceous, demonstrating that this realm was a site of plate convergence during the Late Mesozoic time (Moghadam & Stern, 2015).

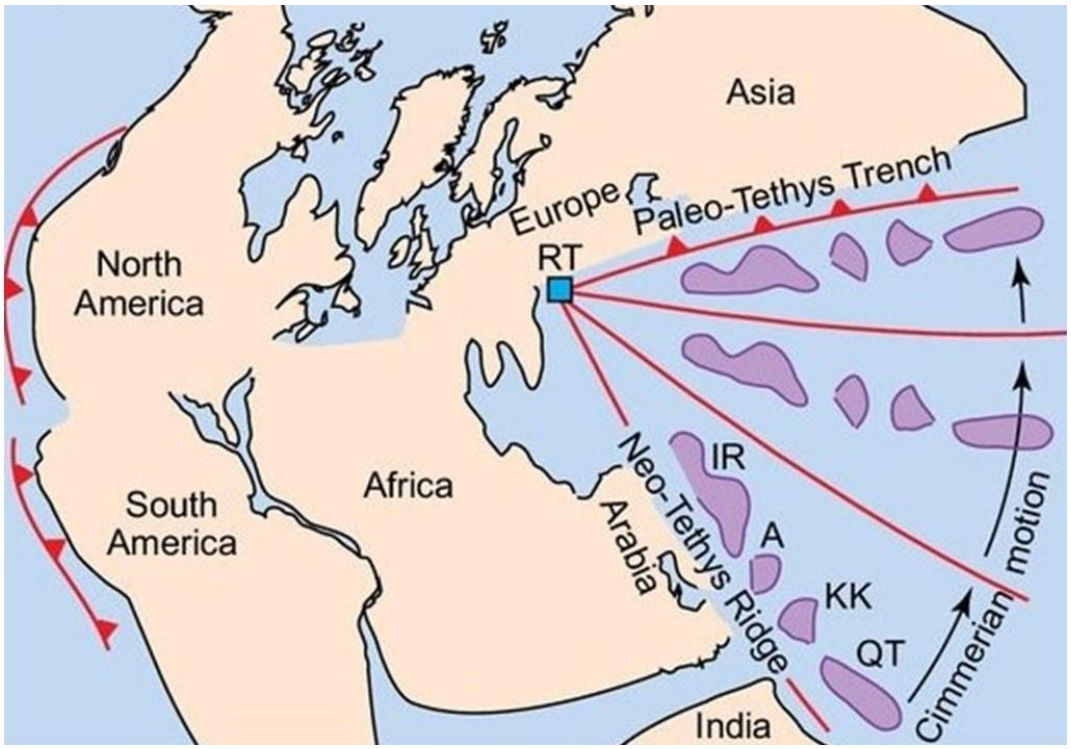

Figure 2. 1. The tectonic scheme of Pangea and the location of the Neo-Tethys, Paleo-Tethys, and the surrounding realms. The Cimmerian terranes movement occurred during the Permian–Triassic time (modified after Muttoni et al., 2009). RT: rotation of the Cimmerian terranes. IR: Iran (NW Iran, Alborz, Central Iran, and Sanandaj-Sirjan; A: Afghanistan (Helmand and Farah); KK: the Karakoram in northern Pakistan; QT: Qiangtang in north Tibet

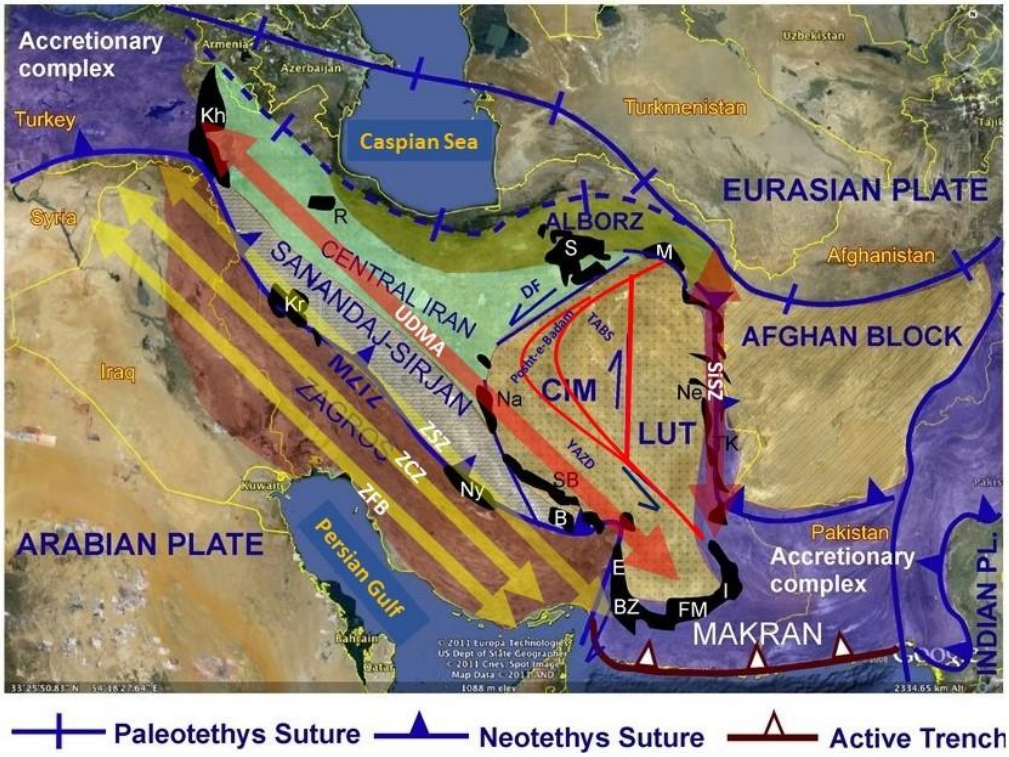

Figure 2. 2. Tectonic scheme of Iran and surrounding areas and location of the Mesozoic ophiolites (modified after Allahyari et al. 2014). MZTZ: Main Zagros Thrust Zone, LUT: Lout Block, CIM: Central Iranian Microcontinent, FD: Doruneh Fault, UDMA: Urumieh-Dokhtar Magmatic Arc, SiSZ: Sistan suture zone, ZSZ: Zagros suture zone, ZFB: The Zagros Fold Belt, ZCZ: Zagros Crush Zone or High Zagros, Ophiolites: M = Mashhad, S = Sabzevar, Kh = Khoy, R = Rasht, Kr = Kermanshah, Ne = Nehbandan, TK = Tchehel Kureh, Ny = Neyriz, I = Iranshahr, BZ = Band-e-Ziarat, E = Esfandagheh, B = Baft, Na = Nain, SB = Shahr-e-Babak

Various scenarios have been proposed for the tectonic evolution of the Arabian-Iranian segment of the Neo-Tethys. Permian to Triassic time has been suggested for the formation of the ocean (Stampfli, 2000). Oceanic spreading continued until the Late Cretaceous, with a NE-dipping intra-oceanic subduction zone present in the northern border of the Arabian plate from the Early to Late Cretaceous. This subduction persisted until the continental collision with the emplacement of the ophiolites in the Late Cretaceous. After the Late Cretaceous, calc-alkaline and alkaline magmatism peaked in the Eocene on the southern margin of the Sanandaj Sirjan Zone (Allahyari et al., 2010; Saccani et al., 2013).

The two parallel domains of the SSZ and UDMA are believed to be the result of the NE-dipping subduction of the Neo-Tethys in this area (Berberian & King, 1981). The consumption of the Neo-Tethys and the associated continental collision is recorded by the southern Iranian

ophiolites (**Fig 2.2, 2.3**)., which surface along the MZTZ (Alavi 1994; Berberian & King, 1981; Stöcklin 1974).

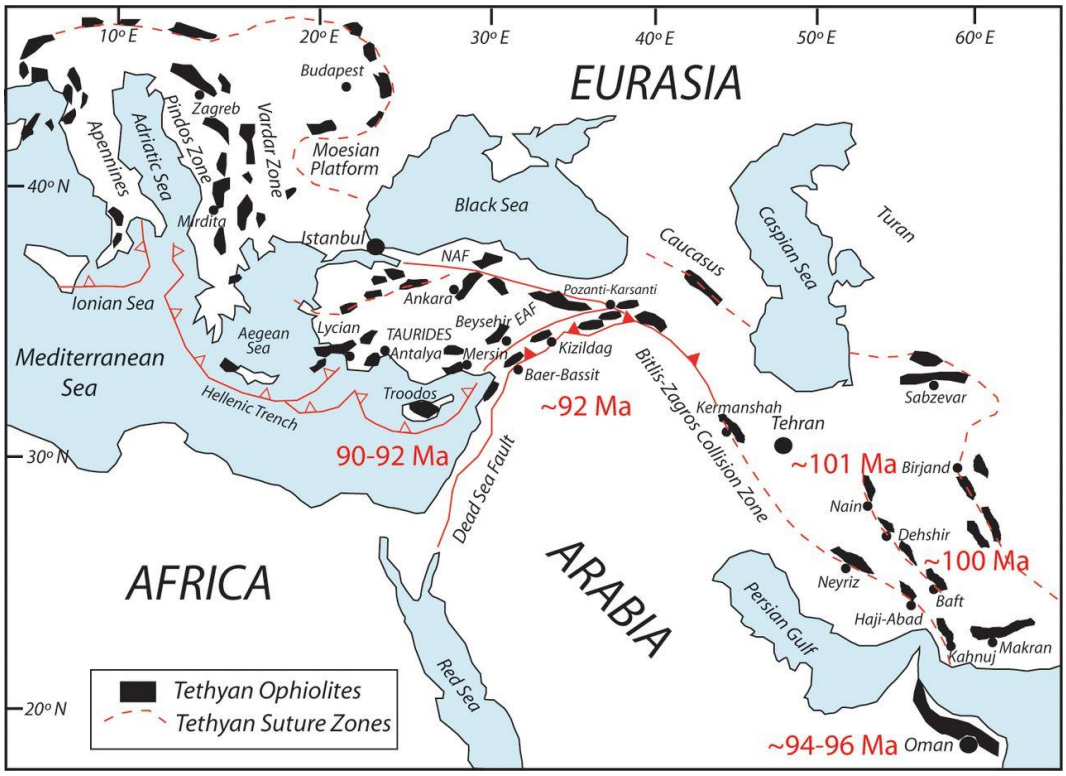

Figure 2. 3. Showing the distribution of Neo-Tethyan ophiolites and suture zones Simplified tectonic map of the eastern Mediterranean–Zagros region (modified after Dilek et al., 2007; Moghadam et al., 2013).

The mineralization at the Mesozoic southern part of the Neo-Tethys is related to shallow-level hydrothermal activity, which is linked to the intrusion-related porphyry copper system of the UDMA and is significantly dominated by substantial volcanic activity. The UDMA hosts abundant mineral deposits, especially copper-molybdenum porphyry—type mineralization and Cu-Zn volcanogenic massive sulfide (VMS) types. The formation of VMS deposits in this area is related to the evolution of an extensional continental margin in a back-arc environment that affected the Central Iranian Microcontinent (CIM). The evolution of this domain is controlled by the Neo-Tethys oceanic crust subduction under the CIM and by the resulting continental arc and back-arc (Maghfouri et al., 2016).

2.2.1 Urumieh-Dokhtar Magmatic Arc

The UDMA (**Fig.2.1, 2.2**) is part of the Alpine-Himalayan orogenic belt in Iran and comprises a subduction zone of voluminous volcanic successions with minor intrusive rocks along the active margin of the southern Iranian plate. This magmatic belt formed as the result of the subduction of the Neo-Tethys oceanic lithosphere beneath Eurasia during the Cenozoic (Alavi 1994;; Berberian & King, 1981). The magmatism resulted in the eruption of large volumes of calc-alkaline rocks, such as; lava flows, pyroclastic layers, tuffs, and ignimbrites (Stocklin, 1968; Berberian & King, 1981). The igneous rocks in the UDMA show geochemical features of tholeiitic, calc-alkalic, shoshonitic, and adakitic magmas (Omrani et al., 2008; Shahabpour, 2007; Shafiei et al., 2009; Mirnejad et al., 2019) and it has long been considered as an Andean-type magmatic arc generated by Neo-Tethyan subduction under the Iranian plate (Mehdi Alavi, 1980; Alavi, 1994; (Berberian & Berberian, 1981; Berberian et al., 1982; Chiu et al., 2017).

The collision between Eurasia and Arabia was one of the most significant continent-continent collision zones during the Tertiary. This event has also been associated with the rifting of the Red Sea, the slowing of Africa-Mediterranean extension (McQuarrie & Van Hinsbergen, 2013), and the development of Eastern and Northern Anatolian fault systems (Okay, Zattin, & Cavazza, 2010). Although the creation of Cenozoic igneous rocks in the UDMA is related to the subduction activity of the Neo-Tethys, the timing of the collision between Eurasia and Arabia is still uncertain, and it varies from Late Cretaceous (Alavi, 1994; Berberian & King, 1981), Eocene (Allen & Armstrong, 2008; Hempton, 1987; Mouthereau et al., 2014), Eocene–Oligocene (Hooper, Bailey, & McCarley Holder, 1995), Oligocene (Agard et al., 2011; Omrani et al., 2008; (Whitechurch et al., 2013; Yilmaz, 1993), Oligocene–Miocene (Berberian et al., 1982), Early to Middle Miocene (Allen, et al., 2011; Richards, 2014; Robertson, 2000), Middle Miocene (Dewey & Sengör, 1979), Middle to Late Miocene (Homke et al., 2004), Late Miocene (McQuarrie, Stock, Verdel, & Wernicke, 2003; Shahabpour, 2007; Stoneley, 1981), to Pliocene (Philip, Cisternas, Gvishiani, & Gorshkov, 1989; Mirnejad et al., 2019).

Meanwhile, the UDMA is believed to be dominated by an Eocene pulse or "flare" stage, although the subduction was active along the north margin of Neo-Tethys for most of the Mesozoic and Cenozoic eras (Berberian & King, 1981; Alavi, 1994; Omrani et al., 2008; Verdel et al., 2011). Several accurate age constraints have been reported and indicate that this magmatic flare-up

episode was longer-lasting, from the Eocene to Oligocene (Chiu et al., 2013). The main igneous and metamorphic rocks reported from the UDMA are summarized in the table (**App.1**).

2.2.2. Sanandaj-Sirjan Zone

The SSZ (**Fig 2.2)** is distributed between MZTZ and UDMA as a Phanerozoic metamorphic belt (Sheikholeslami et al., 2008). This area extends ~1500 km long and 150–250 km wide from Sanandaj (NW) to Sirjan (SE) of Iran. (Stoklin, 1968; Alavi, 1994; Mohajjel & Fergusson, 2000; M. Mohajjel, Fergusson, & Sahandi, 2003). This metamorphic zone, as part of the Tethys orogenic belt (Şengör, 1990), comprises strongly deformed and metamorphosed rocks associated with plutonic intrusions and Mesozoic volcanic rocks (Mohajjel et al., 2003; Azizi & Jahangiri, 2008).

During the Mesozoic, the SSZ represented an active continental margin by subduction of the Arabian plate beneath Eurasia. The resulting magmatism is characterized by calc-alkaline rocks produced during the early stages of the Neo-Tethys subduction. The subduction zone shifted briefly to the SW to the present-day Zagros Crush Zone (Agard et al., 2011; Hassanzadeh & Wernicke, 2016) and references therein), before migrating northward to the UDMA during the Eocene (Berberian & King, 1981; Sengör, 1990; Shakerardakani et al., 2020).

Zircon U-Pb ages of the Late Neoproterozoic-Cambrian (ca. 600–500 Ma) have been reported for granitoids and metamorphic rocks in different areas (Hassanzadeh et al., 2008; Azizi et al., 2011; Nutman et al., 2014; Shakerardakani et al., 2015). The coeval granitoids and metamorphic rocks from Alborz and Central Iran are among the oldest rocks in Iran, whose origins may be related to the northern margin of Gondwana (Hassanzadeh et al., 2008). In addition to the main Middle-Late Jurassic granitoids exposed across the entire zone (Mahmoudi et al., 2011; Chiu et al., 2013), magmatic rocks of the Eocene age have also been recognized in the Kamyaran and Boroujerd regions in the NW of the SSZ (Azizi, et al., 2011; Mahmoudi et al., 2011; Chiu et al., 2017). The main igneous and metamorphic rocks reported from the SSZ are summarized in the table (**App.2**).

2.2.3. Zagros zone

Zagros zone extends for nearly 2000 km from southeastern Turkey through northern Syria and northeastern Iraq to western and southern Iran (Alavi et al. 1997). From southwest to northeast, this zone is divided into three subzones (**Fig. 2.2**):

1. The Zagros Fold Belt (ZFB), which consists of folded deposits from Permo–Triassic to Late Cretaceous/Paleocene age. These sediments in ZFB are similar to their equivalent rocks in Arabia, which have a northeast-southwest trend. They are followed by a more complex pattern of sedimentation to the recent Pliocene. (Berberian & King1981; Agard et al., 2005).

2. High Zagros or Zagros Crush Zone (ZCZ) consists of the imbricated tectonic slices radiolarites, limestones, Mesozoic obducted ophiolite remnants, flysch, and Eocene volcanic rocks. All of the ZCZ Mesozoic deposits are thrusted onto the ZFB (Agard et al., 2005).

3. The Zagros fault or Main Zagros Thrust Zone (MZTZ), which separates the Zagros domain from Sanandaj Sirgan Zone (Agard et al., 2005).

2.2.4. Zagros suture zone

The Zagros Suture Zone (ZSZ) consists of several rock associations, which record the geodynamic evolution of Neo-Tethys. This realm reflects different affinities and continental growth of Neo-Tethys and represents significant collisional tectonic boundaries between the Arabian shield (Gondwana) and the Sanandaj–Sirjan continental block of Iran (e.g., Berberian & King, 1981; Sengor et al., 1988; Robertson, 2007; Allahyari et al., 2010; Saccani et al., 2013).

Continental collision along the Zagros suture zone resulted from the long-lasting convergence of the Arabian plate toward Eurasia (**Fig.2.1, 2.2**) and has provided the main force uplifting the Iranian plateau and raising the Zagros Mountains. The Late Cretaceous ophiolites, cropping out along the MZTZ, represent remnants of the southern Neo-Tethyan oceanic lithosphere (**Fig.2.1**)(e.g., Allahyari et al., 2014; Aswad et al., 2011; Saccani et al., 2013; Saccani et al., 2014 and references within). The well-preserved Neo-Tethyan Zagros ophiolites are of supra-subduction zone type and display a consistent sequence of events during their formation and emplacement (Moghadam et al., 2013). The collision along the Zagros suture zone was started at ~35 Ma and persisted to the final stage at ~12 Ma (e.g., Mouthereau et al. 2012; Madanipour et al. 2013; Motaghi et al. 2017 and references within). This main fault takes up ~10 mm yr−1 of oblique convergence in Zagros (Vernant et al., 2004; Motaghi et al., 2017).

2.2.5. Central Iran

Central Iran (**Fig 2.2)** is bounded by different structural domains and blocks, the Zagros Mountains in the south and west, Alborz Mountains in the north, and SiSZ in the east. However,

the defining geological boundaries of Central Iran remains largely a controversial issue. Stocklin (1968) believed that central Iran was bounded to SSZ in the south-southwest, Lut block in the east, and Alborz Mountains in the north. According to Stocklin (1968), most of Azerbaijan also belongs to Central Iran. Meanwhile, Nabavi (1976) considers the northern part of the Lut Block as a part of Central Iran, and Aghanabati (2004) based on the tectono-sedimentary features, believed that Central Iranian Micro-continent (CIM) and SSZ are parts of the Central Iran domain. However, there is not a consensus regarding the boundaries of Central Iran). The main igneous and metamorphic rocks reported from Central Iran are summarized in the table (**App.3**).

2.2.6. Central Iranian Micro-continent

The Central Iranian Micro-continent (Takin, 1972) in the heart of Central Iran (**Fig 2.2)**, consists of four micro-continental structural units: Yazd, Posht-e-Badam, Tabas, and Lut Blocks (Ghasemi & Talbot, 2006; Verdel et al., 2007; Bagheri & Stampfli, 2008) divided by generally N-S, right-lateral, strike-slip faults, concaved to the E (Aghanabati, 2004; Mehdipour Ghazi et al., 2019). This terrane is constructed in the upper-plate domain of the Neo-Tethyan subduction zone and the present intra-plate domain of the Arabia–Eurasia collision boundary (Alavi, 1991; Bagheri & Stampfli, 2008; Berberian & King, 1981; Stocklin, 1968; Takin, 1972; Tadayon et al., 2019). Furthermore, the area consists of igneous and metamorphic unites, which are dominantly overlain by the major Jurassic-Cretaceous and minor Paleogene sedimentary sequences (Agard et al., 2011).

During the Mesozoic–Cenozoic time, the geodynamic evolution of CIM dominated by multiple opening and closure events of the oceanic back-arc domains of the Neo-Tethys. (Rossetti et al., 2014; Şengör et al., 1988;Moghadam et al., 2009; Moghadam et al., 2014; Stampfli &Borel, 2002; Stöcklin, 1974). These are preserved in the ophiolitic suture zone that surrounds the CIM (**Fig.2.1**).

In Central Iran, a phase of the extensive extensional regime in the Late Precambrian to Early Cambrian is represented by various rift-related deposits (Rajabi et al., 2015a, 2012, 2015b; Ghorbani, 2013; Daliran et al., 2013; Hajsadeghi et al., 2018). Furthermore, high-grade Precambrian metamorphic rocks associated with Gondwana are well documented in this area (Ramezani & Tucker, 2003; Verdel et al., 2007; Bagheri and Stampfli, 2008; (Hassanzadeh et al., 2008; Rahmati-Ilkhchi et al., 2011; Balaghi Einalou et al., 2014; Moghadam & Stern, 2015, 2016;

Rossetti et al., 2015; Chiu et al., 2017). The main igneous and metamorphic rocks reported from the Lut, CIM, and Sistan Suture Zone are summarized in the table (**App.4**).

2.2.6.1. Lut Block

The Lut block (**Fig 2.2),** located in the eastern part of the CIM, extends from the Doruneh Fault in the north to the Jaz-Mourian basin in the south (Berberian & King, 1981; Karimpour & Stern, 2009) and is one of several microcontinental blocks that drifted from the northern margin of Gondwana during the opening phase of the Neo-Tethys in the Permian (Golonka, 2004; Keykhay-Hosseinpoor et al., 2020). The voluminous Late Cretaceous to Neogene/Quaternary volcanic rocks in the Lut block can afford a significant key for understanding the geodynamic evolution of the continental crust and underlying mantle of Neo-Tethys in this area (Saadat & Stern, 2016).

The Supra-Subduction Zone is highlighted by ophiolites between the eastern part of the Lut Block and the Afghan Block to the east (Saccani et al., 2010). Subduction along this zone is associated with emplacement of large porphyry intrusions during the Early Cenozoic, which hosts significant porphyry copper and associated epithermal gold deposits (Malekzadeh Shafaroudi, Karimpour, & Stern, 2015).

The presence of Cretaceous ophiolites in the Lut block represents the consumption of the Sistan arm of Neo-Tethys underneath the Afghan block during the east-dipping subduction and the subsequent collision between the Lut and Afghan continental blocks (Moghadam & Stern, 2015; Saccani et al., 2010; Mehrabi, Tale Fazel, & Yardley, 2019). Meanwhile, the mineralization in this block during the Jurassic to Tertiary phases of magmatism consists of various porphyry Cu and Cu-Au deposits, epithermal Au deposits, Cu-Pb-Zn vein-type deposits, and Cu-Pb-Zn vein-type deposits (Arjmandzadeh et al., 2011; Keykhay-Hosseinpoor et al., 2020).

2.2.7. Afghan Block (Farah)

Afghan block (**Fig 2.2)** consists of the collage of crustal blocks assembled in present-day Afghanistan during the Cimmerian orogeny and located west and north of the Chaman and Konar faults. This block shows a variation of magmatic and tectonic effects that result from the subduction of Tethyan oceanic material beneath the Afghan margin before the Himalayan collision (Treloar & Izatt, 1993). Moreover, the northerly orientation of the Eastern Iranian ranges is mainly composed of Cenozoic rocks. This belt is developed between the Gondwana-derived Afghan block

in the east and the Lut block in the west (Stöcklin, 1968). Furthermore, the eastern Iranian flysch zone (Eftekharnezhad, 1980), accumulating on a remnant oceanic seafloor (Sistan Ocean) between colliding continental margins of Lut and Afghan blocks during the late Paleogene (Tirrul et al., 1983).

The subduction of the Sistan Ocean underneath the Afghan block has been interpreted by several authors, although the polarity of the subduction remains equivocal and controversial. An eastward subduction, proposed by several authors (e.g., Tirrul et al., 1983; Fotoohi Rad et al., 2005; Saccani et al., 2010; Angiboust et al., 2013)is based on the southeast vergence of the thrusts and associated folds, as well as the occurrence of high-pressure metamorphic rocks and the vicinity of Afghan Block to Sefidab forearc basin. The lack of a specific passive margin and presence of magmatic arc as well as associated low P/T metamorphic terrane on the Afghan block along the Sistan suture zone remain problematic (Bagheri & Gol, 2020).

Conversely, a westward subduction of the Sistan Ocean underneath the Lut block is proposed by others based on the development of a Tertiary magmatic arc along the Lut block as well as the existence of ophiolitic sequences along the western margin of the Sistan suture zone (e.g., Eftekharnezhad, 1980; Karimpour et al., 2011; Pang et al., 2013). However, no high-pressure metamorphic rocks, which would be additional supportive evidence have been reported in this area (Bagheri & Gol, 2020).

2.2.8. Sistan Suture Zone

The north-trending Sistan suture zone (SiSZ) that separates the Lut and Afghan continental blocks (**Fig 2.2**) also preserves Cenozoic igneous and metamorphic rocks associated with the subduction of Neo-Tethys in eastern Iran (e.g., Camp & Griffis, 1982; Tirrul et al.,1983; Agard et al., 2009; Guillot et al., 2009; Bröcker et al., 2013). This terrane preserves extensive subduction-related Cretaceous ophiolitic mélanges as well as upper Cretaceous-Eocene flysch deposits (Maastrichtian to Eocene) interpreted to represent a forearc setting (Babazadeh & de Wever, 2004; Fotoohi Rad, Droop, & Burgess, 2009).

In the evolution of the Sistan oceanic basin, the ophiolites are considered relicts of the oceanic lithosphere during the Eocene continental collision between the CIM and the Afghan Block, which was mostly consumed in a subduction zone and, in part, obducted onto the Lut

margin (Tirrul et al., 1983; Dercourt et al., 1986; Sengor et al., 1988; Saccani et al., 2010; Pang et al., 2012).

Calc-alkaline volcanism (volcanic arcs) in SiSZ during Eocene-Oligocene, and consequently during the closure of the Neo-Tethys in Late Cretaceous, has been attributed to the delamination of a thickened lithospheric root (Pang et al., 2012). Meanwhile, magmatism mainly originated from mantle sources and is possibly related to the partial melting of sediments and the fluids released from the subducting plate into the overlying mantle (Pang et al., 2013; Tarabi et al., 2019).

Development of the island arc in the SiSZ in southeast Iran during the Late Cretaceous has been linked to a wide range of interpretations including the E-dipping subduction of an oceanic plate under the Afghan block (Camp & Griffis, 1982; Tirrul et al. 1983), W-dipping subduction under the Lut block (Berberian 1982; Zarrinkoub et al., 2012), two-sided subduction (Arjmandzadeh et al., 2011b), E-dipping intra-oceanic subduction (Saccani et al., 2010) and N-dipping to E-dipping subduction (Verdel et al., 2011; et al., 2019b). The depleted mantle peridotites in SiSZ show a MORB signature; however, some samples in the southern part of the area are considered to be the source of boninitic melts in the Supra-Subduction Zone and may indicate the existence of intra-oceanic subduction from the Turonian to the Maastrichtian (Saccani et al., 2010; Bonnet et al., 2018).

CHAPTER 3: METHODOLOGY

3.1. Data collection

Lithogeochemical, geochronological, and isotopic data were compiled from the 175 published articles and were stored in the DateView (http://sil.usask.ca/Databases.htm). The new database includes 420 U-Pb, and 1147 lithogeochemical samples, 1552 Lu-Hf, and 353 Sm-Nd isotopic composition results. The list of references and the information of all these samples are available in **APPENDIX** (**B-D**) and DateView (**Fig. 3.1., 3.2., 3.3**.).

After extracting the data from available literature and existing databases, some additional information was added to them. The data often excluded sample information that was not accurately related to the U-Pb ratios extracted from zircon analysis. All the dataset was converted into a consistent format and file type for data preprocessing.

For example, supplementary details such as record ID, analytical technique, age of the unit from which the sample was taken, lithology, geographical coordination, isotope ratios, associated one or two sigma uncertainties for ratios and ages were added to the dataset. Furthermore, the final dataset for the available, $^{147}Sm/^{144}Nd$, $^{143}Nd/^{144}Nd$, $^{176}Lu/^{177}Hf$, $^{176}Hf/^{177}Hf$ isotope ratios contains calculated $\varepsilon_{Nd}(T)$ and $\varepsilon_{Hf}(T)$ values and calculated Nd and Hf two-stage depleted mantle model (T_{2DM}).

However, by merging the geochemistry data with relevant geographical coordination and using Microsoft Access, the results were appended to the original dataset. The data then was imported into ArcGIS and transposed onto the plate-tectonic reconstruction. It should be noted that displaying the data in GPlates, with an appropriate symbology appears to show quite clearly the geodynamic settings on western Neo-Tethys through time.

3.1.1 Geochronological data

After data compilation, in order to define, manipulate, retrieve and manage data for any interpretation, all raw data and their original references compiled from published records were stored in the DateView and StratDB online database. It should be noted that the references to all the sources of data used in diagrams and graphs presented in this thesis are therefore not provided, only those relating to topics where appropriate.

By combining geochronological data, isotope ratios, and geographical coordinates of the samples in a unique organized structure like DateView, it would be convenient for any interpretation and analysis in order to reconstruct paleo-plates boundaries by GPlates and Arc Map. The integrated data, as well as the digital geological maps, was then transferred to Geographic Information Systems (GIS) and integrated with the other datasets and with GPlates for visual analysis. The purpose of the visual analysis beyond pattern recognition or the identification of peculiarities in the datasets is to discover the meaning of what can be identified and to be able to infer some sort of geological context for these observations.

Most of the geochronology data collected in this thesis are U-Pb zircon. These data indicate the age of rock formation for igneous rocks, the age of multiple protoliths for sedimentary rocks, and the age of major individual metamorphic events for metamorphic rocks in the western Neo-Tethys.

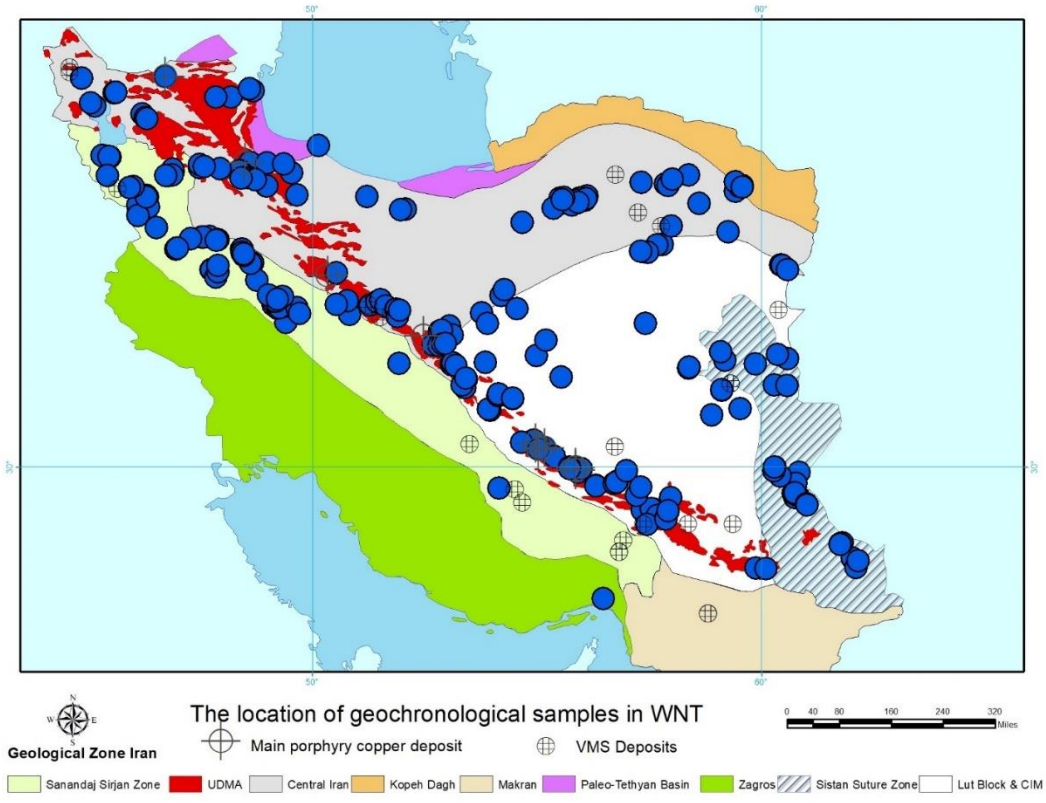

Figure 3. 1. The geological zones of Iran and the location of geochronological samples on WNT. Tectonic and structural maps of Iran, modified after (Aghanabati, 1998; and Alavi, 1996).

3.1.2 Geochemistry data

The compiled literature regarding the WNT includes rock chemistry composition data, which can be useful to either understand what type of tectonic setting the rock formed in (Pearce, Harris, & Tindle, 1984; Pearce, 2014, 2008) or to assess geological processes associated to the development of the samples (e.g. fractionation, partial melting, mineral species, etc.).

In this study, lithochemical data were compiled for 1147 igneous and metamorphic rocks. The location of the samples is shown in (**Fig. 3.2**.) Due to the lack of geographical coordination for some samples, we consider only one point on the map for all samples to be related to the location that has not any coordination. Some lithochemical elements often referred to as mobile elements, are influenced by weathering and alteration. All sample data were, therefore, classified into rock types using immobile element plots (Pearce, 2014).

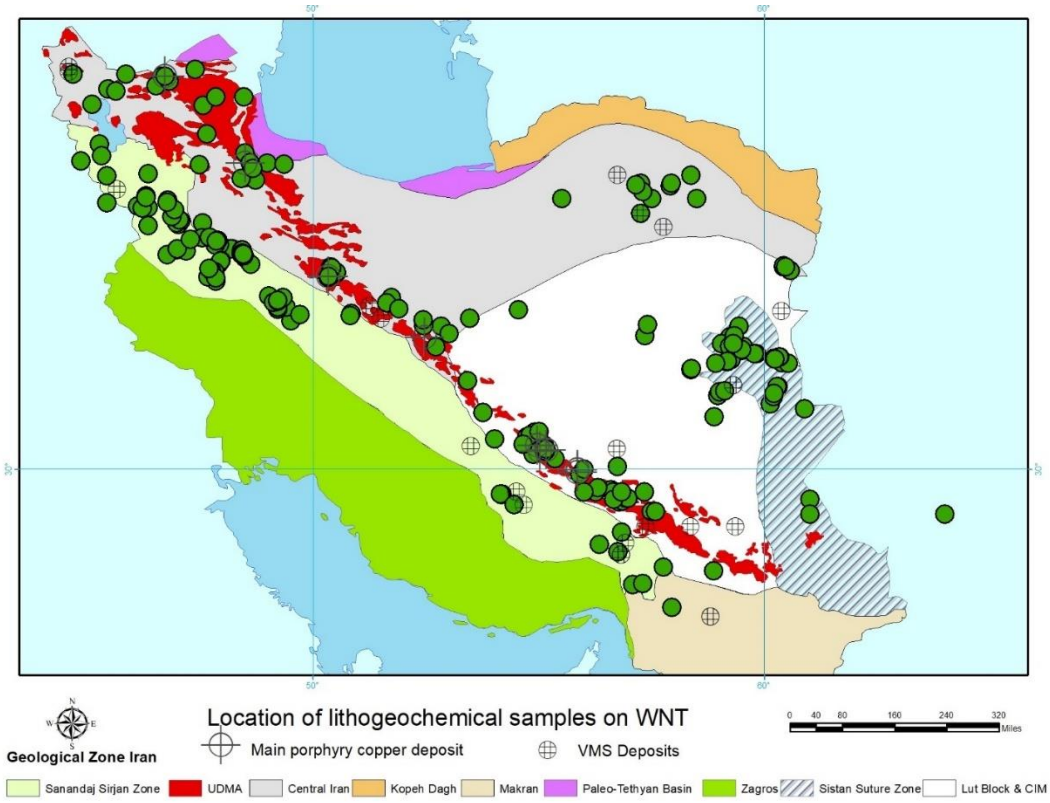

Figure 3. 2. Tectonic scheme of Iran and surrounding areas and lithogeochemical location on western Neo-Tethys (Allahyari et al., 2018). Tectonic and structural maps of Iran, modified after (Aghanabati, 1998; and Alavi, 1996).

3.1.3 Isotope geochemistry data

In order to clarify the juvenile environments from mature tectono-magmatic settings as well as shed light on the oceanic or crustal source of magma, we used Isotope Systems such as U-Pb, Sm-Nd, Rb-Sr. These isotope data were compiled from published references.

The Sm-Nd and Lu-Hf system is used as a tracer to provide information on the nature of the source rocks. The calculation of T_{2DM}, ε_{Nd}, and ε_{Hf} in DateView provides the age of the lithosphere in different parts of the Neo-Tethyan basin. The location of Sm-Nd and Lu-Hf isotopic data for the WNT are shown in the map (**Fig. 3.3.**).

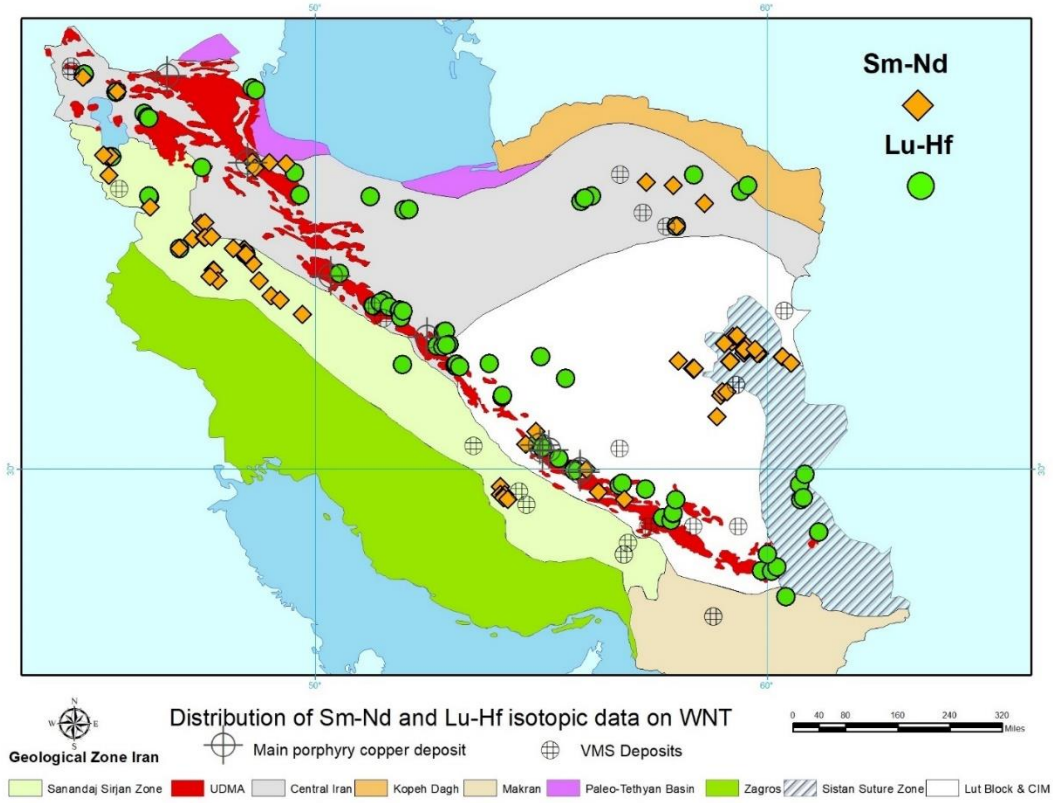

Figure 3. 3. Distribution of Sm-Nd and Lu-Hf isotopic data for the western Neo-Tethys.

3.2. Radiogenic isotope principles and calculations

There is a lot of review literature on isotope systems (e.g., DePaolo, 1988; Champion & Huston, 2016); therefore, only a general introduction is provided here on radiogenic isotope principles and calculations. Radiogenic isotopes are a result of the decay of a radioactive parent isotope (at a constant decay rate, λ) to a more stable daughter product. The volume of daughter

isotope generated by radioactive decay from the parent isotope is a function of the half-life of the parent isotope, and the time, in years, the parent has been decaying:

$(\text{Daughter}) = (\text{Parent Isotope}) * (e^{\lambda t-1})$

In the formula: t = the time in question, and λ = the decay constant. The number of daughter isotope existing in rocks is the sum of the initial daughter isotope concentration, plus the amount of the daughter isotope generated over time from the decay of the parent isotope:

$(\text{Daughter isotope})_{\text{now}} = (\text{Daughter})_{\text{initial}} + (\text{parent isotope})_{\text{now}} * (e^{\lambda t-1})$

In the formula: λ = the decay constant, (now) = abundance of the isotope as measured in the present day, (initial) = abundance of the isotope at time t in the past and, t = the age of the rock, (in years, in this study is crystallization age).

In the Lu-Hf isotope system, ^{176}Lu decays to ^{176}Hf by beta decay with a half-life of 37.12 Ga and decay constant of (1.867±0.008) *10-11 (Vervoort et al., 2014). The decay constant for ^{147}Sm is $6.54*10^{-12,}$ and the half-life is 106 Ma (Champion & Huston, 2016).

Lab results for parents and daughters are commonly reported relative to a stable isotope. For Sm-Nd, the stable isotope is ^{144}Nd, and for Lu-Hf is ^{177}Hf. The initial ratio for $^{176}Hf/^{177}Hf$ samples was calculated with the following formula (Vervoort, 2014):

$$(^{176}Hf/^{177}Hf)_{(i)} = (^{176}Hf/^{177}Hf)_{(P)} - (^{176}Lu/^{177}Hf)_{(P)} * (e^{\lambda t-1})$$

$^{176}Hf/^{177}Hf$ values are generally reported as epsilon (ε) units (Iizuka, Yamaguchi, Itano, Hibiya, & Suzuki, 2017)and references within), which are deviations in part per ten thousand from a chondritic earth reference model (CHUR=Chondritic Uniform Reservoir), as follows:

$$\varepsilon_{Hf} = 10000* [(^{176}Hf/^{177}Hf)_{Sample(T)} - (^{176}Hf/^{177}Hf)_{CHUR(T)}] / (^{176}Hf/^{177}Hf)_{CHUR(T)}$$

The depleted mantle model ages (T_{DM}), two-stage model ages (T_{2DM}), and the CHUR model ages (T_{CHUR}) were also calculated for Hf and Nd isotopes of the igneous rocks in western Neo-Tethys. In the T_{2DM} model age, an estimated (not the measured) isotopic ratio of $^{147}Sm/^{144}Nd$ ratio or $^{176}Lu/^{177}Hf$ is used for calculating the sample evolution curve prior to the crystallization age.

In this thesis present-day CHUR values for Lu-Hf and Sm-Nd isotope calculations are from Bouvier, Vervoort, & Patchett (2008): $(^{176}Lu/^{177}Hf)_{(0)\ CHUR} = 0.0336$ and $(^{176}Hf/^{177}Hf)_{(0)\ CHUR} = 0.282785$, and $(^{147}Sm/^{144}Nd)_{(0)\ CHUR} = 0.1967$ and $(^{143}Nd/^{144}Nd)_{(0)\ CHUR} = 0.51264$.

The present-day DM values for Lu-Hf isotope calculations are from Griffin (Griffin et al., 2000): $(^{176}Lu/^{177}Hf)_{(0)\ DM} = 0.0384$ and $(^{176}Hf/^{177}Hf)_{(0)\ DM} = 0.28325$. The present-day DM values for Sm-Nd isotope calculations are from DePaolo (1981): $^{147}Sm/^{144}Nd_{(0)\ DM} = 0.2136$ and $^{143}Nd/^{144}Nd_{(0)\ DM} = 0.513074$.

In the calculation of T_{2DM}, the present-day average crustal value was suggested for $^{176}Lu/^{177}Hf$: 0.015 (Marchesi et al., 2011; Griffin et al., 2002) and for $^{147}Sm/^{144}Nd$: 0.11 (Champion & Huston, 2016).

The calculation formulae of T_{DM} and T_{2DM} are as follow (Griffin et al., 2002):

$$T_{DM}=(1/\lambda) \times \ln \left(\left(\left(^{176}Hf/^{177}Hf\right)_{(0)\ Sample} - \left(^{176}Hf/^{177}Hf\right)_{(0)\ DM}\right) / \left(\left(^{176}Lu/^{177}Hf\right)_{(0)\ Sample} - \left(^{176}Lu/^{177}Hf\right)_{(0)\ DM}\right) +1\right)$$

$$T_{2DM}= (1/\lambda) \times \ln \left(\left(176Hf/177Hf\right)_{(0)\ CRUST} - \left(^{176}Hf/^{177}Hf\right)_{(0)\ DM}\right) / \left(\left(^{176}Lu/^{177}Hf\right)_{(0)\ CRUST} - \left(^{176}Lu/^{177}Hf\right)_{(0)\ DM}\right) +1\right)$$

$$\left(^{176}Hf/^{177}Hf\right)_{(0)\ CRUST} = \left(^{176}Hf/^{177}Hf\right)_{initial\ sample} + \left(^{176}Lu/^{177}Hf\right)_{(0)}\ CRUST \times \left(e^{\lambda t-1}\right)$$

T_{DM} and T_{2DM} values for Sm-Nd data were calculated using similar formulae to those shown for Lu-Hf earlier.

3.3. Software

3.3.1. GIS

The extracted data were plotted using GIS software. ArcGIS (ArcMap) is also used to create maps (https://www.arcgis.com/home/index.html). Therefore, in order to connect data from Access with ArcMap, the first step required is to create a Personal Geodatabase in Arc Catalog, then open it with Microsoft Access. The second step requires merging raw data in a single table in Microsoft Access, creating the feature class from this merged file, and saving it in our geodatabase in Arc Catalog. Raw datasets are presented as tables of numbers, which may be unintelligible until they are plotted to display their spatial links within GIS software (Bonham-Carter, 1994). This

merged file includes data and sample coordinates. The final step required is a spatial join, whereby attributes from one layer (coordination of geochronological data) are combined to another layer (Plate ID), based on the spatial relationship. The spatial join of the two layers will attach plate identification information, allowing these points to be plotted on the plate-tectonic reconstruction model within GPlates.

3.3.2. GPlates

In order to visualize and manipulate the associated data through geological time, it is essential to work with software such as GPlates (https://www.GPlates.org/). This tool is a segment of the new plate reconstruction software that incorporates functionality familiar from GIS with the added dimension of geological time (Williams et al., 2012). Moreover, GPlates is an open-source and powerful software package for visualizing and reconstructing plate tectonic boundaries and associated data through geological time by using geological and geochronological data sets. We used the visualization capability of GPlates 2.1 to track the evolution of western Neo-Tethys subduction zones from the global geodynamic models.

3.3.3. Microsoft Access

Microsoft Access is used in this research to construct the geochemistry database. It is designed for single users and is suitable for constructing geochemical sample data sets compiled from the scientific literature.

3.3.4. ioGAS

The geochemical analysis in this thesis was conducted in ioGAS since the software has excellent graphical options and allows for rapid visualization. Using ioGAS as a primary tool greatly streamlined data workflows, as well as simplifying data interpretation and analysis.

3.3.5. Other Software

Other software used in this thesis includes Microsoft Excel as part of Microsoft Office, which is a spreadsheet that provides a way to store raw data extracted from literature. It is also used for calculations, drawing graphs, and tables. DVRawData was used (Eglington, 2018a) for compiling original spreadsheet data into a temporary database before uploading it to the DateView database. GEODATE (Eglington, 2018b) was used for calculation model ages (T_{2DM}), initial isotope ratios, and epsilon values (ε_{Nd} and ε_{Hf}).

CHAPTER 4: RESULTS

4.1. Lithochemistry

4.1.1 Rock classification

Lithochemical data can be useful for recognizing the tectonic setting in which the rock formed (Pearce, Harris, & Tindle, 1984; Pearce, 2014, 2008) or for assessing geological processes (e.g., fractionation, partial melting, mineral species) that are related to the history of the rock. Nevertheless, it is necessary to distinguish between altered and non-altered samples before any evaluation of tectonic settings using published tectonic discrimination diagrams.

Some immobile elements (such as Zr, Ti, Nb, and Y) can better identify primary rock compositions even when mobile elements, such as Na2O, K2O, and SiO2, have been affected (Pearce, 2014). All samples are plotted on Zr/Ti vs. Nb/Y diagram (**Fig.4.1**.) in order to classify the rock samples (Pearce, 2014). Selected non-altered lithologies are plotted on $Na_2O + K_2O$vs. SiO_2 diagram (**Fig. 4.2**), also referred to as a TAS classification discrimination diagram (Le Maitre, 1989). Samples plot on the TAS diagram (**Fig.4.2**) indicates a highly variable range of compositions are represented, from ultramafic to felsic compositions in the western Neo-Tethys. Samples that have suspected of being significantly altered were excluded from this study to ensure that the interpretations are based solely on the less altered samples.

In this study, all the igneous rock samples were separated as either felsic or mafic rocks, regardless of whether they were intrusive or extrusive. In this regard, for the use of tectonic discrimination diagrams, only those samples in (**Fig.4.2**.) were considered, which were classified as felsic or mafic rocks. For example, the samples that plot in the andesitic, rhyolitic, and dacitic areas have been accepted for tectonic discrimination as felsic rocks, whereas those samples plotted in the basaltic field were considered to be mafic.

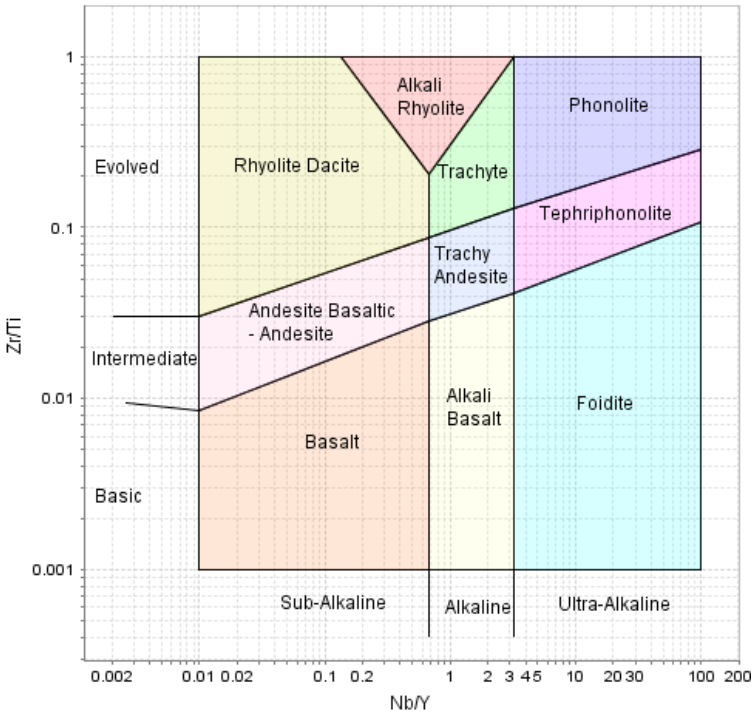

Figure 4. 1. Immobile element classification diagram used to classify the rocks in this study (Modified after Pearce, 1996). Lithology terminology used is for volcanic rocks but should also be taken to include plutonic equivalents.

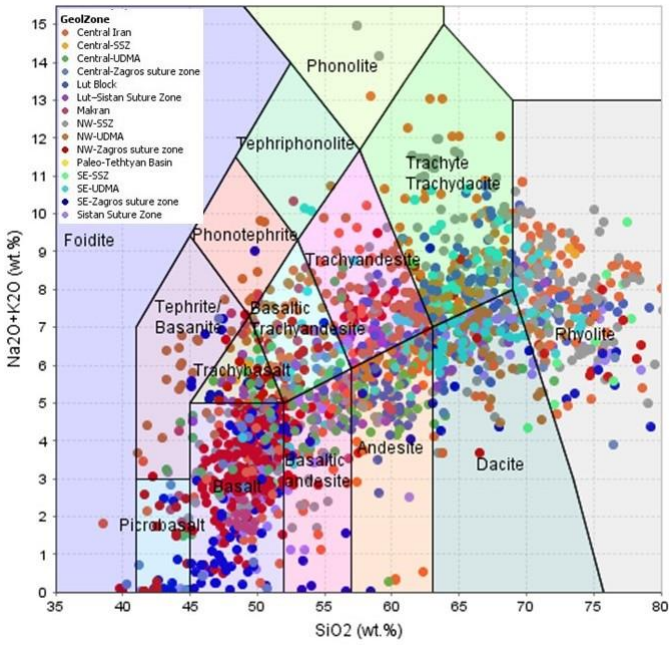

Figure 4. 2. Lithological classification of all the igneous samples in this study (TAS Classification Diagram) for the different geological zone of Iran (Le Maitre, 1989). Lithology terminology used is for volcanic rocks but should also be taken to include plutonic equivalents.

4.1.2 The felsic rock tectonic setting

The trace element discrimination diagrams have sometimes been used to discriminate the tectonic setting in which volcanic rocks have occurred (e.g., Pearce & Cann, 1973; Floyd & Winchester, 1975; Winchester & Floyd, 1977; Shervais, 1982; Pearce, Harris, & Tindle, 1984). Using the classification diagram of immobile element ratios Y+Nb vs. Rb in this study to recognize the tectonic settings of felsic rocks in WNT shows the rocks may be subdivided into four main groups; ocean ridge granites (ORG), volcanic arc granites (VAG), within plate granites (WPG) and collision granites (COLG) (Pearce, Harris, & Tindle, 1984). However, the areas on this kind of discriminant diagrams accurately show the source, crystallization, and melting history of regions, but they do not display tectonic regimes very well (Pearce, Harris, & Tindle, 1984). Thus, using the discrimination diagram is not optimal for categories; all classifications and interpretations must consider all aspects of geological events in the areas (Pearce, Harris, & Tindle, 1984).

The felsic rocks in WNT were classified according to the total alkali-silica (TAS) diagram (Le Maitre, 1989). The barren and ore-related porphyries are divisible into trachyte, trachydacite, trachyandesite, andesite, dacite, and rhyolite with SiO_2 contents ranging from 55 to 80 wt.% (**Fig.4.3. A**). The location of felsic rocks, major porphyries, and VMS deposits, with their geochronological age in WNT, are shown in (**Fig.4.7**).

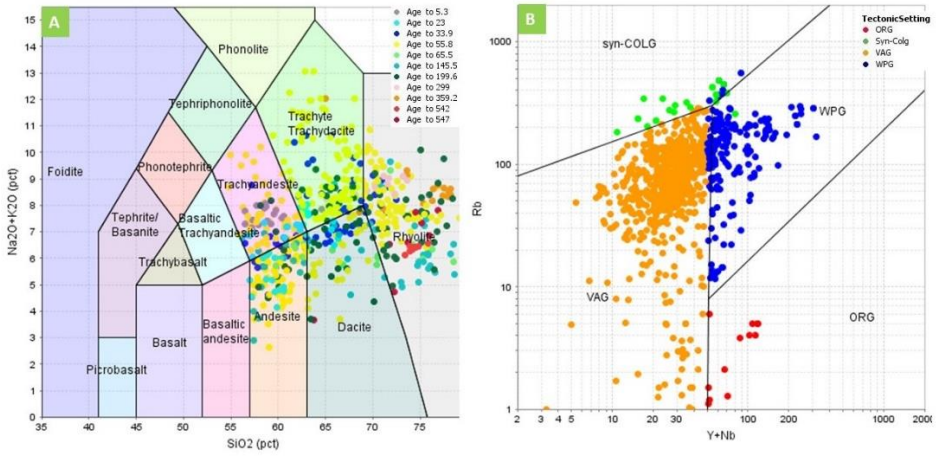

Figure 4. 3. (**A**) Total alkali-silica diagram (Le Maitre, 1989) of felsic rocks from the western Neo-Tethys. (**B**) discriminant diagrams for syn-collision (syn-COL), volcanic arc (VA), within-plate (WP), and normal ocean ridge (OR) granites (Pearce, Harris, & Tindle, 1984).

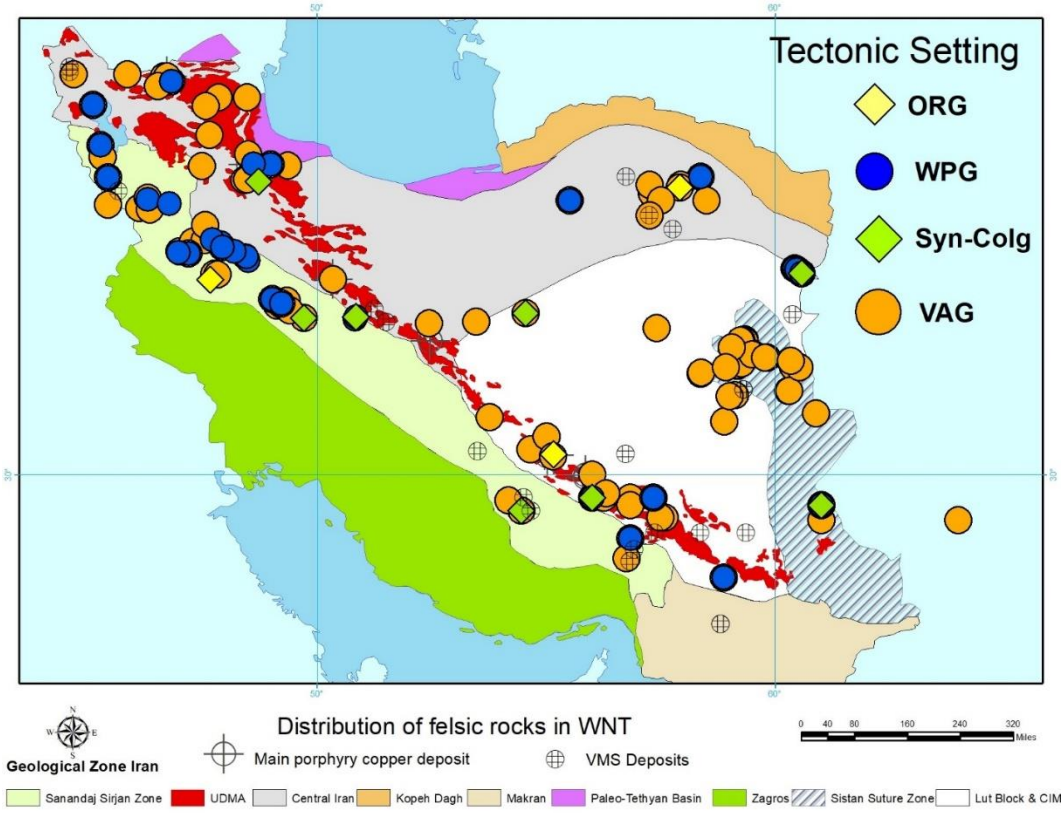

Figure 4. 4. Location of WNT felsic rock samples with their tectonic setting in this study.

4.1.3 The mafic rock tectonic setting

To identify fingerprinting magma type and tectonic setting of mafic rocks, samples were plotted using Th/Yb vs. Nb/Yb (**Fig. 4.5.A**) and TiO_2/Yb vs. Nb/Yb (**Fig. 4.5.B**). Mafic rocks were classified in order to identify between the arc and mid-ocean ridge settings and emphasize the distinction between oceanic (more juvenile) and continental arcs in the study area. In both diagrams, Nb/Yb as a proxy of the alkalinity of the magma and can indicate settings associated with mantle plumes, whereas Th/Nb and TiO_2/Yb can indicate settings associated with subduction zones (Pearce, 2014).

In **Fig.4.5. A** Th/Nb has been recognized as a proxy for subduction or crustal input since it retains an approximately constant ratio during mantle melting. In contrast, they can be decoupled during the subduction stage in most arc environments (Pearce, 2014) since Nb is subduction-immobile and Th is a subduction-mobile element. A few samples in **Fig. 4.5.A** plot outside the fields of continental and oceanic arcs. Therefore, samples above the mantle array with Nb/Yb <1 are considered as oceanic arcs whereas values of Nb/Yb >3 are classified as being from continental

arcs. However, samples with Nb/Yb values between 1 and 3 are considered as changes in the Nb/Yb ratios during the development of arc maturity over time. The MORB settings in the mantle array are separated in this diagram by Nb/Yb values as well. They are classified as N-MORB (Nb/Yb<1), E-MORB (1<Nb/Yb<10), and OIB (Nb/Yb>10).

In Graph (**Fig.4.5. B**), Ti/Yb has been considered as a proxy for plume melting. Through shallow melting (partial melting of spinel peridotites), Ti and Yb are partitioned similarly into the melt. Whereas they are separate for deep melting (partial melting of garnet peridotites) where solely Yb is partitioned significantly into garnet. Therefore, Ti/Yb ratio is high just in the products of deep melting where garnet is stable.

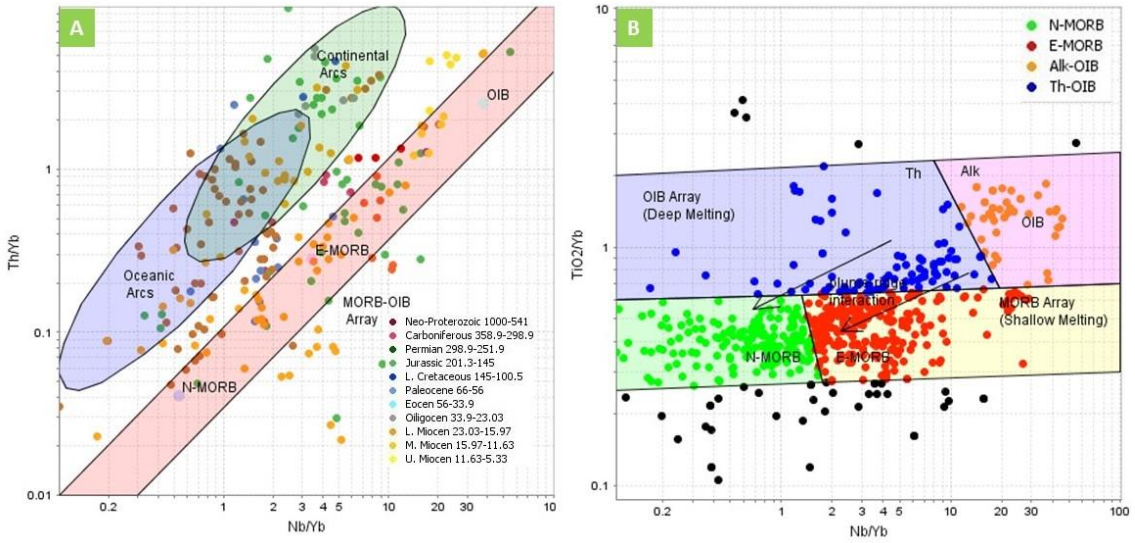

Figure 4. 5. The tectonic settings discrimination diagrams for basaltic rocks (**A**) The Th/Nb as a subduction proxy (Pearce, 2014). (**B**) The Ti/Yb as a plume-melting proxy (Pearce, 2008).

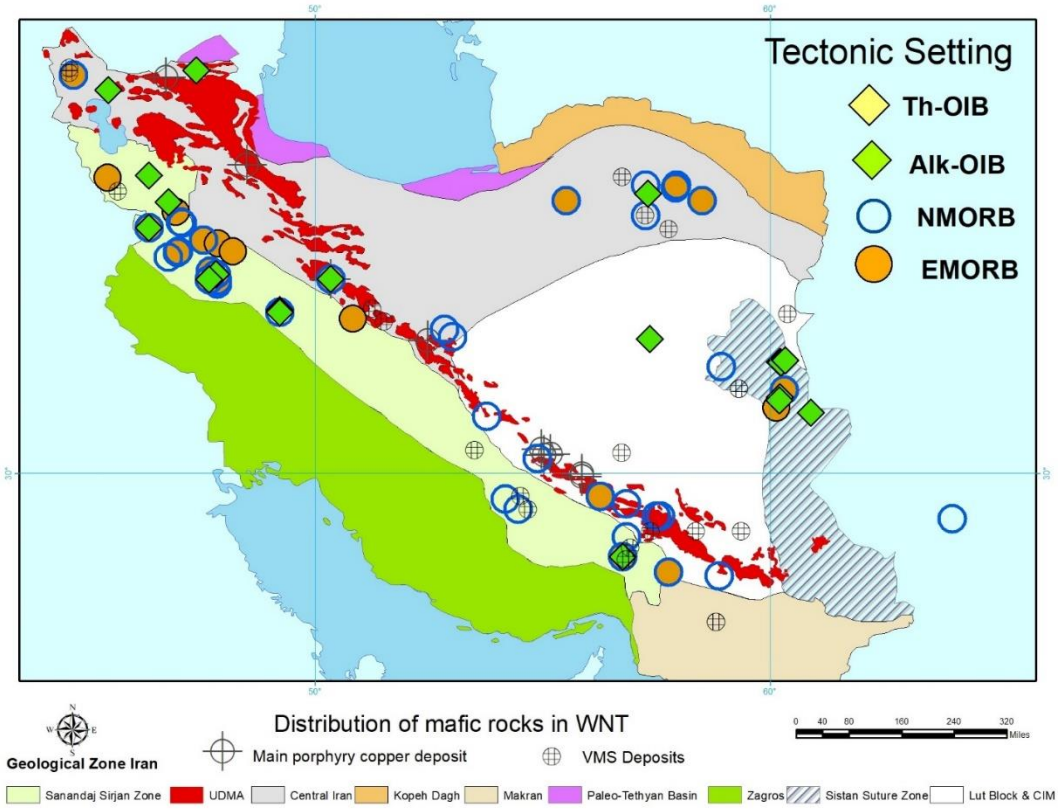

Figure 4. 6. Location of western Neo-Tethys mafic rock samples with their tectonic setting in this study.

4.2. Geochronology

Geochronological data from igneous rocks are of substantial importance for this thesis. More than 420 compiled zircon U-Pb data were compiled from the literature of western Neo-Tethys (**Fig.4.7**). Geographical coordinates provided in the literature were directly used whereas samples without accurate location information are estimated by the proximity of geochemical and geochronology samples that have coordinate information reported (accuracy +/- 25-50 km). Using the estimated location of rock samples will not affect the overall interpretation since the research includes the entirety of the western Neo-Tethys.

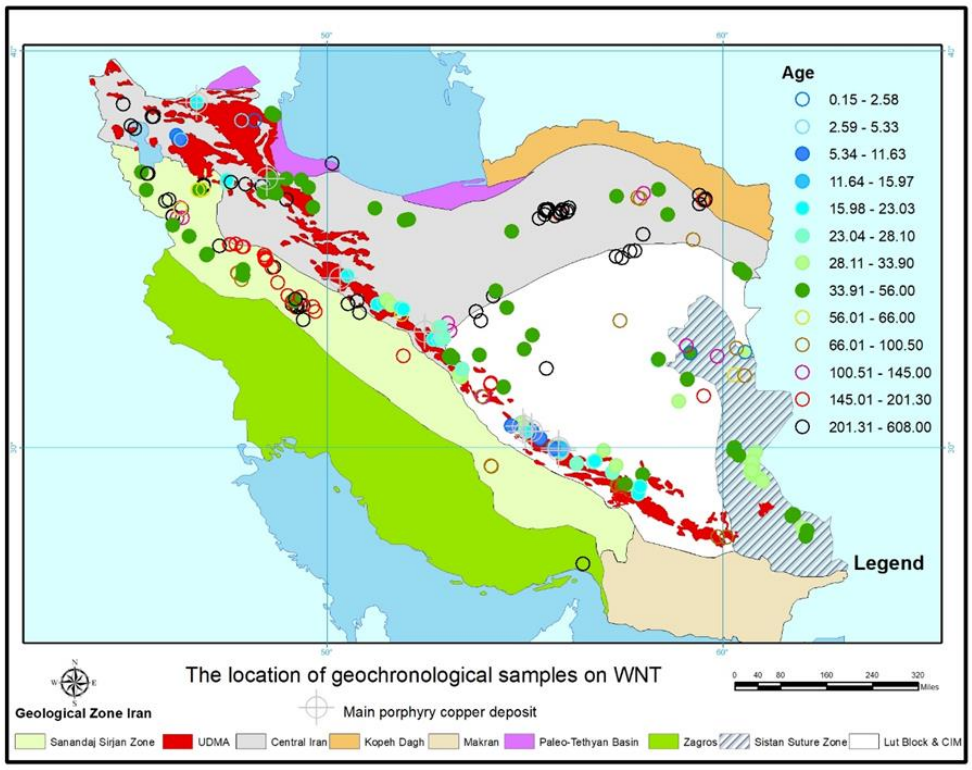

Figure 4. 7. The geological zone of Iran and the location of geochronological samples on western Neo-Tethys. Tectonic and structural maps of Iran, modified after (Aghanabati, 1998; and Alavi, 1996).

4.3. Isotope geochemistry

In addition to the magmatic ages of igneous rocks, Sm-Nd and Lu-Hf isotope data were compiled and have been used to understand the protolith age and composition of igneous rocks in western Neo-Tethys.

Radiogenic isotope tracers can reveal information about the ages and origins of rocks, or processes of mixing between them. These are most powerful when used together with other tracers. An example of this application is the evolution of the crust and mantle through geological time. Higher initial $^{87}Sr/^{86}Sr$ ratios (at equal SiO_2) generally indicate the involvement of an older, more radiogenic lithospheric mantle, assimilation of more radiogenic crustal Sr during differentiation with increasing crustal thickness, or contamination by subduction-related fluids and/or sediments, whereas relatively lower Sr isotope ratios generally reflect mantle source affinities (Haschke et al., 2010).

Furthermore, the isotopic compositions can clarify the juvenile environments from mature tectono-magmatic settings as well as shed light on the oceanic or crustal source of magma. The Sm-Nd and Lu-Hf system can be used as a tracer to provide information on the nature of the source rocks.

In this study, Lu-Hf and Sm-Nd data were compiled from the literature for 1552 separate zircons and 353 igneous rock samples, respectively. Sample locations are shown in the figure (**Fig.3.3**). The calculation of T2DM is shown in **Fig.4.8**, whereas ƐNd and ƐHf are plotted against geological ages for different parts of the Neo-Tethyan basin in **Fig.4.9** and **Fig.4.10** respectively.

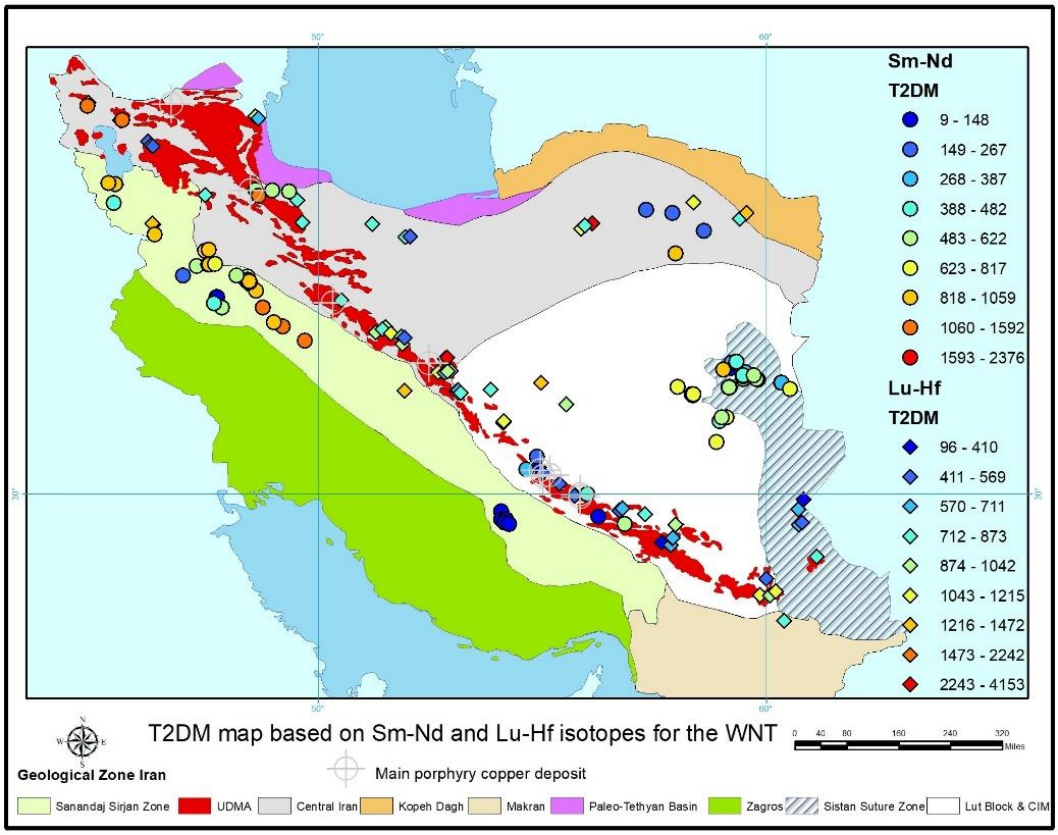

Figure 4. 8. Sm-Nd and Lu-Hf two-stage depleted mantle model age (T_{2DM}) isotopic map for Iran, western Neo-Tethys.

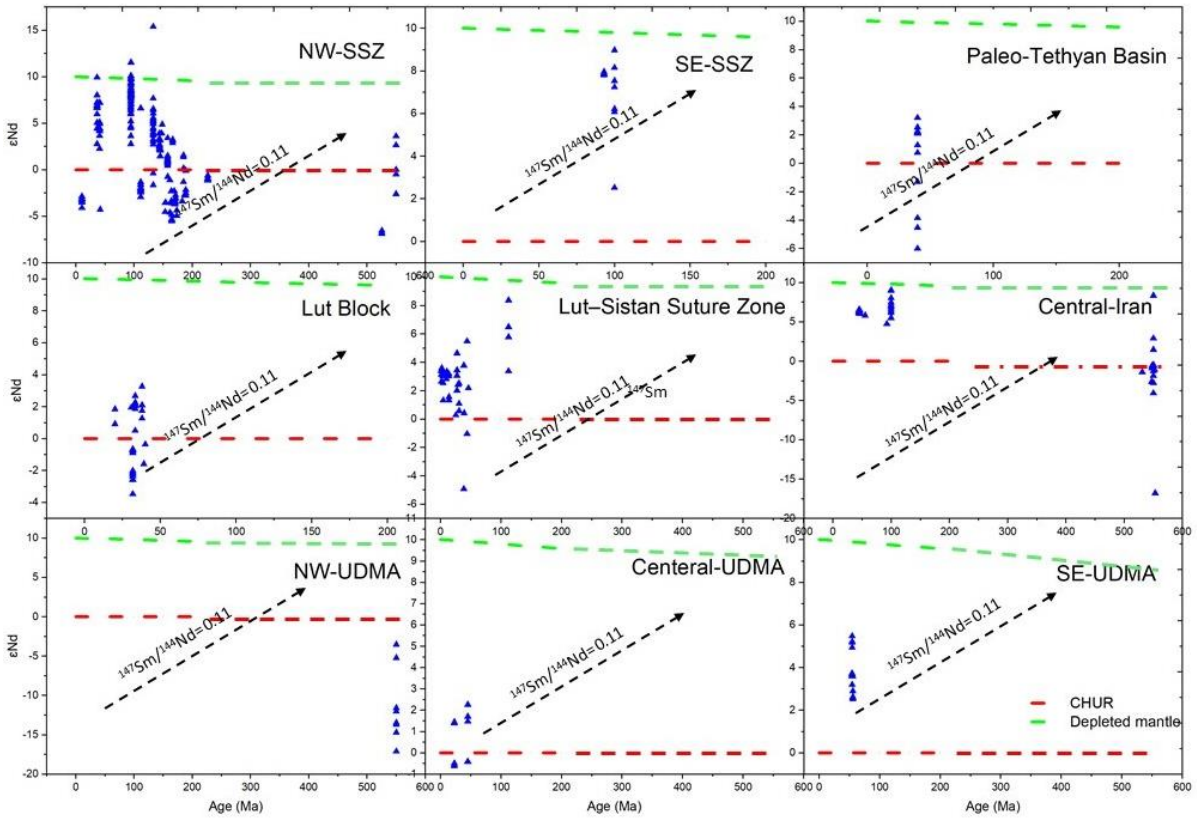

Figure 4. 9. ε_{Nd} versus magmatic ages for the western Neo-Tethys in 9 different geological zones of Iran. The arrow shows the isotope composition trend for the intermediate crustal rocks.

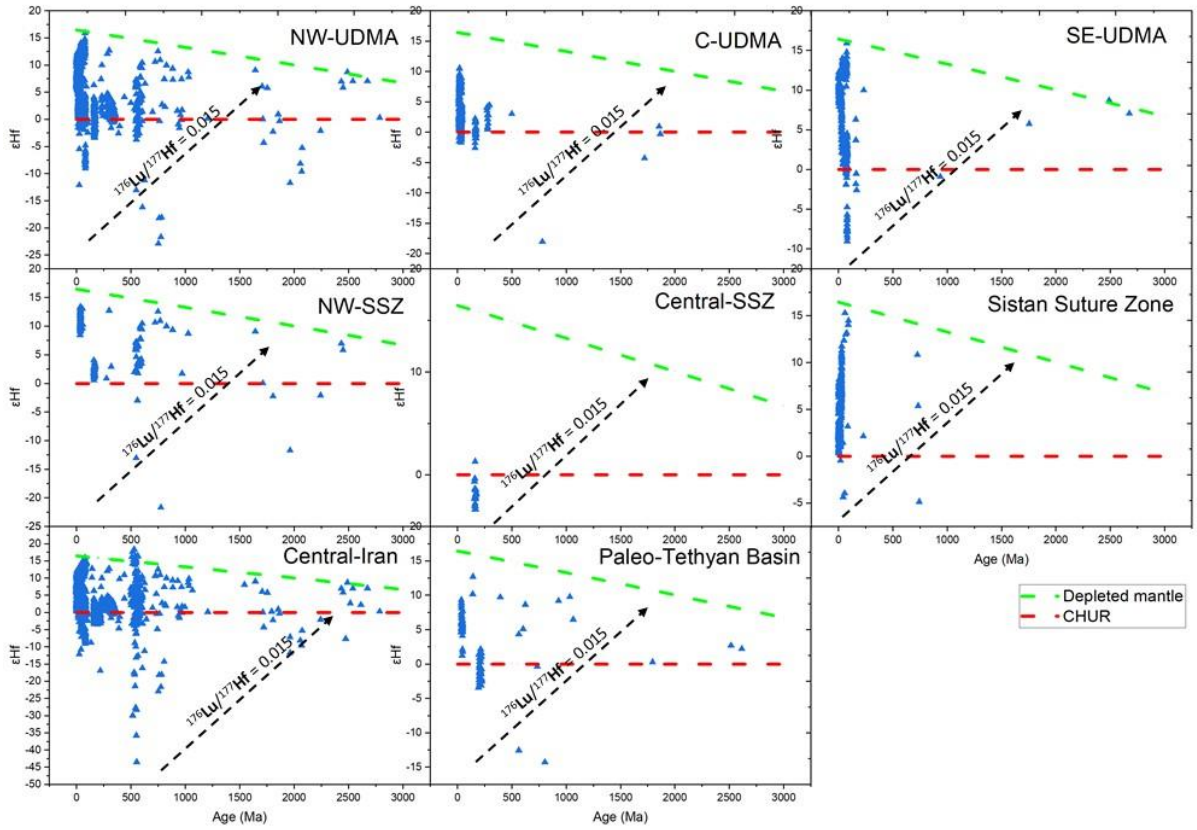

Figure 4. 10. ε_{Hf} versus magmatic ages for the western Neo-Tethys in 8 different geological zones of Iran. The arrow shows the isotope composition trend for the intermediate crustal rocks.

To distinguish the juvenile crust from the older crust and understand the relationship of the barren and fertile crust with respect to mineralization, the incubation age of the rocks (T_{INC}), which is simply T_{2DM} minus the crystallization age, should be calculated ($T_{INC} = T_{2DM} - T_{Cry}$). After these results are plotted on the map, they can demonstrate empirical relationships between mineral systems and isotopic domains in the WNT and can also be used as a variable in isotopic maps (**Fig.4.11**). The combination of the model and the incubation age (T_{2DM}, T_{INC}) with geochronological data is particularly powerful because T_{INC} not only provides an indication of the age of the crust in a region but also when that crust was reworked provides additional constraints on the protolith and components within individual igneous units.

Lu-Hf and Sm-Nd isotopic maps can be informative in identifying potentially favorable paleo-tectonic settings for the mineralization as well as delineating different domains within the Pre-Tethyan rocks and the Tethyan-age rocks. This isotopic data can also be used to assist in identifying older continental margins, accretionary orogenic settings, and juvenile zones, either

marginal or internal, which may display crustal extension and rifting, or primitive arc crust. Furthermore, these maps can provide identification of crustal breaks, which may represent major fault zones and, hence, mantle input and fluid pathways for fluids and magmas, or serve to delineate natural boundaries for metallogenic terranes (Champion & Huston, 2016).

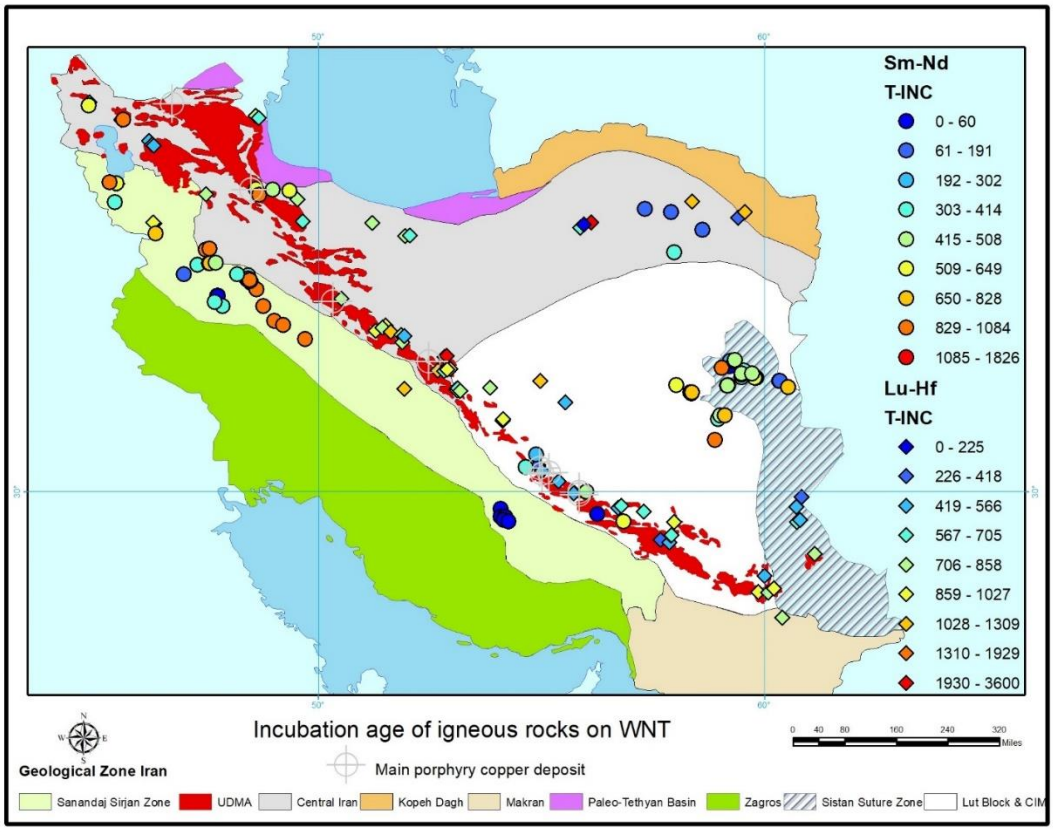

Figure 4. 11. Sm-Nd and Lu-Hf incubation model age (T_{INC}) isotopic map for Iran, western Neo-Tethys.

4.4. Mineralization and Adakitic Signatures

The ore deposits of the Western Neo-Tethys basin in Iran can be divided into three groups showing different metal associations, spatial distributions, and geodynamic settings, as described below.

1. The first group consists of porphyry deposits (**Fig.4.13**) associated with subduction-related granitoids of Eocene to Miocene age. The most famous porphyry deposits in this group (Table, **4.1**) are the Sungun (Hezarkhani & Williams-Jo, 1998), Sarcheshmeh (Waterman & Hamilton, 1975; Shahabpour, 1982; Hezarkhani, 2006), and Miduk deposits (Hassanzadeh, 1993; Taghipour, Aftabi, & Mathur, 2008). This mineralization was formed during the final closure of

the Neo-Tethys Ocean (Atapour, 2007; Aftabi & Atapour, 2009; Aftabi & Atapour, 2011; Shafiei et al., 2009; Richards, Spell, Rameh, Razique, & Fletcher, 2012; Aghazadeh et al., 2015; Golestani et al., 2018).

Statistically, the number of Iranian copper mines is 22, with potential reserves of 3.2 billion tons and a proven reserve of 1.9 billion tons. Fifteen million tons of copper are extracted annually from these mines, which makes Iran the 17th largest copper producer in the world. In terms of reserves, Iran has 3.5% of the world's copper ores (data for Iranian copper deposits, in Persian, is available in the https://www.mimt.gov.ir/). Table (**4.1**) and the diagram (**Fig.4.12**) show the size of Iran's main porphyry deposits. The data for the copper deposits were stored in the IntelligenceMine (www.IntelligenceMine.com).

Table 4. 1. Most important copper deposits in Iran (Ghorbani, 2013).

Name of deposit	Geological Zone	Type of mining	Proved reserve (MT)	Potential reserve (MT)	Average Cu Grade (%)
Sarcheshmeh	SE-UDMA	Open Pit	826.5	1,200	0.68
Meiduk	SE-UDMA	Open Pit	180	500	0.85
Sungun	NW-UDMA	Open Pit	1,000	2,000	0.70

2. The lower Late Cretaceous volcanogenic massive sulfide (VMS) deposits, concentrated mainly in the southern part of the Central Iranian Microcontinent (CIM), make up the second group (**Fig.4.13**). These VMS deposits are mostly related to the evolution of an extensional continental margin in a back-arc environment that affected the CIM during the lower Late Cretaceous volcano-sedimentary sequence (Maghfouri, Rastad, Mousivand, Choulet, & Ye, 2017; Maghfouri, 2012). The most famous VMS deposits of this group are the Bavanat Cu-Zn-Ag (Mousivand et al., 2007), the Sargaz Cu-Zn (Badrzadeh et al., 2011), the Chahgaz Zn-Pb-Cu (Mousivand et al., 2011), the Barika gold-rich (Yarmohammadi, 2006) and the Sheikh Ali Cu (Rastad, Miralipour, & Momenzadeh, 2002). The classification of VMS deposits into various sub-types in WNT is summarized in Table (**4.2**).

Table 4. 2. The classification of VMS deposits in Western Neo-Tethys the new and classical nomenclature proposed by Franklin et al. (2005).

New Classification	Old Classification	World examples	WNT Examples
Mafic	Cyprus-type	*Cyprus*, Oman, and ophiolite-hosted deposits in the Newfoundland Appalachians	*Sheikh Ali* Cu deposit
Bimodal-mafic	Noranda-type	*Noranda* Camp, Flin Flon-Snow Lake, and Kidd Creek	*Sargaz* Cu-Zn deposit
Siliciclastic-mafic (or pelitic-mafic)	Besshi-type	*Besshi* district in Japan and Windy Craggy, British Columbia	*Bavanat* Cu-Zn-Ag deposit, *Nudeh* copper deposit
Siliciclastic-felsic (or bimodal siliciclastic)	Bathurst-type	*Bathurst* District, Iberian Pyrite Belt, and Finlayson Lake	*Chahgaz* Zn-Pb-Cu deposit
Bimodal-felsic	Kuroko-type	*Kuroko*, Buchans, and Skellefte	*Barika* gold-rich deposit

3. The third group is mineralization hosted in some ophiolites of the upper Cretaceous. Examples of this type of mineralization are mainly concentrated along the Main Zagros Thrust Zone (MZTZ, **Fig.2.2**) related to the Neo-Tethys and associated back-arc basins on the southern margin of Eurasia. The ophiolites are part of the 3000 km long ophiolite-rich zone that extends eastwards from Troodos (Cyprus) through Turkey and as far as Semail in Oman (Knipper, Ricou, & Dercourt, 1986; Moores, Kellogg, & Dilek, 2000; Robertson, 2002; Dilek & Furnes, 2009; Allahyari et al., 2010; Saccani et al., 2013; Allahyari et al., 2014; Saccani et al., 2014; Moghadam & Stern, 2015).

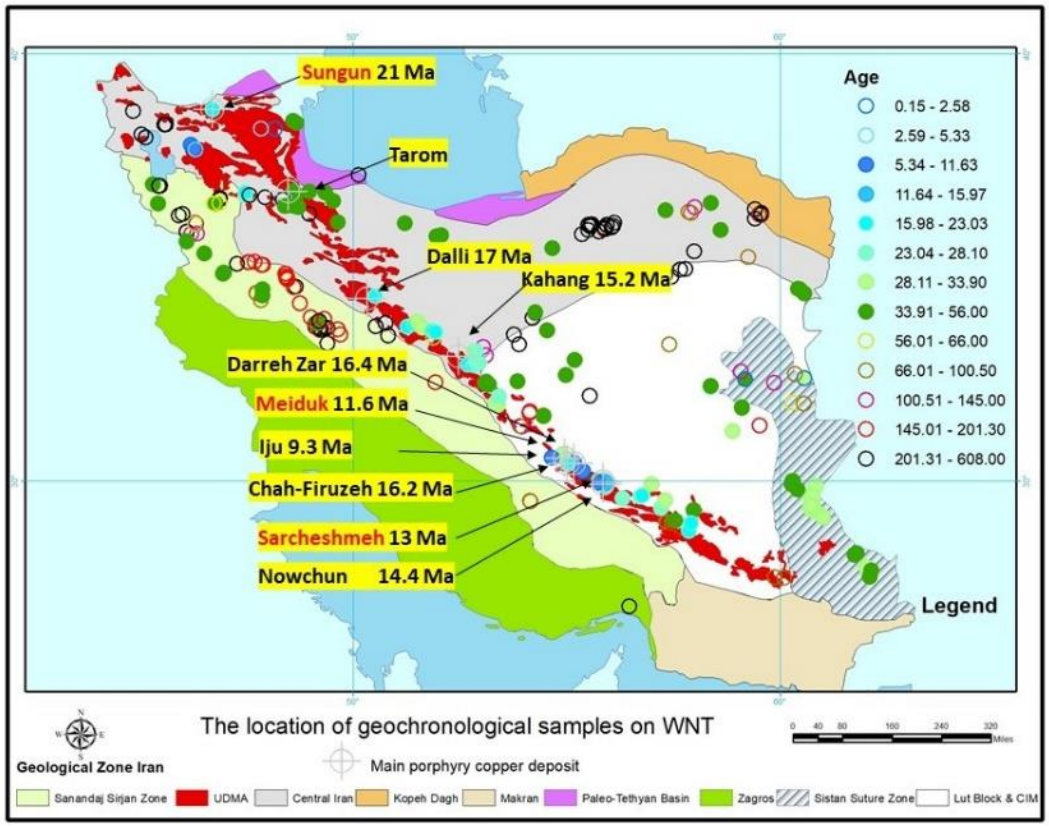

Figure 4. 12. The geological zone of Iran and the location of geochronological samples on Western Neo-Tethys, showing the locations of major named porphyry Cu deposits with known isotopic ages from the Urumieh-Dokhtar Magmatic Arc (UDMA) Published ages from(Aghazadeh et al., 2015) and (Richards et al., 2012b)

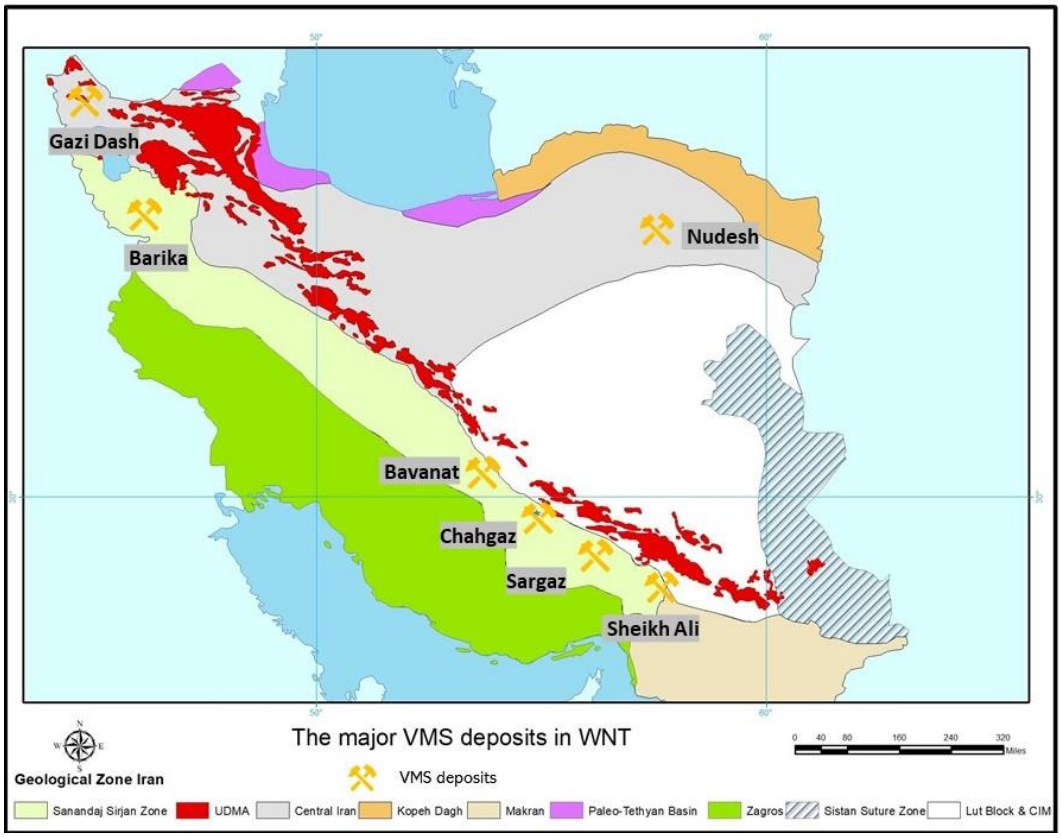

Figure 4. 13. The geological zone and the location of VMS deposits in Iran; UDMA, Urumieh-Dokhtar Magmatic Arc; modified after (Maghfouri et al., 2016). Tectonic and structural map of Iran, modified after (Aghanabati, 1998; and Alavi, 1996).

During partial melting, Sr is compatible at low pressures (<~10 kbar) and strongly incompatible at high pressures (>12 kbar). Conversely, Y is incompatible at low pressures but compatible at high pressures. As a result, Sr/Y can be considered as an indicator of the average crustal pressure, or depth, at which magmatic differentiation occurred. A larger Sr/Y ratio signifies a greater pressure or depth (**Fig.4.14, Fig.4.17**). Loucks (2000) and Loucks & Ballard (2002) showed that more than 80 porphyry copper deposits worldwide are genetically related to felsic intrusions having Sr/Y > 35 (Loucks, 2014). High Sr/Y ratios (≥20) are therefore used in the definition of adakites as an indication of a lack of plagioclase fractionation combined with the presence of garnet in source rocks, together taken to indicate partial melting of an eclogitic source (Defant & Kepezhinskas, 2001). However, high Sr/Y ratios can also indicate high magmatic water contents, which suppress early plagioclase crystallization but promote hornblende crystallization.

Porphyry-related magmas are typically related to adakite-like geochemical signatures. It can be indicated by the high Sr / Y and La / Yb ratios or with partial melting of the thickened

garnetiferous lower crust. This magma can be produced from various arc magmatic series ranging from primary slab melts to slab melts hybridized by peridotites. Recent studies (e.g., Gao et al., 2004; RodrÍguez et al., 2007; Rooney et al., 2011; Wang et al., 2005) show that adakites can be produced by melting of the lower crust or ponded basaltic magmas and magma mixing processes in both, the arc, or non-arc tectonic environments. It is also shown that adakites can be derived from subducting oceanic crust, delamination of the lower crust, slab melting (Stern & Kilian, 1996), and thick lower crust (Jamali & Mehrabi, 2015).

Adakitic melts are produced from the lower basaltic crust under high pressures, where garnet is maintained as a residual phase. This condition is attained when the crust reaches thicknesses of more than 40 km (Castillo, 2006). It is argued that (Haschke et al., 2006; Richards & Kerrich, 2007) hybrid magma containing up to approximately ten percent contribution of garnet amphibolite melting in the lower crust is expected to be triggered by MASH-type processes (melting, assimilation, storage, homogenization).

Other potential sources for increasing heat in the base of thickened arc crust is the upwelling of hot asthenospheric mantle plumes due to slab breakoff and rift-related decompression melting of the collision-modified lithosphere (Haschke & Ben-Avraham, 2005).

Geochemical results show the mineralized Cenozoic rocks of UDMA in WNT generally have a high Sr/Y (**Fig.4.14**) and La/Yb (**Fig.4.15**), and that the main porphyry copper deposits at UDMA are distributed over the areas with Sr/Y ratios of more than 35 (**Fig.4.17**).

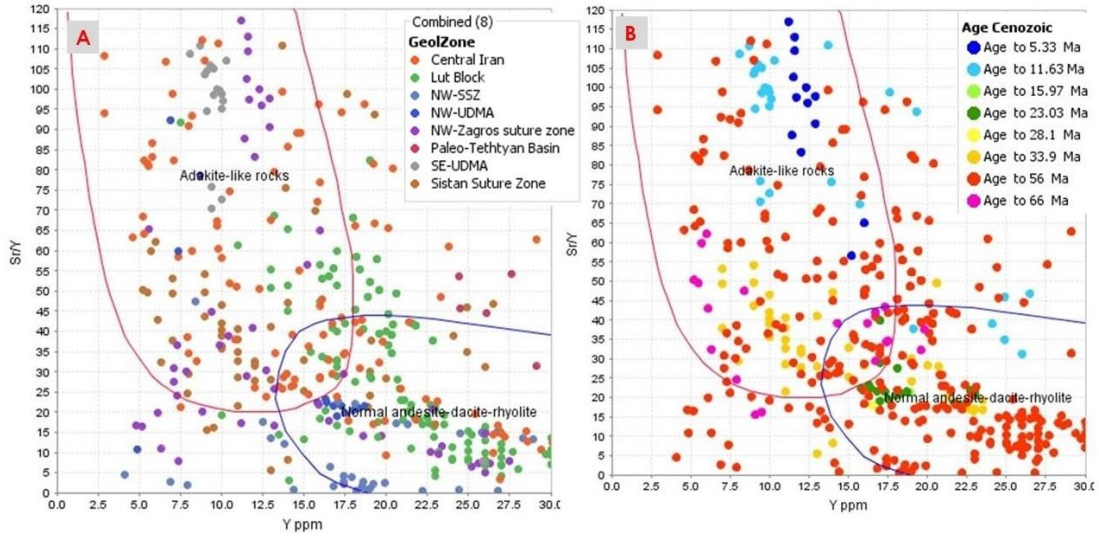

Figure 4. 14. Sr/Y vs. Y (ppm) diagram of Cenozoic intrusive rocks from the western Neo-Tethys**.** (**A**) distribution of samples by age (**B**) distribution of samples by Geological zone (Defant & Drummond, 1993).

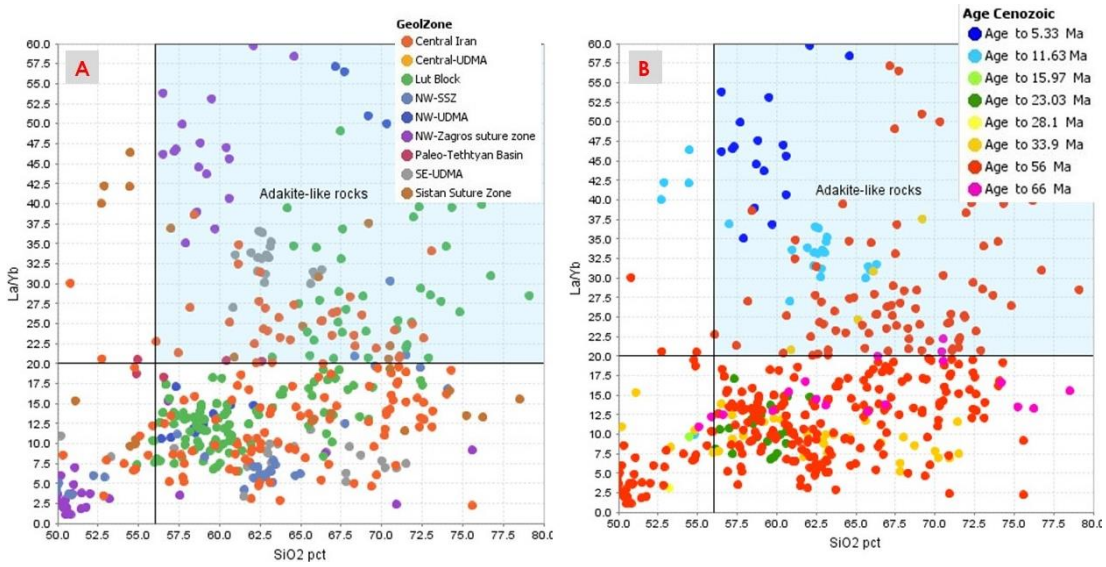

Figure 4. 15. Geochemical classification of the western Neo-Tethys Cenozoic igneous rocks for adakitic signature. La/Yb vs. SiO_2 diagrams of (Defant & Drummond, 1993), (**A**) distribution of samples by Geological zone (**B**) distribution of samples by age.

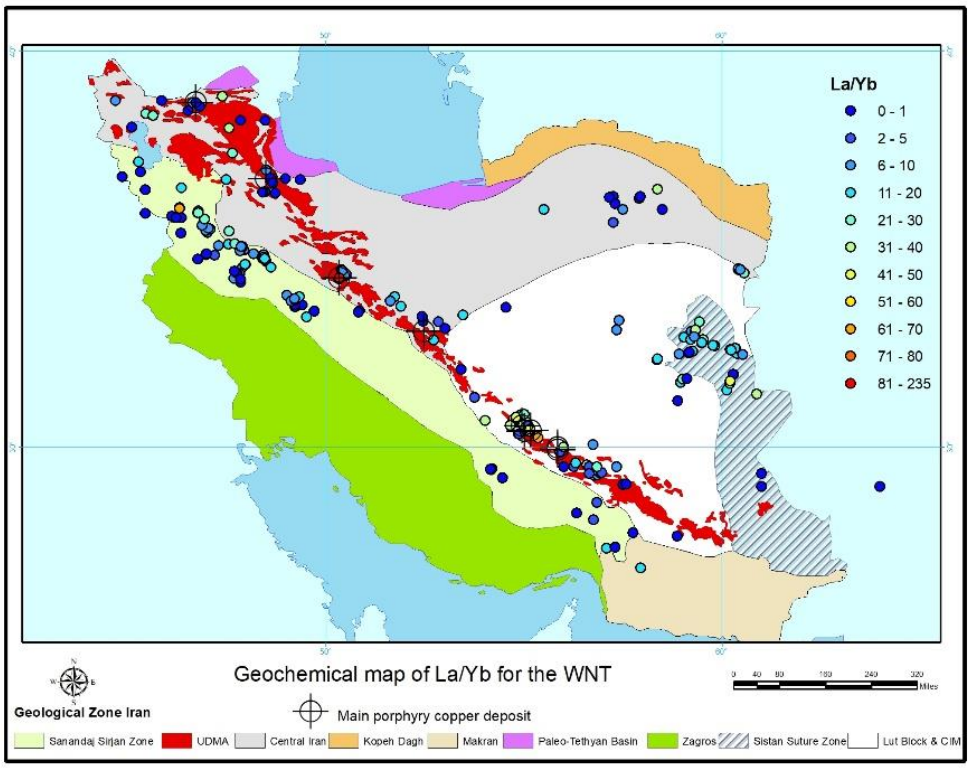

Figure 4. 16. Geological map of Iran and distribution La/Yb ratios as an indicator of average lithosphere pressure or depth at the western Neo-Tethys.

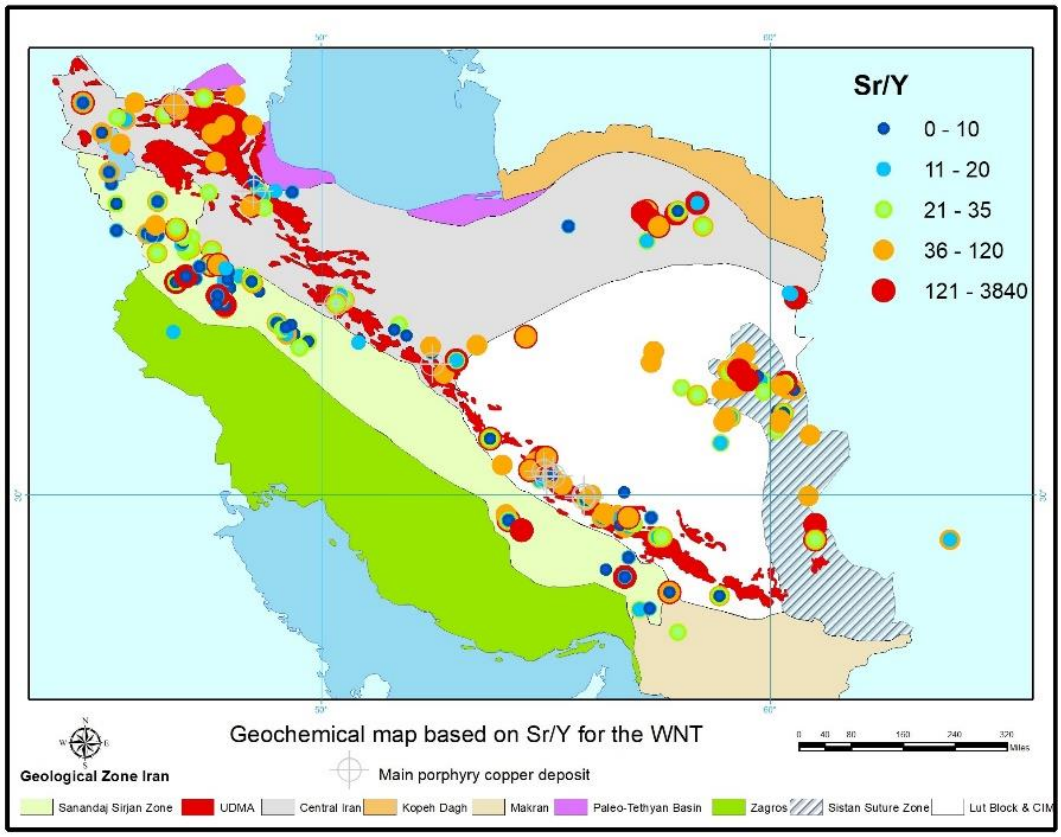

Figure 4. 17. Geological map of Iran and distribution of Sr/Y ratios as an indicator of average lithosphere pressure or depth at the western Neo-Tethys.

CHAPTER 5: DISCUSSION PART 1: MAGMATIC EVOLUTION

5.1. Geochemistry and isotopic signatures during geological time

In this thesis, the lithochemistry and the Nd and Hf isotopic analyses of igneous and metamorphic rocks mainly from the Neo-Tethys and rarely from the Paleo-Tethyan basin have been compiled and compiled, and re-interpreted. The result has been separated according to the geological time and different classifications of the geological zone in Iran. This can provide a comprehensive overview of the magmatic evolution during syn- and post-collision events during the past ~600 (Ma) in western Neo-Tethys. Furthermore, it can improve our understanding of the magmatic and crustal evolution of the Tethys oceans through time in Iran's different geological zone.

It should be noted that the igneous and metamorphic rocks formed before the Permian are related to Paleo-Tethys and the older oceans. There is no relation between Neoproterozoic, Cambrian, Devonian, and Carboniferous rocks and Neo-Tethys. Essentially, these rocks formed the basement to the magmatic systems that developed during the evolution of the Neo-Tethys.

5.1.1. Neoproterozoic 1000-541 (Ma)

Neoproterozoic metamorphic rocks are exposed in the WNT, in the Shotur Kuh Complex. They are considered as an extension of the Paleo-Tethys Ocean terrane in CIM (Rahmati-Ilkhchi et al., 2011). These rocks are comparable with the granitoid rocks of the same age from the Saghand region in the eastern part of Central Iran (Ramezani & Tucker, 2003). The U–Pb age dating of zircon showed that these rocks formed during Late Neoproterozoic continental arc magmatism that has also been distinguished in other tectonic blocks of Central Iran (**Fig.5.1. A**). The geochronological data from granites and orthogneisses from central Iran have confirmed this interpretation (Hassanzadeh et al., 2008). Furthermore, these Late Neoproterozoic to Early Cambrian rocks originated after the main phase of Pan-African orogeny. They are considered juvenile Arabian–Nubian shield and Peri-Gondwanan rocks after the main phase of Pan-African orogeny (Rahmati-Ilkhchi et al., 2011).

A limited occurrence of Neoproterozoic metamorphic rocks occurred around CIM. According to the geochemical discrimination diagram (Defant & Drummond, 1993), there is no adakitic signature in Neoproterozoic Terrans in central Iran (**Fig.5.1. B**).

For the geochemical classification of mafic and felsic rocks of the study area, a combination of two discrimination diagrams (**Fig.5.1, C, D**) has been used. As a first step, the Rb-Yb+Nb diagram of Pearce, Harris, and Tindle (1984) is used to discriminate the tectonic setting of felsic rocks. Felsic rocks in the Neoproterozoic of the CIM plot largely within the VAG setting of this discrimination diagram (**Fig.5.1, C**). However, some rocks that plot within the WPG field are close to the border and therefore are considered to have a close affinity to VAG (**Fig.5.1, C**).

As the second step, the TiO_2/Yb–Nb/Yb of Pearce (2014) is used to separate subduction-related from non-subduction related basalts. In this discrimination diagram the TiO_2/Yb ratio functions as a good indicator of the depth of mantle melting. The majority of mafic rocks in the Neoproterozoic of CIM plot within the E-MORB field of the diagram (**Fig. 5.1.D**).

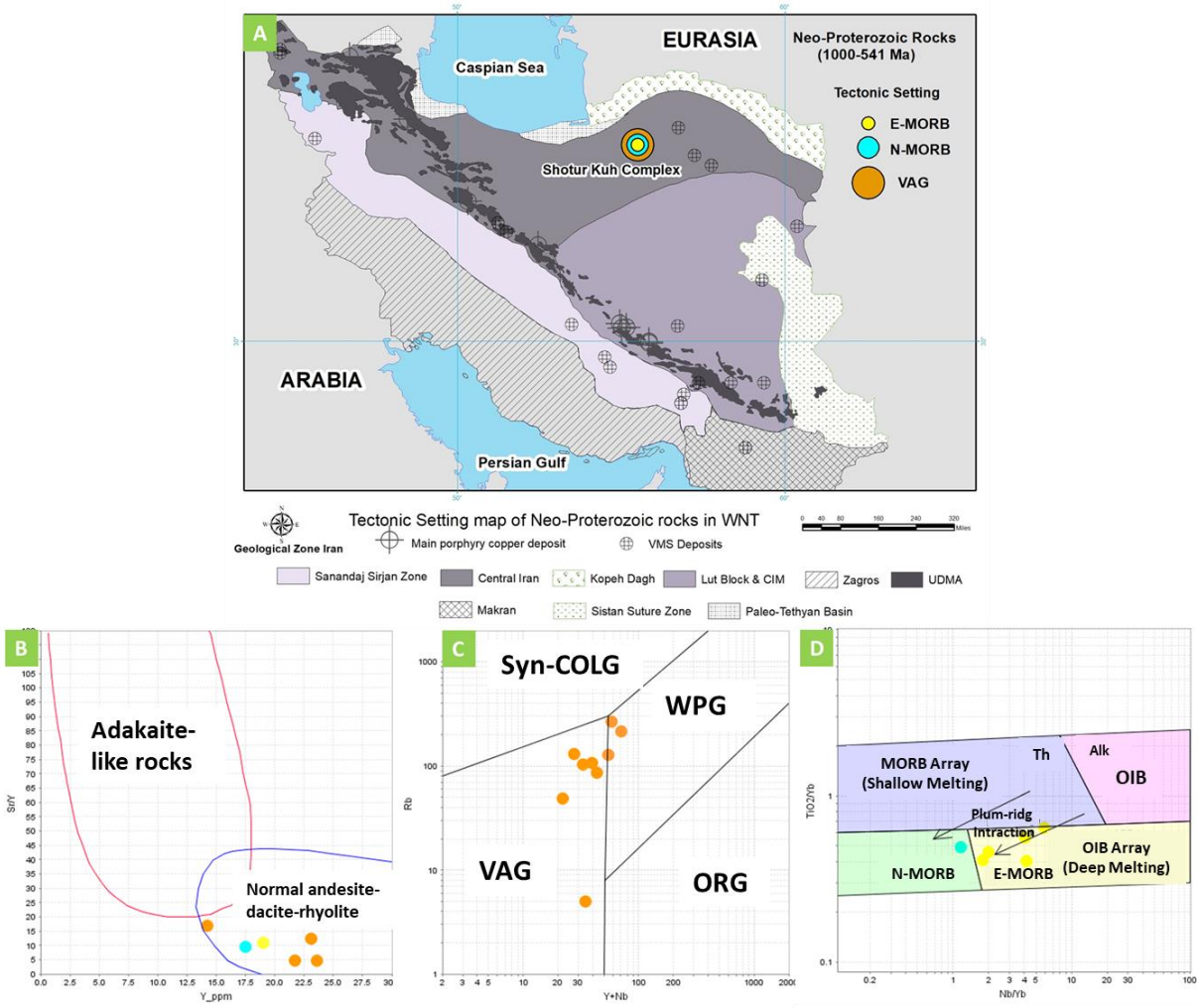

Figure 5. 1. Classification and geochemical characterization of igneous and metamorphic rocks from Neoproterozoic rocks in the western Neo-Tethys (**A**) Location of Shotur Kuh Complex (Rahmati-Ilkhchi et al., 2011). (**B**) Sr/Y vs. Y (ppm) diagram of Neoproterozoic rocks from the western Neo-Tethys (Defant & Drummond, 1993). (**C**) Rb vs. (Y + Nb) discriminant diagrams for the tectonic setting of felsic rocks in the study area (Pearce, Harris, & Tindle, 1984). (**D**) the TiO_2/Yb–Nb/Yb diagrams diagram is used to separate subduction-related from subduction-unrelated mafic rocks (Pearce, 2014).

The Nd and Hf isotopic analyses of Neoproterozoic igneous and metamorphic rocks (**Fig.5.2. A-D**) in this study have been compiled mainly from the Urumieh-Dokhtar Magmatic Arc, Sanandaj Sirjan Zone, Sistan suture son, and Alborz Zone (Paleo -Tethyan basin). Although the sample location belongs to these zones, isotopic data indicate that there are different crustal blocks and protoliths for them (**Table 5.1, Fig.5.2. A-D**).

The Mishu granites yielded the crystallization ages of ca. 550 Ma in the northwest part of the UDMA (Fig.5.2.C). They have been formed along an ancient subduction zone in the Paleo-

Tethyan Ocean. The Mishu granites have formed via interaction between juvenile melts and old (Mesoproterozoic or Archaean) continental crust during Cadomian (Shahzeidi et al., 2017). These granites mainly show S-type characteristics, whereas the leucogranites part have I-type signatures. The S-type granites show high $^{87}Sr/^{86}Sr(i)$ ratios, ranging from 0.7068 to 0.7095. Their ε_{Nd} values change between -11.5 to -17.1, which are interpreted as the product involving an extreme crustal contribution. The I-type granites are characterized by relatively low $^{87}Sr/^{86}Sr(i)$ ratios (0.7048–0.7079) and higher values of ε_{Nd} (-3.2 to -5.2) (Shahzeidi et al., 2017), which are interpreted as the product involving a moderate crustal contribution in a subduction environment affiliated with the arc magmatism in the Paleo-Tethys basin. In comparison with S-type, the I-type granites have shown a juvenile signature. The age, geochemistry, and Isotopic signatures of Cadomian Mishu granites strongly indicate the similarities between these rocks with other Late Neoproterozoic – Early Cambrian (600–520 Ma) granites across Iran and the surrounding areas such as Turkey and Iberia (Shahzeidi et al., 2017)

The isotopic and geochronological data of the Taknar complex, Central Iran (**Fig.5.2. A-B**), is interpreted as the Late Ediacaran–Cambrian or Cadomian arcs that formed along the northern margin of Gondwana (Moghadam et al., 2017). Their ε_{Nd} values change between -2.7 to +8.3, which are interpreted as the product involving a medium crustal contribution to the moderate mantel contribution. Their ε_{Hf} values change between -3.5 to +8.1. The Nd and Hf isotopic data have shown that the igneous rocks were generated by mixing juvenile magmas with older continental crust components at an active continental margin of the Iran–Anatolia Cadomian rocks (Moghadam et al., 2017).

The geochronological data (U–Pb zircon age 554 ± 6 Ma) for Arghash pluton (**Fig.5.2. A-D**) indicated that these igneous rocks most likely are the remnant of the Peri-Gondwana rocks in central Iran. The value of ε_{Nd} (-16.7) indicates that these igneous rocks are formed in an island-arc or back-arc tectonic setting with an extreme crustal contribution (Alaminia et al., 2013).

The results of U–Pb dating for the Khoy metamorphic complex (KMC) in the northwest part of the SSZ (**Fig.5.2. A, B**) suggests a late Proterozoic (550–590 Ma) consolidation of granitic and basaltic magma. Furthermore, the initial $^{143}Nd/^{144}Nd$ and $^{87}Sr/^{86}Sr$ ratios strongly indicate that the original magma originated in the subduction zone from a depleted mantle source and some contamination from recycled sediments (Azizi et al., 2011). Their ε_{Nd} and ε_{Hf} values change

between -2.6 to +3.6, and +1.8 to +10.4 respectively, which are interpreted as the product involving a low crustal contribution to a moderate to high mantle contribution, and the rocks were generated through the mixing of juvenile magmas with older continental crust components at an active continental margin.

The geochronological data of the Delbar Metamorphic-Igneous Complex (DMIC) in Central Iran (**Fig.5.2. A, B**) indicated that they have formed along the northern margin of Gondwana during the Late Ediacaran to Cambrian arc-type magmatism (~545 Ma). It is believed that these rocks are the result of the final collision and amalgamation of Gondwana. This occurred during the closure of the Rheic Ocean and the opening of the coeval Paleo-Tethys basin at the end of the Avalonian–Cadomian orogeny (Balaghi Einalou et al., 2014, and references within). The Delbar Metamorphic-Igneous Complex has yielded a bimodal population of zircon ε_{Hf} (T) values. The first group has ε_{Hf} (T) values from -43.5 to -27.8, which are interpreted as the product of an extreme crustal contribution in a subduction environment. The second group has ε_{Hf} (T) values from -9.9 to +16.4, which is interpreted as a product of moderate crustal contribution to moderate to high mantle contribution and could be attributed to magma partially evolved with juvenile magmas. Both groups are affiliated with arc magmatism in the Paleo-Tethys basin. The U–Pb zircon dating of the Zanjan–Takab core complex in the northwest part of the UDMA (**Fig.5.2. A, B**) supports a Late Neoproterozoic –Early Cambrian age (ca. 548–568 Ma) for meta-granites and orthogneisses rocks (Hassanzadeh et al., 2008). Zircon ε_{Hf}(T) values between -2.8 to +5.9 (Moghadam et al., 2016) are consistent with the mixing of old crust and depleted mantle-derived material.

Zircon analyses from the Marand region of the northwest part of the UDMA have ε_{Hf} (T) values between -3.7 to +6.5 (Chiu et al., 2017) which are consistent with the mixing of old crust and depleted mantle-derived material (**Fig.5.2. A, B**).

Similarly, zircon analyses from the Saghand region of Central Iran have ε_{Hf} (T) values between -4.8 to -0.3 (Chiu et al., 2017), also supportive of melting of old continental crust (**Fig.5.2. A, B**).

In contrast zircons from the Zahedan region in the Sistan Suture Zone have a more moderate ε_{Hf} (T) value of +5.4 (Chiu et al., 2017), which is interpreted to represent juvenile mantle input without significant crustal contamination (**Fig.5.2. A, B**). In the Tehran area of the Alborz

Zone (Paleo -Tethyan basin) zircon ε_{Hf} (T) values are +5.1 (Chiu et al., 2017) and are interpreted to represent juvenile mantle input without significant crustal contamination (**Fig.5.2. A, B**).

The T_{2DM} and epsilon values calculated based on the isotopic data reveal that at least three crustal blocks in Central Iran can be recognized in different Neoproterozoic time periods. Therefore, samples from northwestern Central Iran (Takab, Khoy, Marand), CIM (Saghand), Alborz (Tehran), and northeastern Central Iran (Taknar, part of Delbar Complex) have different epsilon values but similar T_{2DM}, indicating likely derivation for the same source region at different time. (**Fig.5.2. A- D**). The isotope data collected for the Neoproterozoic rocks in WNT are summarized in Table (**5.1**).

Table 5. 1. The summary of isotope data for the Neoproterozoic rocks in western Neo-Tethys.

Location Name	**Geological Zone**	**Crustal Block**	ε_{Hf}	ε_{Nd}	**Age** (Ma)	**Reference**
Mishu	NW-UDMA	NW-Central Iran	_	-11.5 to -17.1 -3.2 to -5.2	550	(Shahzeidi et al., 2017)
Marand	NW-UDMA	NW-Central Iran	-3.7 to +6.5	_	541-698	(Chiu et al., 2017)
Takab	NW-UDMA	NW-Central Iran	-2.8 to +5.9	_	546-557	(Moghadam et al., 2016)
Zahedan	Sistan Suture Zone	Lut	+5.4	_	546-557	(Chiu et al., 2017)
Khoy	SE	NW-Central Iran	+1.8 to +10.4	-2.6 to +3.6	550.1	(Azizi, et al., 2011)
Arghash	CIM	CIM		-16.7	550–590	(Alaminia et al., 2013)
Delbar	Central Iran	NE-Central Iran	-43.5 to -27.8 -9.9 to +16.4	_	~545 Ma	(Balaghi Einalou et al., 2014)
Saghand	CIM	CIM	-4.8 to -0.3	_	733- 548	(Chiu et al., 2017)
Taknar	Central Iran	NE-Central Iran	-3.5 to +8.1	-2.7 to +8.3	550.5-547	(Moghadam et al., 2017)
Tehran	Alborz (Paleo - Tethyan basin)	Central Iran	+5.1	_	606	(Chiu et al., 2017)

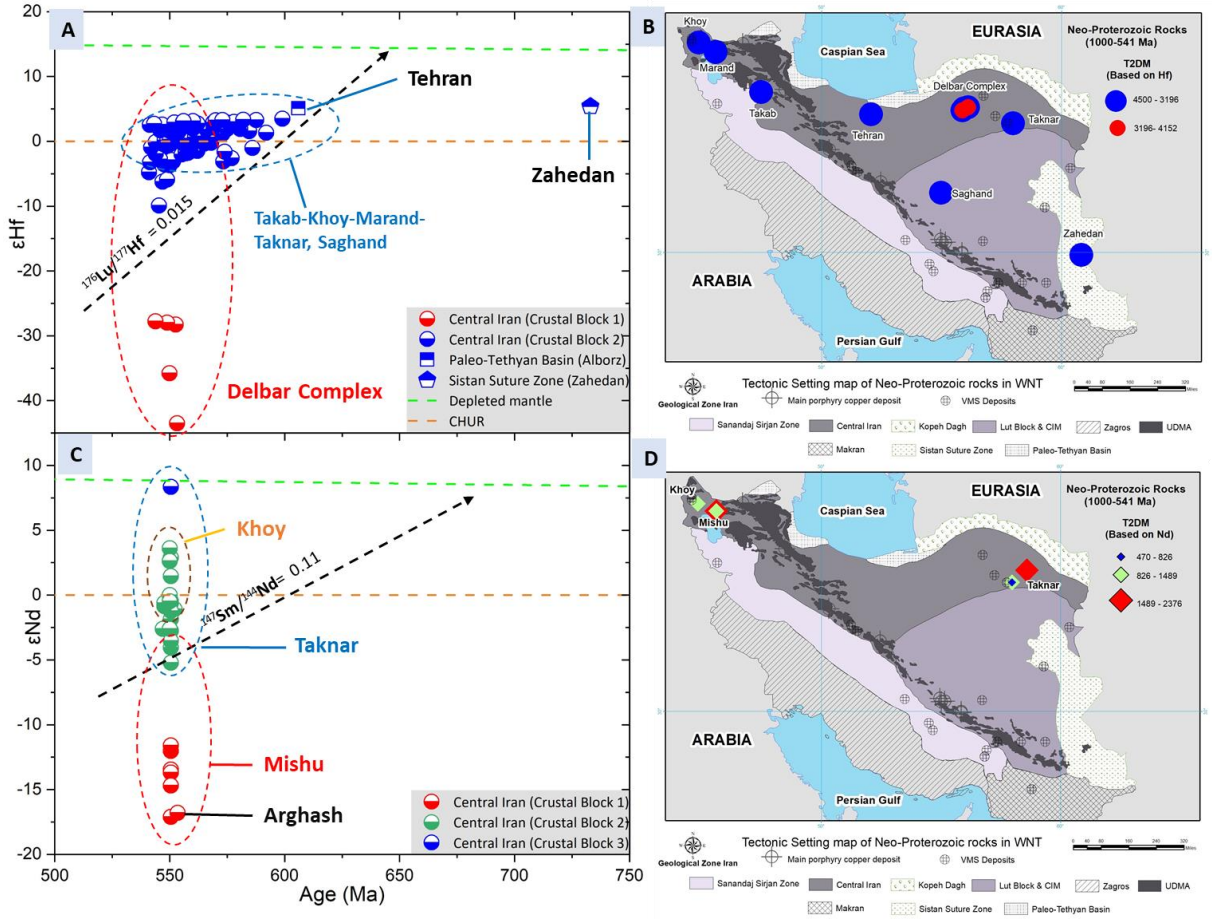

Figure 5. 2. Diagrams of ε_{Hf}(T) and ε_{Nd} (T) versus U-Pb ages and the distribution of the Neoproterozoic rocks on the WNT. The legend corresponds to the different crustal blocks in WNT. The arrow shows the isotope composition trend for the intermediate crustal rocks. (**A**) ε_{Hf} (T) versus magmatic ages (**B**) Distribution of T_{2DM} isotopic data on WNT, calculated based on Hf isotopic composition. (**C**) ε_{Nd} (T) versus magmatic ages (**D**) Distribution of T_{2DM} isotopic data on WNT, calculated based on Nd isotopic composition.

5.1.2. Cambrian 541-485.4 (Ma)

Late Neoproterozoic -Early Cambrian (Cadomian) metamorphic and igneous rocks comprise most of Iran's basement (e.g., Moghadam & Stern, 2015; Shakerardakani et al., 2017; Malek-Mahmoudi et al., 2017). These basement rocks indicate the formation of the Paleo-Tethys Ocean via subduction along the northern margin of the Gondwana supercontinent during the Late Neoproterozoic (Shabanian et al., 2018). Zircon U–Pb ages from the Azna-Dorud region in the northwest part of the SSZ of Iran have a crystallization age of 525.6 ± 4 Ma (Early Cambrian) for the protolith of the basement rocks (Shabanian et al., 2018).

Cambrian metamorphic rocks are not prevalent in the Azna-Dorud region of the northwest part of the SSZ of Iran. Based on data from Defant & Drummond (1993), there is no adakaitic signature in Cambrian rocks in Central Iran (**Fig.5.3. A, C**). Based on the Rb-Yb+Nb discriminant diagram (**Fig.5.3. B**) of Cambrian felsic rocks of the CIM plot within the WPG tectonic setting. However, some samples show the VAG signature but plot close to the border of the WPG field. These WPG rocks may reflect a continental crust or underplated crust that has undergone a cycle of continent-continent collision or island–arc magmatism in a post-orogenic tectonic setting (Whalen, Currie, & Chappell, 1987; Nédélec, Stephens, & Fallick, 1995). These granitoid may have been emplaced after Cadomian orogen, which occurred on the Gondwana supercontinent's northern margin (Shabanian et al., 2018).

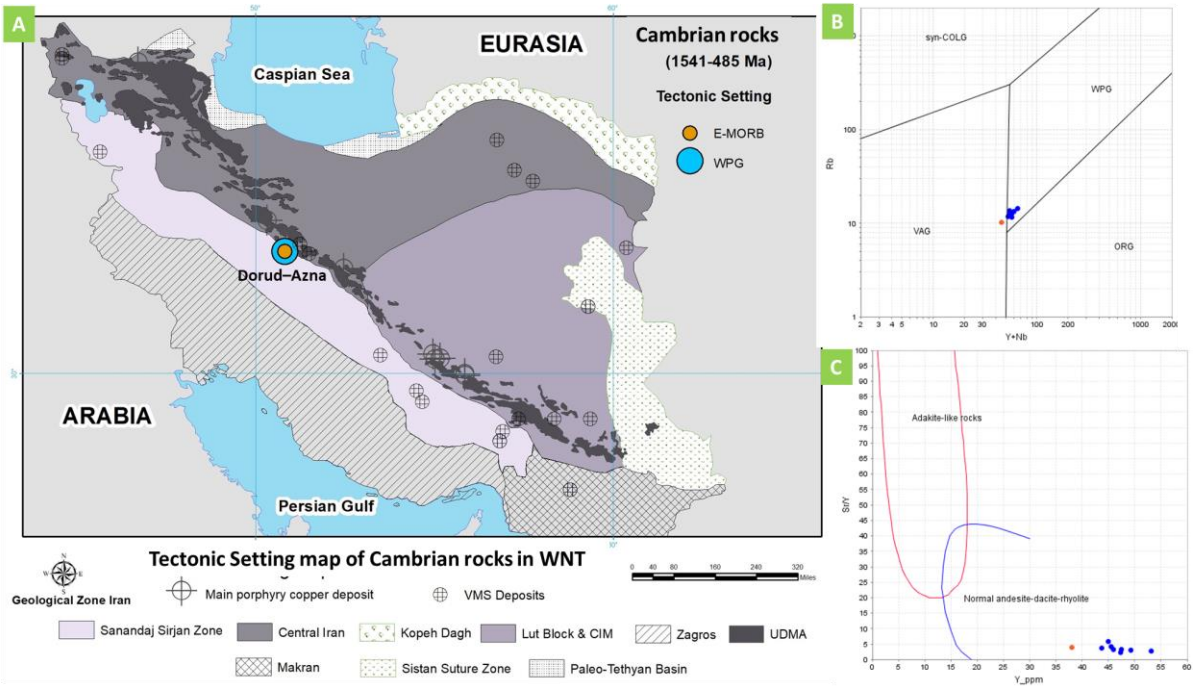

Figure 5. 3. Classification and geochemical characterization of igneous and metamorphic rocks from Cambrian rocks in the WNT (**A**) Location of Dorud–Azna- northwest part of the SSZ (Shabanian et al., 2018). (**B**) Rb vs. (Y + Nb) discriminant diagrams for the tectonic setting of felsic rocks in the study area (Pearce, Harris, & Tindle, 1984). (**C**) Sr/Y vs. Y (ppm) diagram of Cambrian rocks from the WNT (Defant & Drummond, 1993).

The U–Pb zircon dating of the Dorud–Azna protolith rocks in the northwest part of the SSZ (**Fig.5.4. A-D**), represent Late Neoproterozoic –Early Cambrian age (ca. 525.6 ± 4 Ma) like other basement granites in the SSZ (Shabanian et al., 2018). ε_{Nd} (T) values between -6.9 to -6.5 indicated evidence of partial melting of old continental. The new data reveals the association of the SSZ

with the Arabian continental crust before drifting on the Iranian plate in the Late Permian-Triassic time (Shabanian et al., 2018).

The isotopic signature of the Taknar in Central Iran in Cambrian has continued the Ediacaran trend. Indeed, it has formed along the northern margin of Gondwana during the Late Ediacaran to Cambrian arc-type magmatism (~545 Ma) and indicated the final collision and amalgamation of Gondwana. Taknar region yields ε_{Nd} (T), and zircon ε_{Hf}(T) values -1.4 and -3.8 to +4.8, respectively (Moghadam et al., 2017). The Isotopic results (**Fig.5.4. A-D**) have indicated evidence of mixed juvenile and reworked magma sources in continental arcs along the northern margin of Gondwana in Late Ediacaran–Cambrian (Moghadam et al., 2017 and references inside).

The isotopic signature of the Delbar Metamorphic-Igneous Complex in Central Iran in Cambrian is considered a continuation of that established in the Ediacaran. Indeed, Delbar Complex has formed along the northern margin of Gondwana during the Late Ediacaran to Cambrian arc-type magmatism (~545 Ma) and indicated the final collision and amalgamation of Gondwana. The Delbar Complex has yielded a variety of zircon ε_{Hf} (T) values from -30 to +18.4 for Cambrian age rocks. This diversity is interpreted to reflect an extreme crustal contribution in a subduction environment partially evolved with juvenile magmas. These rocks are attributed to the arc magmatism in the Paleo-Tethys basin (Balaghi Einalou et al., 2014).

During the Cambrian in the Saghand region of the CIM, the majority of the rocks yield positive zircon ε_{Hf} (T) values between +3.6 to +7.4 (Chiu, 2017); however, one sample had a value of -1.19. The data is interpreted to reflect a juvenile mantle source magma not significantly contaminated by the crust (**Fig.5.4. A, B**).

During the Cambrian, the Khoy metamorphic complex (KMC) in the northwest part of the SSZ, does not exhibit a significant change in isotopic composition compared with the late Proterozoic. Indeed, there is just one sample reported with ε_{Hf} values +1.98. Therefore, the interpretation of isotopic evolution in the Cambrian is similar to that of the Neoproterozoic in which magmatism occurred in an active continental margin and involved a low crustal contribution to a moderate to high mantle contribution. The rocks having been generated through the mixing of juvenile magmas with an older continental crust.

The T_{2DM} and epsilon values calculated based on the isotopic data reveal that at least two crustal blocks in Central Iran can be recognized in different Cambrian time periods. Therefore, samples from the northwestern (Khoy) and northeastern Central Iran (Taknar and part of Delbar Complex) have different epsilon values but similar T_{2DM}, indicating derivation for the same source region but at different times. (**Fig.5.4. A- D**). Furthermore, based on the calculated T_{2DM}, samples from the CIM (Saghand) and northeastern Central Iran (part of the Delbar complex) also show a similar protolithic source but generation at different times. The isotope data collected for the Cambrian rocks in WNT are summarized in Table (**5.2**).

Table 5. 2. The summary of isotope data for the Cambrian rocks in western Neo-Tethys.

Location Name	**Geological Zone**	**Crustal Block**	ε_{Hf}	ε_{Nd}	**Age** (Ma)	**Reference**
Dorud–Azna	NW-SSZ	NW-Central Iran	_	-6.9 to -6.5	525.6	(Shabanian et al., 2018)
Khoy	NW-SSZ	NW-Central Iran	+1.98	_	533	(Azizi et al., 2011)
Delbar	Central Iran	NE-Central Iran	-30 to +18.4	_	498.4-540.6	(Balaghi Einalou et al., 2014)
Saghand	CIM	CIM	-1.19 to +7.4	_	501- 535	(Chiu et al., 2017)
Taknar	Central Iran	NE-Central Iran	-3.8 to +4.8	-1.4	502-540	(Moghadam et al., 2017)

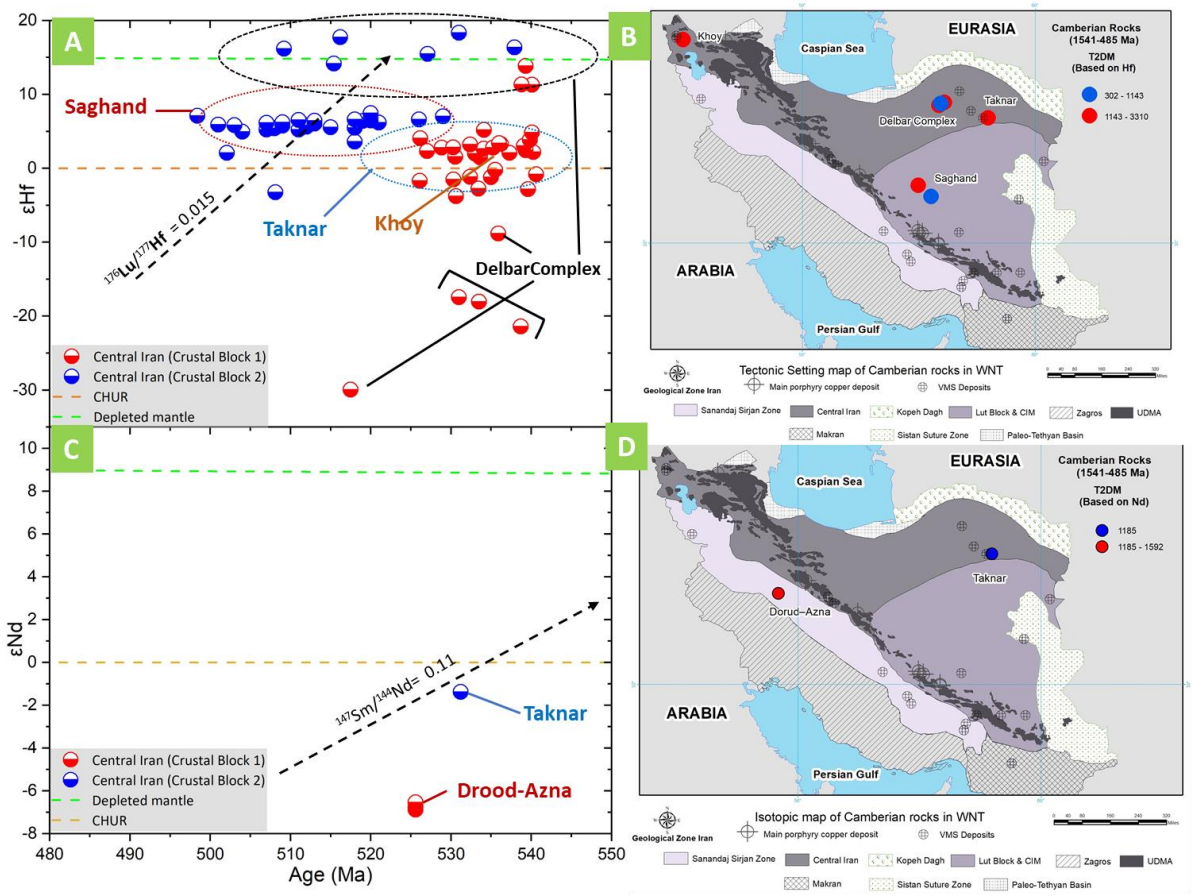

Figure 5. 4. Diagrams of ε_{Hf}(T) and ε_{Nd} (T) versus U-Pb ages and the Cambrian rocks' distribution on the WNT. The legend corresponds to the different crustal blocks in WNT. The arrow shows the isotope composition trend for the intermediate crustal rocks. (**A**) ε_{Hf} (T) versus magmatic ages (**B**) Distribution of T_{2DM} isotopic data on WNT, calculated based on Hf isotopic composition. (**C**) ε_{Nd} (T) versus magmatic ages (**D**) ε_{Nd} (T) Distribution of T_{2DM} isotopic data on WNT, calculated based on Nd isotopic composition.

5.1.3. Devonian 419.2-358.9 (Ma)

A few isotopic data have been reported from Devonian igneous and metamorphic rocks in the western Neo-Tethys (Chiu et al., 2017; Moghadam, 2016; Balaghi Einalou et al., 2014). The samples include the northwest part of the UDMA (Saqqez and Takab area) and Central Iran (Delbar complex). Devonian age rocks from the Delbar Complex have zircon ε_{Hf} (T) values of -4.64 which is interpreted to still reflect crustal contribution in a subduction environment magmatism in Central Iran (**Fig.5.5. A, B)**. Samples from Saqqez and Takab have yielded zircon ε_{Hf} (T) values +0.9 and -1.27 to -2.56, respectively. These data are interpreted as the crustal contribution in a subduction environment with partially evolved juvenile magmas in the Saqqez area based on the slightly positive ε_{Hf} (T) value.

The T_{2DM} and epsilon values calculated based on the isotopic data reveal that at least two crustal blocks in Central Iran can be recognized in different Devonian time periods. Therefore, samples from the northwestern (Takab) and northeastern Central Iran (Delbar Complex) have different epsilon values but similar T_{2DM}, indicating likely derivation for the same source region but at different times. Furthermore, based on the calculated T_{2DM}, in northwestern Central Iran, samples from the Saqqez region show the different sources of protolith from the Takab area during the Devonian (**Fig.5.5. A, B**). The isotope data collected for the Devonian rocks in WNT are summarized in Table (**5.3**).

Table 5. 3. The summary of isotope data for the Devonian rocks in western Neo-Tethys.

Location Name	Geological Zone	Crustal Block	ε_{Hf}	ε_{Nd}	**Age** (Ma)	**Reference**
Saqqez	NW-UDMA	NW-Central Iran	+0.9	_	359	(Chiu et al., 2017)
Takab	NW-UDMA	NW-Central Iran	-1.27 to -2.56	_	386-397	(Moghadam et al., 2016)
Delbar Complex	Central Iran	NE-Central Iran	-4.64	_	390.7	(Balaghi Einalou et al., 2014)

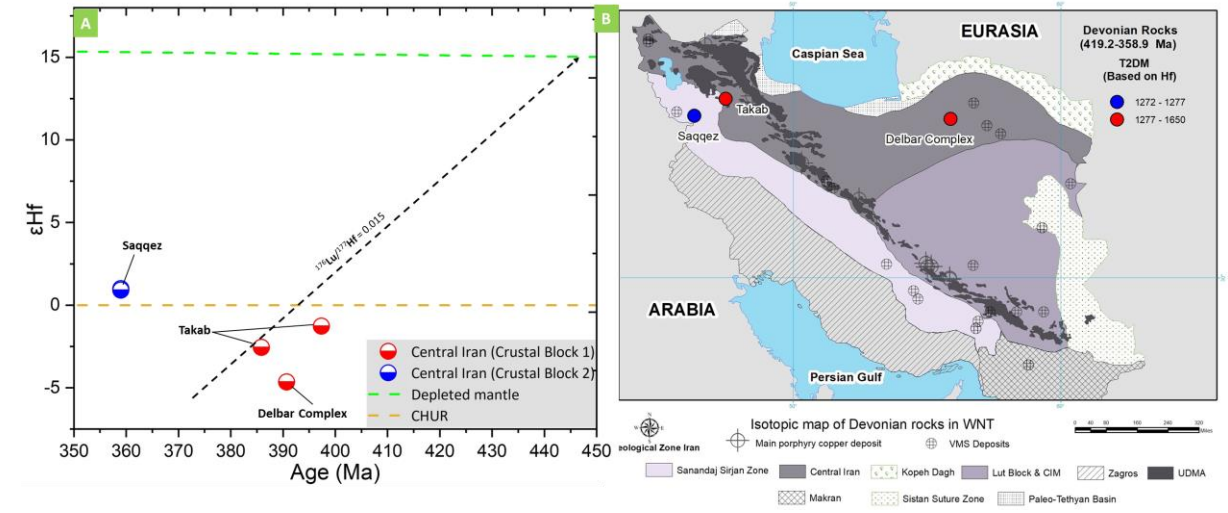

Figure 5. 5. Diagrams of ε_{Hf}(T) versus U-Pb ages and the distribution of the Devonian rocks on the WNT. The legend corresponds to the different crustal blocks in WNT. The arrow shows the isotope composition trend for the intermediate crustal rocks. (**A**) ε_{Hf}(T) versus magmatic ages (**B**) Distribution of T_{2DM} isotopic data on WNT, calculated based on Hf isotopic composition.

5.1.4. Carboniferous 358.9-298.9 (Ma)

Based on the Sr/Y vs. Y geochemical discrimination diagram samples from the northwest part of the UDMA, do not exhibit an adakaitic signature (**Fig.5.6. C**). Furthermore, mafic rocks plot in the OIB signature (**Fig.5.6. B, C**), whereas felsic samples plot in the setting of VAG and

WPG for these areas (**Fig.5.6. A, D**).

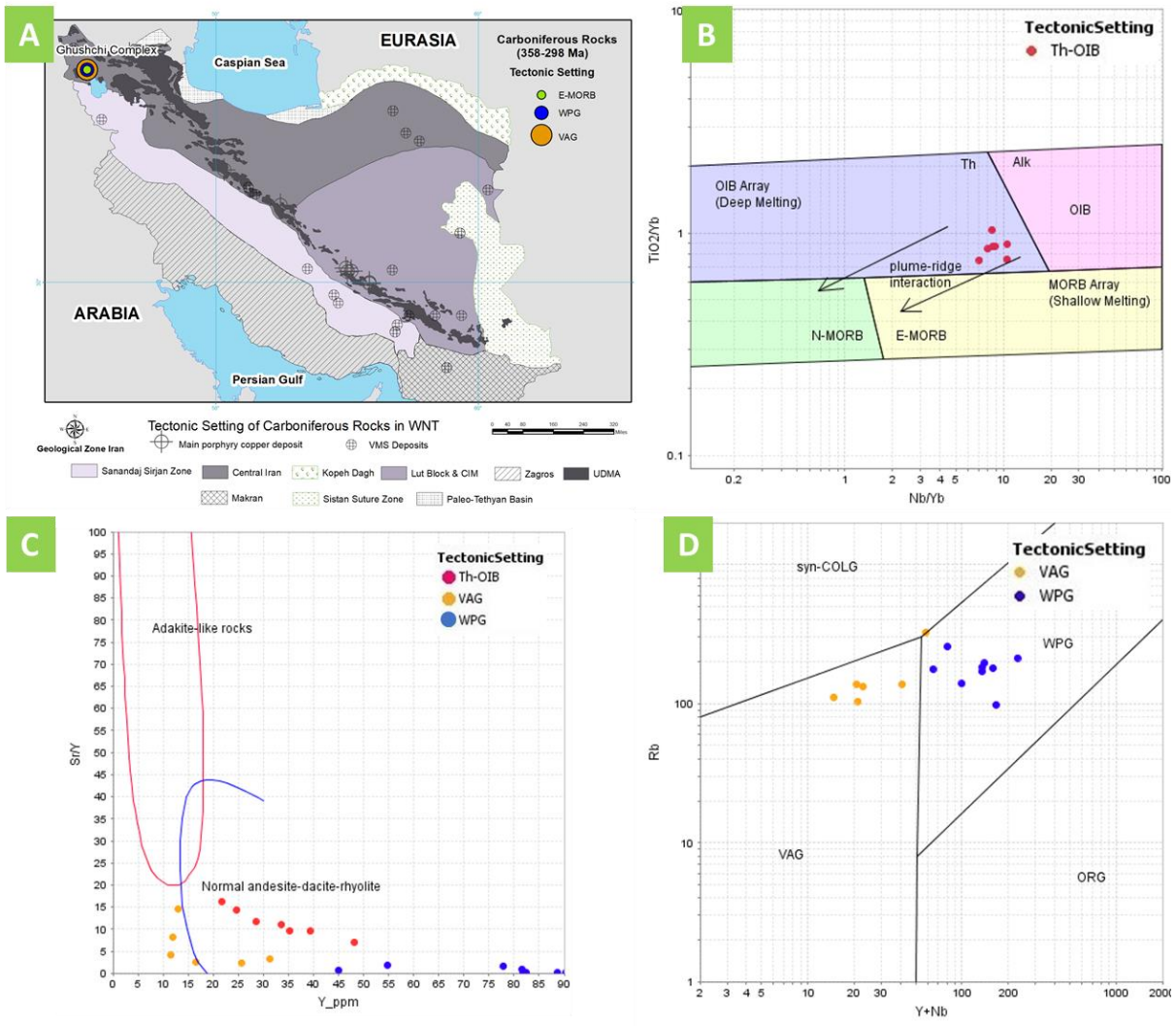

Figure 5. 6. Classification and geochemical characterization of Igneous and metamorphic rocks from Carboniferous rocks in the WNT (**A**) Location of Ghushchi granites on northwest part of the SSZ (Moghadam & Stern, 2015). (**B**) the TiO_2/Yb–Nb/Yb diagrams are used to separate subduction-related from subduction-unrelated mafic rocks (Pearce, 2014). (**C**) Sr/Y vs. Y (ppm) diagram of Cambrian rocks from the WNT (Defant & Drummond, 1993). (**D**) Rb vs. (Y + Nb) discriminant diagrams for the tectonic setting of felsic rocks in the study area (Pearce, Harris, & Tindle, 1984).

Carboniferous magmatism in the northwest part of the UDMA is represented by the Ghushchi granites and gabbronorites which are interpreted to be A-type granites emplaced at ~320 (Ma). In the northwest part of the UDMA, samples from Naqadeh have yielded zircon ε_{Hf} (T) values between -1.56 to +3.19, whereas samples from Saqqez and Takab have yielded zircon ε_{Hf} (T) values -0.51 to +4.15 and +3, respectively. These results are interpreted to represent juvenile mantle input in overall NW-UDMA and partially evolved with mixing the crustal contribution in

a rifting environment. Meanwhile, samples from the Khalifan region in the northwest part of the SSZ have ε_{Nd} (T) values between -1.14 to -0.93 which is interpreted to be the product of slight crustal contribution to of magmas generated during the opening of the Neo-Tethys in the northwest part of the Sanandaj Sirjan Zone.

The T_{2DM} and epsilon values calculated based on the isotopic data reveal that at least two crustal blocks can be recognized in northwestern Central Iran in Carboniferous time, although in different temporal events. Therefore, samples from Saqqez, Naqadeh, Khalilfan, and Takab have different epsilon values but similar T_{2DM}, indicating likely derivation for the same source region but at different times. Furthermore, based on the calculated T_{2DM}, samples from the Saqqez area show two different crustal blocks during the Carboniferous (**Fig.5.7. A-D**). The isotope data collected for the Carboniferous rocks in WNT are summarized in Table (**5.4**).

Table 5. 4. The summary of isotope data for the Carboniferous rocks in western Neo-Tethys.

Location Name	**Geological Zone**	**Crustal Block**	ε_{Hf}	ε_{Nd}	**Age** (Ma)	**Reference**
Saqqez	NW-UDMA	NW- Central Iran	-0.51 to +4.15	_	302-356	(Chiu et al., 2017)
Takab	NW-UDMA	NW- Central Iran	+3	_	325	(Moghadam et al., 2016)
Naqadeh	NW-UDMA	NW- Central Iran	-1.56 to +3.19	_	300-333	(Chiu et al., 2017)
Khalifan	NW-SSZ	NW- Central Iran	_	-1.14 to -0.93	315	(Bea, 2011)

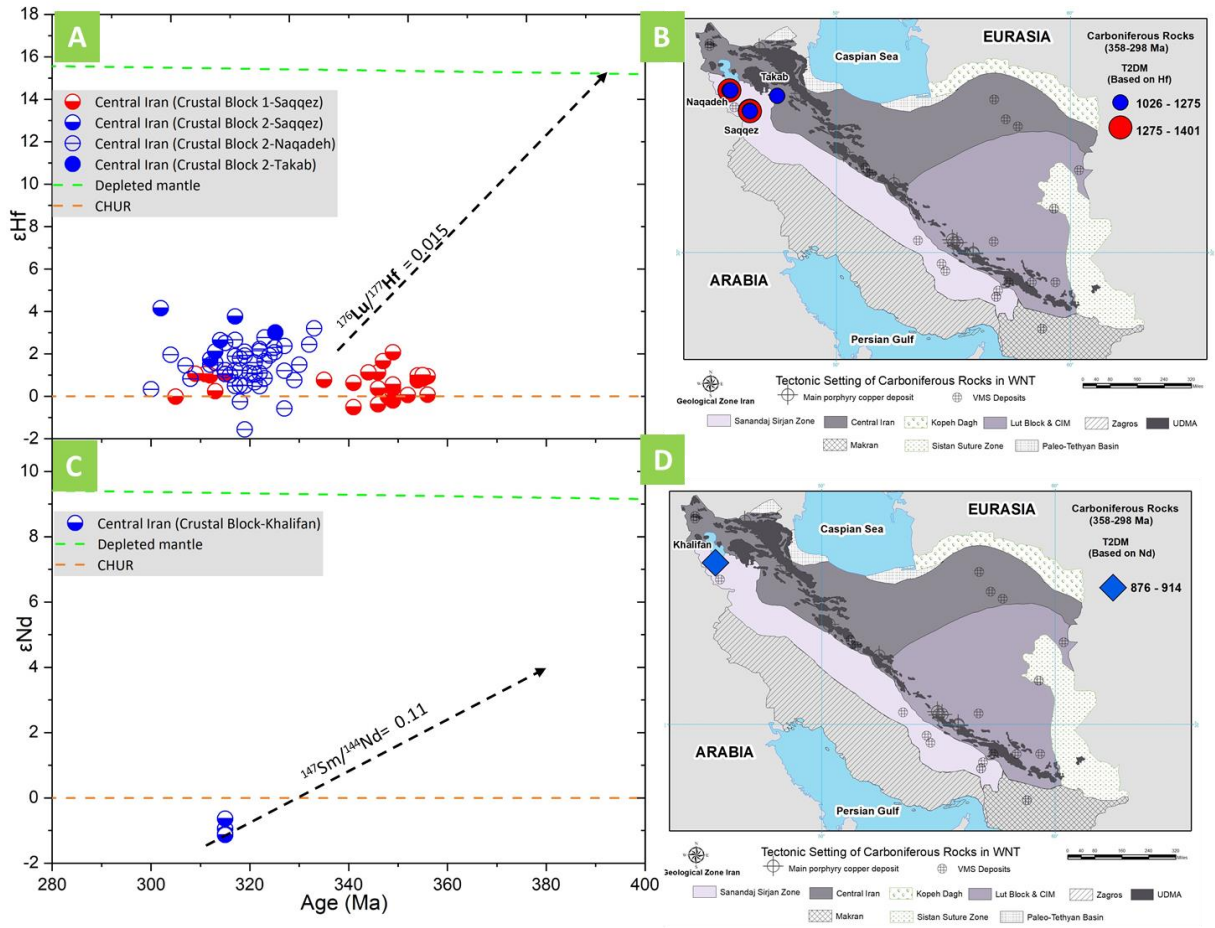

Figure 5. 7. Diagrams of ε_{Hf}(T) and ε_{Nd} (T) versus U-Pb ages and the Carboniferous rocks' distribution on the WNT. The legend corresponds to the different crustal blocks in WNT. The arrow shows the isotope composition trend for the intermediate crustal rocks. (**A**) ε_{Hf} (T) versus magmatic ages (**B** Distribution of T_{2DM} isotopic data on WNT, calculated based on Hf isotopic composition. (**C**) ε_{Nd} (T) versus magmatic ages (**D**) ε_{Nd} (T) Distribution of T_{2DM} isotopic data on WNT, calculated based on Nd isotopic composition.

5.1.5. Permian 298.9-251.9 (Ma)

The Hasanrobat A-type granite in the central part of the SSZ yielded $^{206}Pb/^{238}U$ age of 288.3±3.6 Ma and is interpreted to reflect a period of significant extension and related intraplate magmatism in the Upper Paleozoic of Iran (Alirezaei & Hassanzadeh, 2012). Similar intrusions occur in the Sabalan-Arasbaran, Takab, and Natanz region along the UDMA; the emplacement of these are considered to be related to the opening of Neo-Tethys Ocean between Sanandaj–Sirjan and Zagros during the Gondwana break-up in Lower Permian (Chiu et al., 2013; Moghadam et al., 2016).

It has been proposed that the SSZ and Central Iran began rifting from the Zagros basin during the opening of the Neo-Tethys Ocean in the Permian (Berberian & King, 1981). In contrast,

Mohajjel et al. (2003) found that seafloor spreading, and rifting occurred in the Permian–Triassic periods, followed by the subduction during the Upper Jurassic–Cretaceous.

Based on the Sr/Y vs Y discrimination diagram (Defant & Drummond, 1993), there is no adakaitic signature in these regions during the Permian (**Fig.5.8. C**). Mafic rocks have shown E-MORB signature (**Fig.5.8. B**) whereas felsic rocks plot in the tectonic setting of WPG for these areas (**Fig.5.8. D**).

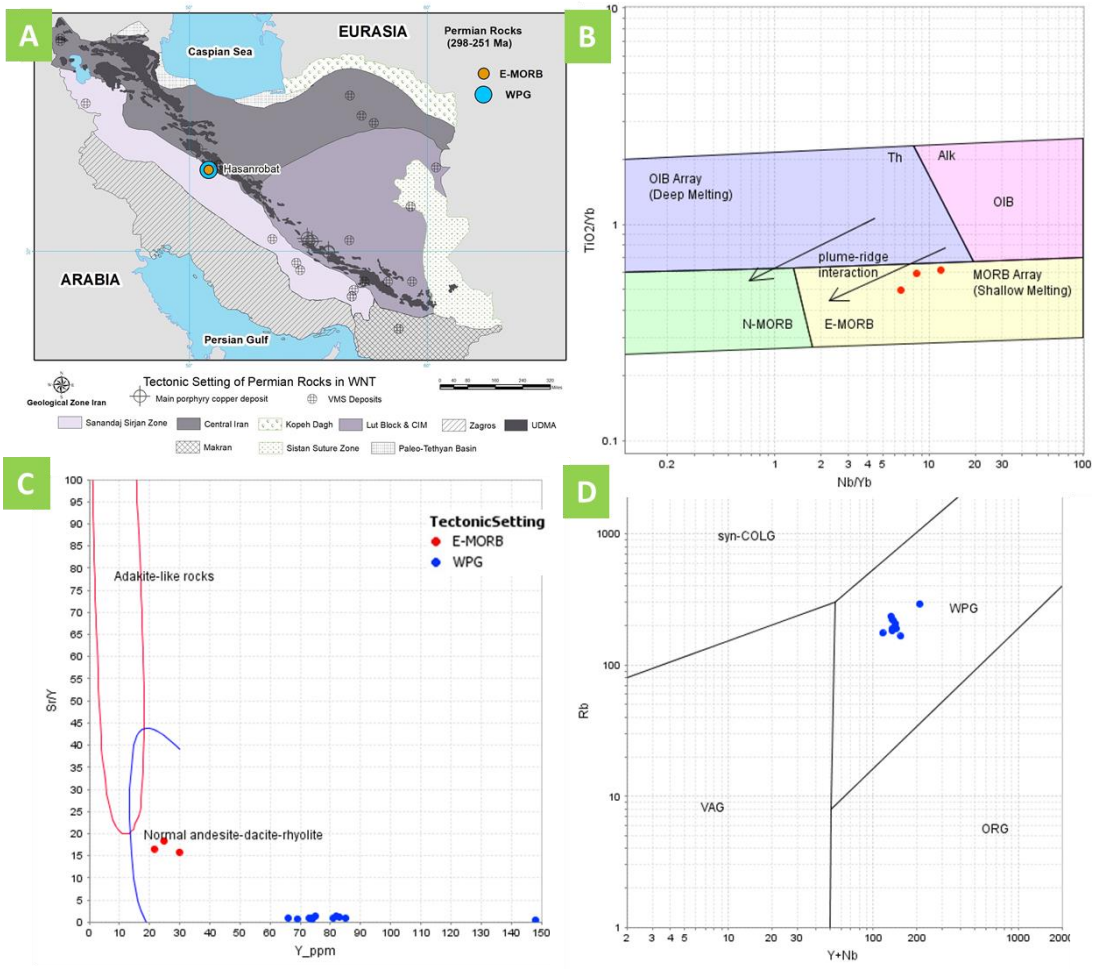

Figure 5. 8. Classification and geochemical characterization of Igneous and metamorphic rocks from Permian rocks in the WNT (**A**) Location of Hasanrobat Granite, the central part of the SSZ (Alirezaei & Hassanzadeh, 2012). (**B**) the TiO_2/Yb–Nb/Yb diagrams diagram is used to separate subduction-related from subduction-unrelated mafic rocks (Pearce, 2014). (**C**) Sr/Y vs. Y (ppm) diagram of Cambrian rocks from the WNT (Defant & Drummond, 1993). (**D**) Rb vs. (Y + Nb) discriminant diagrams for the tectonic setting of felsic rocks in the study area (Pearce, Harris, & Tindle, 1984).

In the northwest part of the UDMA, samples from the Takab and Sabalan-Arasbaran areas have yielded zircon $\varepsilon_{Hf}(T)$ values +12.05 and +4.72, respectively (**Fig.5.9. A, B**). Furthermore,

samples from the Natanz area have zircon $\varepsilon_{Hf}(T)$ values between +0.43 to +4.46. These results are interpreted to represent juvenile mantle input across the northwest part of the UDMA and C-UDMA during Permian–Triassic rifting and seafloor spreading.

The T_{2DM} and epsilon values calculated based on the isotopic data reveal that at least two crustal blocks in northwestern Central Iran can be recognized at different periods during the Permian. Therefore, samples from Takab and Natanz have different epsilon values but similar T_{2DM}, indicating likely derivation for the same source region but at different times. Furthermore, based on the calculated T_{2DM}, compared to the Takab and Natanz areas in northwestern and central Iran, samples from the Sabalan-Arasbaran area show a different crustal block during the Carboniferous (**Fig.5.9. A, B**). The isotope data collected for the Permian rocks in WNT are summarized in Table (**5.5**).

Table 5. 5. The summary of isotope data for the Permian rocks in western Neo-Tethys.

Location Name	**Geological Zone**	**Crustal Block**	ε_{Hf}	ε_{Nd}	**Age** (Ma)	**Reference**
Sabalan-Arasbaran	NW-UDMA	NW- Central Iran	+12.05	_	283	(Chiu, 2013)
Takab	NW-UDMA	NW- Central Iran	+4.72	_	282	(Moghadam et al, 2016)
Natanz	C-UDMA	C-Central Iran	+0.43 to +4.46	_	295 to 271	(Chiu, 2013)

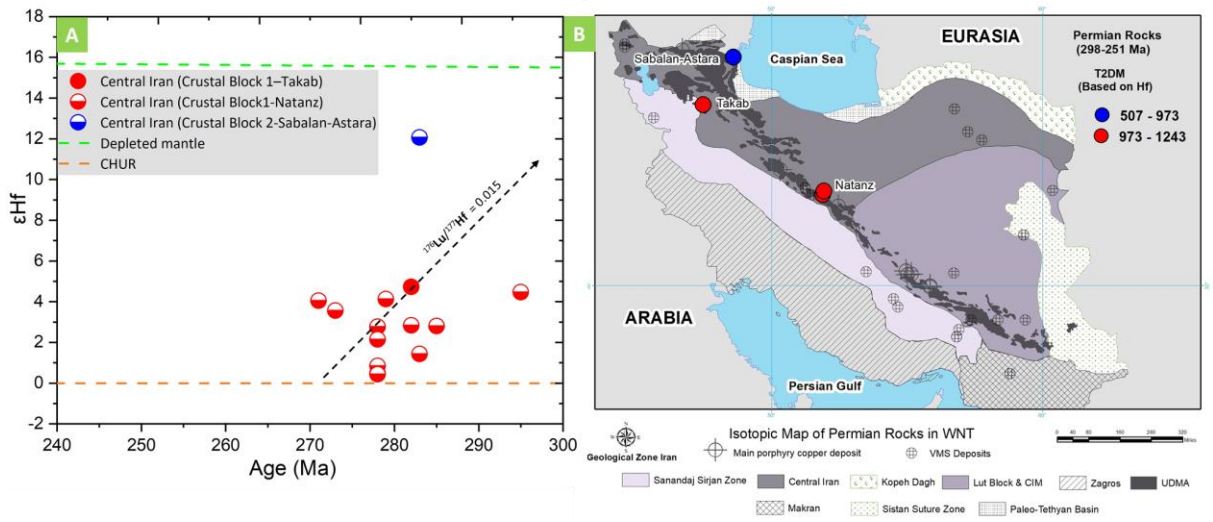

Figure 5. 9. Diagrams of ε_{Hf} (T) versus U-Pb ages and the Permian rocks' distribution on the WNT. The legend corresponds to the different crustal blocks in WNT. The arrow shows the isotope composition trend for the intermediate crustal rocks. (**A**) ε_{Hf} (T) versus magmatic ages (**B**) Distribution of T_{2DM} isotopic data on WNT, calculated based on Hf isotopic composition.

5.1.6. Triassic 251.9-201.3 (Ma)

Zircon ε_{Hf} (T) values from Triassic age rocks from the northwest part of the UDMA show a similar trend as that of Permian samples from this region. Samples from the Sabalan-Astara and Takab area have zircon ε_{Hf} (T) values between +0.60 to +3.45 and +7.41, respectively, in the northwest part of the UDMA (**Fig.5.10. A, B**). They are interpreted as juvenile mantle input throughout the entire UDMA, especially in the northwest part of the UDMA during the rifting and seafloor spreading phase of Neo-Tethys Ocean in Permian–Triassic times. Furthermore, the Mashhad granodiorites and diorites give slightly lower zircon ε_{Hf}(T) values between -3.13 and +2.16, implying a magmatic derivation from mixed juvenile and reworked sources. They are interpreted to be a product of the closing of the Paleo-Tethys in the eastern Alborz Zone.

The T_{2DM} and epsilon values calculated based on the isotopic data reveal that at least two crustal blocks in the northwestern and northeastern parts of Central Iran can be recognized in different Triassic time periods. Samples from Takab and Sablan-Arasbaran regions have different epsilon values but similar T_{2DM}, indicating likely derivation for the same source region but at different times. Furthermore, based on the calculated T_{2DM}, compared to the Takab and Sablan-Arasbaran areas in northwestern, central Iran, the Mashhad area shows a different crustal block during the Triassic time (**Fig.5.10. A, B**). The isotope data collected for the Triassic rocks in WNT are summarized in Table (**5.6**).

Table 5. 6. The summary of isotope data for the Triassic rocks in western Neo-Tethys.

Location Name	Geological Zone	Crustal Block	ε_{Hf}	ε_{Nd}	Age (Ma)	Reference
Sabalan-Astara	NW-UDMA	NW- Central Iran	+0.60 to +3.45	_	224-243	Chiu et al., 2013
Takab	NW-UDMA	NW- Central Iran	+7.41	_	226	(Moghadam et al., 2016)
Mashhad	Central Iran (Paleo-Tethys basin)	NE- Central Iran	-3.13 to +2.16	_	203-227	(Chiu et al., 2017)

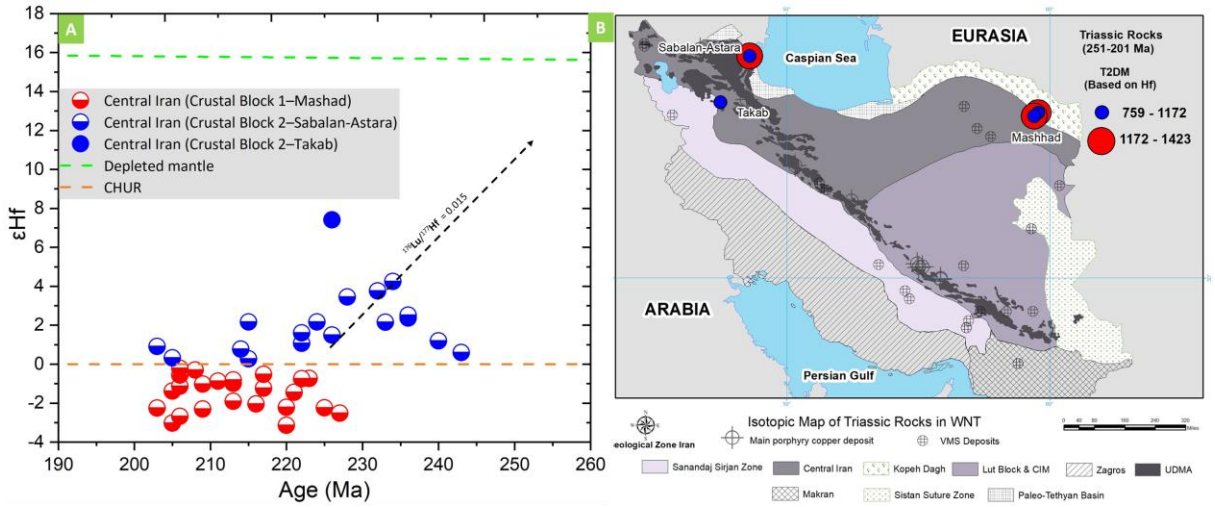

Figure 5. 10. Diagrams of $\varepsilon_{Hf}(T)$ versus U-Pb ages and the distribution of the Triassic rocks on the WNT. The legend corresponds to the different crustal blocks in WNT. The arrow shows the isotope composition trend for the intermediate crustal rocks. (**A**) $\varepsilon_{Hf}(T)$ versus magmatic ages (**B**) Distribution of T_{2DM} isotopic data on WNT, calculated based on Hf isotopic composition.

5.1.7. Jurassic 201.3-145 (Ma)

A series of Triassic-Cretaceous intrusions emplaced in a volcanic arc and back-arc tectonic setting occurs in the Sanandaj-Sirjan Zone of the Zagros orogenic belt in south-central Iran (**Fig.5.11)**. The intrusions are mainly I-type granites and are interpreted to be related to the onset of the subduction of the Neo-Tethys oceanic crust beneath the CIM in Triassic time. (Chiu et al., 2013; Esna-Ashari et al., 2012; Khalaji et al., 2007; Azizi et al., 2015; Ahadnejad et al., 2011; Azizi et al., 2011; Shakerardakani et al., 2015). In addition, dike swarms with an OIB signature are interpreted to have been generated from the enriched mantle in the subduction zone (**Fig.5.12. A**). These dykes have intruded the Kangareh-Taghiabad plutons in Ghorveh, Astaneh, and Droud-Azna area in the northwest part of the Sanandaj Sirjan Zone (Azizi et al., 2015; Esna-Ashari et al., 2012; Shakerardakani et al., 2015).

Azizi et al. (2015) proposed that the low initial $^{87}Sr/^{86}Sr$ ratios (0.7034 to 0.7054) and positive εNd(t) values (+3 to+8) indicate a depleted mantle source for Kangareh-Taghiabad in the northwest part of the Sanandaj Sirjan Zone. However, our calculation values for $\varepsilon_{Nd}(T)$ (-2.76 to +1.54) showed slight crust contamination and depleted mantle source for these rocks. These results propose an arc and back-arc tectonic setting in an intra-oceanic system than the Andean magmatic type regime for the origin of Kangareh-Taghiabad bodies in the Middle to Late Jurassic period. It is believed that intra-oceanic arc systems are built on oceanic crust, whereas Andean-type arcs are built on the pre-existing continental crust (Stern & Scholl, 2010). These plutons merged with the northwest part of the SSZ during accretion-type continental growth in the Late Jurassic. Furthermore, compositions indicate an adakitic signature for Kangareh-Taghiabad intrusions and Ghalaylan Complex during the Jurassic. Simultaneously, there is no such attribute for other regions in the northwest part of the SSZ (**Fig.5.12. B**). However, there is not enough evidence about the existence of the older metamorphic basement in some areas like Ghorveh (Kangareh-Taghiabad and Ghalaylan Complex) in the northwest part of the Sanandaj Sirjan Zone. Moreover, It is believed that the inner ophiolite belt in Iran was related to a back-arc basin and the mafic rocks in the central part of the SSZ originate from the same source (Ghazi et al., 2012; Moghadam & Stern, 2011).

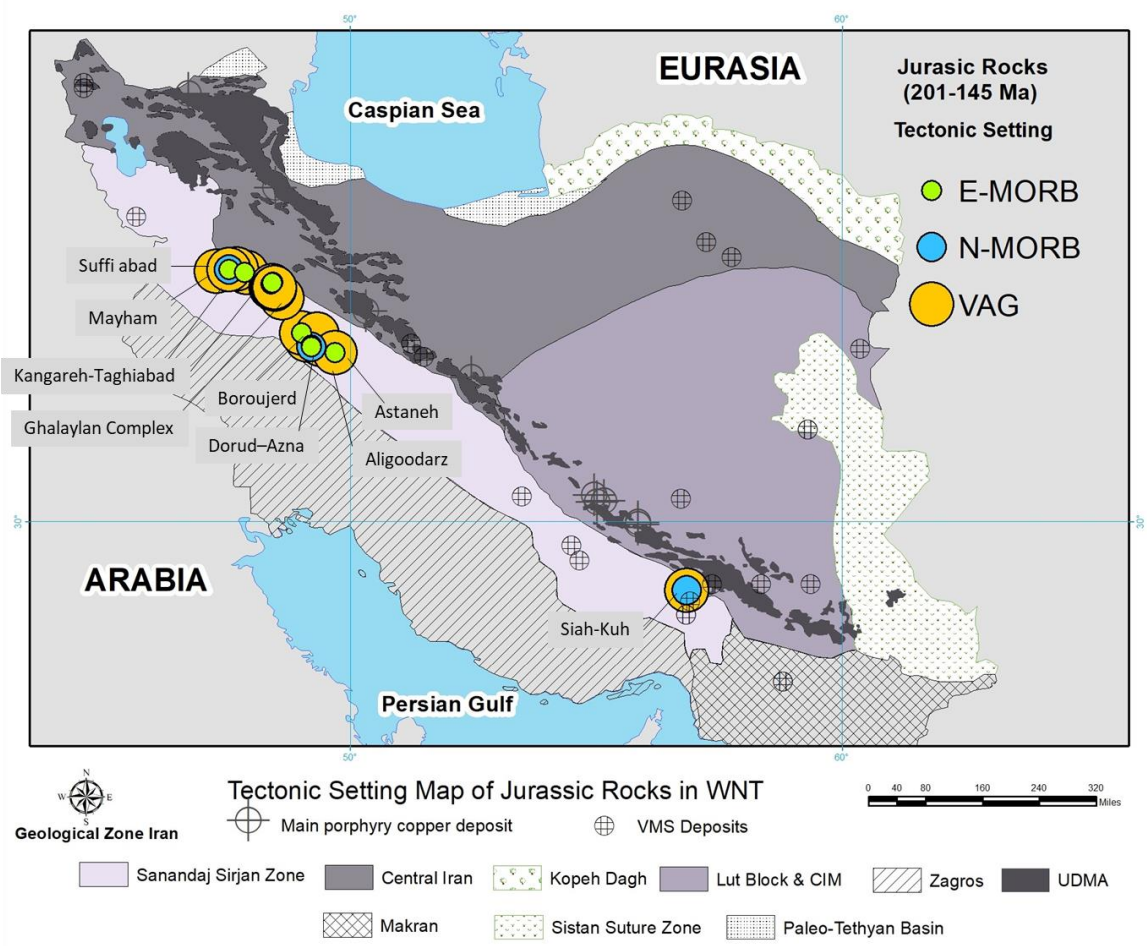

Figure 5. 11. Location of Jurassic rocks with their tectonic setting in the western Neo-Tethys.

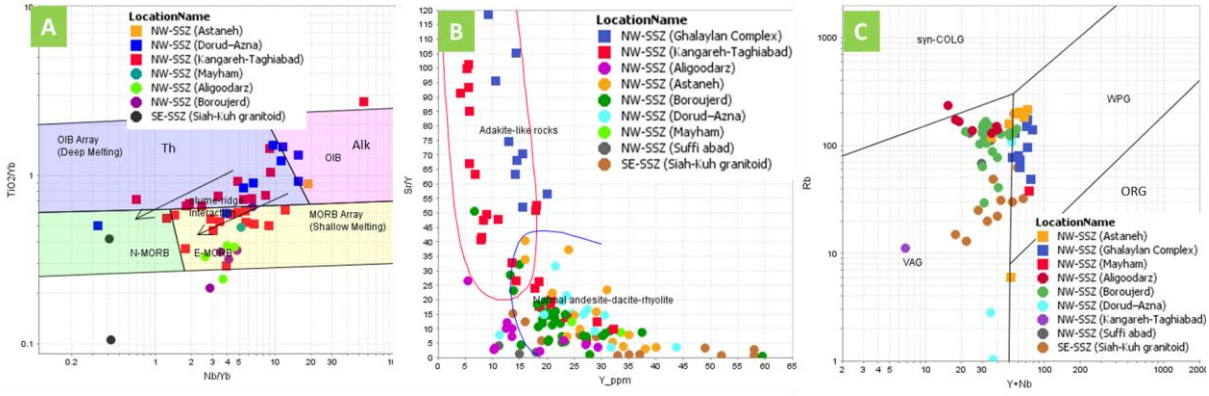

Figure 5. 12. Classification and geochemical characterization of Igneous and metamorphic rocks from Jurassic rocks in the WNT. (**A**) the TiO_2/Yb–Nb/Yb diagrams diagram is used to separate subduction-related from subduction-unrelated mafic rocks (Pearce 2014). (**B**) Sr/Y vs. Y (ppm) diagram of Cambrian rocks from the WNT (Defant & Drummond, 1993). (**C**) Rb vs. (Y + Nb) discriminant diagrams for the tectonic setting of felsic rocks in the study area (Pearce, Harris, & Tindle, 1984).

The Sr-Nd isotope ratios imply high ratios of $^{143}Nd/^{144}Nd$ (0.5125–0.5127) and low initial ratios of $^{87}Sr/^{86}Sr$ (0.7024–0.7069). In particular, the positive ε_{Nd} (+1.44 to +4.87) for the Suffi Abad granite would be consistent with it having been generated from the depleted mantle over the subduction zone (Azizi et al., 2011). Moreover, samples from the Hamdan and Bam-Jiroft areas in the northwest part of the SSZ have zircon ε_{Hf} (T) values between +0.55 to +4.04 and +6.29, respectively. These values are interpreted as reflecting juvenile mantle input throughout the subduction of Neo-Tethys during the Middle to Late Jurassic. In the Esfahan area in the central part of the SSZ samples have zircon ε_{Hf} (T) values between -3.35 to +1.3, whereas samples from the Alvand and Ghalaylan areas have zircon ε_{Nd} (T) values between -3.57 to +3.24 and -0.756 to +3.41, respectively. This range in values is consistent with magmas generated from a mixed juvenile and reworked magma history formed in the subduction zone of Neo-Tethys in the northwest part of the Sanandaj Sirjan Zone.

Samples from the Yazd and Bazman area have zircon ε_{Hf} (T) values between -2.62 to +2.23 and -2.59 to +3.68, respectively, implying an origin of mixed juvenile and reworked sources. These rocks are interpreted to have been formed as a result of the subduction of Neo-Tethys oceanic crust in the central part of the UDMA and southeast part of the UDMA. In addition, a sample from the Bam-Jiroft area yields a zircon εHf (T) value +6.29 which is consistent with derivation from a juvenile mantle source without significant crustal contamination in SE-UDMA. As a result of the closing of the Paleo-Tethys basin in the eastern part of Central Iran, Mashhad plutons yield zircon ε_{Hf}(T) values between -3.41 to +1.38, implying an origin of mixed reworked and juvenile sources to form the magmas (**Fig.5.13. A-C**).

The T_{2DM} and epsilon values calculated based on the Hf isotopic data reveal that at least three crustal blocks in the northwest part of the SSZ, Central part of the SSZ, and CIM can be recognized in different Jurassic periods (**Fig.15.3 A, B**). Furthermore, the T_{2DM} and epsilon values calculated based on the Nd isotopic data recognized two different crustal blocks in the northwest part of the Sanandaj Sirjan Zone. The two blocks are designated, i) crustal block 1 which includes the Aligoodarz, Boroujerd, and Malayer areas and ii) crustal block 2 which includes the Alvand, Suffi Abad, Ghalaylan, and Kangareh-Taghiabad. These two crustal blocks are distinguished on basis of having different epsilon values but similar T_{2DM}, indicating likely derivation for the same

source region at different times (**Fig.15.3. C, D**). The isotope data collected for the Jurassic rocks in WNT are summarized in Table (**5.7**).

Table 5. 7. The summary of isotope data for the Jurassic rocks in western Neo-Tethys.

Location Name	**Geological Zone**	**Crustal Block**	ε_{Hf}	ε_{Nd}	**Age** (Ma)	**Reference**
Yazd	C-UDMA	CIM	-2.62 to +2.23	_	163-174	Chiu et al., 2013
Bazman	SE-UDMA	CIM	-2.59 to +3.68	_	162-168	Chiu et al., 2013
Bam-Jiroft	SE-UDMA	CIM	+6.29	_	161	Chiu et al., 2013
Mashhad	Central Iran (Paleo-Tethys basin)	NE-Central Iran	-3.41 to +1.38	_	161-200	(Chiu et al., 2017)
Esfahan	Central-SSZ	Central-SSZ	-3.35 to +1.3	_	159-177	Chiu et al., 2013
Hamadan	NW-SSZ	NW-SSZ	+0.55 to +4.04	_	163-173	Chiu et al., 2013
Aligoodarz	NW-SSZ	NW-SSZ	_	-5.54 to -3.59	165	(Esna-Ashari, 2012)
Alvand	NW-SSZ	NW-SSZ	_	-3.57 to +3.24	171.7	(Shahbazi et al., 2010)
Boroujerd	NW-SSZ	NW-SSZ	_	-3.67 to -3.08	169.6-170.7	(Khalaji et al., 2007)
Ghalaylan	NW-SSZ	NW-SSZ	_	-0.756 to +3.41	157.8	(Azizi et al., 2015)
Kangareh-Taghiabad	NW-SSZ	NW-SSZ	_	-2.76 to +1.54	185-189	(Azizi et al., 2015)
Malayer	NW-SSZ	NW-SSZ	_	-4.61 to -2.68	161.9-187	(Ahadnejad et al., 2011)
Suffi Abad	NW-SSZ	NW-SSZ	_	+1.44 to +4.87	145-148.5	(Azizi, et al., 2011)

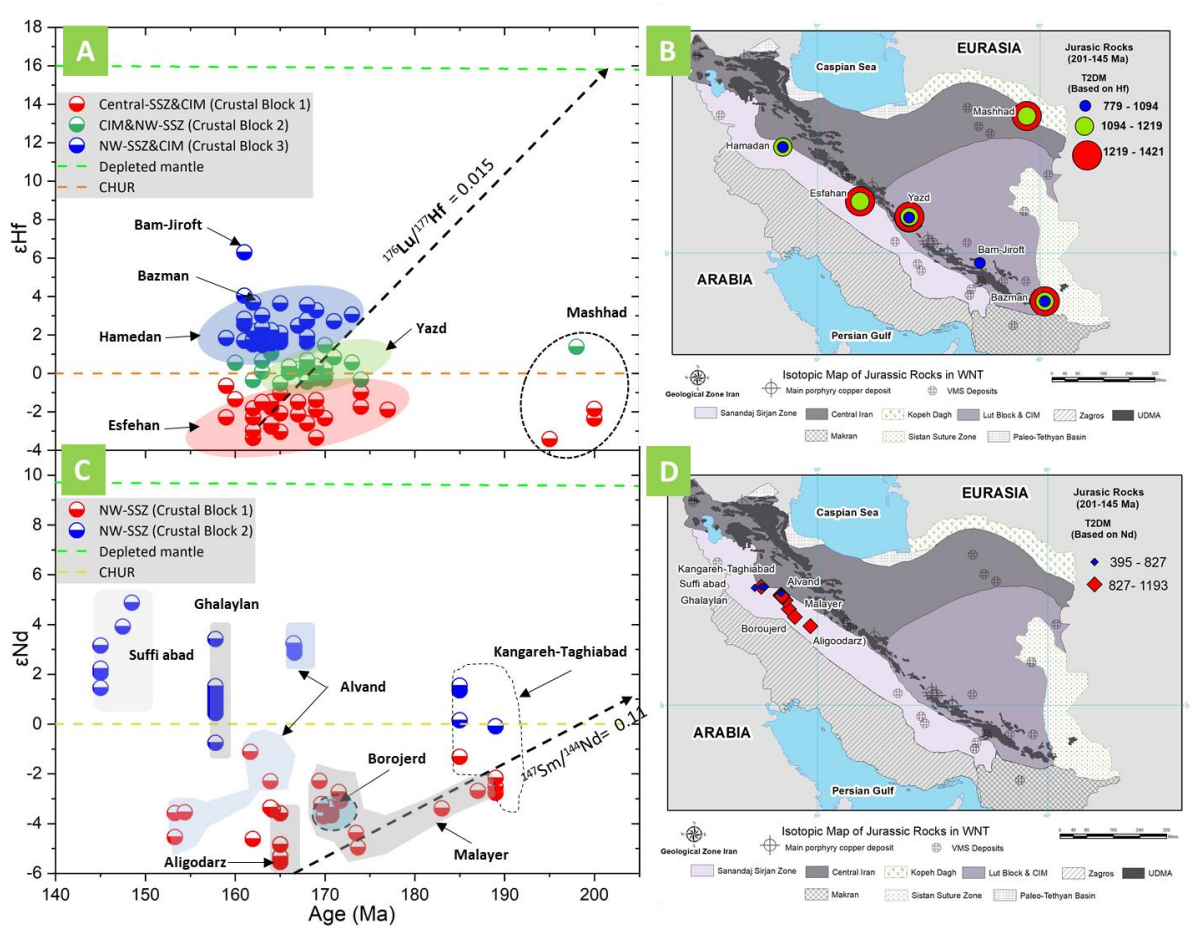

Figure 5. 13. Diagrams of ε_{Hf} (T) versus U-Pb ages and the distribution of the Jurassic rocks on the WNT. The legend corresponds to the different crustal blocks in WNT. The arrow shows the isotope composition trend for the intermediate crustal rocks. (**A**) Diagrams of ε_{Hf} (T) versus U-Pb ages (**B**) Distribution of T_{2DM} isotopic data on WNT, calculated based on Hf isotopic composition. (**C**) Diagrams of ε_{Nd} (T) versus U-Pb ages. (**D**) Distribution of T_{2DM} isotopic data on WNT, calculated based on Nd isotopic composition.

5.1.8. Cretaceous 145-66 (Ma)

The subduction of the Neo-Tethys oceanic crust under the CIM continued into the Cretaceous. Magmatism occurred dominantly in the arc and back-arc tectonic setting and generated the majority of Late Cretaceous ophiolite-arc systems. These Cretaceous rocks and related volcanic and plutonic rocks along the Zagros suture zone such as the Kata–Rash, Mishao, igneous rocks, and the Hasanbag, Kermanshah, Neyriz, Hasan Salary, Band-e-Zeyarat, and Dar Anar ophiolites (Moghadam, 2014; Saccani et al., 2014; Jafari et al., 2013; Moghadam et al., 2014; Ali et al., 2016; Abdulzahra et al., 2018; Babaie et al., 2001; Ghazi et al., 2004; Nouri et al., 2017; Nouri et al., 2016; Khosravi et al., 2017).

The Sabzevar ophiolite has been interpreted to have formed in an embryonic oceanic arc basin between the Lut block and the Binalud mountains (Turan plate) and existed during the mid-Cretaceous times (Hosseini et al., 2017). In the southeast part of the UDMA the Bahr Aseman igneous complex formed in a subduction-related island-arc setting associated with the evolution of the Neo-Tethys Ocean closure (Hosseini et al., 2017). Similarly, the Gazu I-type intrusive rocks were emplaced in a volcanic arc setting between the Lut and Tabas block in CIM (Mahdavi et al., 2016). Additional outcrops of Cretaceous igneous rocks include those of the Bam-Jiroft and Bazman area in the southeast part of the UDMA, the Mirabad, and Birjand ophiolite in Lut–Sistan Suture Zone, and the Almogholagh and Kangareh-Taghiabad bodies in NW- northwest part of the Sanandaj Sirjan Zone. These igneous rocks have been interpreted as related to arc magmatism of Neo-Tethys during the Late Cretaceous (Ghiasvand et al., 2017; Moghadam et al., 2016; Chiu et al. 2017; Chiu et al., 2013; Pang, 2014; Zarrinkoub et al., 2012; Amiri et al., 2017; Azizi et al., 2015; Abdulzahra et al., 2018). (**Fig. 5.14. B**).

On the TiO_2/Yb–Nb/Yb diagram, the Kata–Rash and Band-e-Zeyarat/Dar Anar ophiolites plot in the E-MORb and N-MORB, respectively (**Fig.5.14. A**). On the Rb vs. (Y + Nb) discriminant diagram, except for two samples of Band-e-Zeyarat/Dar Anar ophiolites, almost all the felsic rock samples define a VAG-arc setting (**Fig.5.14. D**). In the Sr/Y vs. Y (ppm) diagram of Cretaceous rocks, just a few samples from Sabzevar, Band-e-Zeyarat/ Dar Anar ophiolites, and Gazu I-type intrusive rocks show adakitic signature (**Fig.5.14. C**).

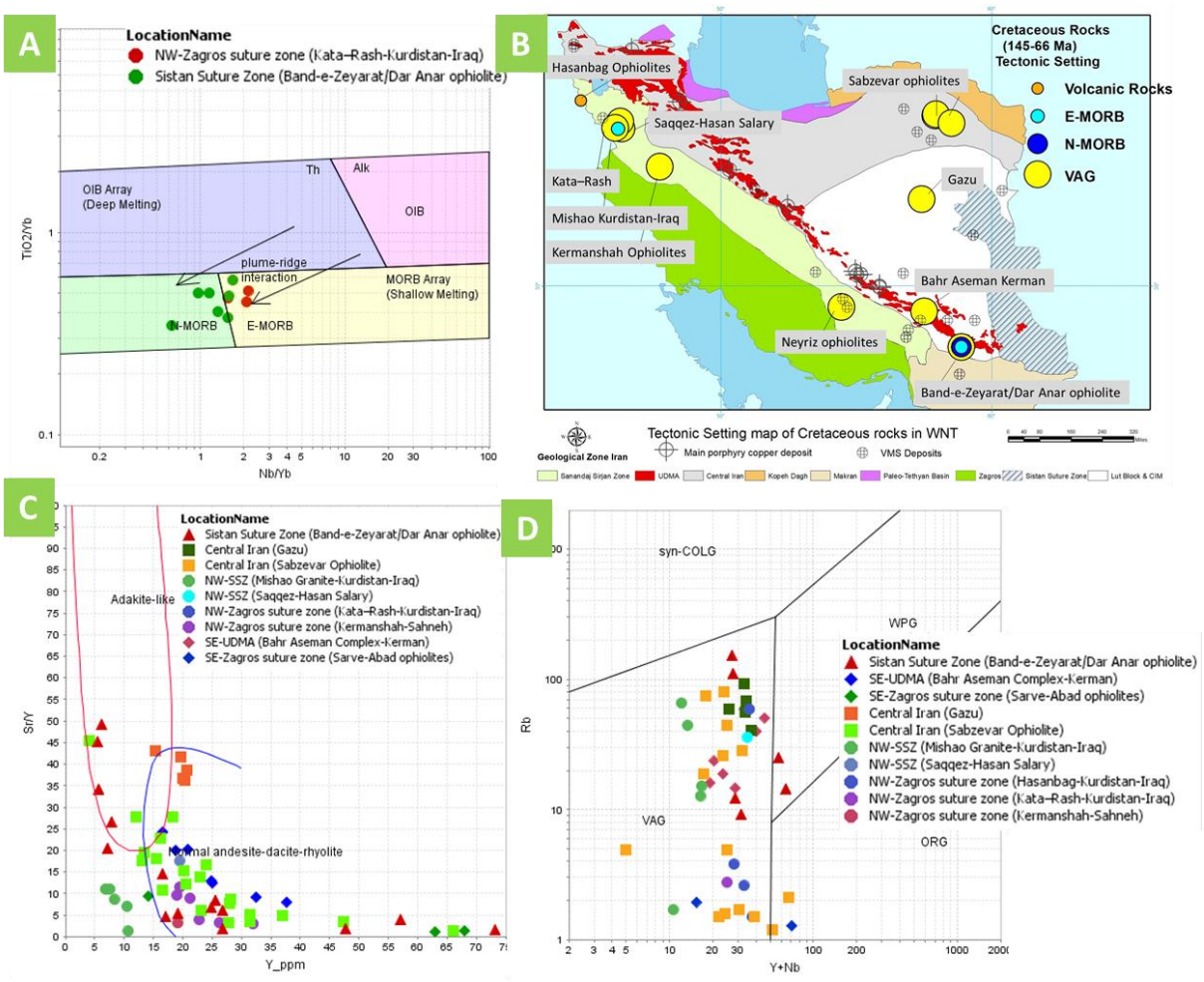

Figure 5. 14. Classification and geochemical characterization of Igneous and metamorphic rocks from Cretaceous rocks in the WNT. (**A, B**) the TiO_2/Yb–Nb/Yb and Th/Yb–Nb/Yb diagrams are used to separate subduction-related from subduction-unrelated mafic rocks (Pearce, 2014). (**C**) The distribution of the Cretaceous rocks on the WNT Geological map of Iran. (**D**) Sr/Y vs. Y (ppm) diagram of Cretaceous rocks from the WNT (Defant & Drummond, 1993). (**E**) Rb vs. (Y + Nb) discriminant diagram for the tectonic setting of felsic rocks in the study area (Pearce, Harris, & Tindle, 1984).

The ε_{Hf} (T) versus U-Pb age diagram (**Fig.5.15. A**) shows ε_{Hf} (T) values -9.03 to -4.76 and -1.90 to +4.53 for Bazman area and +10.46 to +15.91 values for Bam-Jiroft domain. The data is interpreted to reflect subduction-related magmatism during the Late Cretaceous (81–72 Ma) in the southeast part of the UDMA (Chiu et al., 2013). Data from the Bam-Jiroft suites indicate a homogeneous mantle source for the magma, whereas the Bazman data is consistent with an origin of mixed reworked and juvenile sources to form the magmas. Similar to the southeast part of the UDMA area, in the Takab area of the northwest part of the UDMA, rocks exhibit similar bimodal zircon ε_{Hf} (T) values from 0.05 to -2.43 and +6.04 to +7.2. Samples from the Mirabad area in the Sistan Suture Zone have zircon ε_{Hf} (T) values from +3.19 to +14.48, which are indicative of a

homogeneous mantle source (Moghadam et al., 2016). One sample from the Firouzeh mine in Central Iran has remarkably low zircon ε_{Hf}(T) values of -8.74, which is consistent with the melting of old continental crust (Ghiasvand et al., 2017).

In the northwest part of the SSZ, a bimodal zircon ε_{Nd} (T) values +2.74 to +7.67 and -1.66 to -0.36 for Kangareh-Taghiabad intrusion in Ghorveh, as well as -2.93 to -1.34 and +6.61 in Mishao I-type granite in Kurdistan-Iraq regions has been reported (Azizi et al., 2015; Abdulzahra et al., 2018). These values are interpreted as an origin of mixed juvenile and reworked sources to form the magmas during the subduction of Neo-Tethys. Furthermore, the Almogholagh pluton in the northwest part of the SSZ has zircon ε_{Nd} (T) values between +2.27 to +3.90 (Azizi et al., 2015) whereas the Birjand ophiolite in Lut–Sistan Suture Zone has ε_{Nd} (T) values between +3.37 to +8.36 (Zarrinkoub et al., 2012). These values are indicative of a homogeneous mantle source for these areas (**Fig.5.15, C**).

The T_{2DM} and epsilon values calculated based on the Hf isotopic data reveal that at least three crustal blocks in the northwest part of the SSZ and CIM can be recognized in different Cretaceous periods (**Fig.5.15 A, B**). Therefore, the northwestern SSZ and the CIM (Crustal block 1, including the Takab and some samples in Bazman) have different epsilon values but similar T_{2DM}, consistent with derivation from the same source region but at different times (**Fig.15.5 A, B**).

The T_{2DM} and epsilon values calculated based on the Nd isotopic data recognized three different crustal blocks in the northwest part of the SSZ and the CIM zone. Samples of Mishao granite in Iraqi Kurdistan and some samples in the Kangareh-Taghiabad area (Crustal block 1), some samples in Kangareh-Taghiabad area, and the samples of the Almogholagh region (Crustal block 2) from the northwestern SSZ have different epsilon values but similar T_{2DM}. The Birjand Ophiolites in the Lut block show a similar trend with some samples in Kangareh-Taghiabad in the northwestern SSZ (Crustal block 3). The similar trends in T_{2DM} and different epsilon values for these areas indicating likely derivation for these crustal blocks indicate likely derivation from the same source region but at different times (**Fig.15.5 C, D**). The isotope data collected for the Cretaceous rocks in WNT are summarized in Table (**5.8**).

Table 5. 8. The summary of isotope data for the Cretaceous rocks in western Neo-Tethys.

Location Name	Geological Zone	Crustal Block	ε_{Hf}	ε_{Nd}	Age (Ma)	Reference
Firouzeh mine	Central Iran	NE-Central Iran	-8.74	_	134	(Ghiasvand, 2017)
Takab	NW-UDMA	NW- Central Iran	-0.05 to -2.43 +6.04 to +7.2	_	106-76	(Moghadam et al., 2016)
Tehran	Alborz (Paleo-Tethys)	Alborz	+10.16 to +12.71	_	142-144	(Chiu et al., 2017)
Bam-Jiroft	SE-UDMA	Lut	+10.46 to +15.91	_	73-78	Chiu et al., 2013
Bazman	SE-UDMA	Lut	-9.03 to -4.76 -1.90 to +4.53	_	83-71	Chiu et al., 2013
Mirabad	Sistan Suture Zone	Lut	+3.19 to +14.48	_	66-94	(Pang et al., 2014)
Birjand ophiolite	Lut–Sistan Suture Zone	Lut	_	+3.37 to +8.36	112.8	(Zarrinkoub, 2012)
Almogholagh	NW-SSZ	NW-SSZ	_	+2.27 to +3.90	144	(Amiri et al., 2017)
Kangareh-Taghiabad	NW-SSZ	NW-SSZ	_	+2.74 to +7.67 -1.66 to -0.36	113	(Azizi et al., 2015)
Mishao -Kurdistan-Iraq	NW-SSZ	NW-SSZ		-2.93 to -1.34 +6.61	111.8	(Abdulzahra et al., 2018)

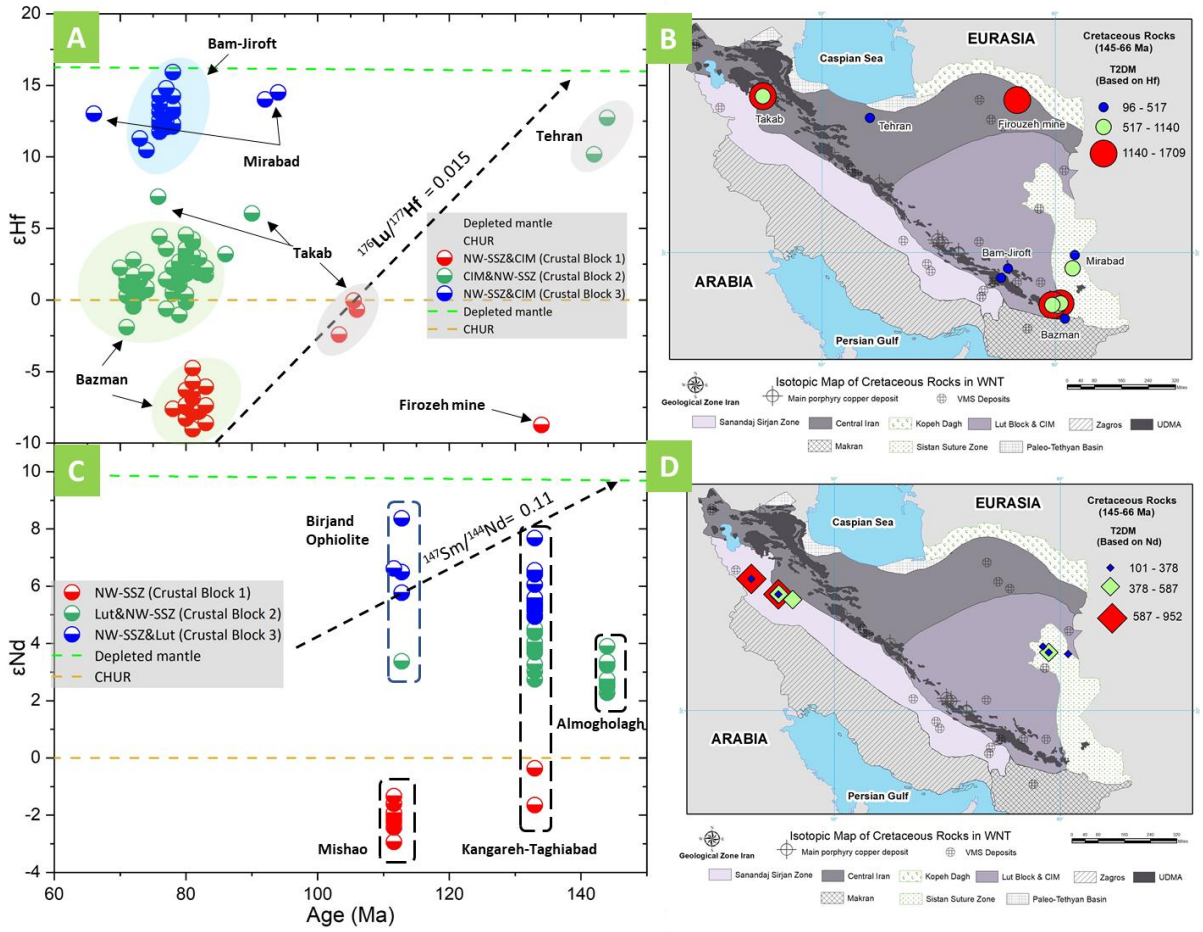

Figure 5. 15. Diagrams of ε_{Hf} (T) versus U-Pb ages and the Cretaceous rocks' distribution on the WNT. The legend corresponds to the different crustal blocks in WNT. The arrow shows the isotope composition trend for the intermediate crustal rocks. (**A**) Diagrams of ε_{Hf} (T) versus U-Pb ages (**B**) Distribution of T_{2DM} isotopic data on WNT, calculated based on Hf isotopic composition. (**C**) Diagrams of ε_{Nd} (T) versus U-Pb ages. (**D**) Distribution of T_{2DM} isotopic data on WNT, calculated based on Nd isotopic composition.

5.1.9. Paleocene 66-56 (Ma)

The subduction of the Neo-Tethys oceanic crust under the CIM continued into the Paleocene. Related volcanic and plutonic rocks revealed the same arc and back-arc tectonic setting as recorded in Late Cretaceous time. The magmatic rocks represent the remnants of the Neo-Tethyan Ocean preserved between the Arabian shield and Cimmerian terranes. They are exposed along the different geological zones (**Fig.5.16. C**) and represented by the Sahneh-Kermanshah, Neyriz, and Sabzevar ophiolites as well as the Saqqez-Hasan Salary, Hasanbag, Bahr Aseman, Bibi-Maryam, and Gazu igneous bodies (Saccani et al., 2014; Jafari et al., 2013; Moghadam et al., 2014; Babaie et al., 2001; Nouri et al., 2016; Allahyari, 2013, Allahyari et al., 2010; 2014; Saccani et al., 2013; Khosravi et al., 2017; Mahmoudi et al., 2011; Ali et al., 2013; Delavari et al.,

2014; Mahdavi et al., 2016; Hosseini et al., 2017; Monsef et al., 2018; Azizi et al., 2011; Pang et al., 2014; Moghadam et al., 2016).

Mafic samples plotted on a TiO_2/Yb–Nb/Yb diagram are distributed in both the E-MORB and N-MORB fields (**Fig.5.16. D**). In contrast, felsic rock samples plotted on Rb vs. (Y + Nb) diagram, fall within a VAG-arc setting (**Fig.5.16. A**). The magmatic ophiolitic rocks are interpreted to have been derived from a MORB-type mantle source and were metasomatized by fluids or melts from subducted sediments which would be consistent with emplacement in a super subduction zone environment in western Neo-Tethys.

In the Sr/Y vs. Y diagram, the majority of Paleocene samples from Bibi-Maryam, Saqqez-Hasan Salary, and Gazu I-type intrusive rocks when plotted on the Sr/Y vs. Y diagram fall within the adakitic field. Additionally, some samples of Bahr Aseman complex and Sahneh-Kermanshah, Sabzevar ophiolites, plot in the adakitic domain (**Fig.5.16. B**).

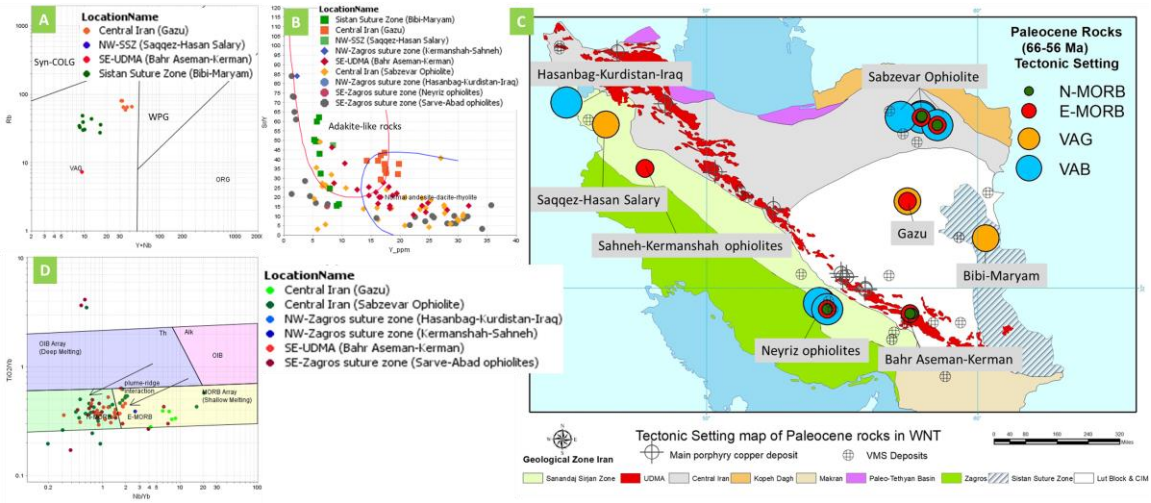

Figure 5. 16. Classification and geochemical characterization of Igneous and metamorphic rocks from Cretaceous rocks in the WNT. (**A**) Rb vs. (Y + Nb) discriminant diagrams for the tectonic setting of felsic rocks in the study area (Pearce, Harris, & Tindle, 1984). (**B**) Sr/Y vs. Y (ppm) diagram of Cretaceous rocks from the WNT (Defant & Drummond, 1993). (**C** The distribution of the Paleocene rocks on the WNT Geological map of Iran. (**D**) the TiO_2/Yb–Nb/Yb diagram is used to separate subduction-related from subduction-unrelated mafic rocks (Pearce, 2014).

Rocks from the Kamyaran area in the northwest part of the SSZ, the Takab region in the northwest part of the UDMA, and the Mirabad granitic pluton in the Sistan Suture Zone yield zircon $\varepsilon_{Hf}(T)$ values +10.27, +6.85 and between +3.95 to +15.29, respectively (Azizi et al., 2011; Moghadam et al., 2016; Pang et al., 2014). Furthermore, the Arghash I-type granitoid in Central

Iran yields an ε_{Nd} (T) value of +5.80 (Alaminia et al., 2013). These isotopic compositions are interpreted to represent a juvenile homogeneous mantle source for the magmas (**Fig.5.17. A-C**). They are interpreted have been emplaced in an arc and back-arc setting during Neo-Tethys subduction after the Cretaceous time (Richards, Wilkinson, & Ullrich, 2006; Moghadam & Stern 2011; Agard et al. 2011).

The T_{2DM} and epsilon values calculated for Paleocene rocks based on the Hf isotopic data identify that at least three crustal blocks are present in the northwestern part of Central Iran, Lut, and CIM terranes (**Fig.5.17 A, B**). Therefore, Crustal block 1, including the Lut (Mirabad), Crustal block 2, including the NW-Central Iran (Takab), and Crustal block 3, including the northwest part of the SSZ (Kamyaran) have different epsilon values but similar T_{2DM}, indicating likely derivation for the same source region at different times (**Fig.5.17 A, B**). Moreover, the T_{2DM} and epsilon values calculated based on the Nd isotopic data recognized one crustal block in NE-Central Iran (Arghash) (**Fig.5.17 B, C**). The isotope data collected for the Cretaceous rocks in WNT are summarized in Table (**5.9**).

Table 5. 9. The summary of isotope data for the Paleocene rocks in western Neo-Tethys.

Location Name	**Geological Zone**	**Crustal Block**	ε_{Hf}	ε_{Nd}	**Age** (Ma)	**Reference**
Kamyaran	NW-SSZ	NW-SSZ	+10.27	_	56	(Azizi et al., 2011)
Takab	NW-UDMA	NW- Central Iran	+6.85	_	59	(Moghadam et al., 2016)
Mirabad	Sistan Suture Zone	Lut	+3.95 to +15.29	_	58-61	(Pang et al., 2014)
Arghash	Central Iran	NE-Central Iran	_	+5.80	55.4	(Alaminia et al., 2013)

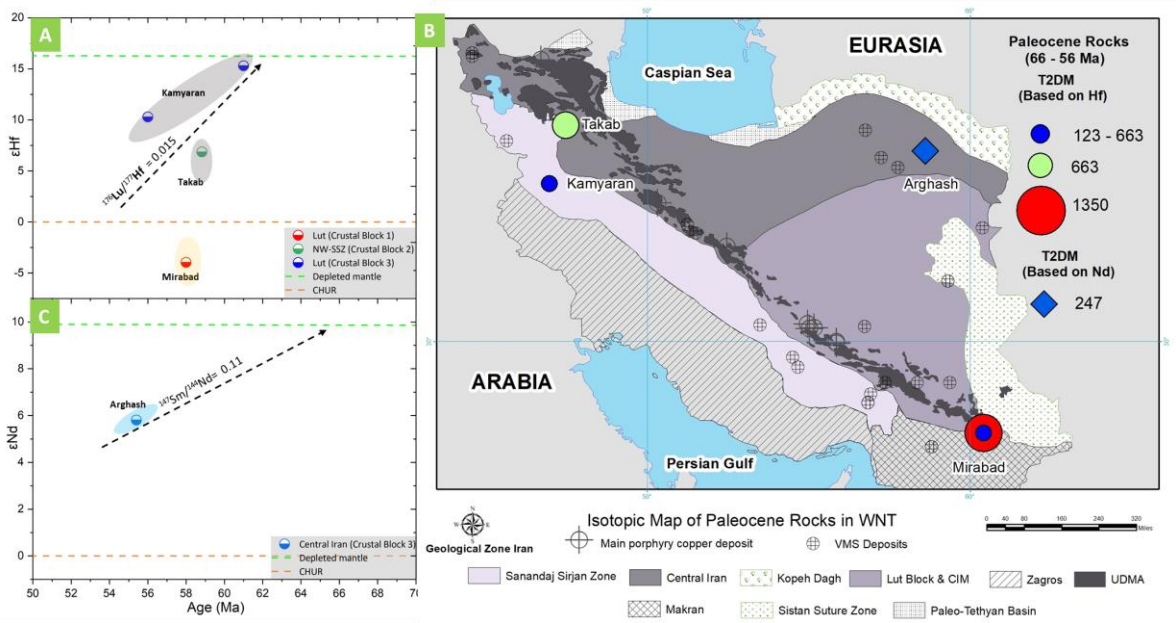

Figure 5. 17. Diagrams of ε_{Hf} (T) versus U-Pb ages and the Paleocene rocks' distribution on the WNT. The legend corresponds to the different crustal blocks in WNT. The arrow shows the isotope composition trend for the intermediate crustal rocks. (**A**) Diagrams of ε_{Hf} (T) versus U-Pb ages (**B**) Distribution of T_{2DM} isotopic data on WNT, calculated based on Hf isotopic composition. (**C**) Diagrams of ε_{Nd} (T) versus U-Pb ages. (**D**) Distribution of T_{2DM} isotopic data on WNT, calculated based on Nd isotopic composition.

5.1.10. Eocene 56-33.9 (Ma)

Subduction-related magmatism in the western Neo-Tethys continued from the Cretaceous to Recent, with extreme magmatic activity occurring during the Eocene to Oligocene (Amidi, Emami, & Michel, 1984; Berberian & King, 1981). This flare-up of magmatism (Stocklin, 1968; Verdel et al., 2011) is probably due to the resumption of oceanic subduction of the Neo-Tethys below Eurasia (Agard et al. 2011). Alternatively, it has been proposed that the Late Jurassic intrusive rocks of the SSZ and younger magmatism in the UDMA (Berberian and Berberian, 1981; Berberian et al., 1982; Berberian & King, 1981) may have been related to the subduction of the Arabian plate below Eurasia **(Fig.5.18**).

Magmatic activity in the Neo-Tethys basin reflects a northeastward migration of the arc in the Middle Eocene. This magmatism may represent a change in the subduction angle and flattening of the Neo-Tethyan slab (e.g., Agard et al., 2011; Berberian & Berberian, 1981; Shahabpour, 2007; Verdel et al., 2011; Shahsavari Alavijeh et al., 2017). Radiometric ages support arc magmatism in the northwest part of the UDMA having started in the Middle Paleocene (~60 Ma; Chiu et al.,

2013), whereas the onset of magmatism in the southeast part of the UDMA was Middle Eocene (Berberian & King, 1981; Hassanzadeh, 1993).

Widespread Cenozoic arc magmatism occurred in many locations (**Fig.5.18**) in the WNT including the Lut–Sistan Suture Zone, Sorkh-Kuh, Khunik, Kamyaran, Taa-Baysaran, Morvarid, Taa-Baysaranm Sabzevar, Ozkol, Rabor-Lalehzar, Lowshan, Nain- Yazd, Takab, Saghand, Firouzeh mine, Naqadeh, GhalaJi, Qazvin, Bam-Jiroft, Anar-Sirjan, Mirabad, Tehran, Tarom areas (Chiu et al., 2017; Chiu et al., 2013; Moghadam et al., 2016; Moghadam et al., 2017; Azizi et al., 2011; Mazhari et al., 2009, 2011; Nakhaei et al., 2015; Samiee et al., 2016; Hosseinkhani et al., 2017; Pang, 2013; Ghiasvand, 2017; Ahmadian et al., 2016; Nabatian; 2017, Shahsavari Alavijeh; 2015; Malekzadeh Shafaroudi et al., 2015; Ahmadian et al., 2016; Golmohammadi et al., 2015; Ao et al., 2016).

Most of the Eocene felsic rocks plot within the VAG-arc field on Rb vs. (Y + Nb) diagram some samples of, although exceptions include samples from the Firoze mine and Tarom in Central Iran, and Sangan in the Lut block, which plotted in the WPG domain of the diagram (**Fig.5.19. A**). Samples from the northwest part of the Zagros suture zone in Kermanshah, the Sarve-Abad ophiolites, and the Taa-Baysaran area plotted on a TiO2/Yb–Nb/ diagram define an OIB setting. Additionally, a few samples from Sabzevar Ophiolite in Central Iran and Piranshahr intrusive rocks in the northwest part of the SSZ show the same tectonic setting environment during the Eocene time. In marked contrast, all the mafic rock samples define the E-MORB and N-MORB tectonic setting (**Fig.5.19. B**).

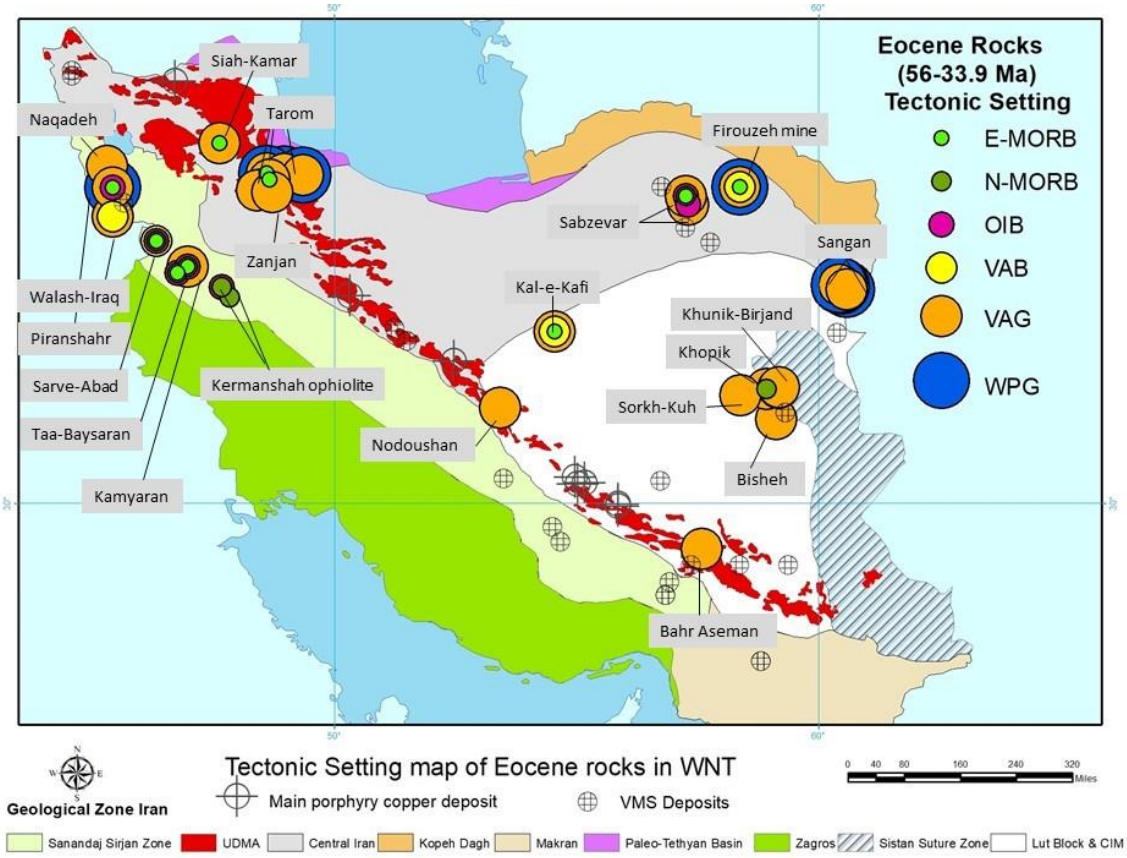

Figure 5. 18. The distribution of the Eocene rocks on the western Neo-Tethys Geological map of Iran.

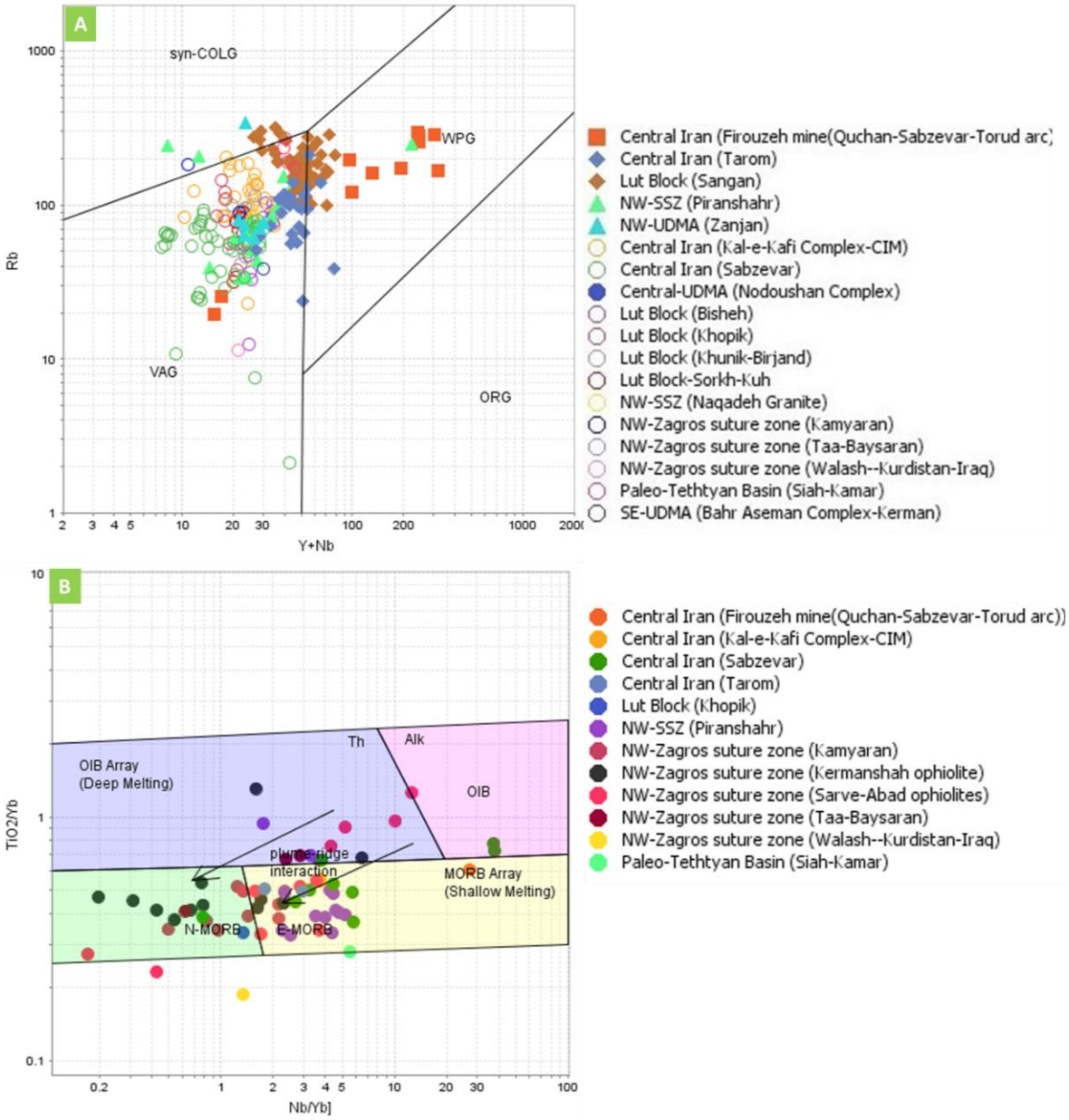

Figure 5. 19. Classification and geochemical characterization of Igneous and metamorphic rocks from Eocene rocks in the WNT. (**A**) Rb vs. (Y + Nb) discriminant diagrams for the tectonic setting of felsic rocks in the study area (Pearce, Harris, & Tindle, 1984). (**B**) the TiO_2/Yb–Nb/Yb diagram is used to separate subduction-related from subduction-unrelated mafic rocks (Pearce, 2014).

In eastern and central Iran, particularly within the Lut Block, there is an excellent potential for various kinds of Eocene age mineralization. Many of the Eocene rocks plotted on Sr/Y vs. Y diagram fall within the adakitic field, in particular the majority of samples from Firozeh mine and Sabzevar ophiolites in Central Iran, samples from the Khopik, Sourkh-Kuh, and Khunik areas in the Lut block, and the Zanjan area in the northwest part of the UDMA.

Some samples from the Tarm region in the Alborz of central Iran, as well as the rocks from the Kamyaran, Taa-Baysaran, Sarvabad areas, and Kermanshah ophiolites in the northwest part of the SSZ and Zagros suture zone also exhibit adakitic affinities (**Fig.5.20. A-D**).

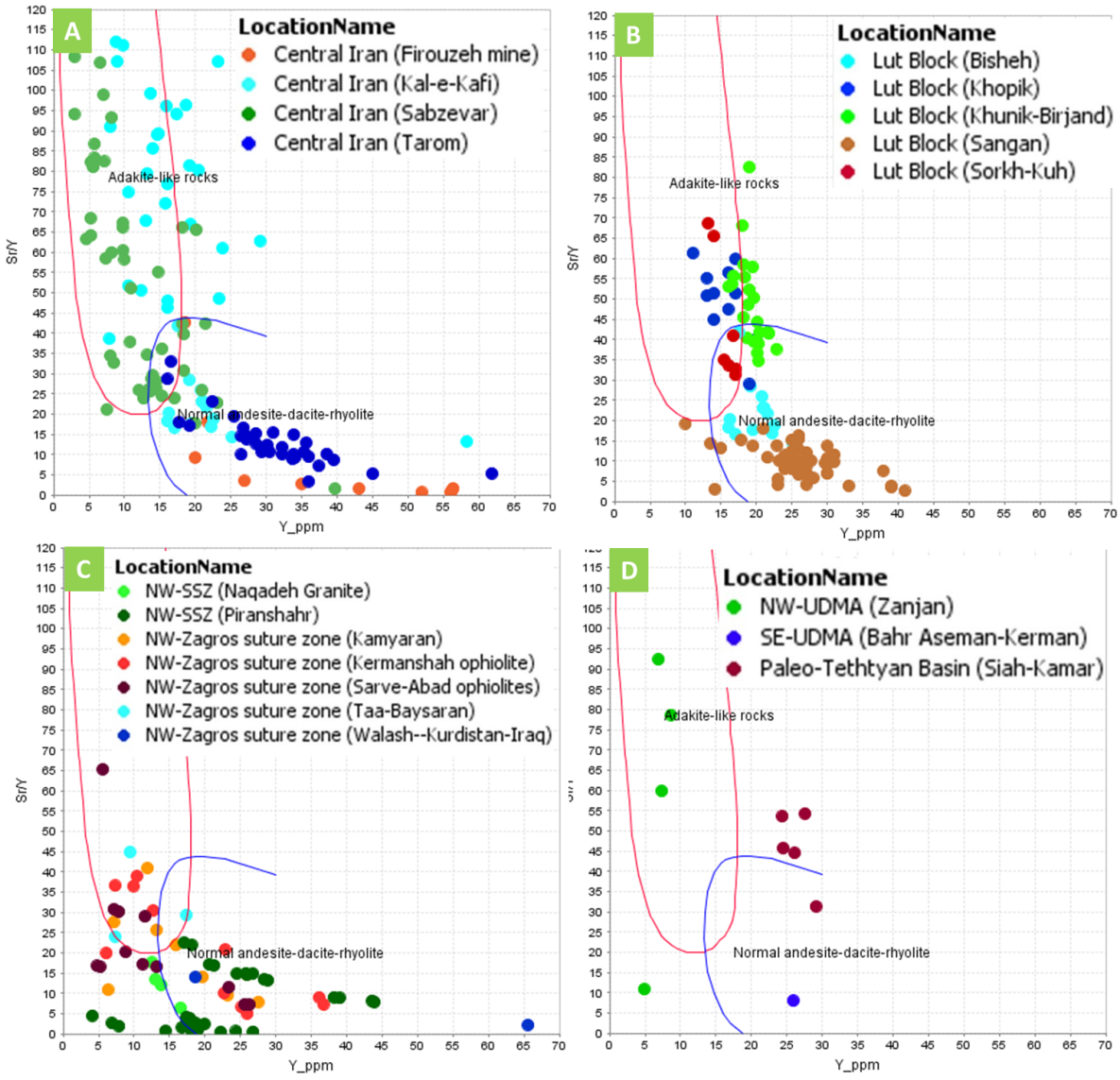

Figure 5. 20. Sr/Y vs. Y (ppm) diagram of Eocene rocks from the WNT (Defant & Drummond, 1993).

Except for the samples from the Saghand region and a few samples from the Firouzeh mine in central Iran, as well as the Mirabad area in the Sistan suture zone in the southeast part of the UDMA, which have negative zircon ε_{Hf} (T) values most Eocene rocks exhibit positive values. Samples from the Firouzeh mine in the northwest part of the UDMA (Chiu et al., 2017) have zircon ε_{Hf} (T) values between +0.34 to +9.89 for granite dikes and -2.07 to +3.25 for meta-granites. This range of values is interpreted to reflect a homogeneous mantle source for the granite dikes and a

mixed juvenile and reworked source for the meta-granites. Two samples from the Mirabad area in Sistan Suture Zone (Chiu et al., 2017) have zircon ε_{Hf} (T) values of -4.36 and +12.39, which suggests partial melting of older crustal material and mixing with juvenile mantle-derived melts in the Eocene. The samples from Nain and Nain-Yazd areas (Chiu et al., 2013) yield zircon ε_{Hf} (T) values between -1.26 to +1.96 and -1.72 to +8.9, respectively, whereas rocks from the Rabor-Lalehzar region shows ε_{Nd} (T) values between -0.42 to +2.25 (Moghadam et al., 2017). These rocks are interpreted as partial melting of older crustal material then mixing with juvenile mantle-derived melts in the central northwest part of the UDMA. In contrast, Eocene age rocks from the Qazvin and Takab regions in the northwest part of the UDMA have zircon ε_{Hf} (T) values between +3.34 to +6.34 and +4.7 to +8.1, respectively. Eocene rocks from the Anar-Sirjan and Bam-Jiroft areas in the southeast part of the UDMA (Chiu et al., 2013) show zircon ε_{Hf}(T) values between +9.67 to +14.02 and +0.6 to +4.02, respectively.

Samples from the northwest part of the SSZ, including the Kamyaran and Taa-Baysaran areas (Azizi et al., 2011), yield zircon ε_{Hf} (T) values between +9.67 to +13.04 and +8.42 to +13.48, respectively. Eocene rocks from the GhalaJi, Kamyaran, Morvarid, Ozkol, Piranshah, and Taa-Baysaran areas in the northwest part of the SSZ (Azizi et al., 2011; Mazhari et al., 2009) show positive ε_{Nd} (T) values between +6.90, +4.43 to +7.99, +5.05 to +7.23, +6.66, +2.25 to +7.25, +2.74 to +2.77, respectively. The strong positive ε_{Hf} (T) and ε_{Nd} (T) values for rocks from the northwest part of the SSZ are consistent with a homogeneous mantle source for Eocene magmatism.

Eocene rocks from the Bisheh, Khunik-Birjand and Sorkh-Kuh areas in the Lut block have ε_{Nd} (T) values between -1.59, +1.26 to +3.26 and -0.36, respectively. In addition, Eocene rocks from the Lut Sistan Suture Zone, have ε_{Nd} (T) values change between 4.93 to +5.47 (Pang, 2013). The ε_{Nd} (T) and ε_{Hf} (T) values in Lut Block and Lut–Sistan Suture Zone, are interpreted to be initially derived from partial melting of older crustal material and subsequent mixing with juvenile mantle-derived melts during the Eocene (Nakhaei et al., 2015; Samiee et al., 2016; Hosseinkhani et al., 2017).

Eocene rocks from the Lowshan area of the Alborz Zone have ε_{Nd} (T) values between +1.2 to +9.33 (Chiu et al., 2017), which is interpreted as the last magma activity related to closing Paleo-Tethys (**Fig.5.21. A-C**).

The T_{2DM} and epsilon values calculated based on the Hf isotopic data reveal that at least three crustal blocks can be distinguished in the northeast part of Central Iran, Alborz, CIM, northwest part of the SSZ, and Lut during the Eocene (**Fig.5.21 A, B**). Crustal Block 1 includes some samples from the Firouzeh mine in northeastern Central Iran, Mirabad area (Lut) and the Saghand area (CIM); Crustal Block 2, includes the Nain-Yazd area (CIM), the Qazvin, Lowshan, Tehran areas (Alborz), and some samples in Kamyaran area (northwest part of the SSZ). Crustal Block 3 includes the Anar-Sirjan area (CIM), Mirabad (Lut), and the Taa-Baysaran area and some samples from the Kamyaran area (northwest part of the SSZ). Samples defining the three crustal blocks have different Hf epsilon values but similar T_{2DM}, thereby indicating likely derivation for the same source region at different times (**Fig.5.21 A, B**).

Moreover, the T_{2DM} and epsilon values calculated based on the Nd isotopic data recognized two different crustal blocks in NE-Central Iran, Alborz, CIM, northwest part of the SSZ, and Lut zone. Crustal Block 1, includes the Rabor-Lalehzar (CIM), the Bisheh, Khunik, Sorkh-Kuh areas (Lut), the Tarom area (Alborz), and the Naqadeh area (northwest part of the SSZ); Crustal Block 2, includes Sabzevar area (northeastern Central Iran) and the Kamyaran, Taa-Baysaran, Morvarid and Ozkol areas (northwest part of the SSZ) Rocks from these two crustal blocks have different Nd epsilon values but similar T_{2DM}, indicating likely derivation for the same source region but at different times during the Eocene (**Fig.5.21 C, D**). The isotope data collected for the Eocene rocks in WNT are summarized in Table (**5.10**).

Table 5. 10. The summary of isotope data for the Eocene rocks in western Neo-Tethys.

Location Name	Geological Zone	Crustal Block	ε_{Hf}	ε_{Nd}	Age (Ma)	Reference
Firouzeh mine	Central Iran	NE-Central Iran	+0.34 to +9.89 -2.07 to +3.25	_	41-43.2	(Chiu et al., 2017)
Qazvin	Alborz (Paleo-Tethys)	Alborz	+3.34 to +6.34	_	46-34.1	Chiu et al., 2013
Takab	NW-UDMA	NW- Central Iran	+4.7 to +8.1	_	40-46	(Moghadam et al., 2016)
Nain	C-UDMA	CIM	-1.26 to +1.96	_	35.7-38.5	Chiu et al., 2013
Nain-Yazd	C-UDMA	CIM	-1.72 to +8.9	_	34-44.7	Chiu et al., 2013
Rabor-Lalehzar	C-UDMA	CIM	_	-0.42 to +2.25	45.7	(Moghadam et al., 2017)
Anar-Sirjan	SE-UDMA	CIM	+9.67 to +14.02	_	34.9-40	Chiu et al., 2013
Bam-Jiroft	SE-UDMA	CIM	+0.6 to +4.02	_	44-46	Chiu et al., 2013)
Kamyaran	NW-SSZ	NW-SSZ	+9.67 to +13.04	_	51-54	(Azizi et al., 2011)
Taa-Baysaran	NW-SSZ	NW-SSZ	+8.42 to +13.48	_	34.7-39.1	(Azizi et al., 2011)
GhalaJi	NW-SSZ	NW-SSZ	_	+6.90	36.63	(Azizi et al., 2011)
Kamyaran	NW-SSZ	NW-SSZ	_	+4.43 to +7.99	36.63	(Azizi et al., 2011)
Morvarid	NW-SSZ	NW-SSZ	_	+5.05 to +7.23	36.63	(Azizi et al., 2011)
Naqadeh	NW-SSZ	NW-SSZ	_	-4.27	41.85	(Mazhari et al., 2011)
Ozkol	NW-SSZ	NW-SSZ	_	+6.66	36.63	(Azizi et al., 2011)
Piranshah	NW-SSZ	NW-SSZ	_	+2.25 to +7.25	41.1	(Mazhari et al., 2009)
Taa-Baysaran	NW-SSZ	NW-SSZ	_	+2.74 to +2.77	36.63	(Azizi, et al., 2011)
Sabzevar	Central Iran	NE-Central Iran	+6.05 to +6.54		45-46.8	(Moghadam et al., 2016)
Saghand	CIM	CIM	-7.10 to -0.29	_	43.8-48.7	(Chiu et al., 2017)
Bisheh	Lut	Lut	_	-1.59	39.16	(Nakhaei et al., 2015)
Khunik-Birjand	Lut	Lut	_	+1.26 to +3.26	38-39.16	(Samieeet al., 2016)
Sorkh-Kuh	Lut	Lut	_	-0.36	40.16	(Hosseinkhani et al., 2017)
Mirabad	Sistan Suture Zone	Lut	-4.36 to +12.39	_	41.1-51	(Chiu et al., 2017)
Lut–Sistan Suture Zone	Lut–Sistan Suture Zone	Lut	_	-4.93 to +5.47	39.1-46.4	(Pang et al., 2013)
Lowshan	Alborz (Paleo-Tethys)	Alborz	+1.2 to +9.33	_	36.7-50	(Chiu et al., 2017)
Tehran	Alborz (Paleo-Tethys)	Alborz		+1.2 to +9.3	43.1-50	(Chiu et al., 2017)
Tarom	Alborz (Paleo-Tethys)	Alborz		-6.01 to +3.19	40.2	(Chiu et al., 2017)

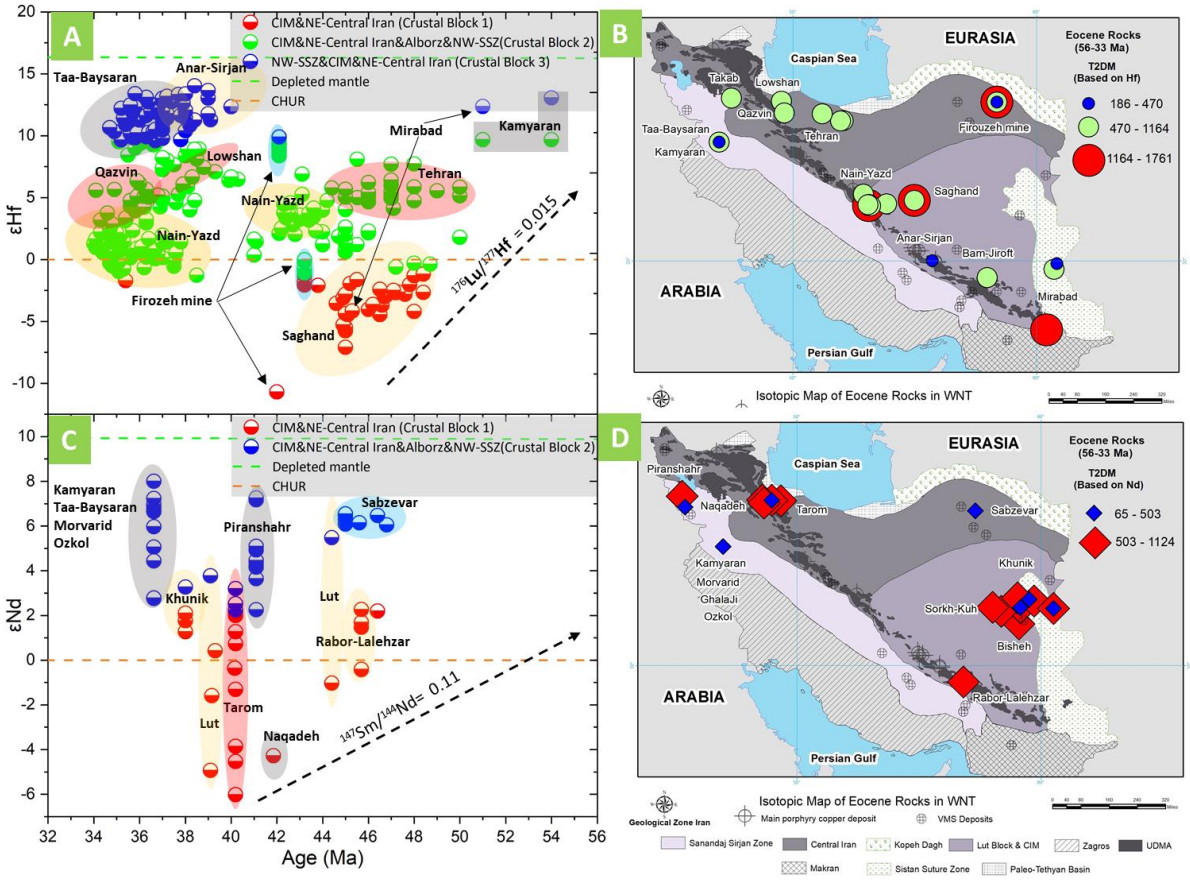

Figure 5. 21. Diagrams of ε_{Hf} (T) versus U-Pb ages and the Eocene rocks' distribution on the WNT. The legend corresponds to the different crustal blocks in WNT. The arrow shows the isotope composition trend for the intermediate crustal rocks. (**A**) Diagrams of ε_{Hf} (T) versus U-Pb ages (**B**) Distribution of T_{2DM} isotopic data on WNT, calculated based on Hf isotopic composition. (**C**) Diagrams of ε_{Nd} (T) versus U-Pb ages. **D**) Distribution of T_{2DM} isotopic data on WNT, calculated based on Nd isotopic composition.

5.1.11. Oligocene 33.9-23.03 (Ma)

The subduction of Neo-Tethys under the active margin of CIM continued from the Upper Triassic to the Oligocene until the Tertiary collision of Arabia with Eurasia (Whitechurch et al., 2013). This evidence is preserved as magmatic arcs, and back-arc tectonic settings across the Lut–Sistan, Alborz, SSZ, and UDMA tectono-stratigraphic domains (**Fig.5.22**). The Sanandaj–Sirjan arc formed in the Mesozoic whereas the Urumieh–Dokhtar arc formed in the Tertiary (Omrani et al., 2008). Oligocene age magmatic rocks in WNT are preserved as different ophiolitic fragments in Khoy, Hasanbag, Walsh, Kermanshah, Neyriz, Nain-Baft, Nehbandan, Dehshir areas. Furthermore, the Oligocene magmatic rocks were exposed in regions such as Horand, Natanz, Taa-Baysaran, Takab, Bam-Jiroft, Kerman, Zahedan, Mahoor, Arasbaran, Mirkuh, Siah-Kamar, Mishu, Ghorveh, Nudeh, and Dalli (Dargahi et al., 2010; Beydokhti et al., 2015; Zarasvandi et al.,

2015; Ghazi et al., 2012; Arvin et al., 2005; Whitechurch et al., 2013; Saccani et al., 2010; Amiri et al., 2017; Maanijou et al., 2013; Jamali et al., 2015; Aghazadeh et al., 2015; Ahmadzadeh et al., 2010; Ali et al., 2013, 2012; Ghazi & Hassanipak, 1999; Khalatbari-Jafari, Juteau, & Cotten, 2006; Hassanipak & Ghazi, 2000; Nouri et al., 2017; Omrani et al., 2008; Hosseini et al., 2017; Peighambariet al., 2011; Sadeghian et al., 2005; Chiu et al., 2017; Chiu et al., 2013; Moghadam et al., 2016, 2009, 2013, 2014, 2017; Azizi et al., 2008; Pang, 2013).

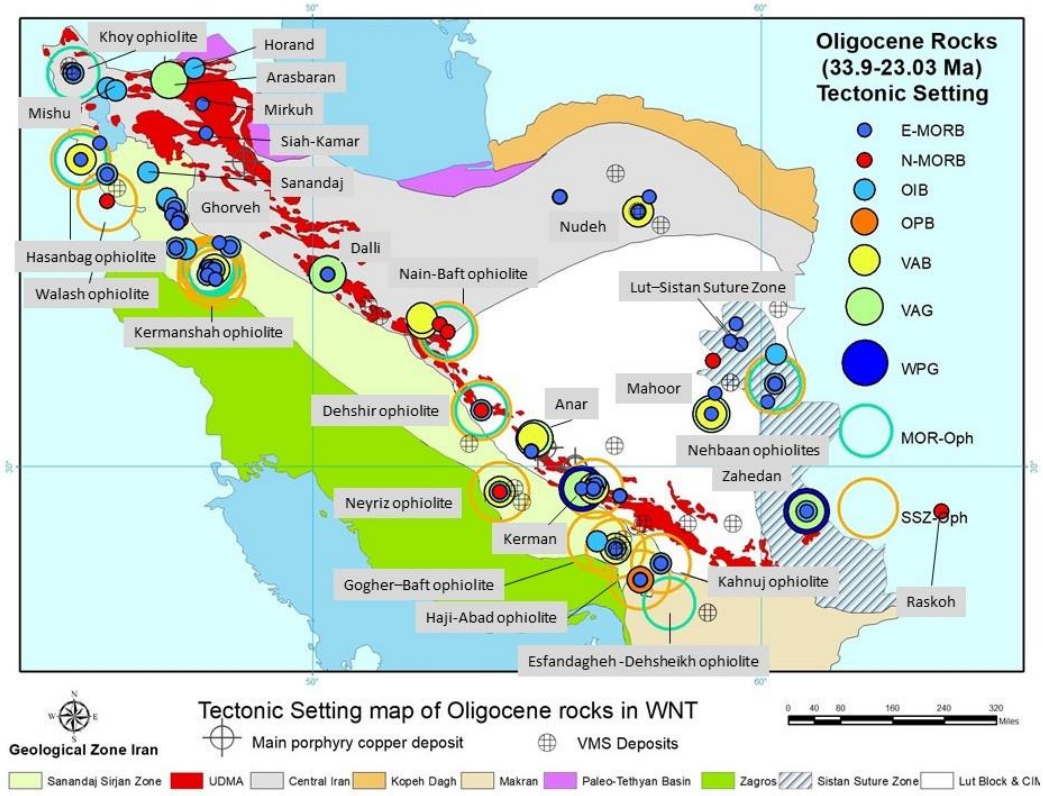

Figure 5. 22. The distribution of the Oligocene rocks on the WNT Geological map of Iran.

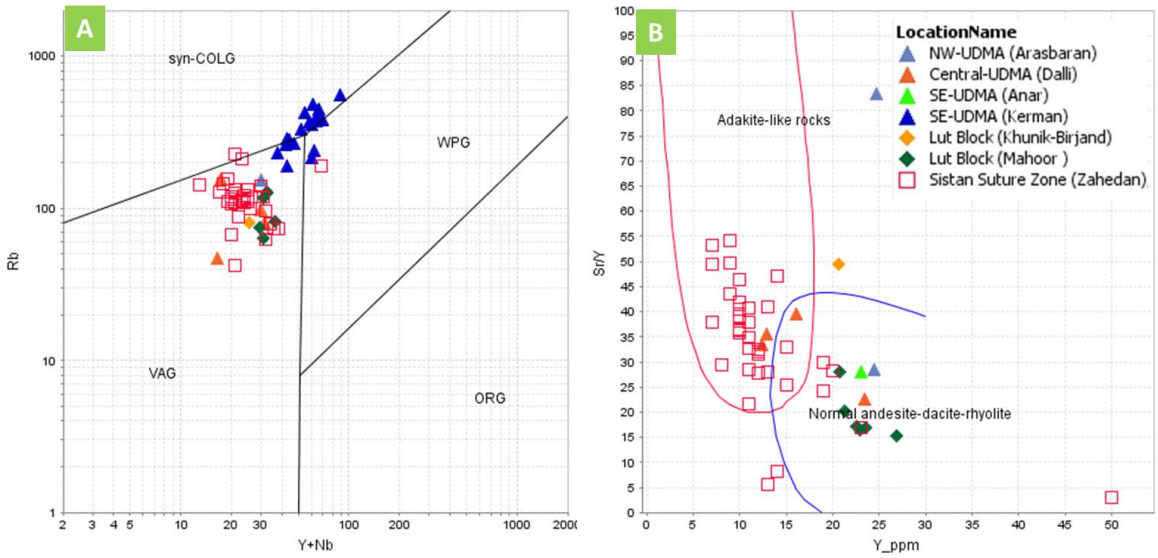

Figure 5. 23. Classification and geochemical characterization of Igneous and metamorphic rocks from Oligocene rocks in Iran's different geological zones in the WNT. (**A**) Rb vs. (Y + Nb) discriminant diagrams for the tectonic setting of felsic rocks in the study area (Pearce, Harris, & Tindle, 1984). (**B**) Sr/Y vs. Y (ppm) diagram of Oligocene felsic rocks from the WNT (Defant & Drummond, 1993).

In the Rb vs. (Y + Nb) of Oligocene felsic rocks, except for some samples from Kerman in the southeast part of the UDMA and Zahedan in Sistan Suture Zone, which are plotted in the WPG and Syn-COLG domains, all the felsic rock samples define a VAG-arc setting (**Fig.5.23. A**). Furthermore, the majority of the samples from Zahedan in the Sistan Suture Zone and Dali in the central part of the UDMA on the Sr/Y vs. Y (ppm) diagram show adakitic signatures (**Fig.5.23. B**).

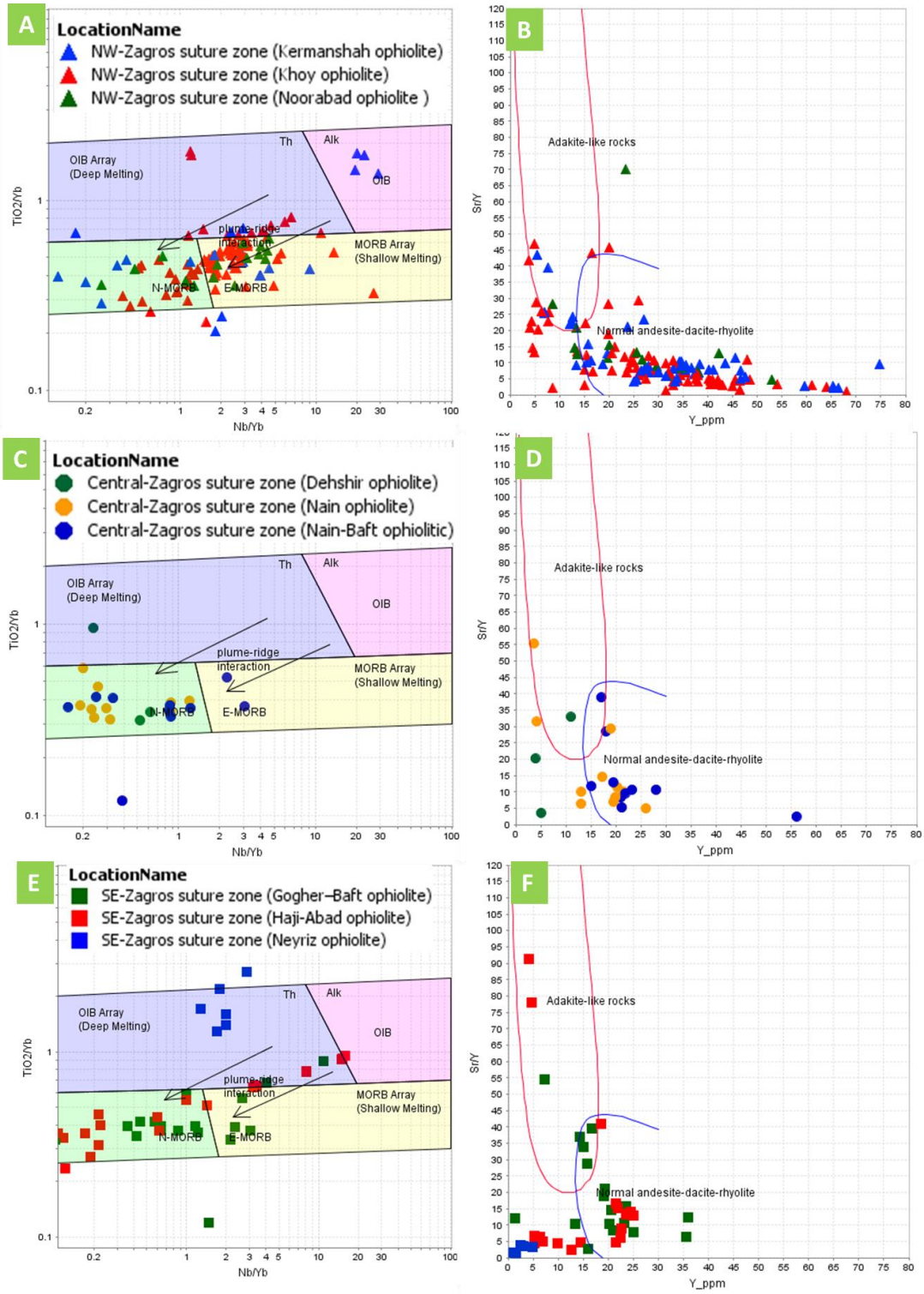
A
LocationName
NW-Zagros suture zone (Kermanshah ophiolite)
NW-Zagros suture zone (Khoy ophiolite)
NW-Zagros suture zone (Noorabad ophiolite)
OIB Array
(Deep Melting)
Th
Alk
OIB
plume-ridge
interaction
MORB Array
(Shallow Melting)
N-MORB
E-MORB
TiO2/Yb
Nb/Yb
B
Adakite-like rocks
Normal andesite-dacite-rhyolite
Sr/Y
Y_ppm
C
LocationName
Central-Zagros suture zone (Dehshir ophiolite)
Central-Zagros suture zone (Nain ophiolite)
Central-Zagros suture zone (Nain-Baft ophiolitic)
OIB Array
(Deep Melting)
Th
Alk
OIB
plume-ridge
interaction
MORB Array
(Shallow Melting)
N-MORB
E-MORB
TiO2/Yb
Nb/Yb
D
Adakite-like rocks
Normal andesite-dacite-rhyolite
Sr/Y
Y_ppm
E
LocationName
SE-Zagros suture zone (Gogher–Baft ophiolite)
SE-Zagros suture zone (Haji-Abad ophiolite)
SE-Zagros suture zone (Neyriz ophiolite)
OIB Array
(Deep Melting)
Th
Alk
OIB
plume-ridge
interaction
MORB Array
(Shallow Melting)
N-MORB
E-MORB
TiO2/Yb
Nb/Yb
F
Adakite-like rocks
Normal andesite-dacite-rhyolite
Sr/Y
Y_ppm

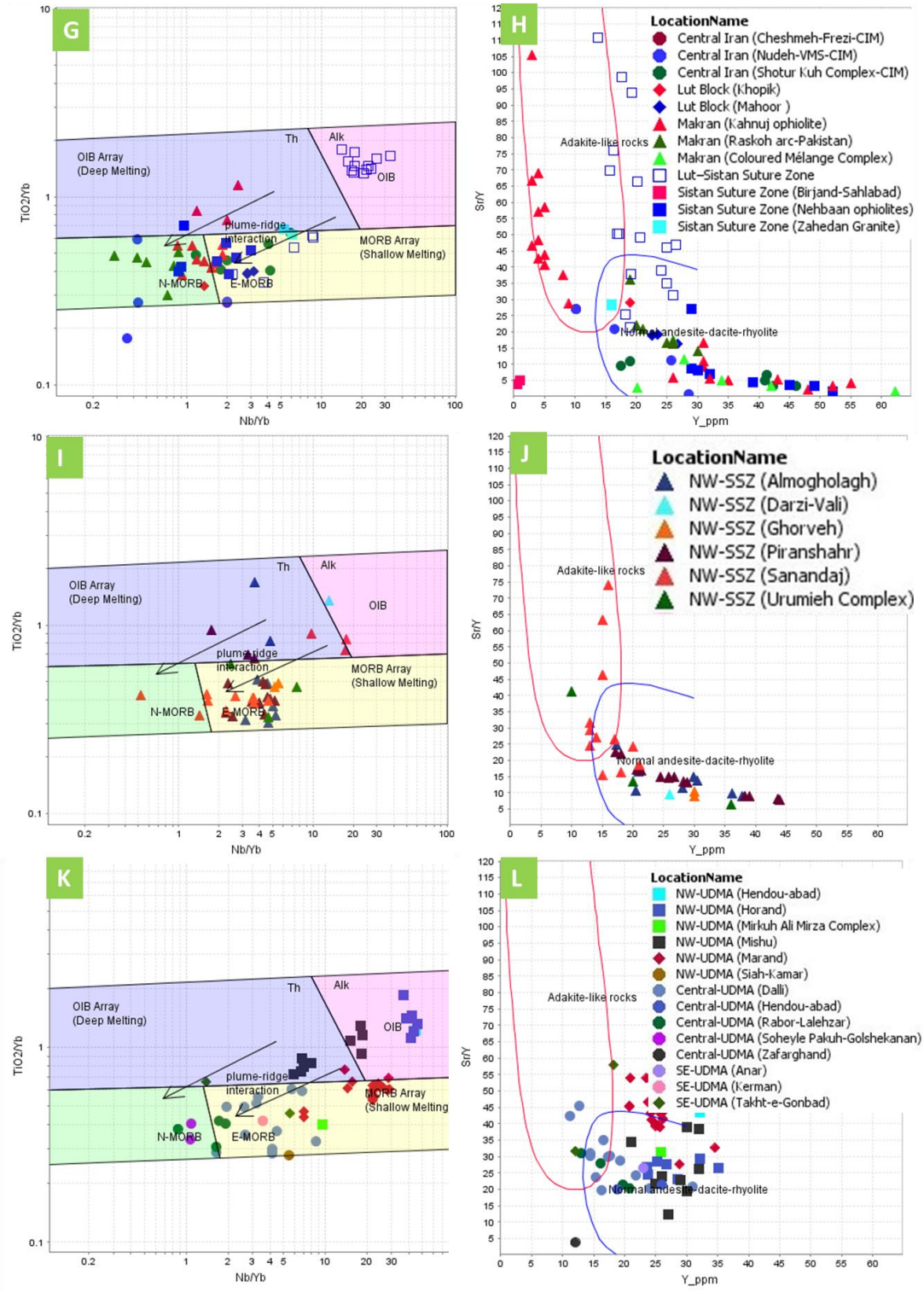

Figure 5. 24. Classification and geochemical characterization of Igneous and metamorphic rocks from Oligocene rocks in Iran's different geological zones in the WNT. (**A, C, E, G, I, K**) TiO_2/Yb–Nb/Yb diagrams are used to separate subduction-related from subduction-unrelated mafic rocks (Pearce, 2014). (**C, F, I, L, O, R**) Sr/Y vs. Y (ppm) diagram of Oligocene mafic rocks from the WNT (Defant & Drummond, 1993).

In the TiO_2/Yb–Nb/Yb diagram for the northwest part of the Zagros suture zone, some samples in Kermanshah and Khoy ophiolites define the OIB tectonic setting, and other areas plot in the E-MORB and N-MORB domain (**Fig.5.24**. **A**). Meanwhile, in the Sr/Y vs. Y diagram of Oligocene rocks of the northwest part of the Zagros suture zone, just a few samples in Kermanshah and Khoy ophiolites show adakitic signatures (**Fig.5.24**. **B**).

In the TiO_2/Yb–Nb/Yb diagram for the of the central part of the Zagros suture zone, except for the three samples in Naein-Baft ophiolitic area, which have been plotted in OIB and E-MORB domains, the majority of the samples show N-MORB signatures (**Fig.5.24**. **C**). Furthermore, in the Sr/Y vs. Y diagram, except for the two samples in Naein-Baft ophiolitic area, almost none of the central part of the Zagros suture zone's samples show adakitic signatures (**Fig.5.24**. **D**).

In the TiO_2/Yb–Nb/Yb diagram for the southeast part of the SE-Zagros suture zone, except for Neyriz ophiolites and the three samples in Haji-Abad ophiolitic area, which have been plotted in the OIB domain, the other samples show N-MORB signatures (**Fig.5.24**. **B**). Moreover, in the Sr/Y vs. Y diagram, just a few rocks in Gohar-Baft and Haji-Abad ophiolites show adakitic signatures (**Fig.5.24**. **F**).

In the east of Iran, the majority of igneous rocks in the Lut-Sistan suture zone and a few samples in the Kahnuj ophiolites show OIB signatures. The other rocks plotted in the TiO2/Yb–Nb/Yb diagram in Central Iran, Makran, Lut block, and Sistan suture zone show N-MORB and E-MORB signatures (**Fig.5.24**. **G**). Additionally, just a few samples in the Lut-Sistan suture zone and the Kahnuj ophiolites show adakitic signatures (**Fig.5.24**. **H**).

In the northwest part of the SSZ, the majority of igneous rocks in Sanandaj and Darzi-Vali, as well as some samples from the Piranshahr and Almagolagh plutons, show OIB signatures. The other rocks which have been plotted in the TiO_2/Yb–Nb/Yb diagram in Ghorveh and Urumieh Complexe show N-MORB and E-MORB signatures (**Fig.5.24**. **I**). In addition, in the Sr/Y vs. Y diagram, almost only samples from the Sanandaj region show adakitic signatures in (**Fig.5.24**. **J**).

In the northwest part of the UDMA, only samples in Misho, Marand, and Horand areas show OIB signatures. The other rocks which have been plotted in the TiO_2/Yb–Nb/Yb diagram in the central part of the UDMA and southeast part of the UDMA show N-MORB and E-MORB signatures (**Fig.5.24**. **K**). Besides, in the Sr/Y vs. Y diagram, only samples from the Daili deposit

in the central part of the UDMA and one sample from Takht-e-Gonbad in the southeast part of the UDMA show adakitic signatures in (**Fig.5.24**. **L**).

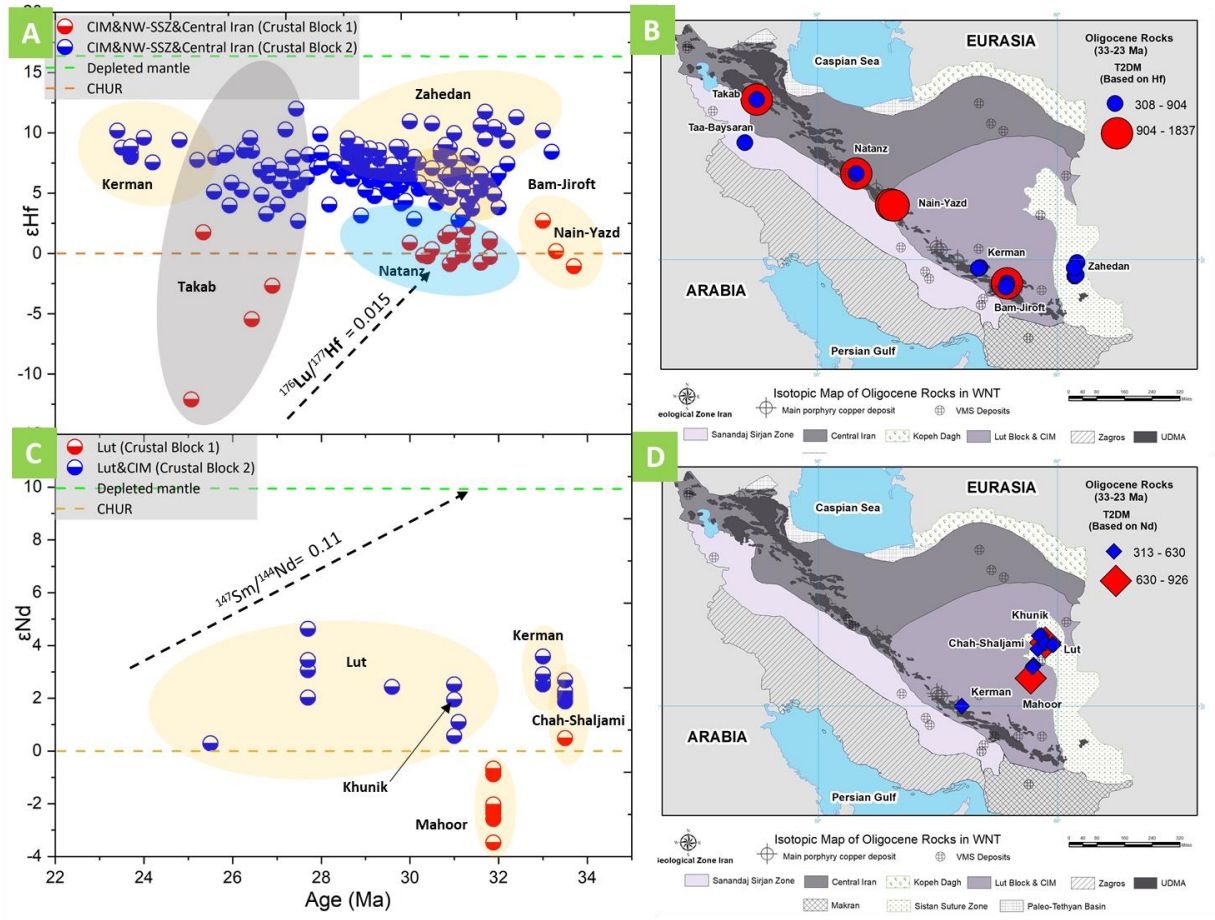

Figure 5. 25. Diagrams of ε_{Hf} (T) versus U-Pb ages and the Oligocene rocks' distribution on the WNT. The legend corresponds to the different crustal blocks in WNT. The arrow shows the isotope composition trend for the intermediate crustal rocks. (**A**) Diagrams of ε_{Hf} (T) versus U-Pb ages (**B**) Distribution of T_{2DM} isotopic data on WNT, calculated based on Hf isotopic composition. (**C**) Diagrams of ε_{Nd} (T) versus U-Pb ages. (**D**) Distribution of T_{2DM} isotopic data on WNT, calculated based on Nd isotopic composition.

Except for the Takab region in the northwest part of the UDMA, which has yielded negative zircon ε_{Hf} (T) values only for a few samples, the other areas in the center part of the UDMA and southeast part of the show positive values during the Oligocene time. Takab area in the northwest part of the UDMA (Moghadam et al., 2016) yields zircon ε_{Hf} (T) values between -12.11 to -2.67 and +1.74 to +12. These types of values indicate that rocks are from the indicate juvenile (newly formed) mantle source and contamination of both crust and Mantle sources in this area. In the central part of the UDMA area, Nain-Yazd and Natanz (Chiu et al., 2013) yield zircon ε_{Hf} (T) values between -1.06 to +2.7 and -0.87 to +3.14, respectively. These values suggest that the

contamination of old crust and juvenile mantle sources in this area is less than the northwest part of the UDMA. In contrast, samples from the southeast part of the UDMA have yielded positive zircon ε_{Hf} (T) and ε_{Nd} (T) values (**Fig.5.25**. **A, B**).

The samples from Bam-Jiroft yielded zircon ε_{Hf} (T) between +2.16 to +8.83 (Chiu et al., 2013). Meanwhile, the Kerman region yields zircon ε_{Hf} (T) values between +5.48 to +10.17 (Chiu et al., 2013) and ε_{Nd} (T) values between +2.51 to +3.58 (Dargahi et al., 2010). Therefore, they indicate a homogeneous mantle source in the southeast part of the UDMA (**Fig.5.25**. **A, B**).

Taa-Baysaran area in the northwest part of the SSZ yielded a positive zircon ε_{Hf} (T) +8.43 (Azizi et al., 2011), and they are interpreted as a homogeneous mantle source in similar southeast part of the UDMA in Oligocene (**Fig.5.25**. **A, B**).

Except for the Mahoor granite in Lut block, which has yielded negative ε_{Nd} (T) values -3.47 to -0.67 (Beydokhti et al., 2015), Chah-Shaljami and Khunik areas with εNd (T) values between +0.48 to +2.67 (Arjmandzadeh et al., 2011) and +1.94 (Samiee et al., 2016) respectively, show positive values during the Oligocene time. These values indicated that a juvenile mantle origin is apparent from the dominance of positive ε_{Nd} (T) values for the Chah-Shaljami and Khunik rocks. Conversely, in the Mahoor areas, suggesting that the rocks involve a reworked crustal component (**Fig.5.25**. **C, D**).

Samples from Lut–Sistan Suture Zone, include the Lut–Sistan area (Pang et al., 2013) and Zahedan granites (Azizi et al., 2011), yield positive ε_{Nd} (T) values between +0.28 to +4.62 and +4.1 to +11.74 respectively. They are interpreted as a homogeneous mantle source in Oligocene, similar to the southeast part of the UDMA and northwest part of the SSZ. (**Fig. 5.25**. **C, D**).

The T_{2DM} and epsilon values calculated based on the Hf isotopic data reveal that at least two crustal blocks in C-Central Iran, CIM, northwest part of the SSZ, and Lut, can be recognized in different Oligocene periods (**Fig.5.25 A, B**). Therefore, Crustal block 1, including the northwest part of the SSZ (a few samples in Takab), C-Central Iran (Natanz), and the CIM (Yazd-Nain), and Crustal block 2, including CIM (Kamyaran and Nain-Yazd), and Lut (Zahedan) have different epsilon values but similar T_{2DM}, indicating likely derivation for the same source region at different times (**Fig.25.5 A, B**).

Moreover, the T_{2DM} and epsilon values calculated based on the Nd isotopic data recognized two crustal blocks in the CIM and Lut zone. Therefore, Crustal block 1, including the Lut (Chah-Shaljami and Mahoor), and Crustal block 2, including the Lut (Khunik and Lut) and CIM (Kerman) have different epsilon values but similar T_{2DM}, indicating likely derivation for the same source region at different times (**Fig.25.5 C, D**). The isotope data collected for the Oligocene rocks in WNT are summarized in Table (**5.11**).

Table 5. 11. The summary of isotope data for the Oligocene rocks in western Neo-Tethys.

Location Name	**Geological Zone**	**Crustal Block**	ε_{Hf}	ε_{Nd}	**Age** (Ma)	**Reference**
Zanjan–Takab	NW-UDMA	NW-Central Iran	-12.11 to -2.67 +1.74 to +12	_	25-32	(Moghadam et al., 2016)
Nain-Yazd	C-UDMA	CIM	-1.06 to +2.7	_	33-33.7	Chiu et al., 2013
Kashan-Natanz	C-UDMA	C-Central Iran	-0.87 to +3.14		28.9-31.8	Chiu et al., 2013
Bam-Jiroft	SE-UDMA	CIM	+2.16 to +8.83	_	28.8-32	Chiu et al., 2013
Kerman	SE-UDMA	CIM	+5.48 to +10.17	_	23.4-33.7	Chiu et al., 2013
Kerman	SE-UDMA	CIM	_	+2.51 to +3.58	33	(Dargahi et al., 2010)
Taa-Baysaran	NW-SSZ	NW-SSZ	+8.43	_	33.2	(Azizi et al., 2011)
Chah-Shaljami	Lut	Lut	_	+0.48 to +2.67	33.5	(Arjmandzadeh et al., 2011)
Khunik	Lut	Lut	_	+1.94	31	(Samiee et al., 2016)
Mahoor	Lut	Lut	_	-3.47 to -0.67	31.88	(Beydokhti et al., 2015)
Lut–Sistan Suture Zone	Lut–Sistan Suture Zone	Lut	_	+0.28 to +4.62	25-31	(Pang et al.,2013)
Zahedan	Sistan Suture Zone	Lut	+4.1 to +11.74	_	29.1-33	(Chiu et al., 2017)

5.1.12. Miocene 23.03-5.33 (Ma)

The convergence history of the Neo-Tethys ocean between Arabia and Eurasia included a long period of subduction followed by continental collision during the Tertiary (Omrani et al., 2008). The time of initial collision continues to be a controversial issue in the geodynamic evolution of WNT and has been interpreted to have started in the Late Cretaceous (Stocklin, 1974; Yilmaz, 1993; Stampfli, 2000), the Late Eocene (Allen & Armstrong, 2008; Hatzfeld & Molnar, 2010), the Late Oligocene (Allen, Jackson, & Walker, 2004; Agard et al., 2005; Fakhari et al., 2008), and the Miocene (McQuarrie et al., 2003; Verdel et al., 2007). However, Pang et al. (2012) argued that since the Middle Miocene two different tectonic regimes have coexisted in WNT, an extensional phase in the east and a contractional phase in the southwestern region of Iran.

The Miocene magmatic rocks in WNT are present in the (**Fig.5.26**. **B**) Lut–Sistan zone, Touzlar, Sorkh-Kuh, Iju, Anar-Sirjan, Kerman, Nain, Natanz, Sabalan-Astara, Sahand, Bazman, Taftan, Mirabad, Rabor-Lalehzar, Akhikamal, and Shida areas (Pang et al., 2012; Heidari et al., 2015; Hosseinkhani et al., 2017; Golestani et al., 2018; Chiu et al., 2013; Pang et al., 2014; Moghadam et al., 2017; Azizi et al., 2014).

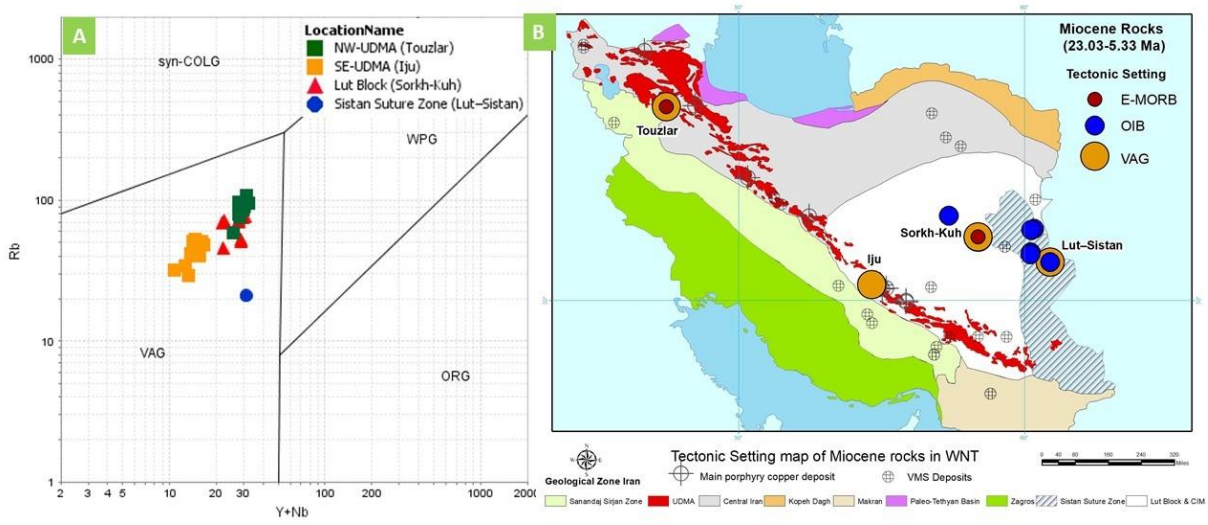

Figure 5. 26. Classification and geochemical characterization of Igneous and metamorphic rocks from Miocene rocks in Iran's different geological zones in the WNT. (**A**) Rb vs. (Y + Nb) discriminant diagrams for the tectonic setting of felsic rocks in the study area (Pearce, Harris, & Tindle, 1984). (**B**) The distribution of the Oligocene rocks on the WNT Geological map of Iran.

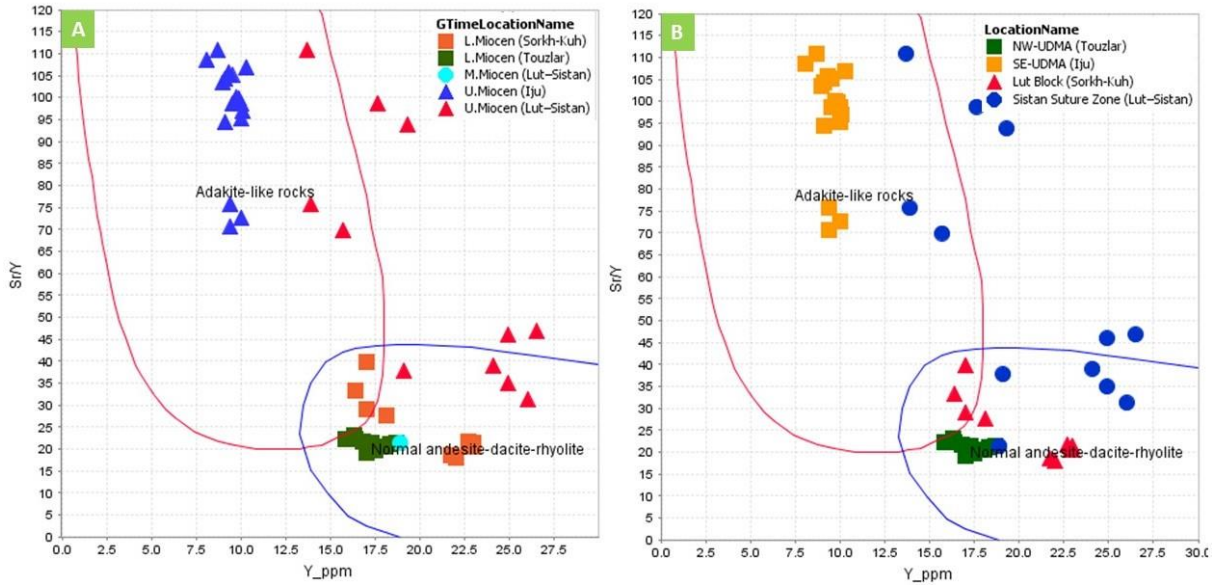

Figure 5. 27. (**A, B**) Sr/Y vs. Y (ppm) diagram of Miocene rocks from the WNT (Defant & Drummond, 1993).

Recent studies on the Late Mesozoic-Cenozoic magmatism in the WNT have proposed that continent-continent type collision of the Arabian and Iranian plates resulted in a thickened lithosphere of the central Iran crust (e.g., Shafiei et al., 2009; Aghazadeh et al., 2015; Richards et al., 2012; Omrani et al., 2008). Post-collision partial melting of a thickened juvenile lower crust is interpreted to have produced adakites over the length of the UDMA (Shahabpour, 1982; Gammons & Williams-Jones, 1997).

Azizi and Asahara (2013) proposed a Late Paleocene age in the southern part of UDMA for partial melting of a thickened juvenile lower-crustal source. Subduction continued until the Mid- to Late Miocene when the Afro-Arabian and CIM collided (Shahabpour, 1982; Gammons & Williams-Jones, 1997). Later, the juvenile mafic lower crust has thickened and converted to garnet-amphibolite due to increasing compressional stress and tectonic shortening (Arvin et al., 2007). Nevertheless, adakites can also be produced in the WNT by other procedures such as slab melting, flat subduction of a hot slab, lower crustal melting, and magma differentiation (Azizi & Asahara, 2013).

Miocene felsic rocks plotted on Rb vs. (Y + Nb) diagram, occur in the VAG-arc field (**Fig.5.26**. **A**). Furthermore, Upper Miocene rocks from the southeast part of the UDMA (Iju) and the Sistan suture zone (Lut-Sistan) plotted on the Sr/Y vs. Y diagram exhibit adakitic signatures. In contrast, Lower Miocene samples from the northwest part of the UDMA (Touzlar) and Lut block (Sorkh-Kuh) plot in the volcanic arc domains (**Fig.5.27**. **A, B**).

In the TiO_2/Yb–Nb/Yb diagram for the Sistan suture zone, Upper-Miocene rocks in Lut-Sistan areas show OIB signatures, whereas Lower-Miocene samples from the Touzlar (northwest part of the UDMA) and Sorkh-Kuh areas (Lut Block) plot in N-MORB and E-MORB domains (**Fig.5.28**. **A, B**).

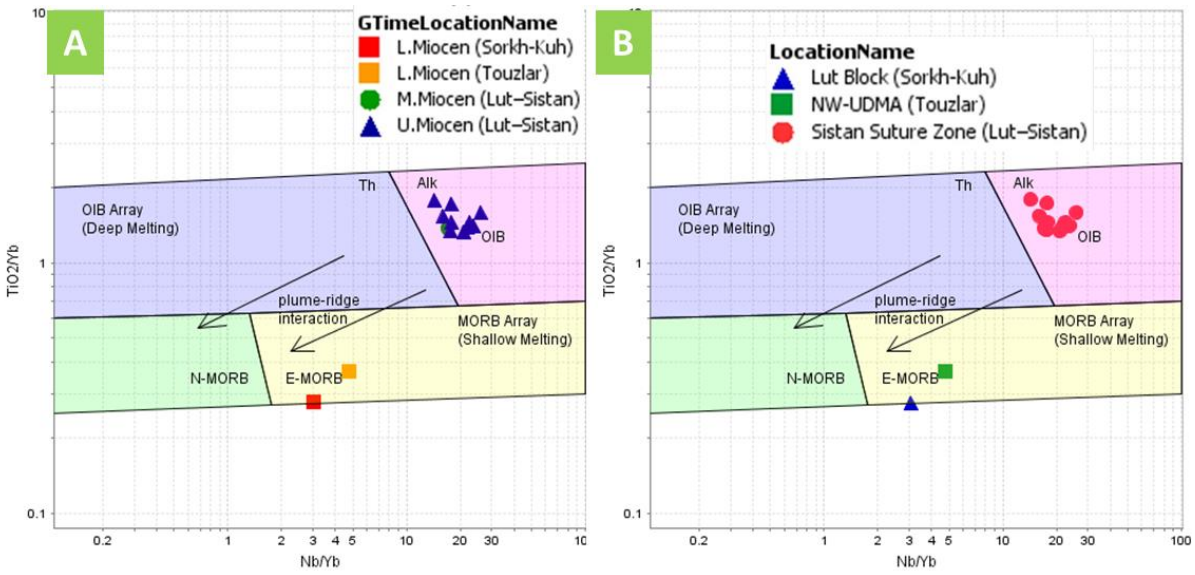

Figure 5. 28. Classification and geochemical characterization of Miocene igneous and metamorphic rocks in Iran's different geological zones in the WNT. (**A, B**) the Th/Yb–Nb/Yb diagram is used to separate subduction-related from subduction-unrelated mafic rocks (Pearce, 2014).

Zircon ε_{Hf} (T) values in the northwest part of the UDMA and southeast part of the UDMA yield positive values during the Miocene time (**Fig. A, C**). Samples from the Natanz region (central part of the UDMA) yield zircon ε_{Hf} (T) values between -1.51 to +10.52 (Chiu et al., 2013), whereas rocks from the Rabor-Lalehzar area have ε_{Nd} (T) values between -0.62 to +1.44 (Moghadam, 2017).

In the southeast part of the UDMA, all the Miocene age samples have positive zircon ε_{Hf} (T) and ε_{Nd} (T) values (**Fig.5.29**. **A-D**). The zircon ε_{Hf} (T) values for Kerman and Anar-Sirjan area, respectively, are between +9.08 to +9.75 (Chiu et al., 2013) and +7.92 to +12.25. Furthermore, Miocene rocks from the Iju area have yielded ε_{Nd} (T) values between +3.6 to +3.7 (Golestani et al., 2018).

Miocene rocks from the Sabalan-Astara and Sahand areas in the northwest part of the UDMA have positive zircon ε_{Hf} (T) values (Chiu et al., 2013) between +2.8 to +5.01 and +5.4 to +9.01, respectively. In contrast, Miocene rocks from the Akhikamal and Shida regions in the northwest part of the SSZ have negative zircon ε_{Hf} (T) values (Azizi et al., 2014) from -4.11 to -3.12, and -3.51 to -2.87 respectively (**Fig.5.29**. **A, B**).

Miocene rocks from the Bazman and Taftan areas in the Sistan Suture Zone (Pang et al., 2014), have positive values from +4.53 to + 8.19 and +4.5 respectively. In contrast, Miocene rocks

from the Mirabad region have a few samples with negative zircon ƐHf (T) values with an overall range between -0.46 and +5.70 (**Fig.5.29**. **A, B**).

Zircon $Ɛ_{Hf}$ (T) and $Ɛ_{Nd}$ (T) values from Miocene rocks in the WNT are interpreted to reflect a dominantly continental- collision in which magma was generated from the melting of continental crust. However, in the northwest part of the SSZ, the negative zircon $Ɛ_{Hf}$ (T) is interpreted to be the result of melting of old continental crust whereas the positive zircon $Ɛ_{Hf}$ (T) values would be indicative of magma generation from a juvenile (newly formed) mantle source along the UDMA. However, in the Natanz and Rabor-Lalehzar area in the central part of the UDMA additional contamination by mixing with crustal sources may have occurred.

Isotopic composition of Miocene rocks in the Taftan, Bazman, and Sorkh-Ku areas of the Sistan Suture Zone and Lut Block are also consistent with a juvenile mantle input. However, Miocene magmatic rocks in the Mirabad and Lut–Sistan areas $Ɛ_{Hf}$ (T) and $Ɛ_{Nd}$ (T) values, could be the result of a mixing of juvenile and older crustal sources (**Fig. Fig.5.29**. **C, D**).

The T_{2DM} and epsilon values calculated based on the Hf isotopic data are interpreted to represent at least two distinct crustal blocks affected by Miocene magmatism in the center and northwest parts of Central Iran, Lut, and CIM (**Fig.5.29 A, B**). Crustal Block 1, which includes the Natanz area in (C-Central Iran), and the Mirabad and parts of the Bazman area (Lut block), whereas Crustal Block 2, includes the Sahad area (northwest parts of Central Iran), the Natanz area (center part of Central Iran), and the Kerman and Anar-Sirjan (CIM). Miocene rocks from these two crustal blocks have different epsilon values but similar T_{2DM}, which is interpreted to reflect derivation for the same source region at different times during the Mesozoic (**Fig.5.29 A, B**).

Moreover, the T_{2DM} and epsilon values calculated based on the Nd isotopic data recognized two crustal blocks in the CIM and Lut zone. Crustal block 1, includes the Sorkh-Ku area (Lut), Akhikamal and Shida areas (northwest part of the SSZ), and Rabor-Lalehzar CIM (Rabor-Lalehzar), and Crustal Block 2, includes the Lut area (Lut) and Iju area (CIM). These two crustal blocks have different epsilon values but similar T_{2DM}, thereby Miocene rocks are interpreted to be derivation for the same source region but at different times (**Fig.5.29. C, D**). The isotope data collected for the Miocene rocks in WNT are summarized in Table (**5.12**).

Table 5. 12. The summary of isotope data for the Miocene rocks in western Neo-Tethys.

Location Name	**Geological Zone**	**Crustal Block**	ε_{Hf}	ε_{Nd}	**Age** (Ma)	**Reference**
Akhikamal	NW-SSZ	NW-SSZ	_	-4.11 to -3.12	10.6	(Azizi et al., 2014)
Shida	NW-SSZ	NW-SSZ	_	-3.51 to -2.87	10.6	(Azizi et al., 2014)
Sabalan-Astara	NW-UDMA	NW-Central Iran	+2.8 to +5.01	_	17.2-18.5	(Chiu et al., 2013)
Sahand	NW-UDMA	NW-Central Iran	+5.4 to +9.01	_	5.3-6.9	(Chiu et al., 2013)
Nain	C-UDMA	CIM	+4.72 to +7.66	_	15.8-17	(Chiu et al., 2013)
Natanz	C-UDMA	C-Central Iran	-1.51 to +10.52	_	15.5-21.7	(Chiu et al., 2013)
Rabor-Lalehzar	SE-UDMA	CIM	_	-0.62 to +1.44	23.2	(Moghadam, et al., 2017)
Kerman	SE-UDMA	CIM	+9.08 to +9.75		22.4-23.2	(Chiu et al., 2013)
Anar-Sirjan	SE-UDMA	CIM	+7.92 to +12.25	_	10.1-5.3	(Chiu et al., 2013)
Iju	SE-UDMA	CIM	_	+3.6 to +3.7	9.01	(Golestani, 2018)
Taftan	Sistan Suture Zone	Lut	+4.5	_	5.3-6.9	(Pang et al., 2014)
Mirabad	Sistan Suture Zone	Lut	-0.46 to +5.70	_	18.3-20	(Pang et al., 2014)
Bazman	Sistan Suture Zone	Lut	+4.53 to + 8.19	_	5.4-7.7	(Pang et al., 2014)
Sorkh-Ku	Lut	Lut	_	+0.92 to +1.84	20.1	(Hosseinkhani et al., 2017)
Lut–Sistan Suture Zone	Lut	Lut	_	-4.11 to +3.34	10.1-14.30	(Pang et al., 2012)

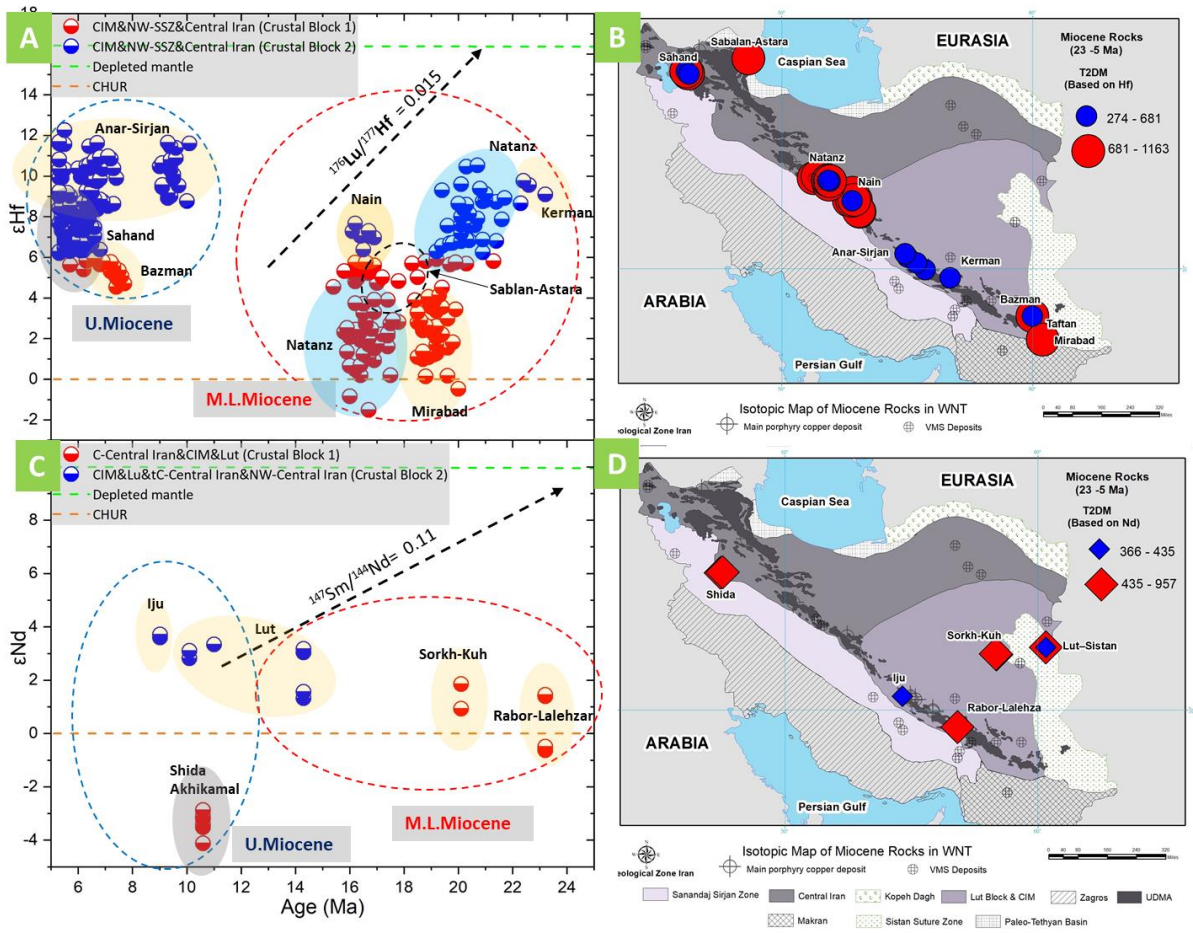

Figure 5. 29. Diagrams of ε_{Hf} (T) versus U-Pb ages and the Miocene rocks' distribution on the WNT. The legend corresponds to the different crustal blocks in WNT. The arrow shows the isotope composition trend for the intermediate crustal rocks. (**A**) Diagrams of ε_{Hf} (T) versus U-Pb ages (**B**) Distribution of T_{2DM} isotopic data on WNT, calculated based on Hf isotopic composition. (**C**) Diagrams of ε_{Nd} (T) versus U-Pb ages. (**D**) Distribution of T_{2DM} isotopic data on WNT, calculated based on Nd isotopic composition.

5.1.13. Plio-Quaternary 5.33-0.0117 (Ma)

As previously discussed Neo-Tethys' subduction was largely ended in Late Eocene and Early Oligocene and was followed by continent-continent collisional style tectonics between the Arabian and Eurasian plates during the Miocene (Allen & Armstrong, 2008; McQuarrie & Van Hinsbergen, 2013; Mouthereau, Lacombe, & Vergés, 2012). Although magmatism in the Late Miocene to Quaternary was largely diminished (Pang et al., 2016)although activity along the WNT includes various ultrapotassic (Ahmadzadeh et al., 2010; Pang et al., 2013, 2015), adakitic (Jahangiri, 2007; Omrani et al., 2008; Pang et al., 2012, 2015), alkali basaltic (Allen et al., 2013; Pang et al., 2012), and high-K calc-alkaline magmas (Davidson et al., 2004).

Adakitic magmatism during the Late Miocene to Plio-Quaternary is associated with the terminal collision between the Arabian and Eurasian plates. Omrani et al. (2008) believe that in the Anar region in the central part of the UDMA, adakites are proposed to be a product of crustal detachment and melting of the subducted slab from ca. 5–10 Ma to present (Omrani et al. 2008). Jahangiri (2007) and Pang et al. (2013) report the presence of adakites in the Marand area in the northwest part of the UDMA, and the Lut–Sistan Suture Zone, respectively. Plio-Quaternary age adakitic magmatism is also documented by Pang et al. (2015, 2016) and (Ghalamghash et al., 2016) in Sabalan volcano located in NW-UDMA (**Fig.5.30**. **B**). Similar aged adakites are described from in Georgia and Armenia (Lin, 2011) (**Fig.5.30**. **B**).

Pliocene felsic rocks plotted on Rb vs. (Y + Nb) diagram, fall within the VAG-arc setting field (**Fig.5.30**. **A**) whereas a Sr/Y vs. Y diagram Pliocene rocks from the Sabalan area in the northwest part of the UDMA all have adakitic signatures (**Fig.5.30**. **C**).

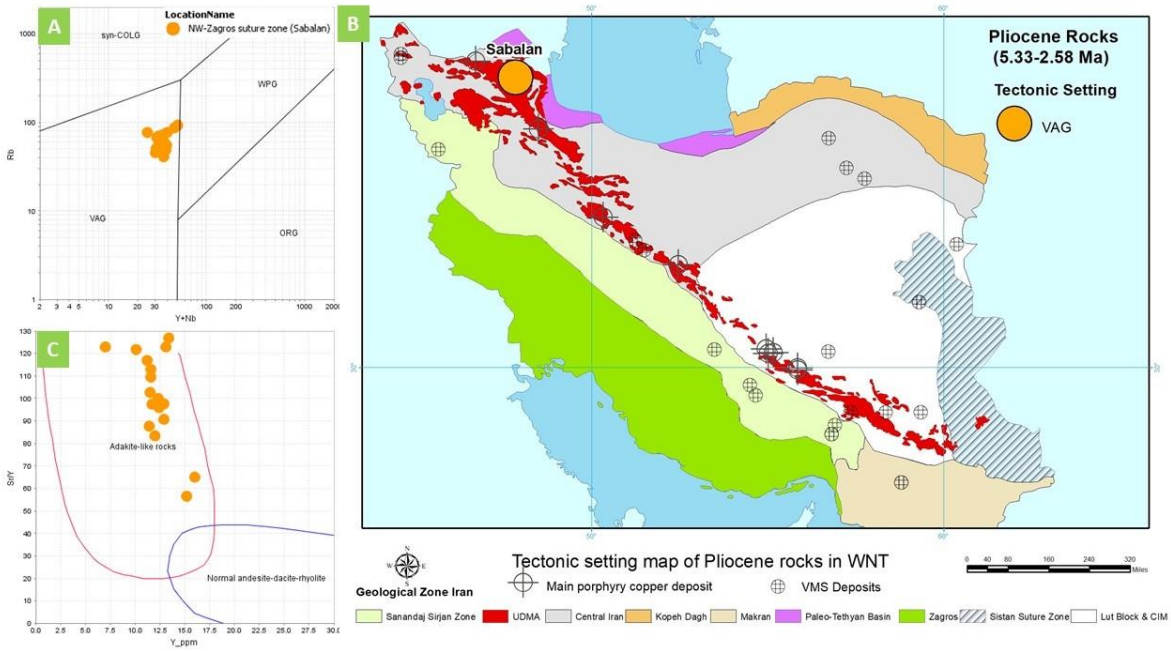

Figure 5. 30. Classification and geochemical characterization of Igneous and metamorphic rocks from Pliocene rocks in Iran's different geological zones in the WNT. (**A**) Rb vs. (Y + Nb) discriminant diagrams for the tectonic setting of felsic rocks in the study area (Pearce, Harris, & Tindle, 1984). (**B**) The distribution of the Pliocene rocks on the WNT Geological map of Iran. (**C**) Sr/Y vs. Y (ppm) diagram of Pliocene rocks from the western Neo-Tethys (Defant & Drummond, 1993).

Plio-Quaternary age rocks show positive zircon ε_{Hf} (T) and ε_{Nd} (T) values (**Fig.5.31**. **A, C**) which is consistent with arc-related post-collisional magmatism, derived from a sub-continental lithospheric mantle (Pang et al., 2012).

In the Sistan Suture Zone and Lut block of eastern Iran alkali basaltic volcanism has been interpreted to have been triggered by a mantle plume in an extensional (Pang et al., 2012). This is presumably due to the thickened lithosphere's delamination after colliding the Lut and Afghan blocks in the Late Cretaceous (Pang et al., 2012). Alternatively, Ghalamghash et al. (2016) propose that in the Sabalan area (northwest part of the UDMA) Neo-Tethyan slab roll-back and break-off, after the termination of subduction and continental collision, resulted in a steeply dipping slab remnant beneath the Eurasian plate.

The T_{2DM} and epsilon values based on the Hf isotopic data from Pliocene and Pleistocene age rocks are interpreted to reflect at least two crustal blocks in the northwest part of Central Iran, Lut, and the CIM regions., (**Fig.5.31 A, B**). Crustal Block 1 includes the Taftan area (Lut), whereas Crustal Block 2, includes the Sahand and Sabalan-Astara areas (NW-Central Iran), and the Bazman and a part of the Taftan areas (Lut). These two crustal blocks have different epsilon values but similar T_{2DM}, which is interpreted to reflect magma derived from the same source region but at different times (**Fig.5.31 A, B**).

The T_{2DM} and epsilon values calculated on the Nd isotopic data recognized two crustal blocks in Pliocene-Pleistocene rocks of the CIM and Lut zone. Crustal Block 1, includes the Lut as well as parts of the Anar area (CIM) whereas Crustal Block 2, includes the Anar area (CIM). These two crustal blocks have different epsilon values but similar T_{2DM}, thereby reflecting magma derivation for the same source region but at different times (**Fig.5.31. C, D**). Isotope data collected for the Pliocene-Pleistocene rocks in WNT are summarized in Table (**5.13**).

Table 5. 13. The summary of isotope data for the Pliocene-Pleistocene rocks in western Neo-Tethys.

Location Name	Geological Zone	Crustal Block	ε_{Hf}	ε_{Nd}	Age (Ma)	Reference
Sabalan-Astara	NW-UDMA	NW-Central Iran	+5.98 to +11.08	_	0.38	(Chiu et al., 2013)
Sahand	NW-UDMA	NW-Central Iran	+6.13 to +9.07	_	5-5.2	(Chiu et al., 2013)
Anar	SE-UDMA	CIM	_	+3.19 to +5.47	1.15	(Pang et al., 2016)
Anar-Sirjan	SE-UDMA	CIM	+9.75 to +11.89	_	5.2	(Chiu et al., 2013)
Taftan	Sistan Suture Zone	Lut	+0.31 to +4.59	_	0.5-3.5	(Pang et al., 2014)
Bazman	Sistan Suture Zone	Lut	+6.83 to +7.46	_	5.1-5.2	(Pang et al., 2014)
Lut–Sistan Suture Zone	Lut Block	Lut	_	+1.32 to +3.42	1.74-4.81	(Pang et al., 2012)

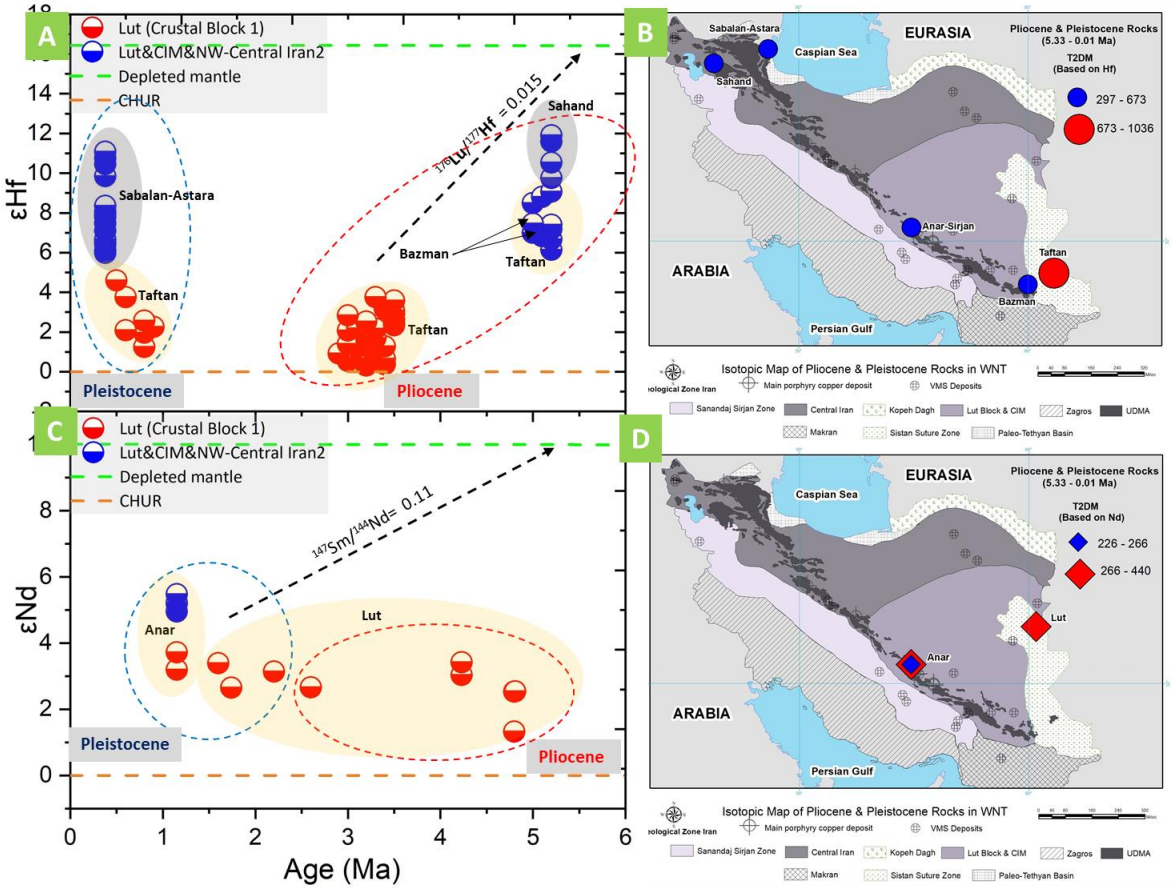

Figure 5. 31. Diagrams of ε_{Hf} (T) versus U-Pb ages and the Pliocene and Pleistocene rocks distribution on the WNT. The legend corresponds to the different crustal blocks in WNT. The arrow shows the isotope composition trend for the intermediate crustal rocks. (**A**) Diagrams of ε_{Hf} (T) versus U-Pb ages (**B**) Distribution of T_{2DM} isotopic data on WNT, calculated based on Hf isotopic composition. (**C**) Diagrams of ε_{Nd} (T) versus U-Pb ages. (**D**) Distribution of T_{2DM} isotopic data on WNT, calculated based on Nd isotopic composition.

5.2. Geochronological signatures during geological time

Data from more than 420 zircon U-Pb citations were compiled from the literature of the western Neo-Tethys (**Fig.4.8, Fig.5.32**). At least six distinct phases of magmatism are identified in the evolution of the WNT on the southern flank of Eurasia. Magmatic in the Neo-Tethys spans from the Mesozoic to Cenozoic and can be subdivided into three phases: i) a peak in the Lower Jurassic time related to the initiation of subduction along the north edge of the western Neo-Tethys; ii) two peaks in the Upper Cretaceous related to the subduction and possibly collisional phases during the Cenomanian and Campanian; and iii) three peaks related to the collisional and post-collisional Cenozoic phases during the Eocene, Oligocene, and Miocene (**Fig.5.32**).

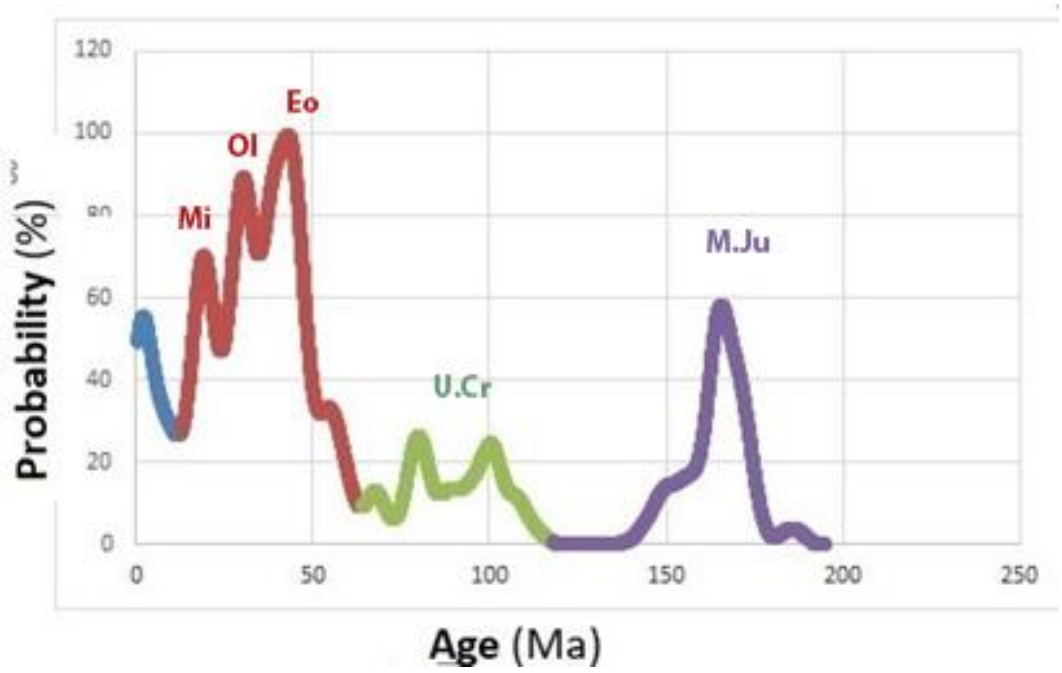

Figure 5. 32. Cumulative frequency plots show the relationship between the different phases of magmatism and their geologic time based on # 420 geochronological data points compiled from the literature on the western Neo-Tethys.

CHAPTER 6: DISCUSSION PART 2; GEODYNAMIC EVOLUTION

6.1. Geodynamic scenario of southern Neo-Tethys Ocean

The geodynamic evolution of the Neo-Tethys in Iran was initiated by rifting during the Late Permian (Stampfli, 2000). Therefore, igneous and metamorphic rocks older than Permian are referred to as basement within the western Neo-Tethys rocks.

The εHf and εNd values calculated in this study revealed that at least five large crustal blocks can be recognized in the western Neo-Tethys. They are Central Iran, Alborz, SSZ, CIM, and Lut; this being a subzone of CIM. However, in the geodynamic evolution of the WNT the Central Iran, CIM, and Lut also existed as basement blocks before the opening of the Neo-Tethys in the late Permian (Stampfli, 2000). Subsequent magmatic events resulted in younger igneous rocks being added to the basement complex; thereby formed new terranes such as the SSZ. Some researchers have proposed that the UDMA is a distinct geological terrane (Alavi 1994; Berberian & King, 1981) although as a magmatic arc it is an integral part of the pre-existing blocks SSZ and Central Iran terranes and should not be recognized as a unique crustal zone in western Neo-Tethys.

6.1.1. The Opening the Neo-Tethys and closure of Paleo-Tethys

The opening of Neo-Tethys corresponds to the closing of the Paleo-Tethys during the Carboniferous Triassic (Stampfli, 2000). This event is related to the drifting of the Cimmerian superterrane which extended from Australia to the eastern Mediterranean during the Late Carboniferous to late Early Permian. The Cimmerian terrane includes crustal blocks along the southern margin of Paleo-Tethys that were separated with the opening of Neo-Tethys during the Late Permian. Subsequent collision of the Cimmerian superterrane with the Eurasian margin (Stampfli, Marcoux, & Baud, 1991; Alavi et al., 1997) resulted in the disappearance of the Late Permian to Middle Triassic back-arc basins of Paleo-Tethys (**Fig 6.1**). These back-arc basins extended along in the southern margin of Eurasia include the Pamirs (Khain, 1994; Leven, 1995), the Caucasus (Nikishin et al., 1998), north of Afghanistan (Boulin, 1988), and the Agh-Darband area in northeast Iran (Baud & Stämpfli, 1989).

Berberian and Berberian (1981) are believed that volcanic rocks on the Precambrian basement and limestones of Lower Permian in Iran can be regarded as syn- to post-rift deposits of the northern margin of Neo-Tethys. Furthermore, the greenschist facies in Iran might be associated

with Neo-Tethys' rifting phase when they became part of the northern Neo-Tethyan active margin in the Permian (Berberian & Berberian 1981).

Isotope data compiled for Carboniferous rocks in WNT includes the Ghushchi, Naqadeh, Saqqez, and Takab A-type granites that represent juvenile mantle input in the overall northwest part of the UDMA (NW-Central Iran crustal block). In the Khalifa region in the northwest part of the SSZ located in the northwest part of Central Iran, crustal blocks lightly negative ε_{Nd} (T) values (-1.14 to -0.93) are interpreted to reflect insignificant crustal contamination during the opening of the Neo-Tethys in the northwest part of Sanandaj Sirjan Zone. Furthermore, the isotopic composition of rocks in the Takab, Sabalan-Astara, and Natanz areas of the northwest part of the UDMA and central part of the UDMA of WNT are consistent with rifting and seafloor spreading of Neo-Tethys during the Permian–Triassic times (**Fig 6.2**). At the same time, isotope data from Mashhad granodiorites and diorites (ε_{Hf} (T) -3.13 and +2.16), are interpreted as a product of a moderate mantle contribution in an extensional environment associated with the rifting of the Paleo-Tethys in the eastern Alborz Zone (**Fig 6.1**). This would contradict the reconstructions of Stampfli (2000) for the final closure of Paleo-Tethys in the eastern Alborz Zone during the Permian–Triassic times (Stampfli and Borel, 2002; Muttoni et al.,2009; Hassanzadeh & Wernicke, 2016). Furthermore, the paleo-plate reconstruction of the WNT, based on GPlates, indicates that the location of the blocks would still be very far from the closure of Paleo-Tethys during the Late Permian - Middle Triassic (291-247 Ma) (**Fig 6.2**). Reconstruction of the WNT, based on GPlates, indicates that the Closure of Paleo-Tethys occurred during the Late Jurassic (**Fig 6.4, B**).

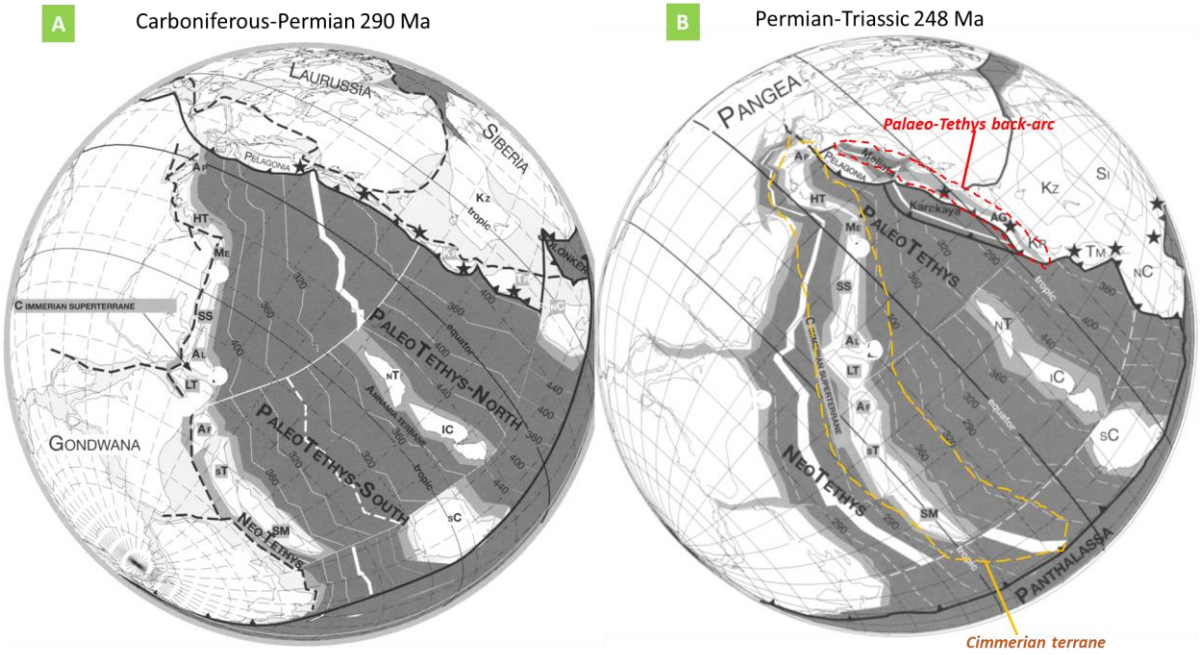

Figure 6.1. Carboniferous-Triassic (290-248 Ma) paleo-plate reconstruction of the WNT area, based on paleomagnetic data (modified after Stampfli, 2000). (**A**) Carboniferous-Permian boundary reconstruction, 290 Ma. (**B**) Permian-Triassic boundary reconstruction, 248 Ma. Abbreviation: **Ap,** Apulia s.str.; **HT,** Hellenides western Taurides externides; **Me,** Menderes-Taurus; **Ss,** Sanandaj-Sirjan; **A1,** Alborz; **Lt,** Lut-Central Iran; **Af,** central Afghanistan; **ST,** south Tibet; **SM,** Sibu Masu; **NT,** North Tibet; **IC,** Indochina and Borneo; **sC,** south China; **NC,** North China **Ka,** Karakaya; **Ag,** Agh-Darband**; Kr,** Karakum-Turan; **Kz,** Kazakhstan; **Si**, Siberia**.**

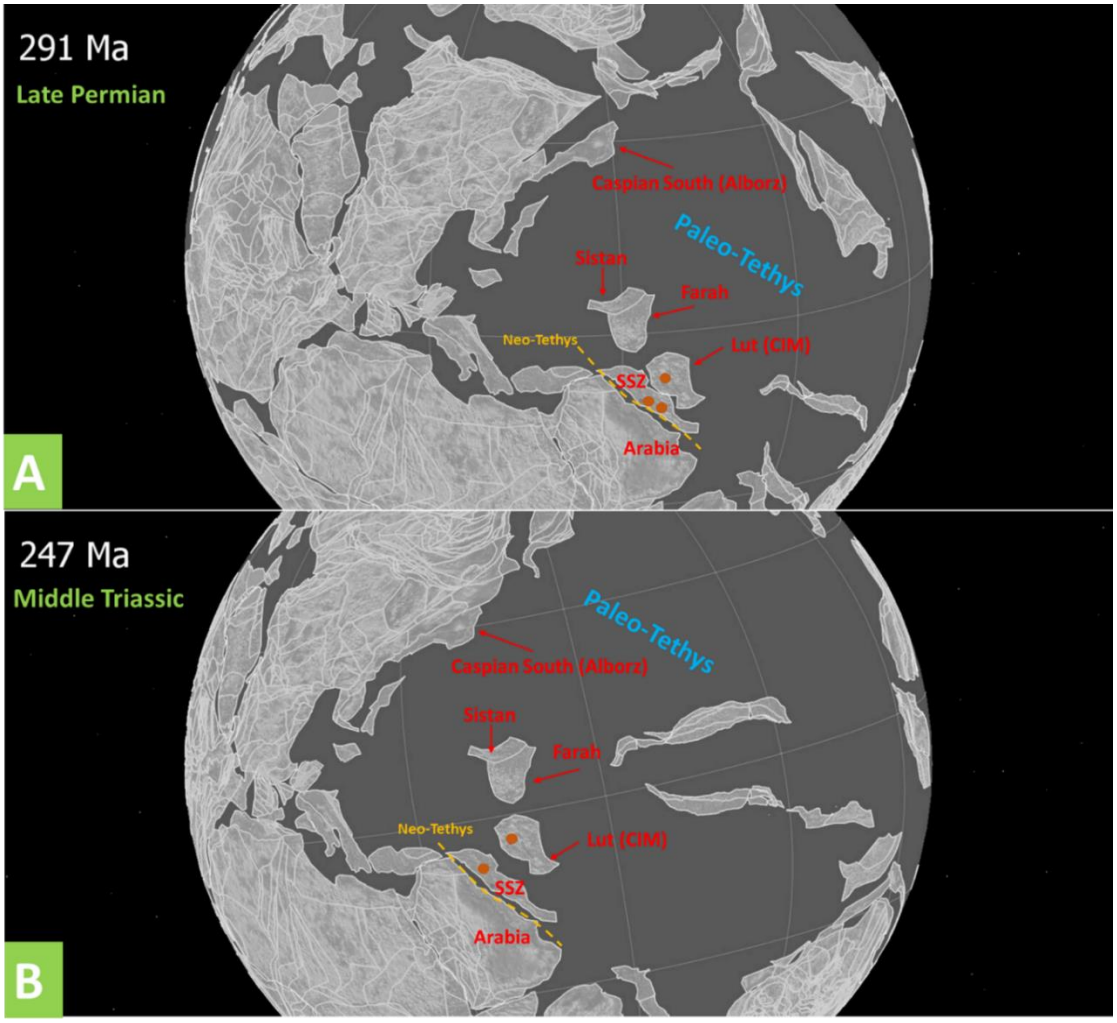

Figure 6.2. Opening of the Neo-Tethys: Late Permian - Middle Triassic (291-247 Ma) paleo-plate reconstruction of the WNT area, based on GPlates. The yellow dashed line indicates the Neo-Tethys domain. The dots show the location of Igneous geochronological samples. Data is available in the DateView database. (**A**) Late Permian boundary reconstruction, 291 Ma. (**B**) Middle Triassic boundary reconstruction, 247 Ma.

6.1.2. The initiation of Subduction

The age of deposition of thick volcano-sedimentary strata and emplacement of calc-alkaline magmas in the SSZ has been proposed to be temporally related to the initiation of subduction along the north edge of the Neo-Tethys during the Late Triassic to Early Jurassic (Stampfli and Borel, 2002; Muttoni et al.,2009; Hassanzadeh & Wernicke, 2016). However, based on GPlates reconstruction of the WNT the initiation of subduction along the Neo-Tethys during the Late Triassic — Early Jurassic is not supported. Modeling using GPlates supports, the initial

opening of the Neo-Tethys during the Late Triassic - Early Jurassic, and initiation of subduction occurred during the Middle Jurassic - Late Jurassic (**Fig.6.3. A, B, Fig.6.4. A, B**).

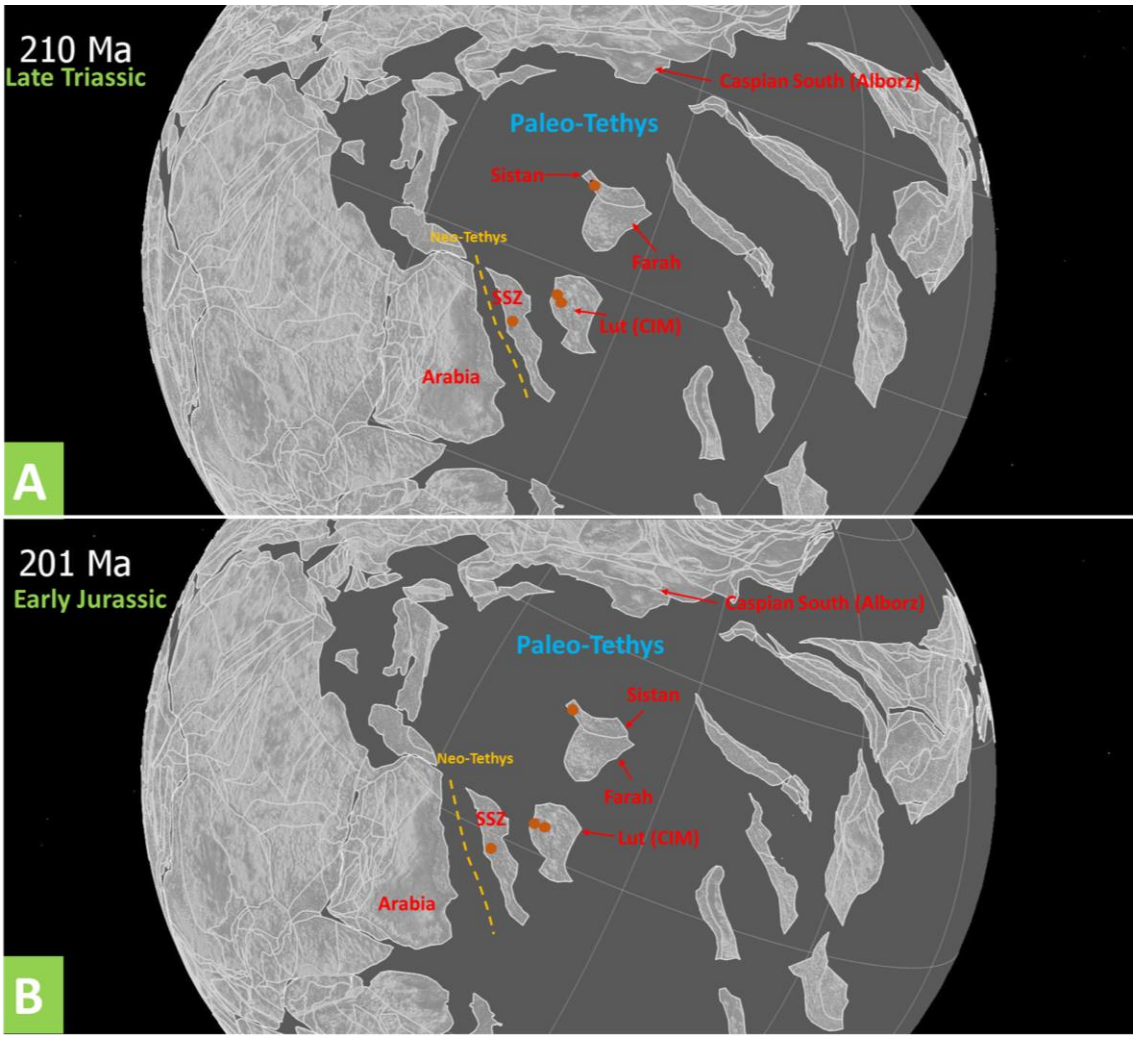

Figure 6. 3. The opening of the Neo-Tethys: Late Triassic - Early Jurassic (210-201 Ma) paleo-plate reconstruction of the WNT area, based on GPlates. The yellow dashed line indicates the Neo-Tethys domain. The dots show the location of Igneous geochronological samples. Data is available in the DateView database. (**A**) Late Triassic boundary reconstruction, 210 Ma. (**B**) Early Jurassic boundary reconstruction, 201 Ma.

The SSZ is a critical terrane for understanding the evolution of the WNT; however, the lack of isotopic data from this region was commonly a significant impediment to understanding the evolution of the collision zone. Alavi (1994), and Shafaii Moghadam and Stern (2011) proposed that the SSZ originally was located to the south, rather than north, of the main Neo-Tethys Ocean prior to the collision. Alternative interpretations considered the SSZ as a part of the

Cimmerian terrains on the northern part of Neo-Tethys before the collision (Bererian & Bererian, 1981; McCall & Kidd, 1982; Agard et al., 2011; Hassanzadeh & Wernicke 2016; this thesis). However, subduction related arc magmatism in WNT is the most distinctive activity of the SSZ, particularly during the Jurassic (**Fig 6.4**). This magmatism represents voluminous calc-alkaline plutonic and volcanic rocks.

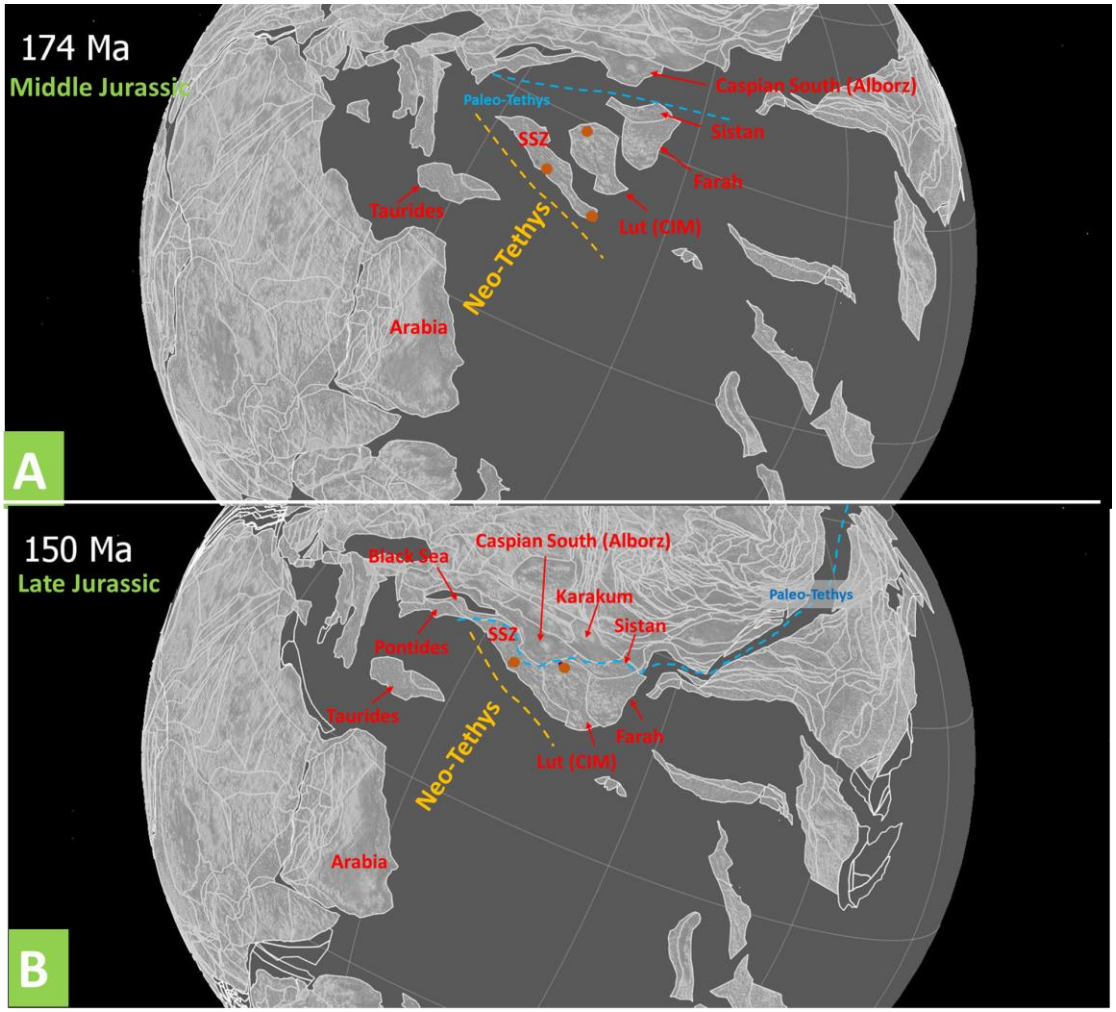

Figure 6. 4. Back-arc spreading in Neo-Tethys subduction and closure of Paleo-Tethys: Middle Jurassic - Late Jurassic (174-150 Ma) paleo-plate reconstruction of the WNT area, based on GPlates. The yellow and blue dashed lines indicate the Neo-Tethys and paleo-Tethys domains, respectively. The dots show the location of Igneous geochronological samples. Data is available in the DateView database. (**A**) Middle Jurassic boundary reconstruction, 174 Ma. (**B**) Closure of Paleo-Tethys, Late Jurassic boundary reconstruction, 150 Ma.

The most dominant episode of plutonic activity in the SSZ is the Jurassic time. From a magmatic perspective, the basement of the SSZ shows some similarities with Central Iran, except

for the Kopet Dagh zone of the pre-Norian Eurasian margin in NE Iran. Data from a total of e 420 zircon U-Pb analyses from intrusive rocks were compiled from the literature on the WNT, with ages ranging from Late Proterozoic to the Pliocene (**Fig. 4.8**). The majority of intrusive rocks are of calc-alkaline arc-related geochemical signatures with the majority representing I-type, although some A-type affinities are present (Arvin et al., 2007; Ahmadi-Khalaji et al., 2007; Shahbazi et al., 2010; Ahadnejad et al., 2011; Mahmoudi et al., 2011; Esna-Ashari et al., 2012). Histograms of the distribution of ages indicate at least six distinct phases of magmatism for the evolution of the WNT and associated back-arc basins on the south flank of Eurasia. This magmatism has flared up during the development of the Neo-Tethys from the Mesozoic to Cenozoic. One peak in the Lower Jurassic time is related to the initiation of subduction along the north edge of the western Neo-Tethys (**Fig.5.32**).

The isotope data (**Table 5.7**) collected for Late Triassic to Early Jurassic (161–200 Ma) in the Mashhad area (Alborz zone) give slightly lower zircon εHf(T) values between -3.41 to +1.38 (Chiu et al., 2017). These results are interpreted as involving a moderate mantle contribution in an extensional environment affiliated with continued rifting of the Paleo-Tethys in the eastern Alborz Zone (**Fig 6.2. A, B**). Middle Jurassic (∼165 Ma) intrusions in the SSZ and Central UDMA represent an early phase of Neo-Tethyan subduction-related magmatism. These intrusions exhibit similar zircon ε_{Hf}(T) values from +4.04 to -3.35 for Central-SSZ and northwest part of the SSZ whereas, zircon ε_{Hf} (T) values from +3.68 to -2.62 for the central part of the UDMA and southeast part of the UDMA, imply a magma origin from mixed juvenile and reworked sources during the subduction of Neo-Tethys (Chiu et al., 2013). Isotope data compiled for a series of Triassic-Cretaceous intrusions exhibit similar ε_{Nd} (T) values between -5.54 to +4.87 for the northwest part of the Sanandaj Sirjan Zone (Chiu et al., 2013; Esna-Ashari et al., 2012; Khalaji et al., 2007; Azizi et al., 2015; Ahadnejad et al., 2011; Azizi et al., 2011; Shakerardakani et al., 2015; Shahbazi et al., 2010).

The distribution of Cretaceous plutons is more limited in WNT, in contrast to the much broader distribution of Jurassic intrusive rocks. However, the Neo-Tethys oceanic crust subduction under the CIM has continued in Cretaceous and Paleocene time (**Fig 6.5, A-D and Fig 6.6, A**). The magmatic rocks represent the arc and back-arc tectonic setting in this area. Late Cretaceous intrusions are only common in the northwest part of the SSZ where three plutonic units are known;

in the Almogholagh and Kangareh-Taghiabad areas, as well as the Mishao granite in Iraqi Kurdistan (Amiri et al., 2017; Azizi et al., 2015; Abdulzahra et al., 2018). The isotope data compiled for these intrusions exhibit ε_{Nd} (T) values between +2.27 to +6.61, implying an magma derivation from juvenile sources during the subduction of Neo-Tethys. Furthermore, the Sistan Suture Zone exhibits similar zircon ε_{Nd} (T) values from +3.19 to +14.48, which indicates the same tectono-magmatic setting in eastern Iran during the Cretaceous period (Pang et al., 2014).

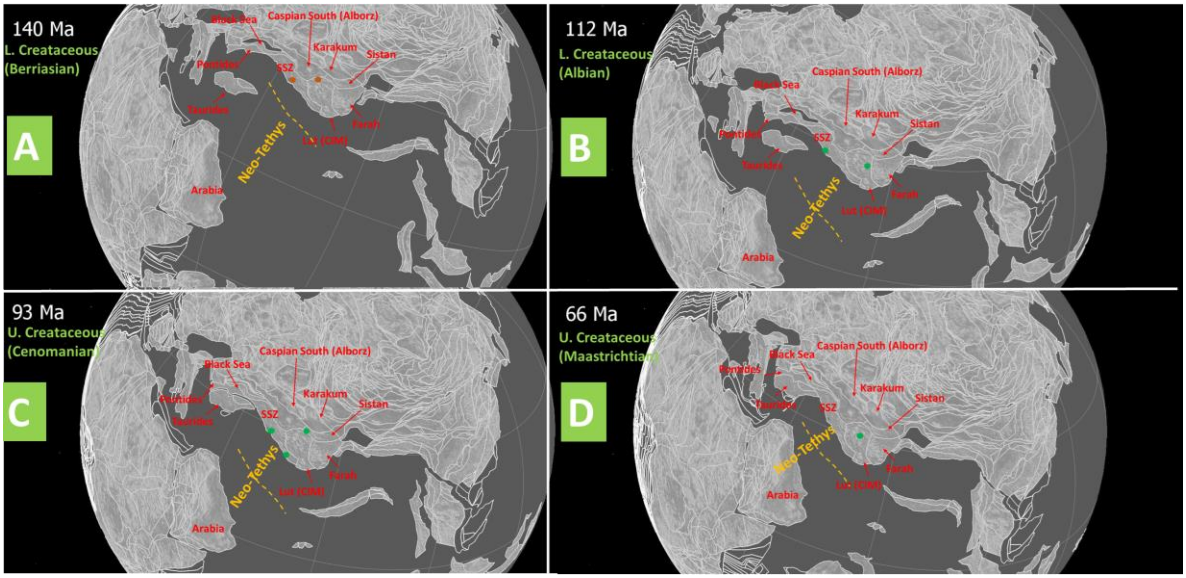

Figure 6. 5. Back-arc spreading in Neo-Tethys subduction: Cretaceous (140-66 Ma) paleo-plate reconstruction of the WNT area, based on GPlates. The yellow dashed line indicates the Neo-Tethys domain. The dots show the location of Igneous geochronological samples. Data is available in the DateView database. (**A**) L. Cretaceous (Berriasian) boundary reconstruction, 140 Ma. (**B**) L. Cretaceous (Albian) reconstruction, 112 Ma. (**C**) U. Cretaceous (Cenomanian) reconstruction, 93 Ma. (**D**) U. Cretaceous (Maastrichtian) reconstruction, 66 Ma.

The subduction of the Neo-Tethys continued during the Paleocene (**Fig 6.6. A)** with examples including (**Fig.5.16. C**) the Sahneh-Kermanshah, Neyriz, and Sabzevar ophiolites as well as Saqqez-Hasan Salary, Hasanbag, Bahr Aseman, Bibi-Maryam, and Gazu intrusive rocks (Saccani et al., 2014; Jafari et al., 2013; Moghadam et al., 2014; Babaie et al., 2001; Nouri et al., 2016; Allahyari, 2013, Allahyari et al., 2010; Saccani et al., 2013; Khosravi et al., 2017; Mahmoudi et al., 2011; Ali et al., 2013; Delavari et al., 2014; Mahdavi et al., 2016; Hosseini et al., 2017; Monsef et al., 2018; Azizi et al., 2011; Pang et al., 2014; Moghadam et al., 2016). Isotope data compiled for the Kamyaran area in the northwest part of the SSZ, Takab region in the northwest part of the UDMA, and the Mirabad granitic pluton in the Sistan Suture Zone have zircon ε_{Hf} (T) values +3.95 to +15.29. Furthermore, the Arghash area in Central Iran exhibits ε_{Nd} (T) value +5.80

(Alaminia et al., 2013). The isotopic compositions of rocks in these regions consistent with magmas generated from juvenile sources during the subduction of Neo-Tethys.

A significant flare-up of arc magmatism affected large parts of the WNT from the collision of the Arabian and Eurasian continents during the Cretaceous to Mid-Tertiary (McQuarrie et al., 2003). The peak of this magmatism occurred between 55 and 35Ma (**Fig 6.6**) with two subparallel magmatic arcs developing; i) the SSZ in a fore-arc setting, and ii) the UDMA in a back-arc setting (Verdel et al., 2011).

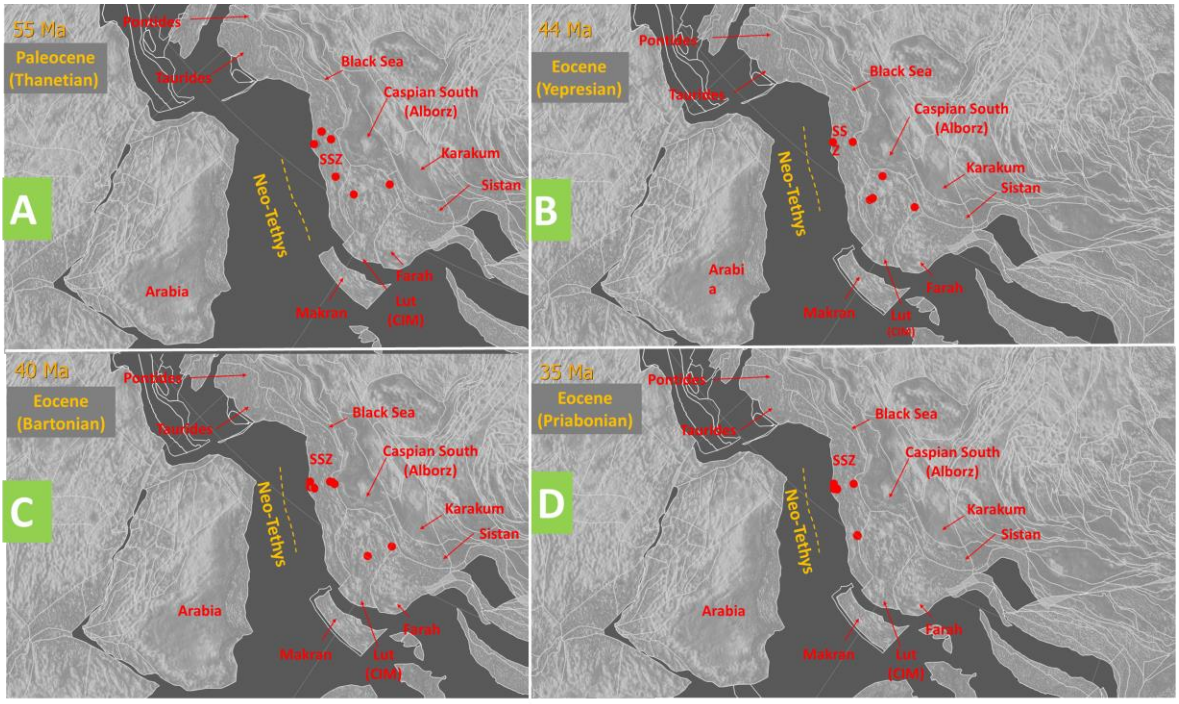

Figure 6. 6. The peak of the magmatism and the back-arc spreading during the Neo-Tethys subduction: Paleocene -Eocene (55-35 Ma) paleo-plate reconstruction of the WNT area, based on GPlates. The yellow dashed line indicates the Neo-Tethys domain. The dots show the location of Igneous geochronological samples. Data is available in the DateView database. (**A**) Paleocene (Thanetian) boundary reconstruction, 55Ma. (**B**) Eocene (Yepresian) reconstruction, 44 Ma. (**C**) Eocene (Bartonian)reconstruction, 40 Ma. (**D**) Eocene (Priabonian)reconstruction, 35 Ma.

The SSZ contains an extensive record of magmatism and has been traditionally regarded as the main suture zone of the closure of the Neo- Tethys Ocean. The boundaries of Main Zagros Thrust Zone (**Fig 2.2**) are marked with dismembered ophiolitic units between the Arabian (Zagros domain) and the SSZ which form an outer belt comprising the Neyriz, Kermanshah, and Oman ophiolites, and an inner belt hosting the Khoy and Nain-Baft ophiolites (Stöcklin, 1981). These ophiolites are considered remnants of the Neo- Tethys' Ocean basins formed during the Mesozoic to Mid-Cenozoic (e.g., Stöcklin, 1974; Sengör, 1979; Berberian & King, 1981; Stampfli and Borel, 2002; Agard et al., 2011, Hassanzadeh & Wernicke 2016).

Most researchers who have worked on the geology of Iran considered the SSZ to be part of the northern margin of the Neo-Tethys. (e.g., Stöcklin, 1968, 1974; Takin, 1972; Berberian & King, 1981; Berberian & Berberian, 1981; Tillman et al., 1981; Dercourt et al., 1986; Agard et al., 2005; Ghasemi & Talbot, 2006; Mohajjel and Fergusson, 2014). However, Alavi (1994) places the SSZ together with the Zagros domain along the southern margin of the Neo-Tethys Ocean.

According to this model, the SSZ was attached to the Arabian plate throughout the history of the Neo-Tethys Ocean. Furthermore, Alavi (1994) proposed that the Late Cretaceous-Tertiary calc-alkaline rocks of the UDMA overlie the ancient southwestern margin of Eurasia and excludes the SSZ. Therefore, in this interpretation, the MZTZ would not represent the Arabia-Eurasia suture zone (**Fig.6.7**). In GPlates reconstruction of the WNT, the location of the SSZ along the northern margin and the Zagros domain, which is part of the Arabian plate, would be located on the southern margin of the Neo-Tethys Ocean **(Fig.6.5. C, D and Fig.6.6. A).**

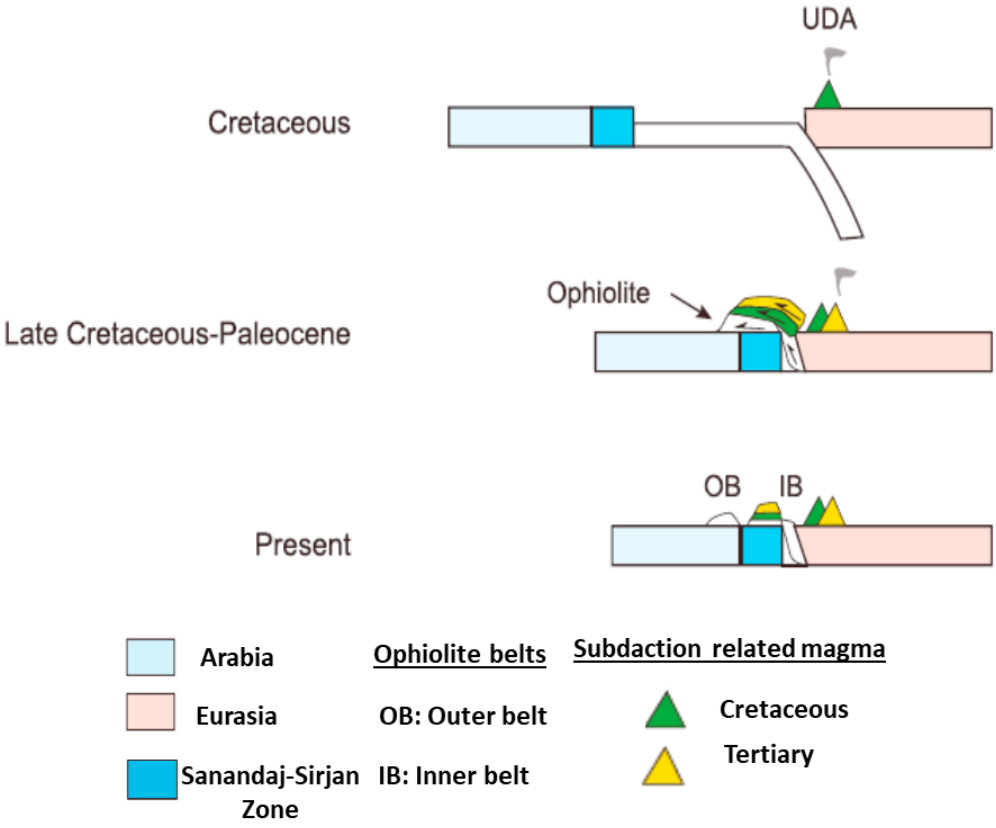

Figure 6. 7. The tectono-setting model for the evolution of WNT by Alavi (1994), considering the SSZ on the southern margin of the Neo-Tethys and viewing the igneous-metamorphic rocks of the SSZ as nappes transported from the Eurasian side after the collision.

Shafaii Moghadam and Stern (2011) proposed that the initiation of subduction of the Neo-Tethys Ocean occurred within the UDMA rather than within the SSZ. In their model both ophiolitic belts formed together in a fore-arc setting to the north of the SSZ and were transported onto the Arabian plate. According to this model, the entire SSZ was a segment along the northeastern border of the Arabian plate, and the thrusting would have occurred before the Late Cretaceous. The plate

was partially subducted, moving to the northeast as a contiguous sheet containing the rocks now represented by the inner and outer ophiolite belts. Subsequently, this plate y was re-exhumed, preserving the Outer Belt ophiolites as a klippe along its southwest margin of the Sanandaj Sirjan Zone (**Fig.6.8**.). This main disadvantage of this model is the lack of evidence in the SSZ for low-temperature metamorphism characteristic of subduction zones except for eclogites in the Shahrekord region, and the Hajiabad blueschists, as well as the blue amphiboles in the mafic inclusions in the diapirs of Hormoz salt (Talbot, 2019), which are likely Early Jurassic (Davoudian et al., 2016), there are no reported high-pressure metamorphic assemblages that would be expected similar to that in Oman and Himalayan belts.

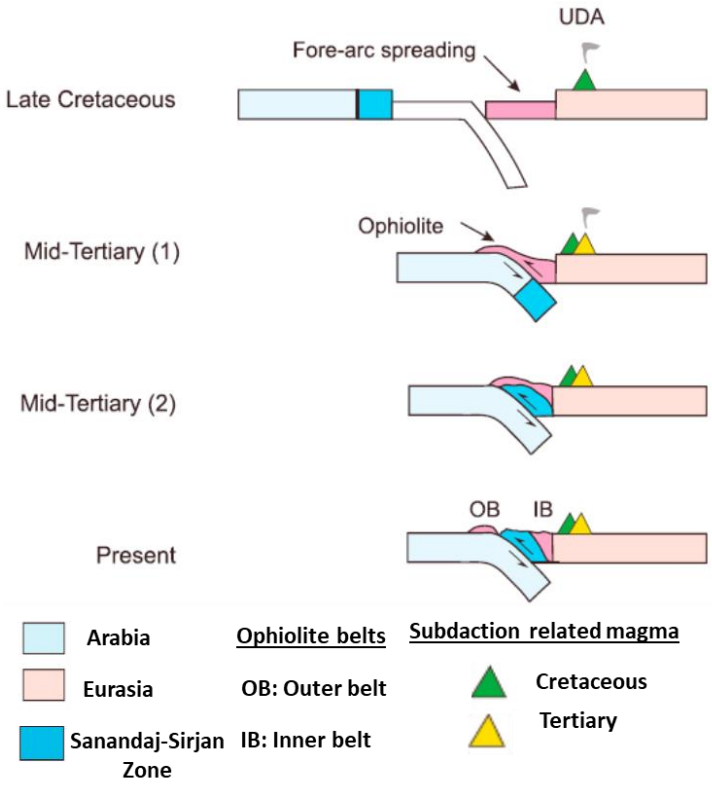

Figure 6. 8. The tectono-setting model for the evolution of WNT by Shafaii Moghadam and Stern (2011), considering the positioning of the SSZ on the southern margin of the Neo-Tethys and proposing complete burial of the SSZ in the subduction channel before rising underneath a hypothetical fore-arc ophiolitic nappe.

In this study, a modified version of the model of Hassanzadeh and Wernicke (2016) is presented. In contrast to previous models, they considered the SSZ to be located on the Neo-Tethys ocean's northern margin based on the Permian-Triassic sedimentary history and development of the Jurassic arc and paleomagnetic data (**Fig.6.9-Fig.6.11**). Accordingly, it is proposed herein, that

voluminous, I-type granitoids, MORB-like arc basalts, and gabbroic bodies in the Takab, Suffiabad, Kangareh-Taghiabad areas and the Ghalaylan Complex of the northwest part of the SSZ (Azizi et al., 2015, 2011), as well as in the Bam-Jiroft area of the southeast part of the SSZ (Sabzehei et al., 1994; Monsef et al., 2010, Chiu et al., 2013) erupted during the Late Triassic to Late Cretaceous as more evolved products of the mature arc magmatic stage.

The initiation of the arc magmatism during the Early to Late Jurassic time in the WNT is represented by the 1200 km long belt of plutonic rocks that extend from the Ghorveh area in the northwest part of the SSZ to the Bam-Jiroft area in the southeast part of the SSZ (Hassanzadeh and Wernicke, 2016, this study). Elsewhere Jurassic age plutonism occurs in the Makran area. The research results of this thesis are in contrast with the previous interpretations that the Jurassic plutonic belt was largely restricted to the northwest part of the Sanandaj Sirjan Zone (e.g., Eftekharnezhad, 1981; Mohajjel and Fergusson, 2014).

The scarcity of the Cretaceous intrusions along the Ghorveh-Jiroft segment of the SSZ has been interpreted by some workers to reflect inland migration of the arc by slab flattening (e.g., Berberian and Berberian, 1981; Verdel et al., 2011). However, the distribution of some Cretaceous plutons in the northwest part of the SSZ (Almogholagh, Kangareh-Taghiabad, and Mishao - Kurdistan-Iraq) and lack of the coeval intrusions between the northwestern and the southeastern part of SSZ can be interpreted by the cessation of arc magmatism in these regions. This could be due to the lack of slab break-off in those areas while the magmatism continued into the Cretaceous (**Fig.6.10**).

Jurassic and Cretaceous magmatic arc rocks are preserved in the Ghorveh and Khoy areas (Hassanzadeh and Wernicke, 2016) in the northwest part of the SSZ and also in the Mishao area of Iraqi Kurdistan. This arc activity continued during the Paleogene and is preserved in the Kamyaran and Takab areas in this part of the Sanandaj Sirjan Zone (**Fig.6.11**). The presence of Paleogene arc magmatism in the SSZ is difficult to explain if the UDMA was located much further to the north at the same time. Hassanzadeh and Wernicke (2016) believed that during the subduction, the slab retained its initial steep inclination in the northwestern segment. This interpretation would be consistent with the scarcity of Paleogene arc rocks in the UDMA (e.g., Stöcklin and Nabavi, 1973). Alternatively, Whitechurch et al. (2013) suggested that a flattened segment with restricted magmatism occurred within the UDMA, whereas a steeper inclined

segment under the SSZ, was associated with the localized renewal of magmatic activity during this period. However, the metamorphic history, notably. the age of metamorphic events and the protoliths remains a controversial issue in SSZ and will require the new isotopic data to resolve.

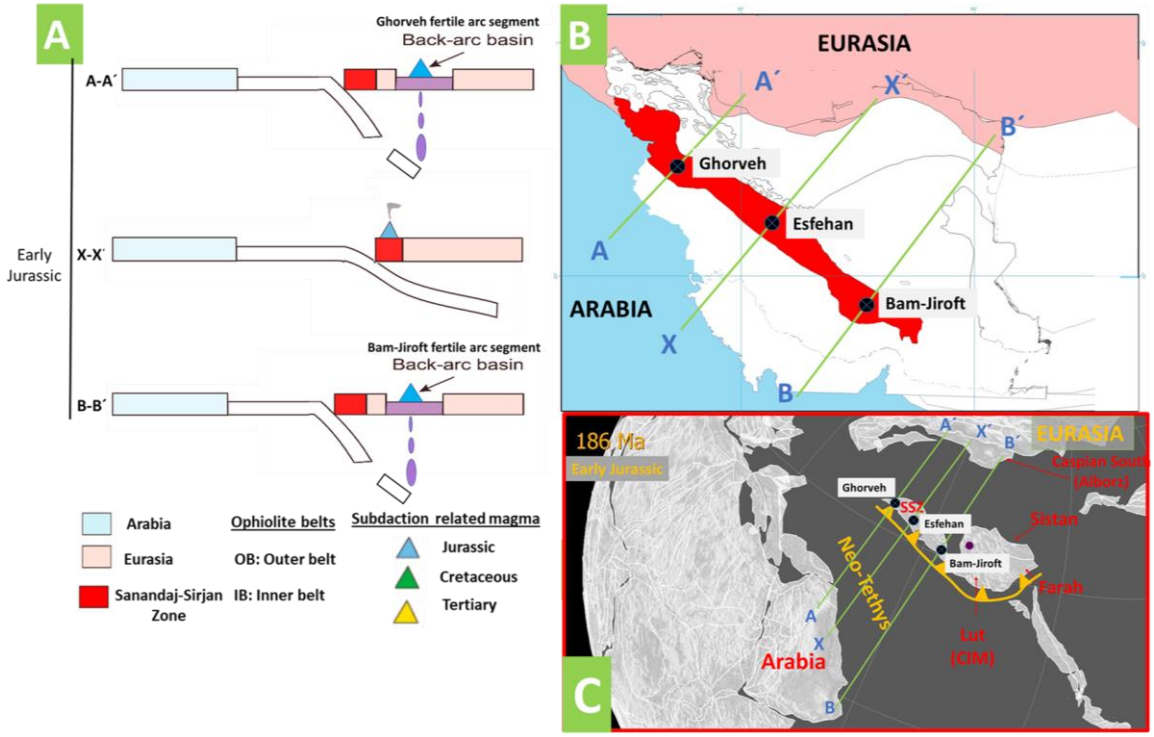

Figure 6. 9. (**A**) The tectono-setting model for the evolution of WNT in the Early Jurassic, modified after Hassanzadeh & Wernicke (2016). The development of the Early Jurassic arc in the northwest part of the SSZ (Ghorveh region), the central part of the SSZ (Esfahan region), and the southeast part of the SSZ (Bam-Jiroft region) are shown in the model. Reference for the position of the SSZ relative to the Neo-Tethys Ocean: Bererian& Bererian (1981); McCall & Kidd (1982); Agard et al., (2011); Hassanzadeh & Wernicke (2016); this study. (**B**) The schematic map shows sections A-A ′, X-X ′, and B-B′ in the northwestern, central, and southeastern parts of the SSZ, respectively. (**C**) Early Jurassic (186 Ma) paleo-plate reconstruction of the WNT area, based on GPlates. The dots show the location of Igneous geochronological samples. Data is available in the DateView database.

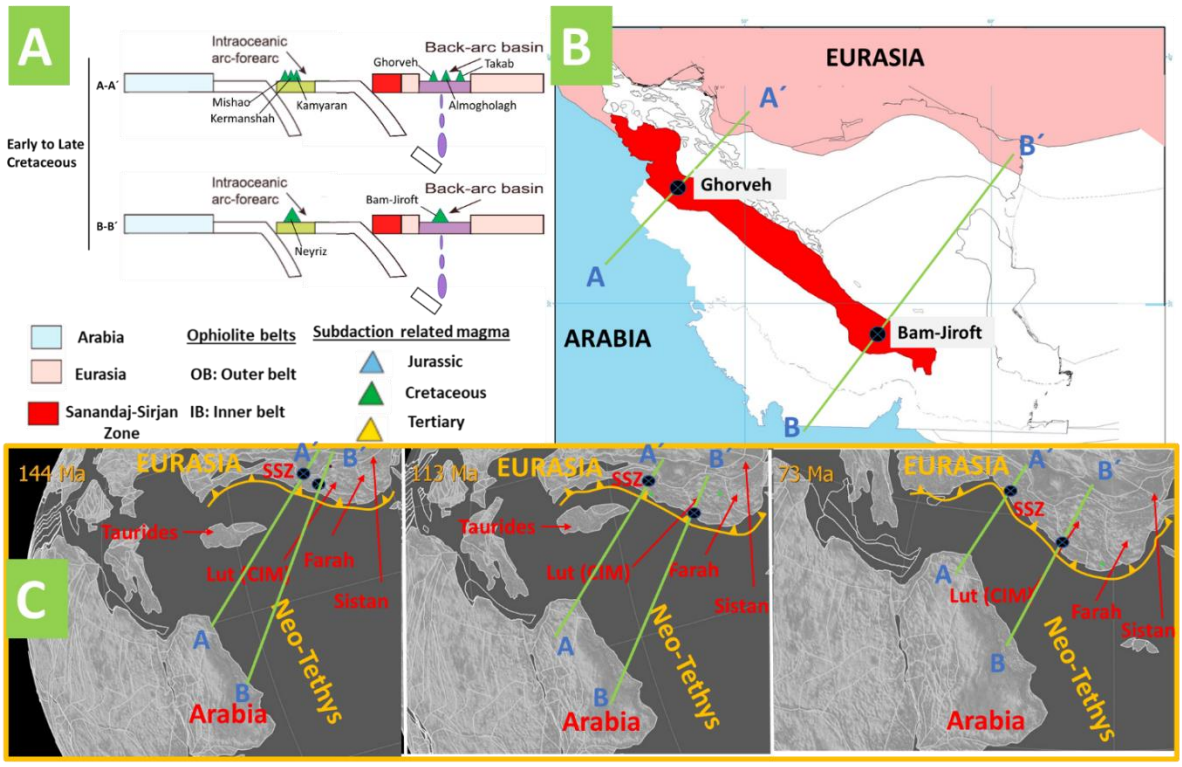

Figure 6. 10. (**A**) The tectono-setting model for the evolution of WNT in the Early to Late Cretaceous (144-73 Ma), modified after Hassanzadeh & Wernicke (2016). The development of the Early to Late Cretaceous arc in the northwest part of the SSZ (Ghorveh and Takab regions) and southeast part of the SSZ (Bam-Jiroft region) are shown in the model. Reference for the position of the SSZ relative to the Neo-Tethys Ocean: Bererian& Bererian (1981); McCall & Kidd (1982); Agard et al., (2011); Hassanzadeh & Wernicke (2016); this study. (**B**) The schematic map shows sections A-A ′, and B-B′ in the northwestern and southeastern parts of the SSZ. (**C**) Early to Late Cretaceous (144-73 Ma) paleo-plate reconstruction of the WNT area, based on GPlates. The dots show the location of Igneous geochronological samples. Data is available in the DateView database.

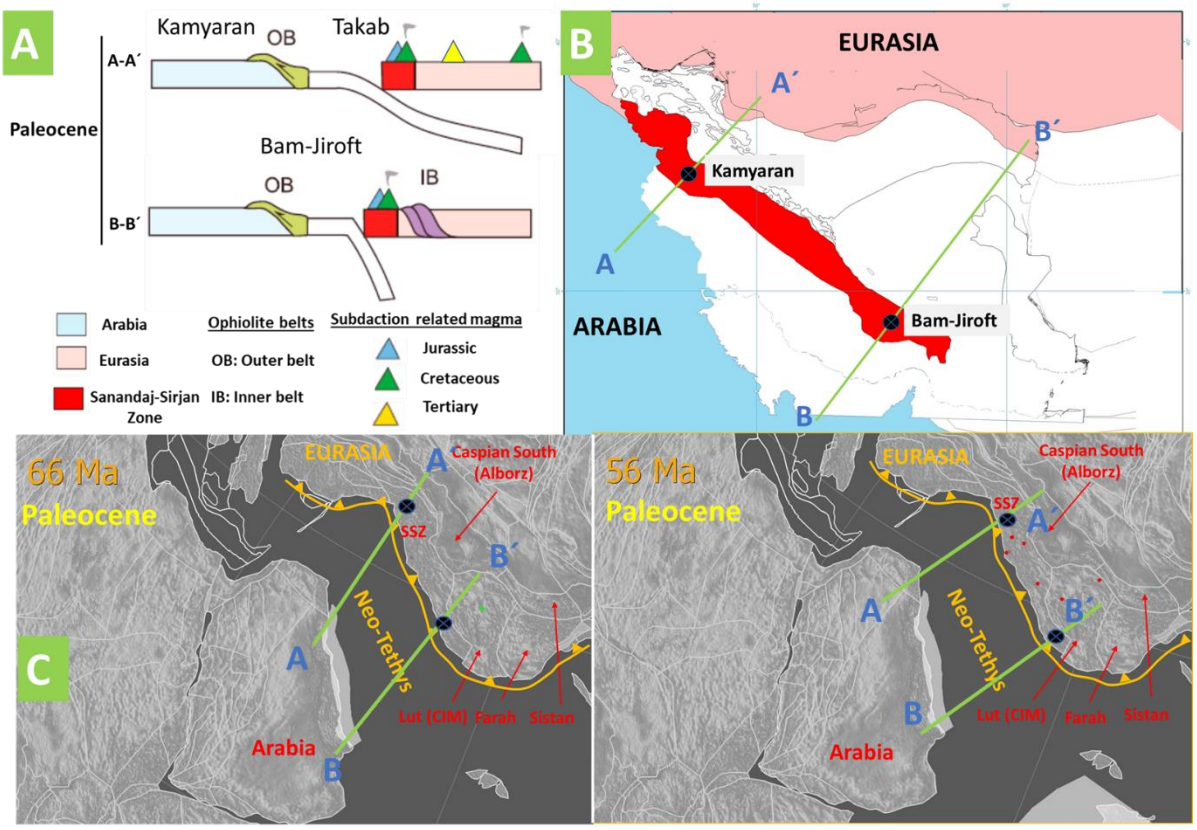

Figure 6. 11. (**A**) The tectono-setting model for the evolution of WNT in the Paleocene (66-56 Ma), modified after Hassanzadeh & Wernicke (2016). The development of the Paleocene arc in the northwest part of the SSZ (Kamyaran and Takab regions) and the southeast part of the SSZ (Bam-Jiroft region) are shown in the model. Reference for the position of the SSZ relative to the Neo-Tethys Ocean: Bererian& Bererian (1981); McCall & Kidd (1982); Agard et al., (2011); Hassanzadeh & Wernicke (2016); this study. (**B**) The schematic map shows sections A-A and B-B′ in the northwestern and southeastern parts of the SSZ. (**C**) Paleocene (66-56 Ma) paleo-plate reconstruction of the WNT area, based on GPlates. The dots show the location of Igneous geochronological samples. Data is available in the DateView database.

6.1.3. The Collision and Post-collision phase

The collision between the Arabian and Eurasian plates has a long protracted and complicated history. A range of ages have been proposed for the collisional events from the Late Cretaceous (Stocklin, 1974; Yilmaz, 1993; Stampfli, 2000), Late Eocene (Allen & Armstrong, 2008; Hatzfeld & Molnar, 2010), Late Oligocene (Allen, Jackson, & Walker, 2004; Agard et al., 2005; Fakhari et al., 2008), and the Miocene (McQuarrie, Stock, Verdel, & Wernicke, 2003; Verdel et al., 2007). However, Pang et al., (2012) proposed that there have been two different tectonic regimes coexisting in the WNT since the Middle Miocene; an extensional phase in the east and a contractional phase in the southwestern region of Iran (**Fig.5.26**. **B**).

Although it should be noted that in contrast with the well known collisional orogens world such as Alpine-Himalayan (e.g., the Pennine in the Alps or Vardar-Cyclades-Menderes in the Aegean region) and the Appalachians (e.g. the Blue Ridge area) the Iranian collision zone does not have a large internal zone or "core" of collision-related metamorphic rocks (Stöcklin, 1968; Berberian & King, 1981; Mohajjel and Fergusson, 2014, Hassanzadeh & Wernicke, 2016). The SSZ in Iran has the nearest similarity to being a metamorphic core zone to the Tethyan collisional arc (e.g., Yin, 2010). However, high-pressure/low-temperature (HP/LT) metamorphic rocks which might be expected are rare. Limited or sparse outcrops of HP/LT metamorphic rocks occur in the southeast part of the SSZ in the Makran (Sabzehei, 1974; Agard et al., 2006) and Hajiabad areas as well as on Hormoz island (Talbot, 2019). Nevertheless, the metamorphic history of the SSZ is complicated and probably occurred in multiple phases. Consequently, in most regions, both the protolith and the recrystallization ages are poorly constrained due to a lack of radiometric data therefore most metamorphic age assignments are speculative (Hassanzadeh & Wernicke, 2016).

Since the peak of subduction-related magmatism in WNT occurred between the Eocene to Oligocene (Amidi et al., 1984; Berberian & King, 1981; Chiu et al., 2013, Ali et al**.,** 2012) and the majority of subduction-related magmatic rocks in the UDMB were emplaced during Oligocene–Miocene, it is proposed that the Arabian–Eurasian continental-continent collision occurred during the Miocene to Pliocene. Furthermore, the paleo-plate reconstruction of the WNT, based on GPlates, indicates that the onset of collision between the Arabian and Eurasian plates likely was initiated between the upper Miocene (10 Ma) to Pliocene (5 Ma) (**Fig.6.12**. **C**-**F**).

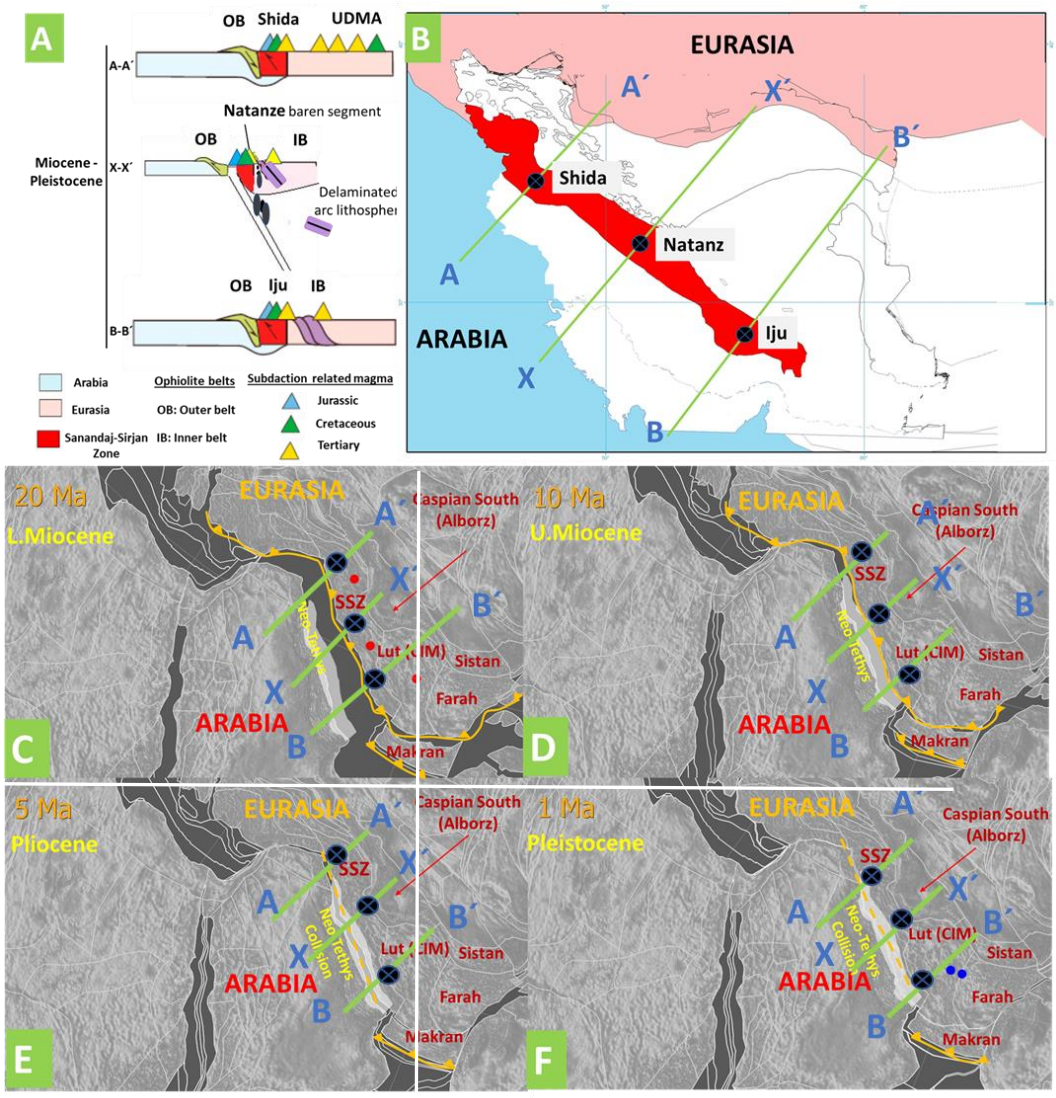

Figure 6. 12. (**A**) The tectono-setting model for the evolution of WNT in the Miocene to Pleistocene (20-1 Ma), modified after Hassanzadeh & Wernicke (2016). The development of the Miocene to Pleistocene arc in the northwest part of the SSZ (Kamyaran and Takab regions) and southeast part of the SSZ (Bam-Jiroft region) are shown in the model. Reference for the position of the SSZ relative to the Neo-Tethys Ocean: Bererian& Bererian (1981); McCall & Kidd (1982); Agard et al., (2011); Hassanzadeh & Wernicke (2016); this study. (**B**) The schematic map shows sections A-A ′, X-X ′, and B-B′ in the northwestern, central, and southeastern parts of the SSZ, respectively. (**C-F**) Miocene to Pleistocene (20-1 Ma) paleo-plate reconstruction of the WNT area, based on GPlates. The dots show the location of Igneous geochronological samples. Data is available in the DateView database.

6. 2. Adakite signatures and porphyry copper mineralization

The term “adakite” is used for intermediate to felsic rocks with high Sr/Y ratio (> 40) and low HREE (Yb<1.8 ppm) values (Defant & Drummond, 1990). These geochemical signatures

indicated the importance of garnet and/or amphibole and the absence of plagioclase in magma sources (Martin, 1999).

Porphyry-related magmas are typically related to adakite-like geochemical signatures reflected in the high Sr / Y and La / Yb ratios. They may also represent partial melting of the thickened garnetiferous lower crust. Porphyry copper deposits worldwide are genetically related to felsic intrusions typically having Sr/Y > 35 (Loucks, 2014). As a result, high Sr/Y ratios are used in the definition of adakitic signatures and porphyry-related mineralization. The Sr/Y ratio can also be used as an indicator of the average crustal pressure, or depth, at which magmatic differentiation occurred. Results from the compilation of geochemical data used in this study indicate the main Cenozoic age porphyry copper deposits in the UDMA of the WNT have high Sr/Y (**Fig.5.15**) and La/Yb (**Fig.5.16**) ratios compared with the barren rocks.

The majority of the known porphyry-type copper deposits in Iran (e.g., Sar Cheshmeh, Sungun, Meiduk, Darreh Zar, Now Chun, and Bagh Khoshk) are associated with collisional-related Miocene intrusions (Zarasvandi et al., 2005), and some Eocene back-arc intrusions (e.g., Kal-e-Kafi, Ahmadian, et al., 2009) in the UDMA. Gravimetric studies indicate a gradient in crustal thickness across the Zagros suture zone from 52 km for the Zagros mountains (Molinaro et al., 2005), and 45 km for the arc segment and 38 to 39 km for the back-arc segment of Natanz regions in the central part of the UDMA (Dehghani & Makris, 1984).

Although the peak of mineralization in WNT and for most porphyry copper deposits in Iran occurred during the Miocene in the UDMA; however, some non-mineralized or barren Miocene porphyry granites are also present in the central part of the UDMA (e.g., Miocene Natanz arc segment). One explanation for the presence of both mineralized and barren Miocene porphyry intrusions has been attributed to collision-induced delamination of the lithospheric arc root in the central part of the UDMA (Haschke et al., 2010) (**Fig.6.12**.). In this proposed geodynamic model, the high Sr and low Y (and Yb) contents of the fertile collision-related Eocene arc rocks in the Natanz area reflect thickened arc crust (~45 km), whereas post-collisional barren Miocene arc rocks (21–19 Ma) in Natanz indicate thin arc crust. This model would involve a change in the mineralogy of the residual melt from Eocene basaltic garnet-bearing (5–30%) amphibolite to Miocene metasomatized mantle peridotite, which could be a result of collision-induced delamination of the arc lithospheric root. Indeed, the lack of copper mineralization in post-

collisional Miocene Natanz arc rocks can be explained by removing the copper- and sulfur enriched metasomatized lithospheric arc root and hydrous cumulate reservoir required to form copper ore deposits with arc-root delamination in this area (**Fig.6.12**.). As a matter of fact, in the Natanz arc segment of the central part of the UDMA, the higher Sr/Y ratios in fertile Eocene rocks can be attributed to the arc crustal thickening (~45 km), as suggested by previous gravimetric studies (Dehghani & Makris, 1984). In contrast, the lower Sr/Y ratios of barren Miocene rocks are related to the melting of garnet-free peridotite in the thin (~38 km) lower arc crust of the Natanz area. Furthermore, the lack of the dense melt residues also provides an alternative interpretation to the Iranian arc plateau (38 km) as a result of ascending by isostatic rebound rather than uplift by anomalous shortening (Haschke et al., 2010).

Porphyry copper deposits in Azerbaijan (northwest part of the UDMA), the Kerman area (southeast part of the UDMA), and the Lut Block (CIM) (). The deposits are related to calc-alkaline arc magmatism. Porphyry deposits in the Lut block region are gold-rich associated with subducted oceanic slabs magmatism (Arjmandzadeh et al., 2011; Malekzadeh Shafaroudi et al., 2015; Arjmandzadeh & Santos, 2014; Mahdavi et al., 2016) whereas deposits in the southeast part of the UDMA are gold-poor, with low $f_{O2,}$ and are interpreted to be hosted by rocks derived from partial melting of the lower crust in a thickened continental arc (Shafiei & Shahabpour, 2008). In the southeast part of the UDMA, the mineralization occurred in the Late Oligocene and Middle to Late Miocene (Mirnejad et al., 2013; McInnes et al., 2005; Aghazadeh et al., 2015). In contrast, porphyry mineralization in the northwest part of the UDMA occurred during the Late Oligocene to Early Miocene (Aghazadeh et al., 2015) whereas in the CIM it ranged from Late Eocene to Early Oligocene (Malekzadeh Shafaroudi et al., 2015; Arjmandzadeh & Santos, 2014).

The presence of Cenozoic adakitic magmatism in central Iran and UDMA depends on successive stages of opening and closing of the Neo-Tethys, including subduction during the Cretaceous-Oligocene and continent-continent collision in the Paleogene (Mohajjel et al., 2003; McClay et al., 2004; Agard et al., 2005). Geochronological results reveal that the porphyry mineralization in the WNT has been moved from the northwest part to the southeast part of the UDMB over time (Aghazadeh et al., 2015) and porphyry copper deposits in the central part of the UDMB (Saveh–Yazd porphyry copper belt) have been formed in the Middle Miocene (17–15 Ma, Aghazadeh, et al., 2015). Recent studies, however, suggest that some porphyry copper deposits

formed after the end of subduction in a post-collisional tectonic setting (Richards, 2009; Hou et al., 2009; Shafiei et al., 2009; Sillitoe, 2010). Recent studies, however, suggest that some porphyry copper deposits formed after the end of subduction in a post-collisional tectonic setting (Richards, 2009; Hou et al., 2009; Shafiei et al., 2009; Sillitoe, 2010).

This study has shown that magmatic rocks of adakitic affinity were first emplaced in the WNT in the Early Jurassic. The first magmatism of adakitic affinity was the Kangareh-Taghiabad and Ghalaylan Complex in the Ghorveh area in the northwest part of the SSZ which was emplaced during the Middle to Late Jurassic for (These rocks belong to a series of Triassic to Cretaceous age intrusions which were emplaced in a volcanic arc and back-arc setting in the SSZ of the Zagros orogenic belt, (Azizi et al., 2015; Esna-Ashari et al., 2012; Shakerardakani et al., 2015). Neo-Tethys subduction of oceanic crust under the CIM has continued from the Jurassic to Paleogene, with adakitic magmatism occurring along segments of the western Neo-Tethys.

Magmatism in the WNT flared-up during the Eocene to the Oligocene (Amidi et al., 1984; Berberian & King, 1981; Chiu et al., 2013, Ali et al., 2012), which coincided with the end of the subduction of Neo-Tethys under the CIM. The result was that the majority of magmatic rocks formed in the UDMA during the Oligocene–Miocene, which coincided with the continent-continent collision of the Arabian and Eurasian plates and post-collisional magmatism. Adakitic magmatism in the WNT is summarized in Table (5.13).

Table 6. 1. Summary of adakitic magmatism in the western Neo-Tethys.

Geological Time	Adakitic signatures	Geological Zone	Location Name	Tectonic Setting
Neoproterozoic to Carboniferous 1000-298.9 (Ma)	-	-	-	Before the formation of the Neo-Tethys
Permian 298.9-251.9 (Ma)	-	-	-	Rifting
Triassic 251.9-201.3 (Ma)	-	-	-	Rifting
Jurassic 201.3-145 (Ma)	*	NW-SSZ	**Majority samples**: Kangareh-Taghiabad and Ghalaylan Complex	The onset of the Subduction (Arc and back-arc)
Cretaceous 145-66 (Ma)	*	Lut Block	**Majority samples**: Sabzevar, Band-e-Zeyarat/ Dar Anar ophiolites, Gazu	Subduction (Arc Setting)
Paleocene 66-56 (Ma)	*	Central Iran NW-SSZ	**Majority samples**: Bibi-Maryam, Saqqez-Hasan Salary, Gazu	Subduction (Arc Setting)
		NW-Zagros suture zone Lut Block	**Some samples**: Kermanshah ophiolites, Sabzevar ophiolites	
Eocene 56-33.9 (Ma)	*	Central Iran Lut Block NW-UDMA Alborz- Central Iran	**Majority samples**: Firozeh mine, Sabzevar ophiolites Khopik, Sourkh-Kuh, Khunik Zanjan	Subduction (Arc Setting)
		NW-SSZ Zagros suture zone	**Some samples**: Tarm, Kamyaran, Taa-Baysaran, Sarvabad, Kermanshah ophiolites	
Oligocene 33.9-23.03 (Ma)	*	Sistan Suture Zone C-UDMA	**Majority samples**: Zahedan, Dali	Pre-collisional-Collisional
		NW-Zagros suture zone C-Zagros suture zone SE-Zagros suture zone Lut Block-Sistan suture zone NW-SSZ C-UDMA SE-UDMA	**Some samples**: Kermanshah ophiolites Khoy ophiolites, Naein-Baft ophiolitic Gohar-Baft and Haji-Abad ophiolites Kahnuj ophiolites Sanandaj Daili deposit Takht-e-Gonbad	
Miocene 23.03-5.33 (Ma)	*	SE-UDMA Sistan suture zone	**Majority samples**: Iju Lut Block -Sistan	Collisional-Post Collisional

		Lut Block		
Plio-Quaternary 5.33-0.0117 (Ma)	*	C-UDMA NW-UDMA Sistan suture zone NW-UDMA	**Majority samples**: Anar Marand Lut Block -Sistan Sabalan	Collisional-Post Collisional

CHAPTER 7: CONCLUSION

The aim of this project was focused on the geodynamic evolution of the WNT and understanding the geochronological and geochemical relationship between magmatism and porphyry-type Cu mineralization in this region.

The hypothesis being tested in this research is: because of the long-recognized analogy between the cordilleran-type UDMA and Andean arcs, porphyry copper deposits form in mature arc settings with the enriched and thickened lithosphere during the evolution of the UDMA.

The thesis methodology incorporated a rigorous comprehensive compilation and regional synthesis of published geochronological and geochemical data of largely Mesozoic magmatism to provide quantitative constraints on the tectonomagmatic evolution of the western Neo-Tethys.

By integrating a large data set of isotopic ratios, geochronological, and geochemical data of magmatic rocks in a unique GIS database, a rigorous correlation of tectonomagmatic events in both time and space could be made with porphyry-style mineral deposits of the western Neo-Tethys. The correlation between the geochemistry and the geochronological data led to a better petrogenetic understanding of the location of porphyry deposits in the western Neo-Tethys.

This study has identified that at least six distinct phases of magmatism for the evolution of the WNT and associated back-arc basins located on the southern margin of the Eurasian plate. This magmatism has flared up during the development of the Neo-Tethys from the Mesozoic to Cenozoic. It can be subdivided into three phases: one peak in the Lower Jurassic, which is related to the initiation of subduction along the north edge of the western Neo-Tethys; two peaks in the Upper Cretaceous, which are related to the subduction and probably collisional phases during Cenomanian and Campanian, and three peaks presumably related to collision and post-collisional magmatic events during the Eocene, Oligocene, and Miocene (**Fig.5.32**).

The geodynamic evolution of the Neo-Tethys in Iran proposed to have started by rifting during the Late Permian. Therefore, igneous and metamorphic rocks older than Permian are considered to form the basement crustal blocks to younger rocks of the western Neo-Tethys. Based on ratios calculated for ε_{Hf} and ε_{Nd} values compiled from published literature at least five large crustal blocks can be recognized in the WNT and include Central Iran, Alborz, SSZ, CIM, and Lut

(as a subzone of CIM). However, Central Iran, CIM, and Lut also existed as basement crustal blocks before the opening of the Neo-Tethys in the late Permian. Subsequently, with further magmatic events additional crustal blocks, such as the SSZ and UDMA were formed and added to the existing basement blocks.

In this study, the following tectonic model is suggested for the development of the western Neo-Tethys:

(1) In agreement with Stampfli's (2000) previous proposal, the initial opening of Neo-Tethys is interpreted to correspond to the final closing of Paleo-Tethys Ocean. This event is related to the drifting of the Cimmerian superterrane in Middle Triassic times. The isotope data collected for the Carboniferous rocks in WNT represent an overall dominance of juvenile mantle input in the northwest part of the UDMA (NW-Central Iran crustal block) and the northwest part of the Sanandaj Sirjan Zone (NW-Central Iran crustal block). Furthermore, the isotopic composition in the northwest part of the UDMA and central part of the UDMA is consistent with the rifting and seafloor spreading of the Neo-Tethys during the Permian and Triassic. At the same time, isotope data from Mashhad granodiorites and diorites are interpreted to be the product of a moderate mantle contribution in an extensional environment affiliated with the rifting of the Paleo-Tethys in the eastern Alborz Zone (**Fig 6.1**). This result contradicts Stampfli's (2000) reconstructions for the final closure of Paleo-Tethys in the east of Alborz Zone during the Permian–Triassic times. Furthermore, reconstruction of the WNT, based on GPlates, indicates that the closure of Paleo-Tethys occurred during the Late Jurassic (**Fig 6.4, B**).

(2) According to previous works, the initiation of subduction along the northern margin of the Neo-Tethys occurred in the Late Triassic to Early Jurassic; however, this event has not been supported by the reconstruction of the WNT using GPlates. Our model shows that the opening of the Neo-Tethys formed during the Late Triassic - Early Jurassic period and the initiation of subduction occurred during the Middle Jurassic - Late Jurassic (**Fig.6.3. A, B, Fig.6.4. A, B**).

Furthermore, the geodynamic evolution of the southern Neo-Tethys Ocean has identified that during convergence between Arabia and Eurasia in WNT, the dip angle of the subducting oceanic lithosphere of the Neo-Tethys Ocean became shallower during the Cretaceous resulting in a migration of arc magmatism northeastward from the SSZ into the UDMA. A significant flare-up of arc magmatism affected huge parts of Iran and WNT from Cretaceous until the mid-Tertiary

collision of the Arabian and Eurasian continents. The peak of this magmatism occurred between 55 and 35Ma. This flare-up has formed two parallel arc regions. The SSZ lay in the fore-arc during this time and UDMA in the back-arc area.

(3) Since the peak of subduction-related magmatism in WNT occurred in Eocene to Oligocene and due to the majority of magmatic rocks formed in the UDMA during Oligocene–Miocene, we proposed that the Arabian–Eurasian continental collision probably occurred during the Miocene–Pliocene. Furthermore, the paleo-plate reconstruction of the WNT, based on GPlates, indicates that the initiation of collision between Arabia and Eurasia occurred between the upper Miocene to Pliocene (10-5 Ma) (**Fig.6.12**. **C-F, Table App 5**).

The peak of porphyry-type mineralization in WNT occurred during the Miocene with the majority of known porphyry copper deposits in Iran located in the UDMA; nevertheless, barren Miocene porphyry granites also are present in the central part of the UDMA notably the Miocene Natanz arc segment. The presence of barren granites might be the result of collision-induced delamination and separation of the fertile lithospheric arc root below the central part of the UDMA (**Fig.6.12**).

Porphyry-related mineralization in the WNT is related to the two parallel domains of the SSZ and UDMA, which are the result of the NE-dipping subduction of the Neo-Tethys in the western Neo-Tethys. Geochemical data, consistent with and adakitic signatures for magmatic rocks in these areas, are similar to Andean-type magmatism. Mineralization is linked to the intrusion-related porphyry copper system of the UDMA which is dominated by substantial volcanic activity. Alternatively, the formation of VMS deposits in the CIM is interpreted to be related to an extensional back-arc environment developed along a continental margin.

Another area in the WNT with potential for mineralization is the SiSZ, located between the Lut and Afghan continental blocks. This area comprises Cenozoic igneous and metamorphic rocks associated with the subduction of Neo-Tethys in Eastern Iran. This area hosts extensive subduction-related Cretaceous ophiolitic mélanges which are followed by Upper Cretaceous-Eocene flysch sediments that are interpreted to have been deposited in a forearc setting. Eocene to Oligocene age volcanic arc magmatism preserved in the SiSZ is interpreted to have originated mainly from mantle sources and have been attributed to the delamination of a thickened lithospheric root.

The Sungun, Sarcheshmeh, and Miduk deposits are the best known examples of Eocene to Miocene subduction-related porphyry-type mineralization in the western Neo-Tethys (**Fig.4.13**). This porphyry-related mineralization is interpreted to have formed during the final closure stage of the Neo-Tethys Ocean. Additionally, the most famous VMS deposits in WNT are the Bavanat, the Sargaz, the Chahgaz, the Barika, and the Sheikh Ali deposits, which are concentrated mainly in the southern part of the CIM (**Fig.4.14**). These VMS deposits are related to the Lower Late Cretaceous volcano-sedimentary sequence developed in an extensional back-arc environment along a continental margin.

Porphyry-related mineralization has a range of ages across Iran. In the southeast part of the UDMA, the age of mineralization is Late Oligocene and Middle to Late Miocene. In contrast, porphyry mineralization in the northwest part of the UDMA and CIM formed during Late Oligocene to Early Miocene and Late Eocene to Early Oligocene, respectively.

This study has shown that no adakitic signatures are observed in WNT rocks until the early Jurassic. The earliest adakitic magmatism is associated with the Middle to Late Jurassic Kangareh-Taghiabad intrusions and Ghalaylan Complex in the Ghorveh area of the northwest part of the SSZ. Subduction of the Neo-Tethys oceanic crust under the CIM continued from Jurassic to Paleogene time with adakitic magmatism being emplaced along segments of the western Neo-Tethys. Furthermore, the magmatism in the WNT flared-up in the Eocene to the Oligocene coinciding with the end of subduction of Neo-Tethys under the CIM. The majority of magmatic rocks formed in the UDMA during Oligocene to Miocene coinciding with the continental collision of the Arabian–Eurasian plates and post-collisional magmatic activity.

REFERENCES

Abdulzahra, I. K., Hadi, A., Asahara, Y., Azizi, H., & Yamamoto, K. (2018). Petrogenesis and geochronology of Mishao peraluminous I-type granites, Shalair valley area, NE Iraq. *Chemie Der Erde*. 78, 215-227 https://doi.org/10.1016/J.CHEMER.2018.01.003

Aftabi, A., & Atapour, H. (2009). Comments on "Arc magmatism and subduction history beneath the Zagros Mountains, Iran: A new report of adakites and geodynamic consequences" by J. Omrani, P. Agard, H. Whitechurch, M. Bennoit, G. Prouteau, L. Jolivet. *Lithos*, *113*(3–4), 844–846. https://doi.org/10.1016/J.LITHOS.2009.04.032

Aftabi, A., & Atapour, H. (2011). Alteration Geochemistry of Volcanic Rocks around Sarcheshmeh Porphyry Copper Deposit, Rafsanjan, Kerman, Iran: Implications for Regional Exploration. *Resource Geology*, *61*(1), 76–90. https://doi.org/10.1111/j.1751-3928.2010.00149.x

Agard, P., Omrani, J., Jolivet, L., & Mouthereau, F. (2005). Convergence history across Zagros (Iran): Constraints from collisional and earlier deformation. *International Journal of Earth Sciences*, *94*(3), 401-419. https://doi.org/10.1007/s00531-005-0481-4

Agard, P., Omrani, J., Jolivet, L., Whitechurch, H., Vrielynck, B., Spakman, W., … Wortel, R. (2011). Zagros orogeny: A subduction-dominated process. *Geological Magazine*, *148*(5–6). https://doi.org/10.1017/S001675681100046X

Agard, P., Yamato, P., Jolivet, L., & Burov, E. (2009). Exhumation of oceanic blueschists and eclogites in subduction zones: Timing and mechanisms. *Earth-Science Reviews*. 92, 53-79. https://doi.org/10.1016/j.earscirev.2008.11.002

Aghanabati, A. (1998). *Major sedimentary and structural units of Iran (map)*.

Aghanabati, A. (2004). *Geology of Iran*.

Aghazadeh, M., Hou, Z., Badrzadeh, Z., & Zhou, L. (2015a). Temporal–spatial distribution and tectonic setting of porphyry copper deposits in Iran: Constraints from zircon U–Pb and molybdenite Re-Os geochronology. *Ore Geology Reviews*, *70*, 385–406. https://doi.org/10.1016/J.OREGEOREV.2015.03.003

Aghazadeh, M., Hou, Z., Badrzadeh, Z., & Zhou, L. (2015b). Temporal–spatial distribution and tectonic setting of porphyry copper deposits in Iran: Constraints from zircon U–Pb and molybdenite Re-Os geochronology. *Ore Geology Reviews*, *70*, 385–406. https://doi.org/10.1016/J.OREGEOREV.2015.03.003

Ahadnejad, V., Valizadeh, M.-V., Deevsalar, R., & Rezaei-Kahkhaei, M. (2011). Age and geotectonic position of the Malayer granitoids: Implication for plutonism in the Sanandaj-Sirjan Zone, W Iran. *Neues Jahrbuch f?R Geologie Und Pal?Ontologie - Abhandlungen*, *261*(1), 61–75. https://doi.org/10.1127/0077-7749/2011/0149

Ahmadian, J., Haschke, M., McDonald, I., Regelous, M., RezaGhorbani, M., Emami, M. H., & Murata, M. (2009). High magmatic flux during Alpine-Himalayan collision: Constraints from the Kal-e-Kafi complex, central Iran. *Geological Society of America Bulletin*, *121*(5–6), 857–868. https://doi.org/10.1130/B26279.1

Ahmadian, Jamshid, Sarjoughian, F., Lentz, D., Esna-Ashari, A., Murata, M., & Ozawa, H. (2016). Eocene K-rich adakitic rocks in Central Iran: Implications for evaluating its Cu–Au–Mo metallogenic potential. *Ore Geology Reviews*, *72*, 323–342. https://doi.org/10.1016/j.oregeorev.2015.07.017

Ahmadzadeh, G., Jahangiri, A., Lentz, D., & Mojtahedi, M. (2010). Petrogenesis of Plio-Quaternary post-collisional ultrapotassic volcanism in NW of Marand, NW Iran. *Journal of Asian Earth Sciences*, *39*(1), 37–50. https://doi.org/10.1016/j.jseaes.2010.02.008

Alaminia, Z., Karimpour, M. H., Homam, S. M., & Finger, F. (2013). The magmatic record in the Arghash region (northeast Iran) and tectonic implications. *International Journal of Earth Sciences*. 102, 1603–1625. https://doi.org/10.1007/s00531-013-0897-1

Alaminia, Z., Salehi, M., & Finger, F. (2017). Discovery of the Hendou-abad copper mineral district and

its association to dikes: A reconstruction scenario for exploration of Cu-porphyry, northeast Isfahan, Iran. *Journal of Geochemical Exploration*, *183*, 88–101. https://doi.org/10.1016/J.GEXPLO.2017.10.006

Alavi, M. (1994). Tectonics of the Zagros orogenic belt of Iran: new data and interpretations. *Tectonophysics*, *229*(3–4). https://doi.org/10.1016/0040-1951(94)90030-2

Alavi, Mehdi. (1980). Tectonostratigraphic evolution of the Zagrosides of Iran. *Geology*. https://doi.org/10.1130/0091-7613(1980)8<144:TEOTZO>2.0.CO;2

Alavi, Mehdi. (1994). Tectonics of the Zagros orogenic belt of Iran: new data and interpretations. *Tectonophysics*, *229*(3–4), 211–238. https://doi.org/10.1016/0040-1951(94)90030-2

Alavi, Mehdi. (1996). Tectonostratigraphic synthesis and structural style of the Alborz mountain system in Northern Iran. *Journal of Geodynamics*, *21*(1), 1–33. https://doi.org/10.1016/0264-3707(95)00009-7

Alavi, Mehdi, Vaziri, H., Seyed-Emami, K., & Lasemi, Y. (1997). The Triassic and associated rocks of the Nakhlak and Aghdarband areas in central and northeastern Iran as remnants of the southern Turanian active continental margin. *Bulletin of the Geological Society of America*. 109 (12), 1563–1575. https://doi.org/10.1130/0016-7606(1997)109<1563:TTAARO>2.3.CO;2

Ali, S. A., Buckman, S., Aswad, K. J., Jones, B. G., Ismail, S. A., & Nutman, A. P. (2012). Recognition of late cretaceous hasanbag ophiolite-arc rocks in the Kurdistan region of the Iraqi Zagros suture zone: A missing link in the paleogeography of the closing neotethys ocean. *Lithosphere*. 4 (5), 395–410. https://doi.org/10.1130/L207.1

Ali, Sarmad A., Buckman, S., Aswad, K. J., Jones, B. G., Ismail, S. A., & Nutman, A. P. (2013). The tectonic evolution of a Neo-Tethyan (Eocene-Oligocene) island-arc (Walash and Naopurdan groups) in the Kurdistan region of the Northeast Iraqi Zagros Suture Zone. *Island Arc*. 22 (1), 104-125. https://doi.org/10.1111/iar.12007

Ali, Sarmad A., Ismail, S. A., Nutman, A. P., Bennett, V. C., Jones, B. G., & Buckman, S. (2016). The intra-oceanic Cretaceous (~108 Ma) Kata–Rash arc fragment in the Kurdistan segment of Iraqi Zagros suture zone: Implications for Neotethys evolution and closure. *Lithos*, *260*, 154–163. Retrieved from http://linkinghub.elsevier.com/retrieve/pii/S002449371630113X

Alirezaei, S., & Hassanzadeh, J. (2012). Geochemistry and zircon geochronology of the Permian A-type Hasanrobat granite, Sanandaj?Sirjan belt: A new record of the Gondwana break-up in Iran. *Lithos*, *151*, 122–134. https://doi.org/10.1016/j.lithos.2011.11.015

Allahyari, K., Saccani, E., Pourmoafi, M., Beccaluva, L., & Masoudi, F. (2010). Petrology of mantle peridotites and intrusive mafic rocks from the Kermanshah ophiolitic complex (Zagros belt, Iran): Implications for the geodynamic evolution of the neo-tethyan oceanic branch between Arabia and Iran. *Ofioliti*, *35*(2).

Allahyari, K., Saccani, E., Rahimzadeh, B., & Zeda, O. (2014). Mineral chemistry and petrology of highly magnesian ultramafic cumulates from the Sarve-Abad (Sawlava) ophiolites (Kurdistan, NW Iran): New evidence for boninitic magmatism in intra-oceanic fore-arc setting in the Neo-Tethys between Arabia and Iran. *Journal of Asian Earth Sciences*, *79*. https://doi.org/10.1016/j.jseaes.2013.10.005

Allahyari, Khalil, Ansdell, K., & Eglington, B. M. (2018). 638-Tectono-magmatic evolution of the Southern Neo-Tethys in relation with ophiolites and mineral deposits: Database development and plate reconstructions. Vancouver, BC, Canada. Retrieved from http://rfg2018.gibsongroup.ca/pdf/rfg1638.pdf

Allahyari, Khalil, Saccani, E., Pourmoafi, M., Beccaluva, L., & Masoudi, F. (2010). Petrology of mantle peridotites and intrusive mafic rocks from the Kermanshah ophiolitic complex (Zagros belt, Iran): Implications for the geodynamic evolution of the neo-tethyan oceanic branch between Arabia and Iran. *Ofioliti*, *35*(2), 71–90.

Allahyari, Khalil, Saccani, E., Rahimzadeh, B., & Zeda, O. (2014). Mineral chemistry and petrology of highly magnesian ultramafic cumulates from the Sarve-Abad (Sawlava) ophiolites (Kurdistan, NW Iran): New evidence for boninitic magmatism in intra-oceanic fore-arc setting in the Neo-Tethys

between Arabia and Iran. *Journal of Asian Earth Sciences*, *79*, 312–328. https://doi.org/10.1016/j.jseaes.2013.10.005

Allen, M. B., Kheirkhah, M., Neill, I., Emami, M. H., & McLeod, C. L. (2013). Generation of arc and within-plate chemical signatures in collision zone magmatism: Quaternary lavas from Kurdistan province, Iran. *Journal of Petrology*. 54 (5), 887–911. https://doi.org/10.1093/petrology/egs090

Allen, M., Jackson, J., & Walker, R. (2004). Late Cenozoic reorganization of the Arabia-Eurasia collision and the comparison of short-term and long-term deformation rates. *Tectonics*, *23*(2), n/a-n/a. https://doi.org/10.1029/2003TC001530

Allen, Mark B., & Armstrong, H. A. (2008). Arabia-Eurasia collision and the forcing of mid-Cenozoic global cooling. *Palaeogeography, Palaeoclimatology, Palaeoecology*. 265, 52-58. https://doi.org/10.1016/j.palaeo.2008.04.021

Allen, Mark B., Kheirkhah, M., Emami, M. H., & Jones, S. J. (2011). Right-lateral shear across Iran and kinematic change in the Arabia-Eurasia collision zone. *Geophysical Journal International*. 184 (2), 555–574. https://doi.org/10.1111/j.1365-246X.2010.04874.x

Amidi, S. M., Emami, M. H., & Michel, R. (1984). Alkaline character of Eocene volcanism in the middle part of central Iran and its geodynamic situation. *Geologische Rundschau*. https://doi.org/10.1007/BF01820882

Amiri, M., Khalaji, A. A., Tahmasbi, Z., Santos, J. F., Sahamieh, R. Z., & Zamanian, H. (2017). Geochemistry, petrogenesis, and tectonic setting of the Almogholagh batholith in the Sanandaj–Sirjan zone, Western Iran. *Journal of African Earth Sciences*. 134, 113-133. https://doi.org/10.1016/j.jafrearsci.2017.06.018

Angiboust, S., Agard, P., De Hoog, J. C. M., Omrani, J., & Plunder, A. (2013). Insights on deep, accretionary subduction processes from the Sistan ophiolitic melange? (Eastern Iran). *Lithos*, *156–159*, 139–158. https://doi.org/10.1016/j.lithos.2012.11.007

Ao, S., Xiao, W., Khalatbari Jafari, M., Talebian, M., Chen, L., Wan, B., … Zhang, Z. (2016). U–Pb zircon ages, field geology and geochemistry of the Kermanshah ophiolite (Iran): From continental rifting at 79Ma to oceanic core complex at ca. 36Ma in the southern Neo-Tethys. *Gondwana Research*, *31*, 305–318. https://doi.org/10.1016/j.gr.2015.01.014

Arjmandzadeh, R., Karimpour, M. H., Mazaheri, S. A., Santos, J. F., Medina, J. M., & Homam, S. M. (2011a). Sr-Nd isotope geochemistry and petrogenesis of the Chah-Shaljami granitoids (Lut Block, Eastern Iran). *Journal of Asian Earth Sciences*, *41*(3), 283–296. https://doi.org/10.1016/J.JSEAES.2011.02.014

Arjmandzadeh, R., Karimpour, M. H., Mazaheri, S. A., Santos, J. F., Medina, J. M., & Homam, S. M. (2011b). Two-sided asymmetric subduction ; implications for tectonomagmatic and metallogenic evolution of the Lut Block, eastern Iran. *Journal of Economic Geology*. 3, 93-93

Arjmandzadeh, R., & Santos, J. F. (2014). Sr-Nd isotope geochemistry and tectonomagmatic setting of the Dehsalm Cu-Mo porphyry mineralizing intrusives from Lut Block, eastern Iran. *International Journal of Earth Sciences*. 103, 123–140. https://doi.org/10.1007/s00531-013-0959-4

Arvin, M., Babaei, A., Ghadami, G., Dargahi, S., & Ardekani, A. S. (2005). The origin of the Kahnuj ophiolitic complex, SE of Iran: Constraints from whole-rock and mineral chemistry of the Bande-Zeyarat gabbroic complex. 30(1), 1-14. *Ofioliti*. https://doi.org/10.4454/ofioliti.v30i1.236

Arvin, M., Pan, Y., Dargahi, S., Malekizadeh, A., & Babaei, A. (2007). Petrochemistry of the Siah-Kuh granitoid stock southwest of Kerman, Iran: Implications for initiation of Neotethys subduction. *Journal of Asian Earth Sciences*, *30*(3), 474–489. https://doi.org/10.1016/j.jseaes.2007.01.001

Aswad, K. J. A., Aziz, N. R. H., & Koyi, H. A. (2011). Cr-spinel compositions in serpentinites and their implications for the petrotectonic history of the Zagros Suture Zone, Kurdistan Region, Iraq. *Geological Magazine*, *148*(5–6), 802–818. https://doi.org/10.1017/S0016756811000422

Atapour, H. (2007). *Geochemical evolution and metallogeny of potassic igneous rocks of the volcano-plutonic belt of Kerman province with particular reference to special elements*. *Ph.D thesis, Shahid Bahonar University of Kerman*. Retrieved from https://ci.nii.ac.jp/naid/10030173954/

Azizi, H., & Asahara, Y. (2013). Juvenile granite in the Sanandaj-Sirjan Zone, NW Iran: Late Jurassic-

Early Cretaceous arc-continent collision. *International Geology Review*. 55(12), 1523-1540. https://doi.org/10.1080/00206814.2013.782959
Azizi, H., Chung, S.-L., Tanaka, T., & Asahara, Y. (2011). Isotopic dating of the Khoy metamorphic complex (KMC), northwestern Iran: A significant revision of the formation age and magma source. *Precambrian Research*, *185*(3), 87–94. https://doi.org/10.1016/j.precamres.2010.12.004
Azizi, H., & Jahangiri, A. (2008). Cretaceous subduction-related volcanism in the northern Sanandaj-Sirjan Zone, Iran. *Journal of Geodynamics*, *45*, 178–190. Retrieved from http://www.sciencedirect.com/science/article/pii/S0264370707000695
Azizi, H., Zanjefili-Beiranvand, M., & Asahara, Y. (2015). Zircon U-Pb ages and petrogenesis of a tonalite-trondhjemite-granodiorite (TTG) complex in the northern Sanandaj-Sirjan zone, northwest Iran: Evidence for Late Jurassic arc-continent collision. *Lithos*. 216, 178-195. https://doi.org/10.1016/j.lithos.2014.11.012
Babaie, H. A., Ghazi, A. M., Babaei, A., La Tour, T. E., & Hassanipak, A. A. (2001). Geochemistry of arc volcanic rocks of the Zagros Crush Zone, Neyriz, Iran. *Journal of Asian Earth Sciences*, *19*(1), 61–76. https://doi.org/10.1016/S1367-9120(00)00012-2
Babazadeh, S. A., & de Wever, P. (2004). Early Cretaceous radiolarian assemblages from radiolarites in the Sistan Suture (eastern Iran). *Geodiversitas*. *26*(2), 185-206.
Badrzadeh, Z., Barrett, T. J., Peter, J. M., Gimeno, D., Sabzehei, M., & Aghazadeh, M. (2011). Geology, mineralogy, and sulfur isotope geochemistry of the Sargaz Cu–Zn volcanogenic massive sulfide deposit, Sanandaj–Sirjan Zone, Iran. *Mineralium Deposita*, *46*(8), 905–923. https://doi.org/10.1007/s00126-011-0357-4
Bagheri, S., & Gol, S. D. (2020). The eastern iranian orocline. *Earth-Science Reviews*. 103322. https://doi.org/10.1016/j.earscirev.2020.103322
Bagheri, S., & Stampfli, G. M. (2008). The Anarak, Jandaq and Posht-e-Badam metamorphic complexes in central Iran: New geological data, relationships, and tectonic implications. *Tectonophysics*, *451*(1), 123–155. https://doi.org/10.1016/j.tecto.2007.11.047
Balaghi Einalou, M., Sadeghian, M., Zhai, M., Ghasemi, H., & Mohajjel, M. (2014). Zircon U–Pb ages, Hf isotopes and geochemistry of the schists, gneisses, and granites in Delbar Metamorphic-Igneous Complex, SE of Shahrood (Iran): Implications for Neoproterozoic geodynamic evolutions of Central Iran. *Journal of Asian Earth Sciences*, *92*, 92–124. https://doi.org/10.1016/j.jseaes.2014.06.011
Baud, A., & Stämpfli, G. M. (1989). Tectonogenesis & Evolution of a Segment of the Cimmerides: The Volcano-Sedimentary Triassic of Aghdarband (Kopet-Dagh, North-East Iran). In *Tectonic Evolution of the Tethyan Region*. 265-275. https://doi.org/10.1007/978-94-009-2253-2_14
Berberian, F., & Berberian, M. (1981). Tectono-plutonic episodes in Iran (pp. 5–32). American Geophysical Union (AGU). https://doi.org/10.1029/GD003p0005
Berberian, F., Muir, I. D., Pankhurst, R. J., & Berberian, M. (1982). Late Cretaceous and early Miocene Andean-type plutonic activity in northern Makran and central Iran. *Journal of the Geological Society*. 139(5), 605-614. https://doi.org/10.1144/gsjgs.139.5.0605
Berberian, M., & King, G. C. P. (1981a). TOWARDS A PALEOGEOGRAPHY AND TECTONIC EVOLUTION OF IRAN. *Canadian Journal of Earth Sciences*, *18*(2).
Berberian, M., & King, G. C. P. (1981b). Towards a paleogeography and tectonic evolution of Iran. *Canadian Journal of Earth Sciences*, *18*(2), 210–265. https://doi.org/10.1139/e81-019
Beydokhti, R. M., Karimpour, M. H., Mazaheri, S. A., Santos, J. F., & Klötzli, U. (2015). U–Pb zircon geochronology, Sr-Nd geochemistry, petrogenesis and tectonic setting of Mahoor granitoid rocks (Lut Block, Eastern Iran). *Journal of Asian Earth Sciences*, *111*, 192–205. https://doi.org/10.1016/j.jseaes.2015.07.028
Bonnet, G., Agard, P., Angiboust, S., Monié, P., Jentzer, M., Omrani, J., … Fournier, M. (2018). Tectonic slicing and mixing processes along the subduction interface: The Sistan example (Eastern Iran).
Bonham-Carter, G. F. (2014). Geographic information systems for geoscientists: modelling with GIS. (3), 9-12. Elsevier. *Lithos*, *310–311*, 269–287. https://doi.org/10.1016/j.lithos.2018.04.016
Boulin, J. (1988). Hercynian and Eocimmerian events in Afghanistan and adjoining regions. 148(3-4),

253-278. *Tectonophysics*. https://doi.org/10.1016/0040-1951(88)90134-5
Bouvier, A., Vervoort, J. D., & Patchett, P. J. (2008). The Lu-Hf and Sm-Nd isotopic composition of CHUR: Constraints from unequilibrated chondrites and implications for the bulk composition of terrestrial planets. *Earth and Planetary Science Letters*. 273(1-2), 48-57. https://doi.org/10.1016/j.epsl.2008.06.010
Bröcker, M., Fotoohi Rad, G., Burgess, R., Theunissen, S., Paderin, I., Rodionov, N., & Salimi, Z. (2013). New age constraints for the geodynamic evolution of the Sistan Suture Zone, eastern Iran. *Lithos*, *170–171*. https://doi.org/10.1016/j.lithos.2013.02.012
Camp, V. E., & Griffis, R. J. (1982). Character, genesis and tectonic setting of igneous rocks in the Sistan suture zone, eastern Iran. *LITHOS*. 15(3), 221-239. https://doi.org/10.1016/0024-4937(82)90014-7
Castillo, P. R. (2006). An overview of adakite petrogenesis. *Chinese Science Bulletin*, *51*(3), 257–268. https://doi.org/10.1007/s11434-006-0257-7
Champion, D. C., & Huston, D. L. (2016). Radiogenic isotopes, ore deposits and metallogenic terranes: Novel approaches based on regional isotopic maps and the mineral systems concept. *Ore Geology Reviews*, *76*, 229–256. https://doi.org/10.1016/j.oregeorev.2015.09.025
Chiu, H.-Y., Chung, S.-L., Zarrinkoub, M. H., Melkonyan, R., Pang, K.-N., Lee, H.-Y., … Khatib, M. M. (2017). Zircon Hf isotopic constraints on magmatic and tectonic evolution in Iran: Implications for crustal growth in the Tethyan orogenic belt. 145, 652-669. *Journal of Asian Earth Sciences*. https://doi.org/10.1016/j.jseaes.2017.06.011
Chiu, H. Y., Chung, S. L., Zarrinkoub, M. H., Mohammadi, S. S., Khatib, M. M., & Iizuka, Y. (2013). Zircon U-Pb age constraints from Iran on the magmatic evolution related to Neotethyan subduction and Zagros orogeny. *Lithos*, *162–163*, 70–87. https://doi.org/10.1016/j.lithos.2013.01.006
Daliran, F., Pride, K., Walther, J., Berner, Z. A., & Bakker, R. J. (2013). The Angouran Zn (Pb) deposit, NW Iran: Evidence for a two stage, hypogene zinc sulfide-zinc carbonate mineralization. *Ore Geology Reviews*. https://doi.org/10.1016/j.oregeorev.2013.02.002
Dargahi, S., Arvin, M., Pan, Y., & Babaei, A. (2010). Petrogenesis of post-collisional A-type granitoids from the Urumieh–Dokhtar magmatic assemblage, Southwestern Kerman, Iran: Constraints on the Arabian–Eurasian continental collision. *Lithos*, *115*, 190–204. Retrieved from https://www.sciencedirect.com/science/article/pii/S0024493709004897
Davidson, J., Hassanzadeh, J., Berzins, R., Stockli, D. F., Bashukooh, B., Turrin, B., & Pandamouz, A. (2004). The geology of Damavand volcano, Alborz Mountains, northern Iran. *Bulletin of the Geological Society of America*. 116(1-2), 16-29. https://doi.org/10.1130/B25344.1
Defant, M. J., & Kepezhinskas, P. (2001). Evidence suggests slab melting in arc magmas. *Eos, Transactions American Geophysical Union*, *82*(6), 65–65. https://doi.org/10.1029/01EO00038
Defant, Marc J., & Drummond, M. S. (1993). Mount St. Helens: Potential example of the partial melting of the subducted lithosphere in a volcanic arc. *Geology*, *21*(6), 547. https://doi.org/10.1130/0091-7613(1993)021<0547:MSHPEO>2.3.CO;2
Dehghani, G. A., & Makris, J. (1984). The Gravity Field and Crustal Structure of Iran. *Neues Jahrbuch Für Geologie Und Paläontologie - Abhandlungen*. https://doi.org/10.1127/njgpa/168/1984/215
Delavari, M., Amini, S., Schmitt, A. K., McKeegan, K. D., & Mark Harrison, T. (2014). U–Pb geochronology and geochemistry of Bibi-Maryam pluton, eastern Iran: Implication for the late stage of the tectonic evolution of the Sistan Ocean. *Lithos*, *200–201*, 197–211. https://doi.org/10.1016/j.lithos.2014.04.015
DePaolo, D. J. (1988). Age dependence of the composition of continental crust: evidence from Nd isotopic variations in granitic rocks. *Earth and Planetary Science Letters*. 90(3), 263-271. https://doi.org/10.1016/0012-821X(88)90130-6
Dercourt, J., Zonenshain, L. P., Ricou, L.-E., Kazmin, V. G., Le Pichon, X., Knipper, A. L., … Biju-Duval, B. (1986). Geological evolution of the tethys belt from the atlantic to the pamirs since the LIAS. *Tectonophysics*, *123*(1–4), 241–315. https://doi.org/10.1016/0040-1951(86)90199-X
Dewey, J. F., & Şengör, A. M. C. (1979). Aegean and surrounding regions: Complex multiplate and continuum tectonics in a convergent zone. *Bulletin of the Geological Society of America*, *90*(1), 84–

92. https://doi.org/10.1130/0016-7606(1979)90<84:AASRCM>2.0.CO;2
Dilek, Y., & Furnes, H. (2009). Structure and geochemistry of Tethyan ophiolites and their petrogenesis in subduction rollback systems. *Lithos*, *113*(1–2), 1–20. https://doi.org/10.1016/J.LITHOS.2009.04.022
Dilek, Y., Furnes, H., & Shallo, M. (2007). Suprasubduction zone ophiolite formation along the periphery of Mesozoic Gondwana. *Gondwana Research*, *11*(4), 453–475. https://doi.org/10.1016/j.gr.2007.01.005
Eftekhar Nejad, J. (1980). Tectonic classification of Iran in relation to depositional basins. Journal of Iranian Petroleum Society, 82, 19-28.
Eglington, B. M. (2018a). FitPDF. Unpublished. Retrieved from http://sil.usask.ca/Software.htm
Eglington, B. M. (2018b). PalaeoPlates Model. Unpublished.
Esna-Ashari, A., Tiepolo, M., Valizadeh, M. V., Hassanzadeh, J., & Sepahi, A. A. (2012). Geochemistry and zircon U-Pb geochronology of Aligoodarz granitoid complex, Sanandaj-Sirjan Zone, Iran. *Journal of Asian Earth Sciences*. 43(1), 11-22. https://doi.org/10.1016/j.jseaes.2011.09.001
Fakhari, M. D., Axen, G. J., Horton, B. K., Hassanzadeh, J., & Amini, A. (2008). Revised age of proximal deposits in the Zagros foreland basin and implications for Cenozoic evolution of the High Zagros. *Tectonophysics*, *451*(1–4), 170–185. https://doi.org/10.1016/j.tecto.2007.11.064
Floyd, P. A., & Winchester, J. A. (1975). Magma type and tectonic setting discrimination using immobile elements. *Earth and Planetary Science Letters*. 27(2), 211-218. https://doi.org/10.1016/0012-821X(75)90031-X
Fotoohi Rad, G. R., Droop, G. T. R., Amini, S., & Moazzen, M. (2005). Eclogites and blueschists of the Sistan Suture Zone, eastern Iran: A comparison of P-T histories from a subduction mélange. *Lithos*. 84(1-2), 1-24. https://doi.org/10.1016/j.lithos.2005.01.007
Fotoohi Rad, G. R., Droop, G. T. R., & Burgess, R. (2009). Early Cretaceous exhumation of high-pressure metamorphic rocks of the Sistan Suture Zone, eastern Iran. *Geological Journal*. 44(1), 104-116. https://doi.org/10.1002/gj.1135
Gammons, C. H., & Williams-Jones, A. E. (1997). Chemical mobility of gold in the porphyry-epithermal environment. *Economic Geology*. 92(1), 45-59. https://doi.org/10.2113/gsecongeo.92.1.45
Gao, S., Rudnick, R. L., Yuan, H.-L., Liu, X.-M., Liu, Y.-S., Xu, W.-L., … Wang, Q.-H. (2004). Recycling lower continental crust in the North China craton. *Nature*, *432*(7019), 892–897. https://doi.org/10.1038/nature03162
Ghalamghash, J., Mousavi, S. Z., Hassanzadeh, J., & Schmitt, A. K. (2016). Geology, zircon geochronology, and petrogenesis of Sabalan volcano (northwestern Iran). *Journal of Volcanology and Geothermal Research*, *327*, 192–207. https://doi.org/10.1016/j.jvolgeores.2016.05.001
Ghasemi, A., & Talbot, C. J. (2006). A new tectonic scenario for the Sanandaj–Sirjan Zone (Iran). *Journal of Asian Earth Sciences*, *26*(6), 683–693. https://doi.org/10.1016/j.jseaes.2005.01.003
Ghazi, A.M., Hassanipak, A. A., Mahoney, J. J., & Duncan, R. A. (2004). Geochemical characteristics, 40Ar–39Ar ages and original tectonic setting of the Band-e-Zeyarat/Dar Anar ophiolite, Makran accretionary prism, S.E. Iran. *Tectonophysics*, *393*(1), 175–196. https://doi.org/10.1016/j.tecto.2004.07.035
Ghazi, A.Mohamad, & Hassanipak, A. . (1999). Geochemistry of subalkaline and alkaline extrusives from the Kermanshah ophiolite, Zagros Suture Zone, Western Iran: implications for Tethyan plate tectonics. *Journal of Asian Earth Sciences*, *17*(3), 319–332. https://doi.org/10.1016/S0743-9547(98)00070-1
Ghazi, J. M., Moazzen, M., Rahgoshay, M., & Shafaii Moghadam, H. (2012). Geochemical characteristics of basaltic rocks from the Nain ophiolite (Central Iran); constraints on mantle wedge source evolution in an oceanic back arc basin and a geodynamical model. *Tectonophysics*, *574–575*, 92–104. https://doi.org/10.1016/j.tecto.2011.10.001
Ghiasvand, A., Karimpour, M. H., Malekzadeh Shafaroudi, A., & Hidarian Shahri, M. R. (2017). Age and origin of subvolcanic rocks from NE Iran: Link between magmatic “flare-up” and mineralization. *Chemie Der Erde*. 78(2), 254-267. https://doi.org/10.1016/J.CHEMER.2017.12.002

Ghorbani, M. (2013). *The economic geology of Iran: Mineral deposits and natural resources*. *The Economic Geology of Iran: Mineral Deposits and Natural Resources*. https://doi.org/10.1007/978-94-007-5625-0

Giese, P., Makris, J., Akashe, B., Roewer, P., Letz, H., & Mostaanpour, M. (1984). The crustal structure in Southern Iran derived from seismic explosion data. Neues Jahrbuch für Geologie und Paläontologie-Abhandlungen, 230-243.

Golestani, M., Karimpour, M. H., Malekzadeh Shafaroudi, A., & Hidarian Shahri, M. R. (2018). Geochemistry, U-Pb geochronology and Sr-Nd isotopes of the Neogene igneous rocks, at the Iju porphyry copper deposit, NW Shahr-e-Babak, Iran. *Ore Geology Reviews*, *93*, 290–307. https://doi.org/10.1016/J.OREGEOREV.2018.01.001

Golmohammadi, A., Karimpour, M. H., Malekzadeh Shafaroudi, A., & Mazaheri, S. A. (2015). Alteration-mineralization, and radiometric ages of the source pluton at the Sangan iron skarn deposit, northeastern Iran. *Ore Geology Reviews*, *65*, 545–563. https://doi.org/10.1016/j.oregeorev.2014.07.005

Golonka, J. (2004). Plate tectonic evolution of the southern margin of Eurasia in the Mesozoic and Cenozoic. *Tectonophysics*. 381(1-4), 235-273. https://doi.org/10.1016/j.tecto.2002.06.004

Griffin, W. L., Pearson, N. J., Belousova, E., Jackson, S. E., Van Achterbergh, E., O'Reilly, S. Y., & Shee, S. R. (2000). The Hf isotope composition of cratonic mantle: LAM-MC-ICPMS analysis of zircon megacrysts in kimberlites. *Geochimica et Cosmochimica Acta*. 64(1), 133-147. https://doi.org/10.1016/S0016-7037(99)00343-9

Griffin, W. L., Wang, X., Jackson, S. E., Pearson, N. J., O'Reilly, S. Y., Xu, X., & Zhou, X. (2002). Zircon chemistry and magma mixing, SE China: In-situ analysis of Hf isotopes, Tonglu and Pingtan igneous complexes. *Lithos*. 61(3-4), 237-269. https://doi.org/10.1016/S0024-4937(02)00082-8

Guillot, S., Hattori, K., Agard, P., Schwartz, S., & Vidal, O. (2009). Exhumation Processes in Oceanic and Continental Subduction Contexts: A Review. 175-205. https://doi.org/10.1007/978-3-540-87974-9_10

Hajsadeghi, S., Mirmohammadi, M., Asghari, O., & Meshkani, S. A. (2018). Geology and mineralization at the copper-rich volcanogenic massive sulfide deposit in Nohkouhi, Posht-e-Badam block, Central Iran. *Ore Geology Reviews*, *92*, 379–396. https://doi.org/10.1016/j.oregeorev.2017.11.030

Haschke, M., Ahmadian, J., Murata, M., & McDonald, I. (2010). COPPER MINERALIZATION PREVENTED BY ARC-ROOT DELAMINATION DURING ALPINE-HIMALAYAN COLLISION IN CENTRAL IRAN. *Economic Geology*, *105*(4), 855–865. https://doi.org/10.2113/gsecongeo.105.4.855

Haschke, M., & Ben-Avraham, Z. (2005). Adakites from collision-modified lithosphere. *Geophysical Research Letters*, *32*(15), L15302. https://doi.org/10.1029/2005GL023468

Haschke, Michael, Günther, A., Melnick, D., Echtler, H., Reutter, K.-J., Scheuber, E., & Oncken, O. (2006). Central and Southern Andean Tectonic Evolution Inferred from Arc Magmatism. In *The Andes* (pp. 337–353). Springer Berlin Heidelberg. https://doi.org/10.1007/978-3-540-48684-8_16

Hassanipak, A. A., & Ghazi, A. M. (2000). Petrology, geochemistry and tectonic setting of the Khoy ophiolite, northwest Iran: implications for Tethyan tectonics. *Journal of Asian Earth Sciences*, *18*(1), 109–121. https://doi.org/10.1016/S1367-9120(99)00023-1

Hassanzadeh, J. (1993). *Metallogenic and tectono-magmatic events in the SE sector of the Cenozoic active continental margin of Iran (Shahr-e-Babak area, Kerman province)*. *(Ph.D. Thesis). University of California*. Retrieved from https://ci.nii.ac.jp/naid/10030516896/

Hassanzadeh, Jamshid, Stockli, D. F., Horton, B. K., Axen, G. J., Stockli, L. D., Grove, M., … Walker, J. D. (2008). U-Pb zircon geochronology of late Neoproterozoic–Early Cambrian granitoids in Iran: Implications for paleogeography, magmatism, and exhumation history of Iranian basement. *Tectonophysics*, *451*(1), 71–96. https://doi.org/10.1016/j.tecto.2007.11.062

Hassanzadeh, Jamshid, & Wernicke, B. P. (2016). The Neotethyan Sanandaj-Sirjan zone of Iran as an archetype for passive margin-arc transitions. 35(3), 586-621. *Tectonics*. https://doi.org/10.1002/2015TC003926

Hatzfeld, D., & Molnar, P. (2010). Comparisons of the kinematics and deep structures of the Zagros and Himalaya and of the Iranian and Tibetan plateaus and geodynamic implications. *Reviews of Geophysics*. 48(2). https://doi.org/10.1029/2009RG000304

Heidari, S. M., Paquette, J.-L., & Gasquet, D. (2015). Geology, timing, and genesis of the high sulfidation Au (–Cu) deposit of Touzlar, NW Iran. *Ore Geology Reviews*, *65*, 460–486. https://doi.org/10.1016/J.OREGEOREV.2014.05.013

Hempton, M. R. (1987). Constraints on Arabian Plate motion and extensional history of the Red Sea. *Tectonics*. 6(6), 687-705. https://doi.org/10.1029/TC006i006p00687

Hezarkhani, A. (2006). Hydrothermal evolution of the Sar-Cheshmeh porphyry Cu–Mo deposit, Iran: Evidence from fluid inclusions. *Journal of Asian Earth Sciences*, *28*(4–6), 409–422. https://doi.org/10.1016/J.JSEAES.2005.11.003

Hezarkhani, A., & Williams-Jo, A. E. (1998). Econotalc Geology Vol. 93, 1998, pp. 651-670. *Econotalc Geolog*, *93*(October), 651–670. https://doi.org/https://doi.org/10.2113/gsecongeo.93.5.651

Homke, S., Vergés, J., Garcés, M., Emami, H., & Karpuz, R. (2004). Magnetostratigraphy of Miocene-Pliocene Zagros foreland deposits in the front of the Push-e Kush Arc (Lurestan Province, Iran). *Earth and Planetary Science Letters*. 225(3-4), 397-410. https://doi.org/10.1016/j.epsl.2004.07.002

Hooper, P. R., Bailey, D. G., & McCarley Holder, G. A. (1995). Tertiary calc-alkaline magmatism associated with lithospheric extension in the Pacific Northwest. *Journal of Geophysical Research*. 25(CONF-9305259-). https://doi.org/10.1029/94jb03328

Hosseini, M. R., Ghaderi, M., Alirezaei, S., & Sun, W. (2017). Geological characteristics and geochronology of the Takht-e-Gonbad copper deposit, SE Iran: A variant of porphyry type deposits. *Ore Geology Reviews*, *86*, 440–458. Retrieved from https://www.sciencedirect.com/science/article/pii/S0169136816303791#!

Hosseini, M. R., Hassanzadeh, J., Alirezaei, S., Sun, W., & Li, C.-Y. (2017). Age revision of the Neotethyan arc migration into the southeast Urumieh-Dokhtar belt of Iran: Geochemistry and U–Pb zircon geochronology. *Lithos*, 296–309. https://doi.org/10.1016/j.lithos.2017.03.012

Hosseinkhani, A., Karimpour, M. H., Malekzadeh Shafaroudi, A., & Santos, J. F. (2017). U-Pb geochronology and petrogenesis of intrusive rocks: Constraints on the mode of genesis and timing of Cu mineralization in SWSK area, Lut Block. *Journal of Geochemical Exploration*, *177*, 11–27. https://doi.org/10.1016/j.gexplo.2017.02.001

Iizuka, T., Yamaguchi, T., Itano, K., Hibiya, Y., & Suzuki, K. (2017). What Hf isotopes in zircon tell us about crust–mantle evolution. *Lithos*. 274, 304-327. https://doi.org/10.1016/j.lithos.2017.01.006

Jafari, M. K., Babaie, H. A., & Mirzaie, M. (2013). Geology, petrology and tectonomagmatic evolution of the plutonic crustal rocks of the Sabzevar ophiolite, NE Iran. *Geological Magazine*. 150(5), 862-884. https://doi.org/10.1017/S0016756812000933

Jahangiri, A. (2007). Post-collisional Miocene adakitic volcanism in NW Iran: Geochemical and geodynamic implications. *Journal of Asian Earth Sciences*, *30*(3), 433–447. https://doi.org/10.1016/j.jseaes.2006.11.008

Jamali, H., & Mehrabi, B. (2015). Relationships between arc maturity and Cu–Mo–Au porphyry and related epithermal mineralization at the Cenozoic Arasbaran magmatic belt. *Ore Geology Reviews*, *65*, 487–501. https://doi.org/10.1016/j.oregeorev.2014.06.017

Karimpour, M. H., & Stern, C. R. (2009). Advanced spaceborne thermal emission and reflection radiometer mineral mapping to discriminate high sulfidation, Reduced intrusion related and iron oxide gold deposits, Eastern Iran. 9. *Journal of Applied Sciences*. https://doi.org/10.3923/jas.2009.815.828

Karimpour, Mohammad Hasan, Stern, C., Farmer, L., & Saadat, S. (2011). Review of age, Rb-Sr geochemistry and petrogenesis of Jurassic to Quaternary igneous rocks in Lut Block, Eastern Iran. *Geopersia*. 1(1), 19-54. https://doi.org/10.22059/JGEOPE.2011.22162

Keykhay-Hosseinpoor, M., Kohsary, A. H., Hossein-Morshedy, A., & Porwal, A. (2020). A machine learning-based approach to exploration targeting of porphyry Cu-Au deposits in the Dehsalm district, eastern Iran. *Ore Geology Reviews*. 116, 103234.

https://doi.org/10.1016/j.oregeorev.2019.103234
Khalaji, A. A., Esmaeily, D., Valizadeh, M. V., & Rahimpour-Bonab, H. (2007). Petrology and geochemistry of the granitoid complex of Boroujerd, Sanandaj-Sirjan Zone, Western Iran. *Journal of Asian Earth Sciences*. 29(5-6), 859-877. https://doi.org/10.1016/j.jseaes.2006.06.005
KHAIN, V. (1994). Geology of Northern Eurasia. Gebrüder Borntraeger, Berlin Stuttgart, 346 p.
KOZUR, H. 1991. The evolution of the Hallstatt ocean and its significance for the early evolution of the Eastern Alps and western Carpathians. In. Paleogeography and paleoceanography of Tethys. Palaeogeogr. Palaeoclimatol. Palaeoecol, 87, 109-135.
Khalatbari-Jafari, M., Juteau, T., & Cotten, J. (2006). Petrological and geochemical study of the Late Cretaceous ophiolite of Khoy (NW Iran), and related geological formations. *Journal of Asian Earth Sciences*, *27*(4), 465–502. https://doi.org/10.1016/j.jseaes.2005.05.006
Khosravi, M., Abedini, A., Alipour, S., & Mongelli, G. (2017). The Darzi-Vali bauxite deposit, West-Azarbaidjan Province, Iran: Critical metals distribution and parental affinities. *Journal of African Earth Sciences*, *129*, 960–972. https://doi.org/10.1016/j.jafrearsci.2017.02.024
Knipper, A., Ricou, L.-E., & Dercourt, J. (1986). Ophiolites as indicators of the geodynamic evolution of the Tethyan ocean. *Tectonophysics*, *123*(1–4), 213–240. https://doi.org/10.1016/0040-1951(86)90198-8
Leturmy, P., & Robin, C. (2010). Tectonic and stratigraphic evolution of Zagros and Makran during the Mesozoic-Cenozoic: introduction. *Geological Society, London, Special Publications*, *330*(1), 1–4. https://doi.org/10.1144/SP330.1
Leven, E. J. (1995). Permian and Triassic of the Rushan-Pshart zone (Pamir). *Rivista Italiana Di Paleontologia e Stratigrafia*. 101(1), 3-16. https://doi.org/10.13130/2039-4942/8562
Loucks, R. R. (2014). Distinctive composition of copper-ore-forming arcmagmas. *Australian Journal of Earth Sciences*, *61*(1), 5–16. https://doi.org/10.1080/08120099.2013.865676
LOUCKS R. R. (2000) Report 1: Development of petrochemical discriminants of metallogenically fertile calc-alkalic igneous suites and their application to regional assessments of gold and copper prospectivity of Neogene and Quaternary volcano-plutonic centers througout Chile and in southwestern Bolivia. Unpublished report for industry-sponsored research project: Predictive Guides to Copper and Gold Mineralisation at Circum-Pacific Convergent Plate Margins, 73 p.
LOUCKS R. R. & BALLARD J. R. (2002) Report 2A: Correlated variation of tectonic stress with chemical composition of arc volcanism: Unpublished report for industry-sponsored research project. Predictive Guides to Copper and Gold Mineralisation at Circum-Pacific Convergent Plate Margins, 99 p.
Lin, Y. C. (2011). Geochemical characteristics and petrogenesis of pre-to post-collisional igneous rocks in Armenia and Caucasian regions. Unpublished Master thesis, National Taiwan University, Taiwan.
Maanijou, M., Aliani, F., Miri, M., & Lentz, D. R. (2013). Geochemistry and petrology of igneous assemblage in the south of Qorveh area, west Iran. *Chemie Der Erde - Geochemistry*, *73*(2), 181–196. https://doi.org/10.1016/J.CHEMER.2013.04.001
Maghfouri, S. (2012). *Geology, mineralogy, geochemistry and genesis of Cu mineralization Within Late Cretaceous Volcano-sedimentary sequence in southwest of Sabzevar, with emphasis on the Nudeh deposit*. University of Tarbiat Modares, Iran.
Maghfouri, S., Rastad, E., Mousivand, F., Choulet, F., & Ye, L. (2017). Geological and geochemical constraints on the Cheshmeh-Frezi volcanogenic stratiform manganese deposit, southwest Sabzevar basin, Iran. *Ore Geology Reviews*, *89*, 96–113. https://doi.org/10.1016/j.oregeorev.2017.06.015
Maghfouri, S., Rastad, E., Mousivand, F., Lin, Y., & Zaw, K. (2016). Geology, ore facies and sulfur isotopes geochemistry of the Nudeh Besshi-type volcanogenic massive sulfide deposit, southwest Sabzevar basin, Iran. *Journal of Asian Earth Sciences*, *125*, 1–21. https://doi.org/10.1016/j.jseaes.2016.04.022
Mahdavi, A., Karimpour, M. H., Mao, J., Haidarian Shahri, M. R., Malekzadeh Shafaroudi, A., & Li, H. (2016). Zircon U–Pb geochronology, Hf isotopes and geochemistry of intrusive rocks in the Gazu copper deposit, Iran: Petrogenesis and geological implications. *Ore Geology Reviews*, *72*, 818–837.

https://doi.org/10.1016/j.oregeorev.2015.09.011
Mahmoudi, S., Corfu, F., Masoudi, F., Mehrabi, B., & Mohajjel, M. (2011). U-Pb dating and emplacement history of granitoid plutons in the northern Sanandaj-Sirjan Zone, Iran. *Journal of Asian Earth Sciences*. 41(3), 238-249. https://doi.org/10.1016/j.jseaes.2011.03.006
Malek-Mahmoudi, F., Reza Davoudian, A., Shabanian, N., Azizi, H., Asahara, Y., Neubauer, F., & Dong, Y. (2017). Geochemistry of metabasites from the North Shahrekord metamorphic complex, Sanandaj-Sirjan Zone: Geodynamic implications for the Pan-African basement in Iran. *Precambrian Research*. 293, 56-72. https://doi.org/10.1016/j.precamres.2017.03.003
Malekzadeh Shafaroudi, A., Karimpour, M. H., & Stern, C. R. (2015). The Khopik porphyry copper prospect, Lut Block, Eastern Iran: Geology, alteration and mineralization, fluid inclusion, and oxygen isotope studies. *Ore Geology Reviews*, *65*, 522–544. https://doi.org/10.1016/j.oregeorev.2014.04.015
Marchesi, C., González-Jiménez, J. M., Gervilla, F., Garrido, C. J., Griffin, W. L., O'Reilly, S. Y., … Pearson, N. J. (2011). In situ Re-Os isotopic analysis of platinum-group minerals from the Mayarí-Cristal ophiolitic massif (Mayarí-Baracoa Ophiolitic Belt, eastern Cuba): implications for the origin of Os-isotope heterogeneities in podiform chromitites. *Contributions to Mineralogy and Petrology*, *161*(6), 977–990. https://doi.org/10.1007/s00410-010-0575-2
Maitre, L. E. (1989). A classification of igneous rocks and glossary of terms. Recommendations of the international union of geological sciences subcommission on the systematics of igneous rocks, 193.
Mazhari, S. A., Bea, F., Amini, S., Ghalamghash, J., Molina, J. F., Montero, P., … Williams, I. S. (2009). The Eocene bimodal Piranshahr massif of the Sanandaj-Sirjan Zone, NW Iran: A marker of the end of the collision in the Zagros orogen. *Journal of the Geological Society*. 166(1), 53-69. https://doi.org/10.1144/0016-76492008-022
McCall, G. J. H., & Kidd, R. G. W. (1982). The Makran, Southeastern Iran: the anatomy of a convergent plate margin active from Cretaceous to Present. *Geological Society Special Publication*. 10(1), 387-397. https://doi.org/10.1144/GSL.SP.1982.010.01.26
McQuarrie, N., Stock, J. M., Verdel, C., & Wernicke, B. P. (2003). Cenozoic evolution of Neotethys and implications for the causes of plate motions. *Geophysical Research Letters*, *30*(20), n/a-n/a. https://doi.org/10.1029/2003GL017992
McQuarrie, Nadine, & Van Hinsbergen, D. J. J. (2013). Retrodeforming the Arabia-Eurasia collision zone: Age of collision versus magnitude of continental subduction. *Geology*. 41(3), 315-318. https://doi.org/10.1130/G33591.1
Mehdipour Ghazi, J., Harris, C., Rahgoshay, M., & Moazzen, M. (2019). Combined igneous and hydrothermal source for the Kiruna-type Bafq magnetite-apatite deposit in Central Iran; trace element and oxygen isotope studies of magnetite. *Ore Geology Reviews*, *105*, 590–604. https://doi.org/10.1016/j.oregeorev.2019.01.006
Mehrabi, B., Tale Fazel, E., & Yardley, B. (2019). Ore geology, fluid inclusions and O-S stable isotope characteristics of Shurab Sb-polymetallic vein deposit, eastern Iran. *Chemie Der Erde*, *79*(2), 307–322. https://doi.org/10.1016/j.geoch.2018.12.004
Mirnejad, H., Raeisi, D., McFarlane, C., & Sheibi, M. (2019). Tafresh intrusive rocks within the Urumieh-Dokhtar Magmatic Arc: Appraisal of Neo-Tethys subduction. *Geological Journal*, *54*(3), 1745–1755. https://doi.org/10.1002/gj.3266
Moghadam, H. S., Corfu, F., Chiaradia, M., Stern, R. J., & Ghorbani, G. (2014). Sabzevar Ophiolite, NE Iran: Progress from embryonic oceanic lithosphere into magmatic arc constrained by new isotopic and geochemical data. *Lithos*, *210*, 224–241. https://doi.org/10.1016/j.lithos.2014.10.004
Moghadam, H. S., Corfu, F., & Stern, R. J. (2013). U–Pb zircon ages of Late Cretaceous Nain Dehshir ophiolites, central Iran. *Journal of the Geological Society, London*, *170*, 175–184. https://doi.org/10.1144/jgs2012-066.U
Moghadam, H. S., Li, X. H., Stern, R. J., Ghorbani, G., & Bakhshizad, F. (2016). Zircon U-Pb ages and Hf-O isotopic composition of migmatites from the Zanjan-Takab complex, NW Iran: Constraints on partial melting of metasediments. *Lithos*, *240–243*. https://doi.org/10.1016/j.lithos.2015.11.004

Moghadam, H. S., Rossetti, F., Lucci, F., Chiaradia, M., Gerdes, A., Martinez, M. L., … Nasrabady, M. (2016). The calc-alkaline and adakitic volcanism of the Sabzevar structural zone (NE Iran): Implications for the Eocene magmatic flare-up in Central Iran. *Lithos*, *248–251*, 517–535. https://doi.org/10.1016/j.lithos.2016.01.019

Moghadam, H. S., & Stern, R. J. (2015). Ophiolites of Iran: Keys to understanding the tectonic evolution of SW Asia: (II) Mesozoic ophiolites. *Journal of Asian Earth Sciences*, *100*, 31–59. Retrieved from http://www.sciencedirect.com/science/article/pii/S1367912015000115

Moghadam, H. S., Stern, R. J., Chiaradia, M., & Rahgoshay, M. (2013). Geochemistry and tectonic evolution of the Late Cretaceous Gogher–Baft ophiolite, central Iran. *Lithos*, *168*, 33–47. https://doi.org/10.1016/j.lithos.2013.01.013

Moghadam, H. S., Whitechurch, H., Rahgoshay, M., & Monsef, I. (2009). Significance of Nain-Baft ophiolitic belt (Iran): Short-lived, transtensional Cretaceous back-arc oceanic basins over the Tethyan subduction zone. *Comptes Rendus Geoscience*, *341*(12), 1016–1028. https://doi.org/10.1016/j.crte.2009.06.011

Moghadam, M. C., Tahmasbi, Z., Ahmadi-Khalaji, A., & Santos, J. F. (2017). Petrogenesis of Rabor-Lalehzar magmatic rocks (SE Iran): Constraints from whole rock chemistry and Sr-Nd isotopes. *Chemie Der Erde - Geochemistry*. 78(1), 58-77. https://doi.org/10.1016/J.CHEMER.2017.11.004

Mohajjel, M., & Fergusson, C. L. (2014). Jurassic to cenozoic tectonics of the zagros orogen in northwestern Iran. *International Geology Review*. 56(3), 263-287. https://doi.org/10.1080/00206814.2013.853919

Mohajjel, M., Fergusson, C. L., & Sahandi, M. R. (2003). Cretaceous-Tertiary convergence and continental collision, Sanandaj-Sirjan Zone, Western Iran. *Journal of Asian Earth Sciences*. 21(4), 397-412. https://doi.org/10.1016/S1367-9120(02)00035-4

Mohajjel, Mohammad, & Fergusson, C. L. (2000). Dextral transpression in Late Cretaceous continental collision, Sanandaj–Sirjan Zone, western Iran. *Journal of Structural Geology*, *22*(8), 1125–1139. https://doi.org/10.1016/S0191-8141(00)00023-7

Molinaro, M., Leturmy, P., Guezou, J.-C., Frizon de Lamotte, D., & Eshraghi, S. A. (2005). The structure and kinematics of the southeastern Zagros fold-thrust belt, Iran: From thin-skinned to thick-skinned tectonics. *Tectonics*, *24*(3), n/a-n/a. https://doi.org/10.1029/2004TC001633

Monsef, I., Monsef, R., Mata, J., Zhang, Z., Pirouz, M., Rezaeian, M., … Xiao, W. (2018). Evidence for an early-MORB to fore-arc evolution within the Zagros suture zone: Constraints from zircon U Pb geochronology and geochemistry of the Neyriz ophiolite (South Iran). 62, 287-305. *Gondwana Research*. https://doi.org/10.1016/j.gr.2018.03.002

Moores, E., Kellogg, L. H., & Dilek, Y. (2000). Tethyan ophiolites, mantle convection, and tectonic "historical contingency": A resolution of the "ophiolite conundrum" Mantle Compositions and Melt Evolution of Tethyan Ophiolites in the Eastern Mediterranean Region View project GOA-G. 3-12. https://doi.org/10.1130/0-8137-2349-3.3

Motaghi, K., Shabanian, E., & Kalvandi, F. (2017). Underplating along the northern portion of the Zagros suture zone, Iran. *Geophysical Journal International*, *210*(1), 375–389. https://doi.org/10.1093/gji/ggx168

Mousivand, F., Rastad, E., Hoshino, K., & Watanabe, M. (2007). The Bavanat Cu-Zn-Ag orebody: First recognition of a Besshi-type VMS deposit in Iran. *Neues Jahrbuch Für Mineralogie - Abhandlungen*, *183*(3), 297–315. https://doi.org/10.1127/0077-7757/2007/0075

Mousivand, Fardin, Rastad, E., Meffre, S., Peter, J. M., Solomon, M., & Zaw, K. (2011). U–Pb geochronology and Pb isotope characteristics of the Chahgaz volcanogenic massive sulphide deposit, southern Iran. *International Geology Review*, *53*(10), 1239–1262. https://doi.org/10.1080/00206811003783364

Mouthereau, F., Lacombe, O., & Vergés, J. (2012). Building the Zagros collisional orogen: Timing, strain distribution and the dynamics of Arabia/Eurasia plate convergence. *Tectonophysics*, *532*, 27–60. https://doi.org/10.1016/j.tecto.2012.01.022

Mouthereau, Frédéric, Filleaudeau, P. Y., Vacherat, A., Pik, R., Lacombe, O., Fellin, M. G., … Masini, E.

(2014). Placing limits to shortening evolution in the Pyrenees: Role of margin architecture and implications for the Iberia/Europe convergence. *Tectonics*. 33(12), 2283-2314. https://doi.org/10.1002/2014TC003663

Muttoni, G., Gaetani, M., Kent, D. V., Sciunnach, D., Angiolini, L., Berra, F., … Zanchi, A. (2009). Opening of the Neo-tethys ocean and the pangea B to pangea A transformation during the permian. *GeoArabia*. 14(4), 17-48. https://doi.org/10.1016/S0012-821X(03)00452-7

Nabavi M (1976) An introduction to the Iranian geology, geological survey of Iran, Tehran. 110. [in Persian]

Nabatian, G., Wan, B., & Honarmand, M. (2017). Whole rock geochemistry, molybdenite Re-Os geochronology, stable isotope and fluid inclusion investigations of the Siah-Kamar deposit, western Alborz-Azarbayjan: New constrains on the porphyry Mo deposit in Iran. *Ore Geology Reviews*, *91*, 638–659. https://doi.org/10.1016/J.OREGEOREV.2017.08.030

Nakhaei, M., Mazaheri, S. A., Karimpour, M. H., Stern, C. R., Zarrinkoub, M. H., Mohammadi, S. S., & Heydarian shahri, M. R. (2015). Geochronologic, geochemical, and isotopic constraints on petrogenesis of the dioritic rocks associated with Fe skarn in the Bisheh area, Eastern Iran. *Arabian Journal of Geosciences*, *8*(10), 8481–8495. https://doi.org/10.1007/s12517-015-1834-3

Nédélec, A., Stephens, E. W., & Fallick, A. E. (1995). The PanAfrican stratoid granites of madagascar: Alkaline magmatism in a post-collisional extensional setting. *Journal of Petrology*. 36(5), 1367-1391. https://doi.org/10.1093/petrology/36.5.1367

Nikishin, A., Cloetingh, S., Brunet, M.-F., Stephenson, R., Bolotov, S., & Ershov, A. (1998). Scythian Platform, Caucasus and Black\tSea region: Mesozoic-Cenozoic tectonic history and dynamics. *Mémoires Du Muséum National d'Histoire Naturelle*. 3, 163-176.

Nouri, F., Asahara, Y., Azizi, H., Yamamoto, K., & Tsuboi, M. (2017). Geochemistry and petrogenesis of the Eocene back arc mafic rocks in the Zagros suture zone, northern Noorabad, western Iran. *Chemie Der Erde - Geochemistry*, *77*(3), 517–533. https://doi.org/10.1016/J.CHEMER.2017.06.002

Nouri, F., Azizi, H., Golonka, J., Asahara, Y., Orihashi, Y., Yamamoto, K., … Anma, R. (2016). Age and petrogenesis of Na-rich felsic rocks in western Iran: Evidence for closure of the southern branch of the Neo-Tethys in the Late Cretaceous. *Tectonophysics*, *671*, 151–172. https://doi.org/10.1016/j.tecto.2015.12.014

Okay, A. I., Zattin, M., & Cavazza, W. (2010). Apatite fission-track data for the Miocene Arabia-Eurasia collision. *Geology*. 38(1), 35-38. https://doi.org/10.1130/G30234.1

Omrani, J., Agard, P., Whitechurch, H., Benoit, M., Prouteau, G., & Jolivet, L. (2008). Arc-magmatism and subduction history beneath the Zagros Mountains, Iran: A new report of adakites and geodynamic consequences. *Lithos*, *106*(3), 380–398. https://doi.org/10.1016/j.lithos.2008.09.008

Pang, K. N., Chung, S. L., Zarrinkoub, M. H., Chiu, H. Y., & Li, X. H. (2014). On the magmatic record of the Makran arc, southeastern Iran: Insights from zircon U-Pb geochronology and bulk-rock geochemistry. *Geochemistry, Geophysics, Geosystems*. 15(6), 2151-2169. https://doi.org/10.1002/2014GC005262

Pang, K. N., Chung, S. L., Zarrinkoub, M. H., Li, X. H., Lee, H. Y., Lin, T. H., & Chiu, H. Y. (2016). New age and geochemical constraints on the origin of Quaternary adakite-like lavas in the Arabia–Eurasia collision zone. *Lithos*. 264, 348-359. https://doi.org/10.1016/j.lithos.2016.08.042

Pang, K. N., Chung, S. L., Zarrinkoub, M. H., Lin, Y. C., Lee, H. Y., Lo, C. H., & Khatib, M. M. (2013). Iranian ultrapotassic volcanism at ~11 Ma signifies the initiation of post-collisional magmatism in the Arabia-Eurasia collision zone. *Terra Nova*. 25(5), 405-413. https://doi.org/10.1111/ter.12050

Pang, K. N., Chung, S. L., Zarrinkoub, M. H., Mohammadi, S. S., Yang, H. M., Chu, C. H., … Lo, C. H. (2012). Age, geochemical characteristics and petrogenesis of Late Cenozoic intraplate alkali basalts in the Lut-Sistan region, eastern Iran. *Chemical Geology*. 306, 40-53. https://doi.org/10.1016/j.chemgeo.2012.02.020

Pang, K. N., Chung, S. L., Zarrinkoub, M. H., Wang, F., Kamenetsky, V. S., & Lee, H. Y. (2015). Quaternary high-Mg ultrapotassic rocks from the Qal'eh Hasan Ali maars, southeastern Iran: petrogenesis and geodynamic implications. *Contributions to Mineralogy and Petrology*. 170(3), 1-

19. https://doi.org/10.1007/s00410-015-1183-y
Paul, A., Hatzfeld, D., Kaviani, A., Tatar, M., & Pequegnat, C. (2010). About this title - Tectonic and Stratigraphic Evolution of Zagros and Makran during the Mesozoic-Cenozoic\rSeismic imaging of the lithospheric structure of the Zagros mountain belt (Iran). *Geological Society, London, Special Publications*. 330(1), 5-18.
Pearce, J.A., & Cann, J. R. (1973). Tectonic setting of basic volcanic rocks determined using trace element analyses. *Earth and Planetary Science Letters*, *19*(2), 290–300. https://doi.org/10.1016/0012-821X(73)90129-5
Pearce, Julian A. (1996). A User's Guide to Basalt Discrimination Diagrams. In *Trace Element Geochemistry of Volcanic Rocks: Applications for Massive Sulfide Exploration*. 12(79), 113.
Pearce, Julian A. (2008). Geochemical fingerprinting of oceanic basalts with applications to ophiolite classification and the search for Archean oceanic crust. *Lithos*, *100*(1–4), 14–48. https://doi.org/10.1016/j.lithos.2007.06.016
Pearce, Julian A. (2014). Immobile element fingerprinting of ophiolites. *Elements*. 10(2), 101-108. https://doi.org/10.2113/gselements.10.2.101
Pearce, Julian A., Harris, N. B. W., & Tindle, A. G. (1984). Trace element discrimination diagrams for the tectonic interpretation of granitic rocks. *Journal of Petrology*. 25(4), 956-983. https://doi.org/10.1093/petrology/25.4.956
Peighambari, S., Ahmadipour, H., Stosch, H.-G., & Daliran, F. (2011). Evidence for multi-stage mantle metasomatism at the Dehsheikh peridotite massif and chromite deposits of the Orzuieh coloured melange belt, southeastern Iran. *Ore Geology Reviews*, *39*(4), 245–264. https://doi.org/10.1016/j.oregeorev.2011.03.004
Philip, H., Cisternas, A., Gvishiani, A., & Gorshkov, A. (1989). The Caucasus: an actual example of the initial stages of continental collision. *Tectonophysics*. 161(1-2), 1-21. https://doi.org/10.1016/0040-1951(89)90297-7
Rahmati-Ilkhchi, M., Faryad, S. W., Holub, F. V., Košler, J., & Frank, W. (2011). Magmatic and metamorphic evolution of the Shotur Kuh metamorphic complex (Central Iran). *International Journal of Earth Sciences*. 100(1), 45-62. https://doi.org/10.1007/s00531-009-0499-0
Rajabi, A., Canet, C., Rastad, E., & Alfonso, P. (2015). Basin evolution and stratigraphic correlation of sedimentary-exhalative Zn-Pb deposits of the Early Cambrian Zarigan-Chahmir Basin, Central Iran. *Ore Geology Reviews*. 64, 328-353. https://doi.org/10.1016/j.oregeorev.2014.07.013
Rajabi, A., Rastad, E., Alfonso, P., & Canet, C. (2012). Geology, ore facies and sulphur isotopes of the Koushk vent-proximal sedimentary-exhalative deposit, Posht-e-Badam Block, Central Iran. *International Geology Review*. 54(14), 1635-1648. https://doi.org/10.1080/00206814.2012.659106
Rajabi, A., Rastad, E., & Canet, C. (2012). Metallogeny of Cretaceous carbonate-hosted Zn-Pb deposits of Iran: Geotectonic setting and data integration for future mineral exploration. *International Geology Review*. 54(14), 1649-1672. https://doi.org/10.1080/00206814.2012.659110
Rajabi, A., Rastad, E., Canet, C., & Alfonso, P. (2015). The early Cambrian Chahmir shale-hosted Zn–Pb deposit, Central Iran: an example of vent-proximal SEDEX mineralization. *Mineralium Deposita*. 50(5), 571-590. https://doi.org/10.1007/s00126-014-0556-x
Ramezani, J., & Tucker, R. D. (2003). The Saghand Region, Central Iran: U-Pb geochronology, petrogenesis and implications for Gondwana tectonics. *American Journal of Science*. 303(7), 622-665. https://doi.org/10.2475/ajs.303.7.622
RICHARDS, J. P. (2014). A Review of Tectonics and Metallogeny of the Tethyan Orogen. *Acta Geologica Sinica - English Edition*, *88*(s2), 923–925. https://doi.org/10.1111/1755-6724.12377_13
Richards, J. P., & Kerrich, R. (2007). Special Paper: Adakite-Like Rocks: Their Diverse Origins and Questionable Role in Metallogenesis. *Economic Geology*, *102*(4), 537–576. https://doi.org/10.2113/gsecongeo.102.4.537
Richards, Jeremy P. (2015). Tectonic, magmatic, and metallogenic evolution of the Tethyan orogen: From subduction to collision. *Ore Geology Reviews*, *70*, 323–345. https://doi.org/10.1016/J.OREGEOREV.2014.11.009

Richards, Jeremy P., Spell, T., Rameh, E., Razique, A., & Fletcher, T. (2012). High Sr/Y Magmas Reflect Arc Maturity, High Magmatic Water Content, and Porphyry Cu ± Mo ± Au Potential: Examples from the Tethyan Arcs of Central and Eastern Iran and Western Pakistan. *Economic Geology*, *107*(2), 295–332. https://doi.org/10.2113/econgeo.107.2.295

Richards, Jeremy P., Wilkinson, D., & Ullrich, T. (2006). Geology of the Sari Gunay epithermal gold deposit, northwest Iran. *Economic Geology*. 101(8), 1455-1496. https://doi.org/10.2113/gsecongeo.101.8.1455

Ricou, L.E., Braud, J., Brunn, J. H. (1977). Le Zagros. *Société Géologique de France. Mémoire Hors Série*, *8*, 33–52.

Ricou, L. E. (1976). Evolution structurale dies Zagrides, la rǵegion clef de Neryriz Zagros iranien. *Mémoires de La Société Géologique de France*, *125*, 140.

Robertson, A. H. F. (2007). Overview of tectonic settings related to the rifting and opening of Mesozoic ocean basins in the Eastern Tethys: Oman, Himalayas and Eastern Mediterranean regions. *Geological Society, London, Special Publications*, *282*(1), 325–388. https://doi.org/10.1144/SP282.15

Robertson, Alastair H.F. (2002). Overview of the genesis and emplacement of Mesozoic ophiolites in the Eastern Mediterranean Tethyan region. *Lithos*, *65*(1–2), 1–67. https://doi.org/10.1016/S0024-4937(02)00160-3

RodrÍguez, C., Sellés, D., Dungan, M., Langmuir, C., & Leeman, W. (2007). Adakitic Dacites Formed by Intracrustal Crystal Fractionation of Water-rich Parent Magmas at Nevado de Longaví Volcano (36·2°S; Andean Southern Volcanic Zone, Central Chile). *Journal of Petrology*, *48*(11), 2033–2061. https://doi.org/10.1093/petrology/egm049

Rooney, T. O., Franceschi, P., & Hall, C. M. (2011). Water-saturated magmas in the Panama Canal region: a precursor to adakite-like magma generation? *Contributions to Mineralogy and Petrology*, *161*(3), 373–388. https://doi.org/10.1007/s00410-010-0537-8

Rossetti, F., Nasrabady, M., Theye, T., Gerdes, A., Monié, P., Lucci, F., & Vignaroli, G. (2014). Adakite differentiation and emplacement in a subduction channel: The late paleocene Sabzevar magmatism (NE Iran). *Bulletin of the Geological Society of America*. 126(3-4), 317-343. https://doi.org/10.1130/B30913.1

Rossetti, F., Nozaem, R., Lucci, F., Vignaroli, G., Gerdes, A., Nasrabadi, M., & Theye, T. (2015). Tectonic setting and geochronology of the Cadomian (Ediacaran-Cambrian) magmatism in Central Iran, Kuh-e-Sarhangi region (NW Lut Block). *Journal of Asian Earth Sciences*, *102*, 24–44. https://doi.org/10.1016/j.jseaes.2014.07.034

Saadat, S., & Stern, C. (2016). Distribution and geochemical variations among paleogene volcanic rocks from the north-central Lut block, eastern Iran. *Iranian Journal of Earth Sciences*. 8(1), 1-24. Retrieved from https://scholar.colorado.edu/geol_facpapers/2

Saccani, E., Allahyari, K., & Rahimzadeh, B. (2014). Petrology and geochemistry of mafic magmatic rocks from the Sarve-Abad ophiolites (Kurdistan region, Iran): Evidence for interaction between MORB-type asthenosphere and OIB-type components in the southern Neo-Tethys Ocean. *Tectonophysics*, *621*. https://doi.org/10.1016/j.tecto.2014.02.011

Saccani, Emilio, Allahyari, K., Beccaluva, L., & Bianchini, G. (2013). Geochemistry and petrology of the Kermanshah ophiolites (Iran): Implication for the interaction between passive rifting, oceanic accretion, and OIB-type components in the Southern Neo-Tethys Ocean. *Gondwana Research*, *24*(1), 392–411. https://doi.org/10.1016/j.gr.2012.10.009

Saccani, Emilio, Allahyari, K., & Rahimzadeh, B. (2014a). Petrology and geochemistry of mafic magmatic rocks from the Sarve-Abad ophiolites (Kurdistan region, Iran): Evidence for interaction between MORB-type asthenosphere and OIB-type components in the southern Neo-Tethys Ocean. *Tectonophysics*, *621*, 132–147. https://doi.org/10.1016/j.tecto.2014.02.011

Saccani, Emilio, Allahyari, K., & Rahimzadeh, B. (2014b). Petrology and geochemistry of mafic magmatic rocks from the Sarve-Abad ophiolites (Kurdistan region, Iran): Evidence for interaction between MORB-type asthenosphere and OIB-type components in the southern Neo-Tethys Ocean.

Tectonophysics, *621*, 132–147. https://doi.org/10.1016/J.TECTO.2014.02.011
Saccani, Emilio, Delavari, M., Beccaluva, L., & Amini, S. (2010). Petrological and geochemical constraints on the origin of the Nehbandan ophiolitic complex (eastern Iran): Implication for the evolution of the Sistan Ocean. *Lithos*, *117*(1), 209–228. https://doi.org/10.1016/j.lithos.2010.02.016
Sadeghian, M., Bouchez, J. L., Nédélec, A., Siqueira, R., & Valizadeh, M. V. (2005). The granite pluton of Zahedan (SE Iran): a petrological and magnetic fabric study of a syntectonic sill emplaced in a transtensional setting. *Journal of Asian Earth Sciences*, *25*(2), 301–327. Retrieved from http://www.sciencedirect.com/science/article/pii/S1367912004000719
Samiee, S., Karimpour, M. H., Ghaderi, M., Haidarian Shahri, M. R., Klöetzli, U., & Santos, J. F. (2016). Petrogenesis of subvolcanic rocks from the Khunik prospecting area, south of Birjand, Iran: Geochemical, Sr–Nd isotopic and U–Pb zircon constraints. *Journal of Asian Earth Sciences*, *115*, 170–182. https://doi.org/10.1016/j.jseaes.2015.09.023
Şengör, A. M. C. (1979). The North Anatolian transform fault: Its age, offset and tectonic significance. *Journal of the Geological Society*. 136(3), 269-282. https://doi.org/10.1144/gsjgs.136.3.0269
Şengör, A. M. C. (1990). A new model for the late Palaeozoic-Mesozoic tectonic evolution of Iran and implications for Oman. *Geological Society Special Publication*. https://doi.org/10.1144/GSL.SP.1992.049.01.49
Şengör, A. M. C., Altıner, D., Cin, A., Ustaömer, T., & Hsü, K. J. (1988). Origin and assembly of the Tethyside orogenic collage at the expense of Gondwana Land. *Geological Society, London, Special Publications*, *37*(1), 119–181. https://doi.org/10.1144/GSL.SP.1988.037.01.09
Shabanian, N., Davoudian, A. R., Dong, Y., & Liu, X. (2018). U-Pb zircon dating, geochemistry and Sr-Nd-Pb isotopic ratios from Azna-Dorud Cadomian metagranites, Sanandaj-Sirjan Zone of western Iran. 306, 41-60. *Precambrian Research*. https://doi.org/10.1016/j.precamres.2017.12.037
Shafaii Moghadam, H., & Stern, R. J. (2011). Geodynamic evolution of Upper Cretaceous Zagros ophiolites: Formation of oceanic lithosphere above a nascent subduction zone. *Geological Magazine*. 148(5-6), 762-801. https://doi.org/10.1017/S0016756811000410
Shafaii Moghadam, H., & Stern, R. J. (2014). Ophiolites of Iran: Keys to understanding the tectonic evolution of SW Asia: (I) Paleozoic ophiolites. *Journal of Asian Earth Sciences*, *91*, 19–38. https://doi.org/10.1016/j.jseaes.2014.04.008
Shafiei, B. (2010). Lead isotope signatures of the igneous rocks and porphyry copper deposits from the Kerman Cenozoic magmatic arc (SE Iran), and their magmatic-metallogenetic implications. *Ore Geology Reviews*, *38*(1–2), 27–36. https://doi.org/10.1016/j.oregeorev.2010.05.004
Shafiei, B., Haschke, M., & Shahabpour, J. (2009). Recycling of orogenic arc crust triggers porphyry Cu mineralization in Kerman Cenozoic arc rocks, southeastern Iran. *Mineralium Deposita*, *44*(3), 265–283. https://doi.org/10.1007/s00126-008-0216-0
Shahabpour, J. (1982). *Aspects of Alteration and Mineralization at the Sar-Cheshmeh Copper-Molybdenum Deposit, Kerman, Iran*. *(Ph.D. Thesis). University of Leeds*. Retrieved from https://ci.nii.ac.jp/naid/10030516930/
Shahabpour, J. (2007). Island-arc affinity of the Central Iranian Volcanic Belt. *Journal of Asian Earth Sciences*, *30*(5–6), 652–665. https://doi.org/10.1016/J.JSEAES.2007.02.004
Shahabpour, J., & Kramers, J. D. (1987). Lead isotope data from the Sar-Cheshmeh porphyry copper deposit, Iran. *Mineralium Deposita*, *22*(4), 278–281. https://doi.org/10.1007/BF00204520
Shahsavari Alavijeh, B., Rashidnejad-Omran, N., & Corfu, F. (2017). Zircon U-Pb ages and emplacement history of the Nodoushan plutonic complex in the central Urumieh-Dokhtar magmatic belt, Central Iran: Product of Neotethyan subduction during the Paleogene. *Journal of Asian Earth Sciences*, *143*, 283–295. Retrieved from http://linkinghub.elsevier.com/retrieve/pii/S1367912017301505
Shahzeidi, M., Moayyed, M., Murata, M., Yui, T. F., Arai, S., Chen, F., … Ahmadian, J. (2017). Late Ediacaran crustal thickening in Iran: Geochemical and isotopic constraints from the ~550 Ma Mishu granitoids (northwest Iran). *International Geology Review*. 59(7), 793-811. https://doi.org/10.1080/00206814.2016.1198728
Shakerardakani, F., Li, X.-H., Neubauer, F., Ling, X.-X., Li, J., Monfaredi, B., & Wu, L.-G. (2020).

Genesis of early cretaceous leucogranites in the Central Sanandaj–Sirjan zone, Iran: Reworking of Neoproterozoic metasedimentary rocks in an active continental margin. *Lithos*, *352–353*, 105330. https://doi.org/10.1016/j.lithos.2019.105330

Shakerardakani, F., Neubauer, F., Bernroider, M., Von Quadt, A., Peytcheva, I., Liu, X., … Masoudi, F. (2017). Geochemical and isotopic evidence for Carboniferous rifting: Mafic dykes in the central Sanandaj-Sirjan zone (Dorud-Azna, West Iran). *Geologica Carpathica*. 68(3), 229-247. https://doi.org/10.1515/geoca-2017-0017

Shakerardakani, F., Neubauer, F., Masoudi, F., Mehrabi, B., Liu, X., Dong, Y., … Friedl, G. (2015). Panafrican basement and Mesozoic gabbro in the Zagros orogenic belt in the Dorud-Azna region (NW Iran): Laser-ablation ICP-MS zircon ages and geochemistry. *Tectonophysics*. 647, 146-171. https://doi.org/10.1016/j.tecto.2015.02.020

Sheikholeslami, M. R., Pique, A., Mobayen, P., Sabzehei, M., Bellon, H., & Emami, M. H. (2008). Tectono-metamorphic evolution of the Neyriz metamorphic complex, Quri-Kor-e-Sefid area (Sanandaj-Sirjan Zone, SW Iran). *Journal of Asian Earth Sciences*. 31(4-6), 504-521. https://doi.org/10.1016/j.jseaes.2007.07.004

Shervais, J. W. (1982). TiV plots and the petrogenesis of modern and ophiolitic lavas. *Earth and Planetary Science Letters*. 59(1), 101-118. https://doi.org/10.1016/0012-821X(82)90120-0

Stampfli, G., Marcoux, J., & Baud, A. (1991). Tethyan margins in space and time. *Palaeogeography, Palaeoclimatology, Palaeoecology*. 87(1-4), 373-409. https://doi.org/10.1016/0031-0182(91)90142-E

Stampfli, G.M, & Borel, G. (2002). A plate tectonic model for the Paleozoic and Mesozoic constrained by dynamic plate boundaries and restored synthetic oceanic isochrons. *Earth and Planetary Science Letters*, *196*(1), 17–33. https://doi.org/10.1016/S0012-821X(01)00588-X

Stampfli, Gérard M. (2000). Tethyan oceans. *Geological Society Special Publication*. 173(1), 1-23. https://doi.org/10.1144/GSL.SP.2000.173.01.01

Stern, C. R., & Kilian, R. (1996). Role of the subducted slab, mantle wedge and continental crust in the generation of adakites from the Andean Austral Volcanic Zone. *Contributions to Mineralogy and Petrology*, *123*(3), 263–281. https://doi.org/10.1007/s004100050155

Stern, R. J., & Scholl, D. W. (2010). Yin and yang of continental crust creation and destruction by plate tectonic processes. *International Geology Review*. 52(1), 1-31. https://doi.org/10.1080/00206810903332322

Stocklin, J. (1968). S T R U C T U R a L H I S T O R Y and T E C T O N I C S of Iran, *7*, 1229–1258.

Stöcklin, J. (1974). Possible Ancient continental margins in Iran. In C. A. Burke & C. L. Drake (Eds.), *The Geology of Continental Margins* (pp. 873–887). Berlin, Heidelberg: Springer. https://doi.org/https://doi.org/10.1007/978-3-662-01141-6_64

Stoneley, R. (1981). The geology of the Kuh-e Dalneshin area of southern Iran, and its bearing on the evolution of southern Tethys. *Journal of the Geological Society*. 138(5), 509-526. https://doi.org/10.1144/gsjgs.138.5.0509

Sun, S. -s., & McDonough, W. F. (1989). Chemical and isotopic systematics of oceanic basalts: implications for mantle composition and processes. *Geological Society, London, Special Publications*, *42*(1), 313–345. https://doi.org/10.1144/GSL.SP.1989.042.01.19

Taghipour, N., Aftabi, A., & Mathur, R. (2008). Geology and Re-Os Geochronology of Mineralization of the Miduk Porphyry Copper Deposit, Iran. *Resource Geology*, *58*(2), 143–160. https://doi.org/10.1111/j.1751-3928.2008.00054.x

Takin, M. (1972). Iranian geology and continental drift in the Middle East. *Nature*. 235(5334), 147-150.https://doi.org/10.1038/235147a0

Tarabi, S., Emami, M.-H., Modabberi, S., & Sheikh-Zakariaee, S.-J. (2019a). Eocene-Oligocene volcanic units of momen abad, east of Iran: petrogenesis and magmatic evolution, 15. Retrieved from http://www.iaujournals.ir/article_665319_f28ff6e4d005678a3d77add47c5369e0.pdf

Tarabi, S., Emami, M. H., Modabberi, S., & Sheikh-Zakariaee, S. J. (2019b). Eocene-Oligocene volcanic units of momen abad, east of Iran: Petrogenesis and magmatic evolution. *Iranian Journal of Earth*

Sciences. 11(2), 126-140.
Tirrul, R., Bell, I. R., Griffis, R. J., & Camp, V. E. (1983). The Sistan suture zone of eastern Iran. *Geological Society of America Bulletin*. 94(1), 134-150. https://doi.org/10.1130/0016-7606(1983)94<134:TSSZOE>2.0.CO;2
Treloar, P. J., & Izatt, C. N. (1993). Tectonics of the Himalayan collision between the Indian Plate and the Afghan Block: A synthesis. *Geological Society Special Publication*. 74(1), 69-87. https://doi.org/10.1144/GSL.SP.1993.074.01.06
Verdel, C., Wernicke, B. P., Hassanzadeh, J., & Guest, B. (2011). A Paleogene extensional arc flare-up in Iran. *Tectonics*, *30*(3), n/a-n/a. https://doi.org/10.1029/2010TC002809
Verdel, C., Wernicke, B. P., Ramezani, J., Hassanzadeh, J., Renne, P. R., & Spell, T. L. (2007). Geology and thermochronology of Tertiary Cordilleran-style metamorphic core complexes in the Saghand region of central Iran. *Bulletin of the Geological Society of America*. 119(7-8), 961-977. https://doi.org/10.1130/B26102.1
Vernant, P., Nilforoushan, F., Hatzfeld, D., Abbassi, M. R., Vigny, C., Masson, F., … Chéry, J. (2004). Present-day crustal deformation and plate kinematics in the Middle East constrained by GPS measurements in Iran and northern Oman. *Geophysical Journal International*. 157(1), 381-398. https://doi.org/10.1111/j.1365-246X.2004.02222.x
Vervoort, A., Min, K. B., Konietzky, H., Cho, J. W., Debecker, B., Dinh, Q. D., … Tavallali, A. (2014). Failure of transversely isotropic rock under Brazilian test conditions. *International Journal of Rock Mechanics and Mining Sciences*. 70, 343-352. https://doi.org/10.1016/j.ijrmms.2014.04.006
Wang, Q., McDermott, F., Xu, J., Bellon, H., & Zhu, Y. (2005). Cenozoic K-rich adakitic volcanic rocks in the Hohxil area, northern Tibet: Lower-crustal melting in an intracontinental setting. *Geology*, *33*(6), 465. https://doi.org/10.1130/G21522.1
Waterman, G. C., & Hamilton, R. L. (1975). The Sar Cheshmeh porphyry copper deposit. *Economic Geology*, *70*(3), 568–576. https://doi.org/10.2113/gsecongeo.70.3.568
Whalen, J. B., Currie, K. L., & Chappell, B. W. (1987). A-type granites: geochemical characteristics, discrimination and petrogenesis. *Contributions to Mineralogy and Petrology*. https://doi.org/10.1007/BF00402202
Whitechurch, H., Omrani, J., Agard, P., Humbert, F., Montigny, R., & Jolivet, L. (2013). Evidence for Paleocene–Eocene evolution of the foot of the Eurasian margin (Kermanshah ophiolite, SW Iran) from back-arc to arc: Implications for regional geodynamics and obduction. *Lithos*, *182*, 11–32. https://doi.org/10.1016/j.lithos.2013.07.017
Williams, S. E., Dietmar Müller, R., Landgrebe, T. C. W., & Whittaker, J. M. (2012). An open-source software environment for visualizing and refining plate tectonic reconstructions using high-resolution geological and geophysical data sets. *GSA Today*. 22(4-5), 4-9. https://doi.org/10.1130/GSATG139A.1
Winchester, J. A., & Floyd, P. A. (1977). Geochemical discrimination of different magma series and their differentiation products using immobile elements. *Chemical Geology*. 20, 325-343. https://doi.org/10.1016/0009-2541(77)90057-2
Yarmohammadi, A. (2006). *Mineralogy, geochemistry and genesis of the Barika gold (and barite and base metal) mineralization, east of Sardasht, northwestern Iran*. Tarbiat Modares University.
Yilmaz, Y. (1993). New evidence and model on the evolution of the southeast Anatolian orogen. *Geological Society of America Bulletin*. https://doi.org/10.1130/0016-7606(1993)105<0251:NEAMOT>2.3.CO;2
Zarasvandi, A., Rezaei, M., Raith, J., Lentz, D., Azimzadeh, A.-M., & Pourkaseb, H. (2015). Geochemistry and fluid characteristics of the Dalli porphyry Cu–Au deposit, Central Iran. *Journal of Asian Earth Sciences*, *111*, 175–191. Retrieved from http://linkinghub.elsevier.com/retrieve/pii/S1367912015300493
Zarrinkoub, M. H., Pang, K.-N., Chung, S.-L., Khatib, M. M., Mohammadi, S. S., Chiu, H.-Y., & Lee, H.-Y. (2012). Zircon U–Pb age and geochemical constraints on the origin of the Birjand ophiolite, Sistan suture zone, eastern Iran. *Lithos*, *154*, 392–405. https://doi.org/10.1016/j.lithos.2012.08.007

Zürcher, L., Bookstrom, A. A., Hammarstrom, J. M., Mars, J. C., Ludington, S., Zientek, M. L., … Richards, J. P. (2015). *Porphyry copper assessment of the Tethys region of western and southern Asia: Chapter V in* Global mineral resource assessment. *Scientific Investigations Report*. https://doi.org/10.3133/sir20105090v

APPENDIX A: MAGMATIC EVENTS

Table App 1. Summary of the main igneous and metamorphic rocks reported from the UDMA.

Geological Time	Geological Zone	Crustal Block	Location Name	Lithology	Age (Ma)	Reference
Neoproterozoic	NW-UDMA	NW-Central Iran	Mishu	Granite	550	(Shahzeidi et al., 2017)
	NW-UDMA	NW-Central Iran	Marand	Ignimbrite, Migmatite Andesite, Paragneiss, Basalt	541-698	(Chiu et al., 2017)
	NW-UDMA	NW-Central Iran	Takab	Migmatite, Andesite, Ignimbrite	546-557	(Moghadam et al., 2016)
Cambrian	–	–	–	–	–	–
Devonian	NW-UDMA	NW-Central Iran	Saqqez	Trachyandesite	359	(Chiu et al., 2017)
	NW-UDMA	NW-Central Iran	Takab	Trachyandesite	386-397	(Moghadam et al., 2016)
Carboniferous	NW-UDMA	NW-Central Iran	Saqqez	Trachyandesite	302-356	(Chiu et al., 2017)
	NW-UDMA	NW-Central Iran	Takab	Trachyandesite	325	(Moghadam et al., 2016)
	NW-UDMA	NW-Central Iran	Naqadeh	Rhyolite	300-333	(Chiu et al., 2017)
Permian	NW-UDMA	NW-Central Iran	Sabalan-Arasbaran	Andesite	283	(Chiu, 2013)
	NW-UDMA	NW-Central Iran	Takab	Andesite	282	(Moghadam et al., 2016)
	C-UDMA	C-Central Iran	Natanz	Diorite, Andesite	295 - 271	(Chiu, 2013)
Triassic	NW-UDMA	NW-Central Iran	Sabalan-Astara	Andesite	224-243	(Chiu et al., 2013)
	NW-UDMA	NW-Central Iran	Takab	Andesite	226	(Moghadam et al., 2016)
Jurassic	C-UDMA	CIM	Yazd	Ignimbrite, Diorite, Andesite	163-174	(Chiu et al., 2013)
	SE-UDMA	CIM	Bazman	Granodiorite, Andesite, Ignimbrite	162-168	(Chiu et al., 2013)
	SE-UDMA	CIM	Bam-Jiroft	Microdiorite	161	(Chiu et al., 2013)
Cretaceous	NW-UDMA	NW-Central Iran	Takab	Microdiorite, Andesite, Tuff	106-76	(Moghadam et al., 2016)
	SE-UDMA	Lut	Bam-Jiroft	Andesite, tuff, Diorite, Rhyolite	73-78	(Chiu et al., 2013)
	SE-UDMA	Lut	Bazman	Andesite, Gabbro, Diorite, Rhyolite	83-71	(Chiu et al., 2013)
	SE-UDMA	_	Bahr Aseman	Intrusive rocks	80.8	(Hosseini et al., 2017)

Paleocene	NW-UDMA	NW-Central Iran	Takab	Granodiorite	59	(Moghadam et al., 2016)
Eocene	NW-UDMA	NW-Central Iran	Takab	Granite, Amphibolite, Gabbro	40-46	(Moghadam et al., 2016)
	C-UDMA	CIM	Nain-Yazd	Gabbro, Diorite, Granite,	34-44.7	(Chiu et al., 2013)
	C-UDMA	CIM	Rabor-Lalehzar	Diorite, Granite, Granodiorite	45.7	(Moghadam et al., 2017)
	C-UDMA	_	Nodoushan	Diorite, Granite, Granodiorite	55.32	(Shahsavari et al., 2017)
	SE-UDMA	CIM	Anar-Sirjan	Diorite, Gabbro, Granite	34.9-40	(Chiu et al., 2013)
	SE-UDMA	CIM	Bam-Jiroft	Amphibolite, Diorite, Granite	44-46	(Chiu et al., 2013)
Oligocene	NW-UDMA	NW-Central Iran	Zanjan–Takab	Diorite, Tuff, Granodiorite	25-32	(Moghadam et al., 2016)
	C-UDMA	CIM	Nain-Yazd	Leucogranite	33-33.7	(Chiu et al., 2013)
	C-UDMA	C-Central Iran	Natanz	Granite, Tuff, Andesite	28.9-31.8	(Chiu et al., 2013)
	SE-UDMA	CIM	Bam-Jiroft	Granite, Andesite	28.8-32	(Chiu et al., 2013)
	SE-UDMA	CIM	Kerman	Diorite, Tuff, Granodiorite, Granite	23.4-33.7	(Dargahi et al., 2010)
Miocene	SE-UDMA	CIM?	Iju	Monzonite, Granodiorite, Andesite	9.33	(Golestaniet al., 2018)
	NW-UDMA	NW-Central Iran	Sabalan-Astara	Diorite	17.2-18.5	(Chiu et al., 2013)
	NW-UDMA	NW-Central Iran	Sahand	Monzonite, Andesite, Granite	5.3-6.9	(Chiu et al., 2013)
	C-UDMA	CIM	Nain	Andesite, Diorite	15.8-17	(Chiu et al., 2013)
	C-UDMA	C-Central Iran	Natanz	Andesite, Diorite, Granodiorite	15.5-21.7	(Chiu et al., 2013)
	SE-UDMA	CIM	Rabor-Lalehzar	Granite, Granodiorite	23.2	(Moghadam et al., 2017)
	SE-UDMA	CIM	Kerman	Rhyolite, Diorite	22.4-23.2	(Chiu et al., 2013)
	SE-UDMA	CIM	Anar-Sirjan	Monzonite, Andesite, Diorite	10.1-5.3	(Chiu et al., 2013)
	SE-UDMA	CIM	Iju	Granodiorite, Quartz-monzonite	9.01	(Golestani, 2018)
Plio-Quaternary	NW-UDMA	NW-Central Iran	Sabalan-Astara	Granodioritic, Gabbro	0.38	(Chiu et al., 2013)
	NW-UDMA	NW-Central Iran	Sahand	Rhyolite, Granodioritic, Gabbro	5-5.2	(Chiu et al., 2013)

	SE-UDMA	CIM	Anar-Sirjan	Volcanic	1.15-5.2	(Pang et al., 2016)

Table App 2. Summary of the main igneous and metamorphic rocks reported from the SSZ.

Geological Time	Geological Zone	Crustal Block	Location Name	Lithology	Age (Ma)	Reference
Neoproterozoic	NW-SSZ	NW-Central Iran	Khoy	Basalt, Andesite, Migmatite, Paragneiss, Ignimbrite	550.1	(Azizi, et al., 2011)
Cambrian	NW-SSZ	NW-Central Iran	Dorud–Azna	Meta-granites	525.6	(Shabanian et al. , 2018)
	NW-SSZ	NW-Central Iran	Khoy	Gabbro	533	(Azizi et al., 2011)
Carboniferous	NW-SSZ	NW-Central Iran	Khalifan	Granite	315	(Bea, 2011)
Permian	Central-SSZ	_	Hasanrobat	Granite	288.3	(Alirezaei et al., 2012)
Triassic	_	_	_	_	_	_
Jurassic	SE-SSZ	_	Siah-Kuh	Granodiorite, Monzonite, Granite	199	(Arvinet al., 2007)
	Central-SSZ	Central-SSZ	Esfahan	Granodiorite, Ignimbrite Andesite, Diorite	159-177	(Chiu et al., 2013)
	NW-SSZ	NW-SSZ	Hamadan	Granodiorite, Andesite, Ignimbrite, Microdiorite	163-173	(Chiu et al., 2013)
	NW-SSZ	NW-SSZ	Aligoodarz	Granodiorite	165	(Esna-Ashari, 2012)
	NW-SSZ	NW-SSZ	Alvand	Granite	171.7	(Shahbazi et al., 2010)
	NW-SSZ	NW-SSZ	Boroujerd	Monzogranite	170.7	(Khalaji et al., 2007)
	NW-SSZ	NW-SSZ	Ghalaylan	Granitoid, Subvolcanic	157.8	(Azizi et al., 2015)
	NW-SSZ	NW-SSZ	Kangareh-Taghiabad	Granitic dyke	185-189	(Azizi et al., 2015)
	NW-SSZ	NW-SSZ	Malayer	Meta-Granite, Diorite, Granodiorite	187	(Ahadnejad et al., 2011)
	NW-SSZ	NW-SSZ	Suffi Abad	leucogranite	145-148	(Azizi, et al., 2011)
Cretaceous	NW-SSZ	NW-SSZ	Almogholagh	Quartz-Monzonite	144	(Amiri et al., 2017)
	NW-SSZ	NW-SSZ	Kangareh-Taghiabad	Gabbro	113	(Azizi et al., 2015)
	NW-SSZ	NW-SSZ	Mishao -Iraq	Granite	111.8	(Abdulzahra et al., 2018)
	NW-SSZ	_	Kata–Rash-Iraq	Rhyolite	108.1	(Ali S.I.et al., 2016)
	NW-SSZ	_	Sahneh	volcanic	95	(NouriI.et al., 2016)
	SE-Zagros suture zone	_	Neyriz ophiolite	Rhyodacite, Plagiogranite	93.19	(Babaei.et al., 2006)
Paleocene	NW-SSZ	NW-SSZ	Kamyaran	Granodiorite	56	(Azizi, et al., 2011)
Eocene	NW-SSZ	NW-SSZ	Kamyaran	Granodiorite	51-54	(Azizi, et al., 2011)

	NW-SSZ	NW-SSZ	Taa-Baysaran	Granite	34.7-39.1	(Azizi et al., 2011)
	NW-SSZ	NW-SSZ	GhalaJi	Gabbro	36.63	(Azizi et al., 2011)
	NW-SSZ	NW-SSZ	Kamyaran	Basalt, Gabbro	36.63	(Azizi et al., 2011)
	NW-SSZ	NW-SSZ	Morvarid	Gabbro	36.63	(Azizi et al., 2011)
	NW-SSZ	NW-SSZ	Naqadeh	Monzogranite	41.85	(Mazhari et al., 2011)
	NW-SSZ	NW-SSZ	Ozkol	Basalt	36.63	(Azizi et al., 2011)
	NW-SSZ	NW-SSZ	Piranshah	Syenite, Gabbro, Granite	41.1	(Mazhari et al., 2009)
	NW-SSZ	NW-SSZ	Taa-Baysaran	Gabbro	36.63	(Azizi et al., 2011)
	NW-SSZ	_	Walash -Iraq	volcanic	43.01	(Ali S.I.et al., 2013)
Oligocene	NW-SSZ	NW-SSZ	Taa-Baysaran	Leucogranite	33.2	(Azizi, et al., 2011)
Miocene	NW-SSZ	NW-SSZ	Akhikamal	Rhyolite	10.6	(Azizi et al., 2014)
	NW-SSZ	NW-SSZ	Shida	Dacite, Trachy-Dacite	10.6	(Azizi et al., 2014)

Table App 3. Summary of the main igneous and metamorphic rocks reported from Central Iran.

Geological Time	**Geological Zone**	**Crustal Block**	**Location Name**	**Lithology**	**Age** (Ma)	**Reference**
Neoproterozoic	Central Iran	NE-Central Iran	Taknar	Andesite	550-547	(Moghadam et al., 2017)
	Central Iran	NE-Central Iran	Delbar	Basalt, Diorite, Andesite	~545 Ma	(Balaghi Einalou et al., 2014)
	Central Iran	NE-Central Iran	Shotur Kuh	Orthogneiss	547	(Rahmati-Ilkhchi et al., 2011)
Cambrian	Central Iran	NE-Central Iran	Delbar	Basalt, Diorite, Andesite	498-540	(Balaghi Einalou et al., 2014)
	Central Iran	NE-Central Iran	Taknar	Basalt, Migmatite, Ignimbrite	502-540	(Moghadam et al., 2017)
Devonian	Central Iran	NE-Central Iran	Delbar	Basalt, Diorite, Andesite	390.7	(Balaghi Einalou et al., 2014)
Carboniferous	Central Iran	_	Ghushchi	Granite	319.9	(Moghadam et al., 2015)
Permian	_	_	_	_	_	_
Triassic	Central Iran (Paleo-Tethys)	NE- Central Iran	Mashhad	Diorite, Granodiorite, Andesite	203-227	(Chiu et al., 2017)
Jurassic	Central Iran (Paleo-Tethys)	NE- Central Iran	Mashhad	Diorite	161-200	(Chiu et al., 2017)
Cretaceous	Central Iran	NE-Central Iran	Firouzeh mine	Microdiorite	134	(Ghiasvand, 2017)
	Central Iran	_	Sabzevar Ophiolite	Peridotite, gabbro, pillow lava	98.4	(Shojaat et al., 2003)

Paleocene	Central Iran	NE-Central Iran	Arghash		55.4	(Alaminia et al., 2013)
Eocene	Central Iran	NE-Central Iran	Firouzeh mine	Metagranite	41-43.2	(Chiu et al., 2017)
	Central Iran	NE-Central Iran	Sabzevar	Microdiorite, Trachyte, Rhyolite Trachy-Andesite	45-46.8	(Moghadam et al., 2016)
	Central Iran		Siah-Kamar	porphyry quartz monzonite	41.9	(Nabatianet al., 2017)
Oligocene	–	–	–	–	–	–
Plio-Quaternary	Central Iran		Sabalan	Volcanices	4.51	(Ghalamghashet al., 2016)

Table App 4. Summary of the main igneous and metamorphic rocks reported from the Lut, CIM, and SiSZ.

Geological Time	**Geological Zone**	**Crustal Block**	**Location Name**	**Lithology**	**Age** (Ma)	**Reference**
Neoproterozoic	Sistan Suture Zone	Lut	Zahedan	Gneissic amphibolite	546-557	(Chiu et al., 2017)
	CIM	CIM	Arghash	Diorite	550–590	(Alaminia et al., 2013)
	CIM	CIM	Saghand	Basalt, Granodiorite, Granite	733- 548	(Chiu et al., 2017)
Cambrian	CIM	CIM	Saghand	Basalt, Granodiorite, Granite	501- 535	(Chiu et al., 2017)
Devonian	–	–	–	–	–	–
Carboniferous	–	–	–	–	–	–
Permian	–	–	–	–	–	–
Cretaceous	Sistan Suture Zone	Lut	Mirabad	Andesite, Granodiorite, Green tuff	66-94	(Pang et al., 2014)
	Lut–Sistan Suture Zone	Lut	Birjand ophiolite	Leucogabbro, Basalt	112.8	(Zarrinkoub, 2012)
	Lut	–	Band-e-Zeyarat/Dar Anar ophiolite	Diorites Trohjemites	141.7	(Ghazi et al., 2004)
Paleocene	Sistan Suture Zone	Lut	Mirabad	Granodiorite	58-61	(Pang et al., 2014)
	CIM	–	Gazu	Granite	66- 65	(Mahdavi et al., 2016)
	Sistan Suture Zone	Lut?	Bibi-Maryam	Granodiorite, Tonalite, Granite	58.6	(Delavarial et al., 2014)
Eocene	CIM	CIM	Saghand	Diorite, Granite, Gabbro, Amphibolite	43.8-48.7	(Chiu et al., 2017)
	Lut	Lut	Bisheh	Diorite	39.16	(Nakhaei et al., 2015)
	Lut	Lut	Khunik-Birjand	Monzodiorite	38-39.16	(Samieeet al., 2016)
	Lut	Lut	Sorkh-Kuh	Biotite quartz-monzonite	40.16	(Hosseinkhani et al., 2017)

	Lut	Sistan Suture Zone	Mirabad	Granite, Granodiorite	41.1-51	(Chiu et al., 2017)
	Lut	Lut–Sistan Suture Zone	Lut–Sistan Suture Zone	Andesite, Dacite, Rhyolite, Basalt	39.1-46.4	(Pang et al., 2013)
	Lut	_	Sangan	Granite, quartz monzonite	39.3-43.9	(Mazhari et al., 2017)
	Lut	_	Bisheh	diorite porphyry	39.3-43.9	(Nakhaei et al., 2015)
	CIM	_	Kal-e-Kafi	Quartz monzonite, Diorite, Granite	52	(Ahmadian et al., 2016)
	Lut	_	Khopik	Monzonite	39	(Malekzadeh et al., 2015)
Oligocene	CIM	_	Kerman	Syenogranite, diorite, syenite, monzogranite	33	(Dargahiet al., 2007)
	Lut	Lut	Chah-Shaljami	Qtz monzonite, Bt granodiorite	33.5	(Arjmandzadeh et al., 2011)
	Lut	Lut	Khunik	Granodiorite porphyry	31	(Samiee et al., 2016)
	Lut	Lut	Mahoor	Granitoid	31.88	(Beydokhti et al., 2015)
	Lut	Lut–Sistan Suture Zone	Lut–Sistan Suture Zone	Andesite, Dacite	25-31	(Pang et al.,2013)
	Lut	Sistan Suture Zone	Zahedan	Tuff, Granodiorite, Diorite, Andesite	29.1-33	(Chiu et al., 2017)
Miocene	Lut	Sistan Suture Zone	Taftan	Andesitic dyke	5.3-6.9	(Pang et al., 2014)
	Lut	Sistan Suture Zone	Mirabad	Granodiorite, Granite, Andesitic dyke Diorite	18.3-20	(Pang et al., 2014)
	Lut	Sistan Suture Zone	Bazman	Diorite, Andesite, Granite, Quartz-monzosyenite porphyry	5.4-7.7	(Pang et al., 2014)
	Lut	Lut	Sorkh-Ku	Diorite	20.1	(Hosseinkhani et al., 2017)
	Lut	Lut	Lut–Sistan Suture Zone	Dacite, Andesite	10.1-14.30	(Pang et al., 2012)
Plio-Quaternary	Lut	Sistan Suture Zone	Taftan	Rhyolite, Granite, Gabbro	0.5-3.5	(Pang et al., 2014)
	Lut	Sistan Suture Zone	Bazman	Granite	5.1-5.2	(Pang et al., 2014)

	Lut	Lut Block	Lut–Sistan Suture Zone	Alkali basalts	1.74-4.81	(Pang et al., 2012)

Table App 5. Comparison of the results of this research and previous studies on the timing of geodynamic events at WNT.

Event	**Previous Research**	**This Research** (Confirmed by Gplates and Isotopic composition)
Closure of **Paleo-Tethys**	**Permian - Triassic** (Stampfli, 2000)	**Late Jurassic** Drifting of the Cimmerian superterrane **in contrast with**: isotope data- **Mashhad** granodiorites (**extensional environment**)
Opening Neo-Tethys	**Permian - Triassic** (Stampfli, 2000) **Triassic** (Lippard et al. 1986)	**Permian–Triassic** Confirmed by Isotopic composition
Initiation of subduction	**Late Triassic - Early Jurassic** (Stampfli and Borel, 2002; Muttoni et al.,2009; Hassanzadeh & Wernicke, 2016)	**Middle Jurassic - Late Jurassic**
Initiation of Collision	**Late Cretaceous** (Alavi, 1994; Berberian & King, 1981) **Eocene** (Allen & Armstrong, 2008; Hempton, 1987; Mouthereau et al., 2014) **Eocene–Oligocene** (Hooper, Bailey, & McCarley Holder, 1995	**U. Miocene to Pliocene (10-5 Ma)**

APPENDIX B: GEOCHRONOLOGICAL DATA REFERENCES

Abdulzahra, I. K., Hadi, A., Asahara, Y., Azizi, H., & Yamamoto, K. (2016). Zircon U–Pb ages and geochemistry of Devonian A-type granites in the Iraqi Zagros Suture Zone (Damamna area): New evidence for magmatic activity related to the Hercynian orogeny. Lithos, 264, 360-374.

Abdulzahra, I. K., Hadi, A., Asahara, Y., Azizi, H., & Yamamoto, K. (2018a). Petrogenesis and geochronology of Mishao peraluminous I-type granites, Shalair valley area, NE Iraq. *Chemie Der Erde*. 78, 215-227. https://doi.org/10.1016/J.CHEMER.2018.01.003

Alaminia, Z., Karimpour, M. H., Homam, S. M., & Finger, F. (2013). The magmatic record in the Arghash region (northeast Iran) and tectonic implications. *International Journal of Earth Sciences*. 102, 1603–1625. https://doi.org/10.1007/s00531-013-0897-1

Alaminia, Z., Salehi, M., & Finger, F. (2017). Discovery of the Hendou-abad copper mineral district and its association to dikes: A reconstruction scenario for exploration of Cu-porphyry, northeast Isfahan, Iran. *Journal of Geochemical Exploration*, *183*, 88–101. https://doi.org/10.1016/J.GEXPLO.2017.10.006

Ali, Sarmad A., Ismail, S. A., Nutman, A. P., Bennett, V. C., Jones, B. G., & Buckman, S. (2016). The intra-oceanic Cretaceous (~108 Ma) Kata–Rash arc fragment in the Kurdistan segment of Iraqi Zagros suture zone: Implications for Neotethys evolution and closure. *Lithos*, *260*, 154–163. Retrieved from http://linkinghub.elsevier.com/retrieve/pii/S002449371630113X

Alirezaei, S., & Hassanzadeh, J. (2012). Geochemistry and zircon geochronology of the Permian A-type Hasanrobat granite, Sanandaj?Sirjan belt: A new record of the Gondwana break-up in Iran. *Lithos*, *151*, 122–134. https://doi.org/10.1016/j.lithos.2011.11.015

Ao, S., Xiao, W., Khalatbari Jafari, M., Talebian, M., Chen, L., Wan, B., … Zhang, Z. (2016). U–Pb zircon ages, field geology and geochemistry of the Kermanshah ophiolite (Iran): From continental rifting at 79Ma to oceanic core complex at ca. 36Ma in the southern Neo-Tethys. *Gondwana Research*, *31*, 305–318. https://doi.org/10.1016/j.gr.2015.01.014

Azizi, H., & Asahara, Y. (2013). Juvenile granite in the Sanandaj-Sirjan Zone, NW Iran: Late Jurassic-Early Cretaceous arc-continent collision. *International Geology Review*. 55(12), 1523-1540. https://doi.org/10.1080/00206814.2013.782959

Azizi, H., Chung, S.-L., Tanaka, T., & Asahara, Y. (2011). Isotopic dating of the Khoy metamorphic complex (KMC), northwestern Iran: A significant revision of the formation age and magma source. *Precambrian Research*, *185*(3), 87–94. https://doi.org/10.1016/j.precamres.2010.12.004

Azizi, H., Najari, M., Asahara, Y., Catlos, E. J., Shimizu, M., & Yamamoto, K. (2015). U–Pb zircon ages and geochemistry of Kangareh and Taghiabad mafic bodies in northern Sanandaj–Sirjan Zone, Iran: evidence for intra-oceanic arc and back-arc tectonic regime in Late Jurassic. *Tectonophysics*, *660*, 47-64.

Azizi, H., Zanjefili-Beiranvand, M., & Asahara, Y. (2015). Zircon U-Pb ages and petrogenesis of a tonalite-trondhjemite-granodiorite (TTG) complex in the northern Sanandaj-Sirjan zone, northwest Iran: Evidence for Late Jurassic arc-continent collision. *Lithos*. 216, 178-195. https://doi.org/10.1016/j.lithos.2014.11.012

Badr, M. J., Collins, A. S., & Masoudi, F. (2013). The U-Pb age, geochemistry and tectonic significance of granitoids in the Soursat Complex, Northwest Iran. Turkish Journal of Earth Sciences, 22(1), 1-31.

Bagheri, S., & Stampfli, G. M. (2008). The Anarak, Jandaq and Posht-e-Badam metamorphic complexes in central Iran: New geological data, relationships and tectonic implications. *Tectonophysics*, *451*(1), 123–155. https://doi.org/10.1016/j.tecto.2007.11.047

Balaghi Einalou, M., Sadeghian, M., Zhai, M., Ghasemi, H., & Mohajjel, M. (2014). Zircon U–Pb ages, Hf isotopes and geochemistry of the schists, gneisses and granites in Delbar Metamorphic-Igneous Complex, SE of Shahrood (Iran): Implications for Neoproterozoic geodynamic evolutions of Central

Iran. *Journal of Asian Earth Sciences*, *92*, 92–124. https://doi.org/10.1016/j.jseaes.2014.06.011
Bea, F., Mazhari, A., Montero, P., Amini, S., & Ghalamghash, J. (2011). Zircon dating, Sr and Nd isotopes, and element geochemistry of the Khalifan pluton, NW Iran: Evidence for Variscan magmatism in a supposedly Cimmerian superterrane. *Journal of Asian Earth Sciences*, *40*(1), 172-179.
Berra, F., Zanchi, A., Angiolini, L., Vachard, D., Vezzoli, G., Zanchetta, S., ... & Kouhpeyma, M. (2017). The upper Palaeozoic Godar-e-Siah Complex of Jandaq: evidence and significance of a North Palaeotethyan succession in Central Iran. *Journal of Asian Earth Sciences*, *138*, 272-290.
Beydokhti, R. M., Karimpour, M. H., Mazaheri, S. A., Santos, J. F., & Klötzli, U. (2015). U–Pb zircon geochronology, Sr-Nd geochemistry, petrogenesis and tectonic setting of Mahoor granitoid rocks (Lut Block, Eastern Iran). *Journal of Asian Earth Sciences*, *111*, 192–205. https://doi.org/10.1016/j.jseaes.2015.07.028
Bröcker, M., Fotoohi Rad, G., Burgess, R., Theunissen, S., Paderin, I., Rodionov, N., & Salimi, Z. (2013). New age constraints for the geodynamic evolution of the Sistan Suture Zone, eastern Iran. *Lithos*, *170–171*. https://doi.org/10.1016/j.lithos.2013.02.012
Chiu, H.-Y., Chung, S.-L., Zarrinkoub, M. H., Melkonyan, R., Pang, K.-N., Lee, H.-Y., … Khatib, M. M. (2017). Zircon Hf isotopic constraints on magmatic and tectonic evolution in Iran: Implications for crustal growth in the Tethyan orogenic belt. *Journal of Asian Earth Sciences*. 145, 652-669. https://doi.org/10.1016/j.jseaes.2017.06.011
Chiu, H. Y., Chung, S. L., Zarrinkoub, M. H., Mohammadi, S. S., Khatib, M. M., & Iizuka, Y. (2013). Zircon U-Pb age constraints from Iran on the magmatic evolution related to Neotethyan subduction and Zagros orogeny. *Lithos*, *162–163*, 70–87. https://doi.org/10.1016/j.lithos.2013.01.006
Delavari, M., Amini, S., Schmitt, A. K., McKeegan, K. D., & Mark Harrison, T. (2014). U–Pb geochronology and geochemistry of Bibi-Maryam pluton, eastern Iran: Implication for the late stage of the tectonic evolution of the Sistan Ocean. *Lithos*, *200–201*, 197–211. https://doi.org/10.1016/j.lithos.2014.04.015
Esna-Ashari, A., Tiepolo, M., Valizadeh, M. V., Hassanzadeh, J., & Sepahi, A. A. (2012). Geochemistry and zircon U-Pb geochronology of Aligoodarz granitoid complex, Sanandaj-Sirjan Zone, Iran. *Journal of Asian Earth Sciences*. 43(1), 11-22. https://doi.org/10.1016/j.jseaes.2011.09.001
Faramarzi, N. S., Amini, S., Schmitt, A. K., Hassanzadeh, J., Borg, G., McKeegan, K., ... & Mortazavi, S. M. (2015). Geochronology and geochemistry of rhyolites from Hormuz Island, southern Iran: A new record of Cadomian arc magmatism in the Hormuz Formation. Lithos, 236, 203-211.
Ghalamghash, J., Mousavi, S. Z., Hassanzadeh, J., & Schmitt, A. K. (2016). Geology, zircon geochronology, and petrogenesis of Sabalan volcano (northwestern Iran). *Journal of Volcanology and Geothermal Research*, *327*, 192–207. https://doi.org/10.1016/j.jvolgeores.2016.05.001
Ghiasvand, A., Karimpour, M. H., Malekzadeh Shafaroudi, A., & Hidarian Shahri, M. R. (2017). Age and origin of subvolcanic rocks from NE Iran: Link between magmatic “flare-up” and mineralization. *Chemie Der Erde*. https://doi.org/10.1016/J.CHEMER.2017.12.002
Golestani, M., Karimpour, M. H., Malekzadeh Shafaroudi, A., & Hidarian Shahri, M. R. (2018). Geochemistry, U-Pb geochronology and Sr-Nd isotopes of the Neogene igneous rocks, at the Iju porphyry copper deposit, NW Shahr-e-Babak, Iran. *Ore Geology Reviews*, *93*, 290–307. https://doi.org/10.1016/J.OREGEOREV.2018.01.001
Golmohammadi, A., Karimpour, M. H., Malekzadeh Shafaroudi, A., & Mazaheri, S. A. (2015). Alteration-mineralization, and radiometric ages of the source pluton at the Sangan iron skarn deposit, northeastern Iran. *Ore Geology Reviews*, *65*, 545–563. https://doi.org/10.1016/j.oregeorev.2014.07.005
Hassanpour, S., Alirezaei, S., Selby, D., & Sergeev, S. (2015). SHRIMP zircon U–Pb and biotite and hornblende Ar–Ar geochronology of Sungun, Haftcheshmeh, Kighal, and Niaz porphyry Cu–Mo systems: evidence for an early Miocene porphyry-style mineralization in northwest Iran. International Journal of Earth Sciences, 104(1), 45-59.
Hassanzadeh, Jamshid, Stockli, D. F., Horton, B. K., Axen, G. J., Stockli, L. D., Grove, M., … Walker, J.

D. (2008). U-Pb zircon geochronology of late Neoproterozoic–Early Cambrian granitoids in Iran: Implications for paleogeography, magmatism, and exhumation history of Iranian basement. *Tectonophysics, 451*(1), 71–96. https://doi.org/10.1016/j.tecto.2007.11.062

Heidari, S. M., Paquette, J.-L., & Gasquet, D. (2015). Geology, timing, and genesis of the high sulfidation Au (–Cu) deposit of Touzlar, NW Iran. *Ore Geology Reviews*, *65*, 460–486. https://doi.org/10.1016/J.OREGEOREV.2014.05.013

Hosseini, M. R., Ghaderi, M., Alirezaei, S., & Sun, W. (2017). Geological characteristics and geochronology of the Takht-e-Gonbad copper deposit, SE Iran: A variant of porphyry type deposits. *Ore Geology Reviews*, *86*, 440–458. Retrieved from https://www.sciencedirect.com/science/article/pii/S0169136816303791#!

Hosseini, S. H., Sadeghian, M., Zhai, M., & Ghasemi, H. (2015). Petrology, geochemistry and zircon U–Pb dating of Band-e-Hezarchah metabasites (NE Iran): An evidence for back-arc magmatism along the northern active margin of Gondwana. Geochemistry, 75(2), 207-218.

Hosseini, M. R., Hassanzadeh, J., Alirezaei, S., Sun, W., & Li, C.-Y. (2017). Age revision of the Neotethyan arc migration into the southeast Urumieh-Dokhtar belt of Iran: Geochemistry and U–Pb zircon geochronology. *Lithos*, 296–309. https://doi.org/10.1016/j.lithos.2017.03.012

Hosseinkhani, A., Karimpour, M. H., Malekzadeh Shafaroudi, A., & Santos, J. F. (2017). U-Pb geochronology and petrogenesis of intrusive rocks: Constraints on the mode of genesis and timing of Cu mineralization in SWSK area, Lut Block. *Journal of Geochemical Exploration*, *177*, 11–27. https://doi.org/10.1016/j.gexplo.2017.02.001

K*arimpour, M. H., Stern, C. R., & Farmer, G. L. (2010). Zircon U–Pb geochronology, Sr–Nd isotope analyses, and petrogenetic study of the Dehnow diorite and Kuhsangi granodiorite (Paleo-Tethys), NE Iran. Journal of Asian Earth Sciences, 37(4), 384-393.*

Khalaji, A. A., Esmaeily, D., Valizadeh, M. V., & Rahimpour-Bonab, H. (2007). Petrology and geochemistry of the granitoid complex of Boroujerd, Sanandaj-Sirjan Zone, Western Iran. *Journal of Asian Earth Sciences*. 29(5-6), 859-877. https://doi.org/10.1016/j.jseaes.2006.06.005

Mahdavi, A., Karimpour, M. H., Mao, J., Haidarian Shahri, M. R., Malekzadeh Shafaroudi, A., & Li, H. (2016). Zircon U–Pb geochronology, Hf isotopes and geochemistry of intrusive rocks in the Gazu copper deposit, Iran: Petrogenesis and geological implications. *Ore Geology Reviews, 72*, 818–837. https://doi.org/10.1016/j.oregeorev.2015.09.011

Mahmoudi, S., Corfu, F., Masoudi, F., Mehrabi, B., & Mohajjel, M. (2011). U-Pb dating and emplacement history of granitoid plutons in the northern Sanandaj-Sirjan Zone, Iran. *Journal of Asian Earth Sciences*. 41(3), 238-249. https://doi.org/10.1016/j.jseaes.2011.03.006

Mazhari, S. A., Bea, F., Amini, S., Ghalamghash, J., Molina, J. F., Montero, P., … Williams, I. S. (2009). The Eocene bimodal Piranshahr massif of the Sanandaj-Sirjan Zone, NW Iran: A marker of the end of the collision in the Zagros orogen. *Journal of the Geological Society*. 166(1), 53-69. https://doi.org/10.1144/0016-76492*008-022*

Mazhari, S. A., Amini, S., Ghalamghash, J., & Bea, F. (2011). Petrogenesis of granitic unit of Naqadeh complex, Sanandaj–Sirjan Zone, NW Iran. Arabian Journal of Geosciences, 4(1-2), 59-67.

Mazhari, N., Shafaroudi, A. M., Ghaderi, M., Lackey, J. S., Farmer, G. L., & Karimpour, M. H. (2017). Geochronological and geochemical characteristics of fractionated I-type granites associated with the skarn mineralization in the Sangan mining region, NE Iran. Ore Geology Reviews, 84, 116-133.

Mirnejad, H., Lalonde, A. E., Obeid, M., & Hassanzadeh, J. (2013). Geochemistry and petrogenesis of Mashhad granitoids: An insight into the geodynamic history of the Paleo-Tethys in northeast of Iran. Lithos, 170, 105-116.

Mirnejad, H., Mathur, R., Hassanzadeh, J., Shafie, B., & Nourali, S. (2013). Linking Cu mineralization to host porphyry emplacement: Re-Os ages of molybdenites versus U-Pb ages of zircons and sulfur isotope compositions of pyrite and chalcopyrite from the Iju and Sarkuh porphyry deposits in Southeast Iran. Economic Geology, 108(4), 861-870.

Moghadam, H. S., Li, X. H., Ling, X. X., Santos, J. F., Stern, R. J., Li, Q. L., & Ghorbani, G. (2015). Eocene Kashmar granitoids (NE Iran): petrogenetic constraints from U–Pb zircon geochronology

and isotope geochemistry. Lithos, 216, 118-135.
Moghadam, H. S., Li, X. H., Santos, J. F., Stern, R. J., Griffin, W. L., Ghorbani, G., & Sarebani, N. (2017). Neoproterozoic magmatic flare-up along the N. margin of Gondwana: The Taknar complex, NE Iran. Earth and Planetary Science Letters, 474, 83-96.
Moghadam, H. S., Li, X. H., Stern, R. J., Ghorbani, G., & Bakhshizad, F. (2016). Zircon U-Pb ages and Hf-O isotopic composition of migmatites from the Zanjan-Takab complex, NW Iran: Constraints on partial melting of metasediments. Lithos, 240–243. https://doi.org/10.1016/j.lithos.2015.11.004
Moghadam, H. S., Corfu, F., Chiaradia, M., Stern, R. J., & Ghorbani, G. (2014). Sabzevar Ophiolite, NE Iran: Progress from embryonic oceanic lithosphere into magmatic arc constrained by new isotopic and geochemical data. Lithos, 210, 224-241.
Moghadam, H. S., Corfu, F., & Stern, R. J. (2013). U–Pb zircon ages of Late Cretaceous Nain–Dehshir ophiolites, central Iran. Journal of the Geological Society, 170(1), 175-184.
Moghadam, H. S., Rossetti, F., Lucci, F., Chiaradia, M., Gerdes, A., Martinez, M. L., … Nasrabady, M. (2016). The calc-alkaline and adakitic volcanism of the Sabzevar structural zone (NE Iran): Implications for the Eocene magmatic flare-up in Central Iran. *Lithos*, *248–251*, 517–535. https://doi.org/10.1016/j.lithos.2016.01.019
Mohammaddoost, H., Ghaderi, M., Kumar, T. V., Hassanzadeh, J., Alirezaei, S., Stein, H. J., & Babu, E. V. S. S. K. (2017). Zircon U–Pb and molybdenite Re–Os geochronology, with S isotopic composition of sulfides from the Chah-Firouzeh porphyry Cu deposit, Kerman Cenozoic arc, SE Iran. Ore Geology Reviews, 88, 384-399.
Mohammadi, A., Burg, J. P., Bouilhol, P., & Ruh, J. (2016). U–Pb geochronology and geochemistry of Zahedan and Shah Kuh plutons, southeast Iran: Implication for closure of the South Sistan suture zone. Lithos, 248, 293-308.
Monsef, I., Monsef, R., Mata, J., Zhang, Z., Pirouz, M., Rezaeian, M., … Xiao, W. (2018). Evidence for an early-MORB to fore-arc evolution within the Zagros suture zone: Constraints from zircon U Pb geochronology and geochemistry of the Neyriz ophiolite (South Iran). *Gondwana Research*. 62, 287-305. https://doi.org/10.1016/j.gr.2018.03.002
Nabatian, G., Ghaderi, M., Neubauer, F., Honarmand, M., Liu, X., Dong, Y., ... & Bernroider, M. (2014). Petrogenesis of Tarom high-potassic granitoids in the Alborz–Azarbaijan belt, Iran: Geochemical, U–Pb zircon and Sr–Nd–Pb isotopic constraints. Lithos, 184, 324-345.
Nakhaei, M., Mazaheri, S. A., Karimpour, M. H., Stern, C. R., Zarrinkoub, M. H., Mohammadi, S. S., & Heydarian shahri, M. R. (2015). Geochronologic, geochemical, and isotopic constraints on petrogenesis of the dioritic rocks associated with Fe skarn in the Bisheh area, Eastern Iran. *Arabian Journal of Geosciences*, *8*(10), 8481–8495. https://doi.org/10.1007/s12517-015-1834-3
Niroomand, S., Hassanzadeh, J., Tajeddin, H. A., & Asadi, S. (2018). Hydrothermal evolution and isotope studies of the Baghu intrusion-related gold deposit, Semnan province, north-central Iran. Ore Geology Reviews, 95, 1028-1048.
Nutman, A. P., Mohajjel, M., Bennett, V. C., & Fergusson, C. L. (2014). Gondwanan Eoarchean–Neoproterozoic ancient crustal material in Iran and Turkey: zircon U–Pb–Hf isotopic evidence. Canadian Journal of Earth Sciences, 51(3), 272-285.
Nouri, F., Azizi, H., Golonka, J., Asahara, Y., Orihashi, Y., Yamamoto, K., … Anma, R. (2016). Age and petrogenesis of Na-rich felsic rocks in western Iran: Evidence for closure of the southern branch of the Neo-Tethys in the Late Cretaceous. *Tectonophysics*, *671*, 151–172. https://doi.org/10.1016/j.tecto.2015.12.014
Pang, K. N., Chung, S. L., Zarrinkoub, M. H., Li, X. H., Lee, H. Y., Lin, T. H., & Chiu, H. Y. (2016). New age and geochemical constraints on the origin of Quaternary adakite-like lavas in the Arabia–Eurasia collision zone. *Lithos*. 264, 348-359. https://doi.org/10.1016/j.lithos.2016.08.042
Rahmati-Ilkhchi, M., Faryad, S. W., Holub, F. V., Košler, J., & Frank, W. (2011). Magmatic and metamorphic evolution of the Shotur Kuh metamorphic complex (Central Iran). *International Journal of Earth Sciences*. 100(1), 45-62. https://doi.org/10.1007/s00531-009-0499-0
Ramezani, J., & Tucker, R. D. (2003). The Saghand Region, Central Iran: U-Pb geochronology,

petrogenesis and implications for Gondwana tectonics. *American Journal of Science*. 303(7), 622-665. https://doi.org/10.2475/ajs.303.7.622

Rossetti, F., Nasrabady, M., Vignaroli, G., Theye, T., Gerdes, A., Razavi, M. H., & Vaziri, H. M. (2010). Early Cretaceous migmatitic mafic granulites from the Sabzevar range (NE Iran): implications for the closure of the Mesozoic peri-Tethyan oceans in central Iran. Terra Nova, 22(1), 26-34.

Samiee, S., Karimpour, M. H., Ghaderi, M., Haidarian Shahri, M. R., Klöetzli, U., & Santos, J. F. (2016). Petrogenesis of subvolcanic rocks from the Khunik prospecting area, south of Birjand, Iran: Geochemical, Sr–Nd isotopic and U–Pb zircon constraints. *Journal of Asian Earth Sciences*, *115*, 170–182. https://doi.org/10.1016/j.jseaes.2015.09.023

Sepahi, A. A., Shahbazi, H., Siebel, W., & Ranin, A. (2014). Geochronology of plutonic rocks from the Sanandaj-Sirjan zone, Iran and new zircon and titanite U-Th-Pb ages for granitoids from the Marivan pluton. Geochronometria, 41(3), 207-215.

Shabanian, N., Davoudian, A. R., Dong, Y., & Liu, X. (2018). U-Pb zircon dating, geochemistry and Sr-Nd-Pb isotopic ratios from Azna-Dorud Cadomian metagranites, Sanandaj-Sirjan Zone of western Iran. *Precambrian Research*. 306, 41-60. https://doi.org/10.1016/j.precamres.2017.12.037

Shafaroudi, A. M., Karimpour, M. H., & Golmohammadi, A. (2013). Zircon U–Pb geochronology and petrology of intrusive rocks in the C-North and Baghak districts, Sangan iron mine, NE Iran. Journal of Asian Earth Sciences, 64, 256-271.

Shahbazi, H., Siebel, W., Pourmoafee, M., Ghorbani, M., Sepahi, A. A., Shang, C. K., & Abedini, M. V. (2010). Geochemistry and U–Pb zircon geochronology of the Alvand plutonic complex in Sanandaj–Sirjan Zone (Iran): New evidence for Jurassic magmatism. Journal of Asian Earth Sciences, 39(6), 668-683.

Shahsavari Alavijeh, B., Rashidnejad-Omran, N., & Corfu, F. (2017). Zircon U-Pb ages and emplacement history of the Nodoushan plutonic complex in the central Urumieh-Dokhtar magmatic belt, Central Iran: Product of Neotethyan subduction during the Paleogene. *Journal of Asian Earth Sciences*, *143*, 283–295. Retrieved from http://linkinghub.elsevier.com/retrieve/pii/S1367912017301505

Shahzeidi, M., Moayyed, M., Murata, M., Yui, T. F., Arai, S., Chen, F., … Ahmadian, J. (2017). Late Ediacaran crustal thickening in Iran: Geochemical and isotopic constraints from the ~550 Ma Mishu granitoids (northwest Iran). *International Geology Review*. 59(7), 793-811. https://doi.org/10.1080/00206814.2016.1198728

Shakerardakani, F., Neubauer, F., Masoudi, F., Mehrabi, B., Liu, X., Dong, Y., … Friedl, G. (2015). Panafrican basement and Mesozoic gabbro in the Zagros orogenic belt in the Dorud-Azna region (NW Iran): Laser-ablation ICP-MS zircon ages and geochemistry. *Tectonophysics*. 647, 146-171. https://doi.org/10.1016/j.tecto.2015.02.020

Zarrinkoub, M. H., Pang, K.-N., Chung, S.-L., Khatib, M. M., Mohammadi, S. S., Chiu, H.-Y., & Lee, H.-Y. (2012). Zircon U–Pb age and geochemical constraints on the origin of the Birjand ophiolite, Sistan suture zone, eastern Iran. *Lithos*, *154*, 392–405. https://doi.org/10.1016/j.lithos.2012.08.007

APPENDIX C: LITHOGEOCHEMICAL DATA REFERENCES

Abdulzahra, I. K., Hadi, A., Asahara, Y., Azizi, H., & Yamamoto, K. (2018a). Petrogenesis and geochronology of Mishao peraluminous I-type granites, Shalair valley area, NE Iraq. *Chemie Der Erde*. 78, 215-227. https://doi.org/10.1016/J.CHEMER.2018.01.003

Ahmadian, Jamshid, Sarjoughian, F., Lentz, D., Esna-Ashari, A., Murata, M., & Ozawa, H. (2016). Eocene K-rich adakitic rocks in Central Iran: Implications for evaluating its Cu–Au–Mo metallogenic potential. *Ore Geology Reviews*, *72*, 323–342. https://doi.org/10.1016/j.oregeorev.2015.07.017

Ali, S. A., Buckman, S., Aswad, K. J., Jones, B. G., Ismail, S. A., & Nutman, A. P. (2012). Recognition of late cretaceous hasanbag ophiolite-arc rocks in the Kurdistan region of the Iraqi Zagros suture zone: A missing link in the paleogeography of the closing neotethys ocean. *Lithosphere*. 4 (5), 395–410. https://doi.org/10.1130/L207.1

Ali, Sarmad A., Buckman, S., Aswad, K. J., Jones, B. G., Ismail, S. A., & Nutman, A. P. (2013). The tectonic evolution of a Neo-Tethyan (Eocene-Oligocene) island-arc (Walash and Naopurdan groups) in the Kurdistan region of the Northeast Iraqi Zagros Suture Zone. *Island Arc*. 22 (1), 104-125. https://doi.org/10.1111/iar.12007.

Ali, Sarmad A., Ismail, S. A., Nutman, A. P., Bennett, V. C., Jones, B. G., & Buckman, S. (2016). The intra-oceanic Cretaceous (~108 Ma) Kata–Rash arc fragment in the Kurdistan segment of Iraqi Zagros suture zone: Implications for Neotethys evolution and closure. *Lithos*, *260*, 154–163. Retrieved from http://linkinghub.elsevier.com/retrieve/pii/S002449371630113X

Alirezaei, S., & Hassanzadeh, J. (2012). Geochemistry and zircon geochronology of the Permian A-type Hasanrobat granite, Sanandaj-Sirjan belt: A new record of the Gondwana break-up in Iran. *Lithos*, *151*, 122–134. https://doi.org/10.1016/j.lithos.2011.11.015

Ao, S., Xiao, W., Khalatbari Jafari, M., Talebian, M., Chen, L., Wan, B., … Zhang, Z. (2016). U–Pb zircon ages, field geology and geochemistry of the Kermanshah ophiolite (Iran): From continental rifting at 79Ma to oceanic core complex at ca. 36Ma in the southern Neo-Tethys. *Gondwana Research*, *31*, 305–318. https://doi.org/10.1016/j.gr.2015.01.014

Arvin, M., Pan, Y., Dargahi, S., Malekizadeh, A., & Babaei, A. (2007). Petrochemistry of the Siah-Kuh granitoid stock southwest of Kerman, Iran: Implications for initiation of Neotethys subduction. *Journal of Asian Earth Sciences*, *30*(3), 474–489. https://doi.org/10.1016/j.jseaes.2007.01.001 *Bahonar University of Kerman*. Retrieved from https://ci.nii.ac.jp/naid/10030173954/

Azizi, H., Tanaka, T., Asahara, Y., Chung, S. L., & Zarrinkoub, M. H. (2011). Discrimination of the age and tectonic setting for magmatic rocks along the Zagros thrust zone, northwest Iran, using the zircon U–Pb age and Sr–Nd isotopes. Journal of Geodynamics, 52(3-4), 304-320.

Azizi, H., Asahara, Y., Mehrabi, B., & Chung, S. L. (2011). Geochronological and geochemical constraints on the petrogenesis of high-K granite from the Suffi abad area, Sanandaj-Sirjan Zone, NW Iran. Geochemistry, 71(4), 363-376.

Azizi, H., Najari, M., Asahara, Y., Catlos, E. J., Shimizu, M., & Yamamoto, K. (2015). U–Pb zircon ages and geochemistry of Kangareh and Taghiabad mafic bodies in northern Sanandaj–Sirjan Zone, Iran: evidence for intra-oceanic arc and back-arc tectonic regime in Late Jurassic. *Tectonophysics*, *660*, 47-64.

Babaie, H. A., Babaei, A., Ghazi, A. M., & Arvin, M. (2006). Geochemical, 40Ar/39Ar age, and isotopic data for crustal rocks of the Neyriz ophiolite, Iran. Canadian Journal of Earth Sciences, 43(1), 57-70.

Beydokhti, R. M., Karimpour, M. H., Mazaheri, S. A., Santos, J. F., & Klötzli, U. (2015). U–Pb zircon geochronology, Sr-Nd geochemistry, petrogenesis and tectonic setting of Mahoor granitoid rocks (Lut Block, Eastern Iran). *Journal of Asian Earth Sciences*, *111*, 192–205. https://doi.org/10.1016/j.jseaes.2015.07.028

Dargahi, S., Arvin, M., Pan, Y., & Babaei, A. (2010). Petrogenesis of post-collisional A-type granitoids from the Urumieh–Dokhtar magmatic assemblage, Southwestern Kerman, Iran: Constraints on the Arabian–Eurasian continental collision. *Lithos*, *115*, 190–204. Retrieved from https://www.sciencedirect.com/science/article/pii/S0024493709004897

Delavari, M., Amini, S., Schmitt, A. K., McKeegan, K. D., & Mark Harrison, T. (2014). U–Pb geochronology and geochemistry of Bibi-Maryam pluton, eastern Iran: Implication for the late stage of the tectonic evolution of the Sistan Ocean. *Lithos*, *200–201*, 197–211. https://doi.org/10.1016/j.lithos.2014.04.015

Esna-Ashari, A., Tiepolo, M., Valizadeh, M. V., Hassanzadeh, J., & Sepahi, A. A. (2012). Geochemistry and zircon U-Pb geochronology of Aligoodarz granitoid complex, Sanandaj-Sirjan Zone, Iran. *Journal of Asian Earth Sciences*. 43(1), 11-22. https://doi.org/10.1016/j.jseaes.2011.09.001

Ghalamghash, J., Mousavi, S. Z., Hassanzadeh, J., & Schmitt, A. K. (2016). Geology, zircon geochronology, and petrogenesis of Sabalan volcano (northwestern Iran). *Journal of Volcanology and Geothermal Research*, *327*, 192–207. https://doi.org/10.1016/j.jvolgeores.2016.05.001

Ghazi, A.M., Hassanipak, A. A., Mahoney, J. J., & Duncan, R. A. (2004). Geochemical characteristics, 40Ar–39Ar ages and original tectonic setting of the Band-e-Zeyarat/Dar Anar ophiolite, Makran accretionary prism, S.E. Iran. *Tectonophysics*, *393*(1), 175–196. https://doi.org/10.1016/j.tecto.2004.07.035

Ghiasvand, A., Karimpour, M. H., Malekzadeh Shafaroudi, A., & Hidarian Shahri, M. R. (2017). Age and origin of subvolcanic rocks from NE Iran: Link between magmatic "flare-up" and mineralization. *Chemie Der Erde*. 78(2), 254-267. https://doi.org/10.1016/J.CHEMER.2017.12.002

Golestani, M., Karimpour, M. H., Malekzadeh Shafaroudi, A., & Hidarian Shahri, M. R. (2018). Geochemistry, U-Pb geochronology and Sr-Nd isotopes of the Neogene igneous rocks, at the Iju porphyry copper deposit, NW Shahr-e-Babak, Iran. *Ore Geology Reviews*, *93*, 290–307. https://doi.org/10.1016/J.OREGEOREV.2018.01.001

Golmohammadi, A., Karimpour, M. H., Malekzadeh Shafaroudi, A., & Mazaheri, S. A. (2015). Alteration-mineralization, and radiometric ages of the source pluton at the Sangan iron skarn deposit, northeastern Iran. *Ore Geology Reviews*, *65*, 545–563. https://doi.org/10.1016/j.oregeorev.2014.07.005

Heidari, S. M., Paquette, J.-L., & Gasquet, D. (2015). Geology, timing, and genesis of the high sulfidation Au (–Cu) deposit of Touzlar, NW Iran. *Ore Geology Reviews*, *65*, 460–486. https://doi.org/10.1016/J.OREGEOREV.2014.05.013

Hosseini, M. R., Hassanzadeh, J., Alirezaei, S., Sun, W., & Li, C.-Y. (2017). Age revision of the Neotethyan arc migration into the southeast Urumieh-Dokhtar belt of Iran: Geochemistry and U–Pb zircon geochronology. *Lithos*, 296–309. https://doi.org/10.1016/j.lithos.2017.03.012

Hosseinkhani, A., Karimpour, M. H., Malekzadeh Shafaroudi, A., & Santos, J. F. (2017). U-Pb geochronology and petrogenesis of intrusive rocks: Constraints on the mode of genesis and timing of Cu mineralization in SWSK area, Lut Block. *Journal of Geochemical Exploration*, *177*, 11–27. https://doi.org/10.1016/j.gexplo.2017.02.001

Jafari, M. K., Babaie, H. A., & Mirzaie, M. (2013). Geology, petrology and tectonomagmatic evolution of the plutonic crustal rocks of the Sabzevar ophiolite, NE Iran. Geological Magazine, 150(5), 862-884.

Khalaji, A. A., Esmaeily, D., Valizadeh, M. V., & Rahimpour-Bonab, H. (2007). Petrology and geochemistry of the granitoid complex of Boroujerd, Sanandaj-Sirjan Zone, Western Iran. *Journal of Asian Earth Sciences*. 29(5-6), 859-877. https://doi.org/10.1016/j.jseaes.2006.06.005

Mahdavi, A., Karimpour, M. H., Mao, J., Haidarian Shahri, M. R., Malekzadeh Shafaroudi, A., & Li, H. (2016). Zircon U–Pb geochronology, Hf isotopes and geochemistry of intrusive rocks in the Gazu copper deposit, Iran: Petrogenesis and geological implications. *Ore Geology Reviews*, *72*, 818–837. https://doi.org/10.1016/j.oregeorev.2015.09.011

Mahmoudi, S., Corfu, F., Masoudi, F., Mehrabi, B., & Mohajjel, M. (2011). U-Pb dating and emplacement history of granitoid plutons in the northern Sanandaj-Sirjan Zone, Iran. *Journal of*

Asian Earth Sciences. 41(3), 238-249. https://doi.org/10.1016/j.jseaes.2011.03.006
Malekzadeh Shafaroudi, A., Karimpour, M. H., & Stern, C. R. (2015). The Khopik porphyry copper prospect, Lut Block, Eastern Iran: Geology, alteration and mineralization, fluid inclusion, and oxygen isotope studies. *Ore Geology Reviews, 65*, 522–544. https://doi.org/10.1016/j.oregeorev.2014.04.015
Mazhari, S. A., Bea, F., Amini, S., Ghalamghash, J., Molina, J. F., Montero, P., … Williams, I. S. (2009). The Eocene bimodal Piranshahr massif of the Sanandaj-Sirjan Zone, NW Iran: A marker of the end of the collision in the Zagros orogen. *Journal of the Geological Society*. 166(1), 53-69. https://doi.org/10.1144/0016-76492*008-022*
Mazhari, S. A., Amini, S., Ghalamghash, J., & Bea, F. (2011). Petrogenesis of granitic unit of Naqadeh complex, Sanandaj–Sirjan Zone, NW Iran. Arabian Journal of Geosciences, 4(1-2), 59-67.
Mazhari, S. A. (2016). Petrogenesis of adakite and high-Nb basalt association in the SW of Sabzevar Zone, NE of Iran: Evidence for slab melt–mantle interaction. *Journal of African Earth Sciences, 116*, 170-181.
Mazhari, N., Shafaroudi, A. M., Ghaderi, M., Lackey, J. S., Farmer, G. L., & Karimpour, M. H. (2017). Geochronological and geochemical characteristics of fractionated I-type granites associated with the skarn mineralization in the Sangan mining region, NE Iran. Ore Geology Reviews, 84, 116-133.
Moghadam, H. S., Li, X. H., Ling, X. X., Stern, R. J., Santos, J. F., Meinhold, G., ... & Shahabi, S. (2015). Petrogenesis and tectonic implications of Late Carboniferous A-type granites and gabbronorites in NW Iran: Geochronological and geochemical constraints. *Lithos*, *212*, 266-279.
Moghadam, H. S., Rossetti, F., Lucci, F., Chiaradia, M., Gerdes, A., Martinez, M. L., … Nasrabady, M. (2016). The calc-alkaline and adakitic volcanism of the Sabzevar structural zone (NE Iran): Implications for the Eocene magmatic flare-up in Central Iran. *Lithos, 248–251*, 517–535. https://doi.org/10.1016/j.lithos.2016.01.019
Moghadam, H. S., Corfu, F., Chiaradia, M., Stern, R. J., & Ghorbani, G. (2014). Sabzevar Ophiolite, NE Iran: Progress from embryonic oceanic lithosphere into magmatic arc constrained by new isotopic and geochemical data. Lithos, 210, 224-241.
Moghadam, H. S., Khedr, M. Z., Arai, S., Stern, R. J., Ghorbani, G., Tamura, A., & Ottley, C. J. (2015). Arc-related harzburgite–dunite–chromitite complexes in the mantle section of the Sabzevar ophiolite, Iran: a model for formation of podiform chromitites. *Gondwana Research*, *27*(2), 575-593.
Monsef, I., Monsef, R., Mata, J., Zhang, Z., Pirouz, M., Rezaeian, M., … Xiao, W. (2018). Evidence for an early-MORB to fore-arc evolution within the Zagros suture zone: Constraints from zircon U Pb geochronology and geochemistry of the Neyriz ophiolite (South Iran). *Gondwana Research*. 62, 287-305. https://doi.org/10.1016/j.gr.2018.03.002
Nabatian, G., Wan, B., & Honarmand, M. (2017). Whole rock geochemistry, molybdenite Re-Os geochronology, stable isotope and fluid inclusion investigations of the Siah-Kamar deposit, western Alborz-Azarbayjan: New constrains on the porphyry Mo deposit in Iran. *Ore Geology Reviews*, *91*, 638–659. https://doi.org/10.1016/J.OREGEOREV.2017.08.030
Nabatian, G., Li, X. H., Honarmand, M., & Melgarejo, J. C. (2017). Geology, mineralogy and evolution of iron skarn deposits in the Zanjan district, NW Iran: Constraints from U-Pb dating, Hf and O isotope analyses of zircons and stable isotope geochemistry. *Ore Geology Reviews*, *84*, 42-66.
Nakhaei, M., Mazaheri, S. A., Karimpour, M. H., Stern, C. R., Zarrinkoub, M. H., Mohammadi, S. S., & Heydarian shahri, M. R. (2015). Geochronologic, geochemical, and isotopic constraints on petrogenesis of the dioritic rocks associated with Fe skarn in the Bisheh area, Eastern Iran. *Arabian Journal of Geosciences*, *8*(10), 8481–8495. https://doi.org/10.1007/s12517-015-1834-3
Nouri, F., Azizi, H., Golonka, J., Asahara, Y., Orihashi, Y., Yamamoto, K., … Anma, R. (2016). Age and petrogenesis of Na-rich felsic rocks in western Iran: Evidence for closure of the southern branch of the Neo-Tethys in the Late Cretaceous. *Tectonophysics*, *671*, 151–172. https://doi.org/10.1016/j.tecto.2015.12.014
Pang, K. N., Chung, S. L., Zarrinkoub, M. H., Mohammadi, S. S., Yang, H. M., Chu, C. H., … Lo, C. H.

(2012). Age, geochemical characteristics and petrogenesis of Late Cenozoic intraplate alkali basalts in the Lut-Sistan region, eastern Iran. *Chemical Geology*. https://doi.org/10.1016/j.chemgeo.2012.02.020

Rahmati-Ilkhchi, M., Faryad, S. W., Holub, F. V., Košler, J., & Frank, W. (2011). Magmatic and metamorphic evolution of the Shotur Kuh metamorphic complex (Central Iran). *International Journal of Earth Sciences*. 100(1), 45-62. https://doi.org/10.1007/s00531-009-0499-0

Saccani, Emilio, Allahyari, K., & Rahimzadeh, B. (2014a). Petrology and geochemistry of mafic magmatic rocks from the Sarve-Abad ophiolites (Kurdistan region, Iran): Evidence for interaction between MORB-type asthenosphere and OIB-type components in the southern Neo-Tethys Ocean. *Tectonophysics*, *621*, 132–147. https://doi.org/10.1016/j.tecto.2014.02.011

Sadeghian, M., Bouchez, J. L., Nédélec, A., Siqueira, R., & Valizadeh, M. V. (2005). The granite pluton of Zahedan (SE Iran): a petrological and magnetic fabric study of a syntectonic sill emplaced in a transtensional setting. *Journal of Asian Earth Sciences*, *25*(2), 301–327. Retrieved from http://www.sciencedirect.com/science/article/pii/S1367912004000719

Samiee, S., Karimpour, M. H., Ghaderi, M., Haidarian Shahri, M. R., Klöetzli, U., & Santos, J. F. (2016). Petrogenesis of subvolcanic rocks from the Khunik prospecting area, south of Birjand, Iran: Geochemical, Sr–Nd isotopic and U–Pb zircon constraints. *Journal of Asian Earth Sciences*, *115*, 170–182. https://doi.org/10.1016/j.jseaes.2015.09.023

Shabanian, N., Davoudian, A. R., Dong, Y., & Liu, X. (2018). U-Pb zircon dating, geochemistry and Sr-Nd-Pb isotopic ratios from Azna-Dorud Cadomian metagranites, Sanandaj-Sirjan Zone of western Iran. *Precambrian Research*. 306, 41-60. https://doi.org/10.1016/j.precamres.2017.12.037

Shafaroudi, A. M., Karimpour, M. H., & Golmohammadi, A. (2013). Zircon U–Pb geochronology and petrology of intrusive rocks in the C-North and Baghak districts, Sangan iron mine, NE Iran. Journal of Asian Earth Sciences, 64, 256-271.

Shahbazi, H., Siebel, W., Pourmoafee, M., Ghorbani, M., Sepahi, A. A., Shang, C. K., & Abedini, M. V. (2010). Geochemistry and U–Pb zircon geochronology of the Alvand plutonic complex in Sanandaj–Sirjan Zone (Iran): New evidence for Jurassic magmatism. Journal of Asian Earth Sciences, 39(6), 668-683.

Shakerardakani, F., Neubauer, F., Masoudi, F., Mehrabi, B., Liu, X., Dong, Y., … Friedl, G. (2015). Panafrican basement and Mesozoic gabbro in the Zagros orogenic belt in the Dorud-Azna region (NW Iran): Laser-ablation ICP-MS zircon ages and geochemistry. *Tectonophysics*. 647, 146-171. https://doi.org/10.1016/j.tecto.2015.02.020

Shojaat, B., Hassanipak, A. A., Mobasher, K., & Ghazi, A. M. (2003). Petrology, geochemistry and tectonics of the Sabzevar ophiolite, North Central Iran. Journal of Asian Earth Sciences, 21(9), 1053-1067.

APPENDIX D: ISOTOPIC DATA REFERENCES

Abdulzahra, I. K., Hadi, A., Asahara, Y., Azizi, H., & Yamamoto, K. (2018). Petrogenesis and geochronology of Mishao peraluminous I-type granites, Shalair valley area, NE Iraq. *Chemie Der Erde*. 78, 215-227 .https://doi.org/10.1016/J.CHEMER.2018.01.003

Ahadnejad, V., Valizadeh, M.-V., Deevsalar, R., & Rezaei-Kahkhaei, M. (2011). Age and geotectonic position of the Malayer granitoids: Implication for plutonism in the Sanandaj-Sirjan Zone, W Iran. *Neues Jahrbuch f?R Geologie Und Pal?Ontologie - Abhandlungen*, *261*(1), 61–75. https://doi.org/10.1127/0077-7749/2011/0149

Alaminia, Z., Karimpour, M. H., Homam, S. M., & Finger, F. (2013). The magmatic record in the Arghash region (northeast Iran) and tectonic implications. *International Journal of Earth Sciences*. 102, 1603–1625. https://doi.org/10.1007/s00531-013-0897-1

Amiri, M., Khalaji, A. A., Tahmasbi, Z., Santos, J. F., Sahamieh, R. Z., & Zamanian, H. (2017). Geochemistry, petrogenesis, and tectonic setting of the Almogholagh batholith in the Sanandaj–Sirjan zone, Western Iran. *Journal of African Earth Sciences*. 134, 113-133. https://doi.org/10.1016/j.jafrearsci.2017.06.018

Arjmandzadeh, R., Karimpour, M. H., Mazaheri, S. A., Santos, J. F., Medina, J. M., & Homam, S. M. (2011a). Sr-Nd isotope geochemistry and petrogenesis of the Chah-Shaljami granitoids (Lut Block, Eastern Iran). *Journal of Asian Earth Sciences*, *41*(3), 283–296. https://doi.org/10.1016/J.JSEAES.2011.02.014

Azizi, H., Tanaka, T., Asahara, Y., Chung, S. L., & Zarrinkoub, M. H. (2011). Discrimination of the age and tectonic setting for magmatic rocks along the Zagros thrust zone, northwest Iran, using the zircon U–Pb age and Sr–Nd isotopes. Journal of Geodynamics, 52(3-4), 304-320.

Azizi, H., Asahara, Y., Mehrabi, B., & Chung, S. L. (2011). Geochronological and geochemical constraints on the petrogenesis of high-K granite from the Suffi abad area, Sanandaj-Sirjan Zone, NW Iran. Geochemistry, 71(4), 363-376.

Azizi, H., Chung, S.-L., Tanaka, T., & Asahara, Y. (2011). Isotopic dating of the Khoy metamorphic complex (KMC), northwestern Iran: A significant revision of the formation age and magma source. *Precambrian Research*, *185*(3), 87–94. https://doi.org/10.1016/j.precamres.2010.12.004

Azizi, H., Asahara, Y., Tsuboi, M., Takemura, K., & Razyani, S. (2014). The role of heterogenetic mantle in the genesis of adakites northeast of Sanandaj, northwestern Iran. *Geochemistry*, *74*(1), 87-97.

Azizi, H., Najari, M., Asahara, Y., Catlos, E. J., Shimizu, M., & Yamamoto, K. (2015). U–Pb zircon ages and geochemistry of Kangareh and Taghiabad mafic bodies in northern Sanandaj–Sirjan Zone, Iran: evidence for intra-oceanic arc and back-arc tectonic regime in Late Jurassic. *Tectonophysics*, *660*, 47-64.

Azizi, H., Zanjefili-Beiranvand, M., & Asahara, Y. (2015). Zircon U-Pb ages and petrogenesis of a tonalite-trondhjemite-granodiorite (TTG) complex in the northern Sanandaj-Sirjan zone, northwest Iran: Evidence for Late Jurassic arc-continent collision. *Lithos*. 216, 178-195. https://doi.org/10.1016/j.lithos.2014.11.012

Babaie, H. A., Babaei, A., Ghazi, A. M., & Arvin, M. (2006). Geochemical, 40Ar/39Ar age, and isotopic data for crustal rocks of the Neyriz ophiolite, Iran. Canadian Journal of Earth Sciences, 43(1), 57-70.

Balaghi Einalou, M., Sadeghian, M., Zhai, M., Ghasemi, H., & Mohajjel, M. (2014). Zircon U–Pb ages, Hf isotopes and geochemistry of the schists, gneisses and granites in Delbar Metamorphic-Igneous Complex, SE of Shahrood (Iran): Implications for Neoproterozoic geodynamic evolutions of Central Iran. *Journal of Asian Earth Sciences*, *92*, 92–124. https://doi.org/10.1016/j.jseaes.2014.06.011

Bea, F., Mazhari, A., Montero, P., Amini, S., & Ghalamghash, J. (2011). Zircon dating, Sr and Nd isotopes, and element geochemistry of the Khalifan pluton, NW Iran: Evidence for Variscan magmatism in a supposedly Cimmerian superterrane. *Journal of Asian Earth Sciences*, *40*(1), 172-179.

Beydokhti, R. M., Karimpour, M. H., Mazaheri, S. A., Santos, J. F., & Klötzli, U. (2015). U–Pb zircon

geochronology, Sr-Nd geochemistry, petrogenesis and tectonic setting of Mahoor granitoid rocks (Lut Block, Eastern Iran). *Journal of Asian Earth Sciences*, *111*, 192–205. https://doi.org/10.1016/j.jseaes.2015.07.028

Chiu, H.-Y., Chung, S.-L., Zarrinkoub, M. H., Melkonyan, R., Pang, K.-N., Lee, H.-Y., … Khatib, M. M. (2017). Zircon Hf isotopic constraints on magmatic and tectonic evolution in Iran: Implications for crustal growth in the Tethyan orogenic belt. *Journal of Asian Earth Sciences*. 145, 652-669. https://doi.org/10.1016/j.jseaes.2017.06.011

Chiu, H. Y., Chung, S. L., Zarrinkoub, M. H., Mohammadi, S. S., Khatib, M. M., & Iizuka, Y. (2013). Zircon U-Pb age constraints from Iran on the magmatic evolution related to Neotethyan subduction and Zagros orogeny. *Lithos*, *162–163*, 70–87. https://doi.org/10.1016/j.lithos.2013.01.006

Dargahi, S., Arvin, M., Pan, Y., & Babaei, A. (2010). Petrogenesis of post-collisional A-type granitoids from the Urumieh–Dokhtar magmatic assemblage, Southwestern Kerman, Iran: Constraints on the Arabian–Eurasian continental collision. *Lithos*, *115*, 190–204. Retrieved from https://www.sciencedirect.com/science/article/pii/S0024493709004897

Esna-Ashari, A., Tiepolo, M., Valizadeh, M. V., Hassanzadeh, J., & Sepahi, A. A. (2012). Geochemistry and zircon U-Pb geochronology of Aligoodarz granitoid complex, Sanandaj-Sirjan Zone, Iran. *Journal of Asian Earth Sciences*. 43(1), 11-22. https://doi.org/10.1016/j.jseaes.2011.09.001

Ghiasvand, A., Karimpour, M. H., Malekzadeh Shafaroudi, A., & Hidarian Shahri, M. R. (2017). Age and origin of subvolcanic rocks from NE Iran: Link between magmatic "flare-up" and mineralization. *Chemie Der Erde*. 78(2), 254-267. https://doi.org/10.1016/J.CHEMER.2017.12.002

Golestani, M., Karimpour, M. H., Malekzadeh Shafaroudi, A., & Hidarian Shahri, M. R. (2018). Geochemistry, U-Pb geochronology and Sr-Nd isotopes of the Neogene igneous rocks, at the Iju porphyry copper deposit, NW Shahr-e-Babak, Iran. *Ore Geology Reviews*, *93*, 290–307. https://doi.org/10.1016/J.OREGEOREV.2018.01.001

Hosseinkhani, A., Karimpour, M. H., Malekzadeh Shafaroudi, A., & Santos, J. F. (2017). U-Pb geochronology and petrogenesis of intrusive rocks: Constraints on the mode of genesis and timing of Cu mineralization in SWSK area, Lut Block. *Journal of Geochemical Exploration*, *177*, 11–27. https://doi.org/10.1016/j.gexplo.2017.02.001

Khalaji, A. A., Esmaeily, D., Valizadeh, M. V., & Rahimpour-Bonab, H. (2007). Petrology and geochemistry of the granitoid complex of Boroujerd, Sanandaj-Sirjan Zone, Western Iran. *Journal of Asian Earth Sciences*. 29(5-6), 859-877. https://doi.org/10.1016/j.jseaes.2006.06.005

Mazhari, S. A., Bea, F., Amini, S., Ghalamghash, J., Molina, J. F., Montero, P., … Williams, I. S. (2009). The Eocene bimodal Piranshahr massif of the Sanandaj-Sirjan Zone, NW Iran: A marker of the end of the collision in the Zagros orogen. *Journal of the Geological Society*. 166(1), 53-69. https://doi.org/10.1144/0016-76492*008-022*

Mazhari, S. A., Amini, S., Ghalamghash, J., & Bea, F. (2011). Petrogenesis of granitic unit of Naqadeh complex, Sanandaj–Sirjan Zone, NW Iran. Arabian Journal of Geosciences, 4(1-2), 59-67.

Moghadam, H. S., Zaki Khedr, M., Chiaradia, M., Stern, R. J., Bakhshizad, F., Arai, S., ... & Tamura, A. (2014). Supra-subduction zone magmatism of the Neyriz ophiolite, Iran: constraints from geochemistry and Sr-Nd-Pb isotopes. *International Geology Review*, *56*(11), 1395-1412.

Moghadam, H. S., Li, X. H., Santos, J. F., Stern, R. J., Griffin, W. L., Ghorbani, G., & Sarebani, N. (2017). Neoproterozoic magmatic flare-up along the N. margin of Gondwana: The Taknar complex, NE Iran. Earth and Planetary Science Letters, 474, 83-96.

Moghadam, H. S., Li, X. H., Stern, R. J., Ghorbani, G., & Bakhshizad, F. (2016). Zircon U–Pb ages and Hf–O isotopic composition of migmatites from the Zanjan–Takab complex, NW Iran: constraints on partial melting of metasediments. *Lithos*, *240*, 34-48.

Moghadam, H. S., Rossetti, F., Lucci, F., Chiaradia, M., Gerdes, A., Martinez, M. L., … Nasrabady, M. (2016). The calc-alkaline and adakitic volcanism of the Sabzevar structural zone (NE Iran): Implications for the Eocene magmatic flare-up in Central Iran. *Lithos*, *248–251*, 517–535. https://doi.org/10.1016/j.lithos.2016.01.019

Moghadam, H. S., Corfu, F., Chiaradia, M., Stern, R. J., & Ghorbani, G. (2014). Sabzevar Ophiolite, NE

Iran: Progress from embryonic oceanic lithosphere into magmatic arc constrained by new isotopic and geochemical data. Lithos, 210, 224-241.
Moghadam, H. S., Stern, R. J., Chiaradia, M., & Rahgoshay, M. (2013). Geochemistry and tectonic evolution of the Late Cretaceous Gogher–Baft ophiolite, central Iran. *Lithos, 168*, 33–47. https://doi.org/10.1016/j.lithos.2013.01.013
Moghadam, M. C., Tahmasbi, Z., Ahmadi-Khalaji, A., & Santos, J. F. (2017). Petrogenesis of Rabor-Lalehzar magmatic rocks (SE Iran): Constraints from whole rock chemistry and Sr-Nd isotopes. *Chemie Der Erde - Geochemistry*. 78(1), 58-77. https://doi.org/10.1016/J.CHEMER.2017.11.004
Nabatian, G., Ghaderi, M., Neubauer, F., Honarmand, M., Liu, X., Dong, Y., ... & Bernroider, M. (2014). Petrogenesis of Tarom high-potassic granitoids in the Alborz–Azarbaijan belt, Iran: Geochemical, U–Pb zircon and Sr–Nd–Pb isotopic constraints. *Lithos*, *184*, 324-345.
Nakhaei, M., Mazaheri, S. A., Karimpour, M. H., Stern, C. R., Zarrinkoub, M. H., Mohammadi, S. S., & Heydarian shahri, M. R. (2015). Geochronologic, geochemical, and isotopic constraints on petrogenesis of the dioritic rocks associated with Fe skarn in the Bisheh area, Eastern Iran. *Arabian Journal of Geosciences*, *8*(10), 8481–8495. https://doi.org/10.1007/s12517-015-1834-3
Nouri, F., Asahara, Y., Azizi, H., Yamamoto, K., & Tsuboi, M. (2017). Geochemistry and petrogensis of the Eocene back arc mafic rocks in the Zagros suture zone, northern Noorabad, western Iran. *Chemie Der Erde - Geochemistry*. 77(3), 517–533. https://doi.org/10.1016/j.chemer.2017.06.002
Nouri, F., Azizi, H., Golonka, J., Asahara, Y., Orihashi, Y., Yamamoto, K., … Anma, R. (2016). Age and petrogenesis of Na-rich felsic rocks in western Iran: Evidence for closure of the southern branch of the Neo-Tethys in the Late Cretaceous. *Tectonophysics*, *671*, 151–172. https://doi.org/10.1016/j.tecto.2015.12.014
Pang, K. N., Chung, S. L., Zarrinkoub, M. H., Chiu, H. Y., & Li, X. H. (2014). On the magmatic record of the Makran arc, southeastern Iran: Insights from zircon U-Pb geochronology and bulk-rock geochemistry. *Geochemistry, Geophysics, Geosystems*. 15(6), 2151-2169. https://doi.org/10.1002/2014GC005262
Pang, K. N., Chung, S. L., Zarrinkoub, M. H., Li, X. H., Lee, H. Y., Lin, T. H., & Chiu, H. Y. (2016). New age and geochemical constraints on the origin of Quaternary adakite-like lavas in the Arabia–Eurasia collision zone. *Lithos*. 264, 348-359. https://doi.org/10.1016/j.lithos.2016.08.042
Pang, K. N., Chung, S. L., Zarrinkoub, M. H., Khatib, M. M., Mohammadi, S. S., Chiu, H. Y., ... & Lo, C. H. (2013). Eocene–Oligocene post-collisional magmatism in the Lut–Sistan region, eastern Iran: Magma genesis and tectonic implications. *Lithos*, *180*, 234-251.
Pang, K. N., Chung, S. L., Zarrinkoub, M. H., Mohammadi, S. S., Yang, H. M., Chu, C. H., … Lo, C. H. (2012). Age, geochemical characteristics and petrogenesis of Late Cenozoic intraplate alkali basalts in the Lut-Sistan region, eastern Iran. *Chemical Geology*. 306, 40-53. https://doi.org/10.1016/j.chemgeo.2012.02.020
Samiee, S., Karimpour, M. H., Ghaderi, M., Haidarian Shahri, M. R., Klöetzli, U., & Santos, J. F. (2016). Petrogenesis of subvolcanic rocks from the Khunik prospecting area, south of Birjand, Iran: Geochemical, Sr–Nd isotopic and U–Pb zircon constraints. *Journal of Asian Earth Sciences*, *115*, 170–182. https://doi.org/10.1016/j.jseaes.2015.09.023
Shabanian, N., Davoudian, A. R., Dong, Y., & Liu, X. (2018). U-Pb zircon dating, geochemistry and Sr-Nd-Pb isotopic ratios from Azna-Dorud Cadomian metagranites, Sanandaj-Sirjan Zone of western Iran. *Precambrian Research*. 306, 41-60. https://doi.org/10.1016/j.precamres.2017.12.037
Shahbazi, H., Siebel, W., Pourmoafee, M., Ghorbani, M., Sepahi, A. A., Shang, C. K., & Abedini, M. V. (2010). Geochemistry and U–Pb zircon geochronology of the Alvand plutonic complex in Sanandaj–Sirjan Zone (Iran): New evidence for Jurassic magmatism. Journal of Asian Earth Sciences, 39(6), 668-683.
Shahzeidi, M., Moayyed, M., Murata, M., Yui, T. F., Arai, S., Chen, F., … Ahmadian, J. (2017). Late Ediacaran crustal thickening in Iran: Geochemical and isotopic constraints from the ~550 Ma Mishu granitoids (northwest Iran). *International Geology Review*. 59(7), 793-811. https://doi.org/10.1080/00206814.2016.1198728

Zarrinkoub, M. H., Pang, K. N., Chung, S. L., Khatib, M. M., Mohammadi, S. S., Chiu, H. Y., & Lee, H. Y. (2012b). Zircon U-Pb age and geochemical constraints on the origin of the Birjand ophiolite, Sistan suture zone, eastern Iran. 154, 392–405. *Lithos*. https://doi.org/10.1016/j.lithos.2012.08.007

APPENDIX E: LOCATION OF GEOGRAPHICAL AREAS

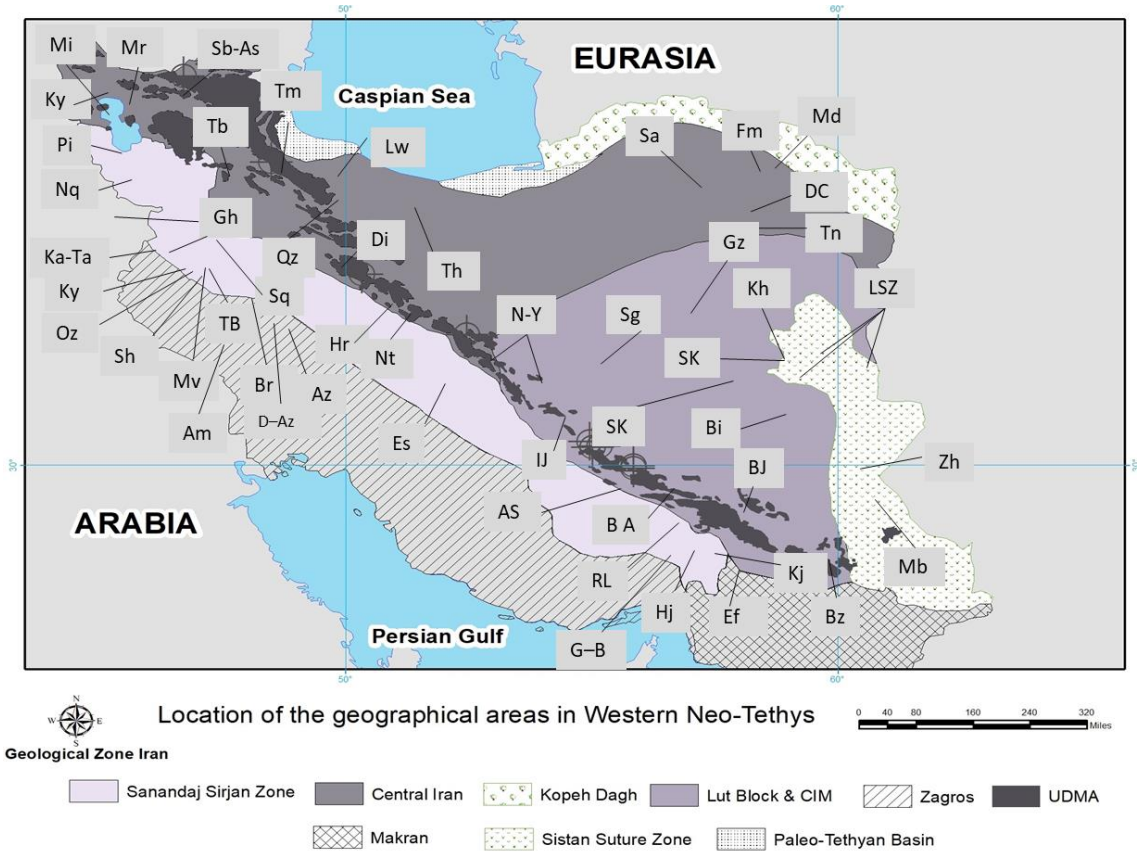

LSZ: Lut–Sistan Suture Zone, **Bi**: Bisheh, **Gh:** GhalaJi, **Sa**: Sabzevar, **Mv**: Morvarid, **Kh**:Khunik, **Pi**: Piranshahr, **Nq**: Naqadeh, **RL**: Rabor-Lalehzar, **Oz**: Ozkol, **Tm**:Tarom, **Tb**: Takab, **Lw**: Lowshan, **Ky**: Kamyaran, **TB**: Taa-Baysaran, **Qz**: Qazvin, **AS**: Anar-Sirjan, **Th**: Tehran, **N-Y**: Nain- Yazd, **Sg**: Saghand, **Fm**: Firouzeh mine, **BJ**: Bam-Jiroft, **Mb**: Mirabad, **DC:** Delbar Complex, **Zh**: Zahedan, **Tn:** Taknar, **Mr:** Mrand, **Ky:** Khoy, **Mr:** Mrand, **Mi:** Misho, **Sq:** Saqqez, **Hr:** Hasanrobat, **Nt:** Natanz, **Sb-As:** Sabalan-Astara, **Md:** Mashhad, **Ka-Ta:** Kangareh-Taghiabad, **Br:** Boroujerd, **Az:** Aligoodarz**, Bz:** Bazman**, Es:** Esfahan**, Gz:** Gazu**, BA:** Bahr Aseman**, Am:** Almogholagh**, Sk:** Sorkh-Kuh, **Kh:** Khunik, **Di:** Dalli, **D-Az:** Drood-Azna, **Ef:** Esfandagheh, **Hj:** Haji-Abad, **Kj:** Kahnuj, **G-B:** Gogher–Baft, **IJ:** Iju